

**POTENTIAL FOR USING TREES TO LIMIT THE INGRESS OF WATER  
INTO MINE WORKINGS: A COMPARISON OF TOTAL EVAPORATION  
AND SOIL WATER RELATIONS FOR *EUCALYPTUS* AND GRASSLAND**

by

**CAREN JARMAIN**

MScAgric (University of Natal, Pietermaritzburg)

Submitted in partial fulfilment of the requirement for the degree of

**DOCTOR OF PHILOSOPHY**

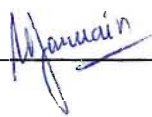
in Agrometeorology, SPACRU, School of Applied Environmental Sciences  
Faculty of Science and Agriculture  
University of Natal  
Pietermaritzburg  
South Africa

November 2003

## DECLARATION

I declare that the results contained in this thesis are from my own original work except where acknowledged.

Signed



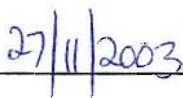
Caren Jarmain

Signed



Professor M.J. Savage  
(Supervisor)

Date



## ABSTRACT

Current mining methods used to extract coal from underground mine workings disturb the natural environment and the existing stable geological structures. As a result, the ingress of water into the mines increases and the quality of the water passing through the mine workings deteriorates, irrespective of the operational status of the mines. Water ingress is generated by regional aquifers, local aquifers, recharge from the surface through rainfall, natural drainage paths on the surface, and surface water bodies. The quality of water in the mines deteriorates as a result of contact with the remaining coal in the mine workings. Mining can therefore cause an increased influx of water into a mine and the degradation of this water. The solution to reducing the impact of mines on the environment is to prevent, or at least reduce, the amount of water entering the mines, and to manage this water to prevent further degradation in water quality.

This study focused on afforestation with *Eucalyptus viminalis* trees to manage or inhibit ingress of water into underground mine workings. The hypothesis of this study was that a change in vegetation, from grassland to fast-growing and potentially high water-using trees like *Eucalyptus*, could possibly reduce the drainage of water below the root-zone and into the mine workings. The hypothesis was tested by estimating the components of the soil water balance for a grassland site and a *Eucalyptus* tree site. The research site was situated in Mpumalanga, (26° 36' S and 29° 08' E, 1650 m a.m.s.l.), one of South Africa's major coal bearing areas. Although the Secunda area is a treeless environment and conditions are not optimal for forestry, some *Eucalyptus* species are suited for conditions (frost and periodic droughts) encountered in this area.

The soil water balance of grassland and *E. viminalis* trees were studied through a field experiment and a long-term (30 years) modelling exercise. Total evaporation of the grassland site was estimated using the Bowen ratio energy balance technique. The transpiration of six representative *E. viminalis* trees were estimated using the heat pulse velocity technique. The soil water storage changes at both sites were determined from the soil water content, estimated using water content reflectometers. Measurements were performed in a smectic clay soil which resulted in measurements difficulties. Vertical cracks were formed under soil drying. To establish the importance of climate and plant growth on the drainage beyond the root-zone, the soil water balance of a grassland and an *E. viminalis* site were simulated over a 30-year period with the Soil Water Atmosphere Plant (SWAP) model.

It was concluded from the comparative field experiment and modelling, that a change in vegetation from grassland to *E. viminalis* will reduce the drainage of water below the root-zone, especially under above-average rainfall conditions. The reduction in drainage beyond the root-zone at the *E. viminalis* sites, compared to the grassland site,

was demonstrated in the modelling exercise and can be deduced from the total evaporation and soil water storage estimated at both sites. The results from the field experiment confirmed the modelling results and showed that usually there were higher transpiration rates for the *E. viminalis* tree site, compared to the grassland site. The higher transpiration rates for *E. viminalis* trees resulted in lower relative saturation of soil layers and lower profile soil water contents at the *E. viminalis* site, and higher daily soil water storage changes at the *E. viminalis* site compared to the grassland site. These differences were more pronounced during winter when the grassland was dormant.

The results from the modelling exercise showed that an *E. viminalis* tree stand, with a closed canopy, reduced drainage below the root-zone compared to a grassland. The drainage at the grassland site contributed to up to 54 % of the rainfall, compared to the 43 % at the *E. viminalis* site. However, under below-average rainfall conditions the annual drainage at both sites, were similar. Further, the absolute magnitude of the drainage was similar to the total evaporation at the grassland site under certain conditions. The results not only suggest that a change in vegetation, from grassland to *E. viminalis* trees, would reduce the drainage beyond the root-zone, but that it may delay the onset of drainage. Under above-average rainfall conditions, the modelled drainage at the *E. viminalis* site only exceeded 20 mm, a month later than at the grassland site. The simulation results also showed that under conditions of above-average rainfall, drainage occurs whenever the rainfall exceeds the long-term average rainfall, irrespective of the existing vegetation. However, when the rainfall is below-average drainage at both sites are limited to large rainfall events. This simulation showed that over a period of eight years, *E. viminalis* trees could potentially reduce the drainage by 1235 mm more than grassland, which is equivalent to  $1540 \text{ m}^3 \text{ ha}^{-1} \text{ a}^{-1}$ , or  $1.54 \text{ M} \ell \text{ ha}^{-1} \text{ a}^{-1}$ . The annual average reduction in drainage below the root-zone caused by *E. viminalis* trees ( $1.79 \text{ M} \ell \text{ ha}^{-1} \text{ a}^{-1}$ ), is a small reduction when compared to the influx of water into mineworkings. E.g. the influx of water into a bord-and-pillar mine range between  $0.5$  and  $4 \text{ M} \ell \text{ d}^{-1}$  per area mined and up to  $17000 \text{ M} \ell \text{ d}^{-1}$  per area mined under high extraction mining (Hodgson and Krantz, 1998; Hodgson *et al.*, 2001).

This work gave a comprehensive account of the differences in the soil water relations of grassland and *E. viminalis* trees overlying coal mine working. Few other studies in South Africa compared the total evaporation and soil water relations of grassland and *E. viminalis* trees in so much detail. State of the art monitoring techniques were used and produced valuable comparison of their use in expansive clay profiles. The work should contribute to management decisions focussed on limiting ingress of water into mine workings.

## RELEVANCE TO MINE MANAGERS

A number of solutions address the problem of ingress of water into mine workings. Some like Evaporators and Crystallisers are extremely expensive (e.g. a 9 Ml d-1 end-of-pipe treatment plant at a cost of R360 000 000) (Kotze, 2000), and not economically viable in the long run. Environmentally related solutions, like afforestation with potentially high water using trees, provide an alternative way to prevent or reduce water movement below the root-zone. The hypothesis is that the replacement of natural grassland overlaying mine working with e.g. *E. viminalis* trees, should cause an increase in total evaporation and a decrease in the soil water storage. This in turn will reduce soil water movement below the root-zone and into mine workings.

This hypothesis was tested in a generally treeless environment: the Mpumalanga mining area. The conditions in this area are less favourable for forestry than in other forestry areas in South Africa. Hostile conditions experienced at the research site in Secunda included severe frost and possible root pruning by the movement of smectic clay soils during winter. Despite these conditions, the results from the study comparing the soil water relations of grassland and *E. viminalis* trees, showed that *E. viminalis* trees have the potential to decrease the soil water movement below the root-zone, when compared to grassland.

The results from the study showed that under above-average rainfall conditions, afforestation with *E. viminalis* trees cause a decrease in the soil water movement below the root-zone, when compared to grassland. The differences in the soil water relations were most pronounced during autumn and winter when the grassland was dormant. However, although the *E. viminalis* trees caused a larger reduction in water movement below the root-zone, compared to grassland, drainage will occur whenever the rainfall exceeds the long-term average rainfall, irrespective of the overlaying vegetation type. Under below-average rainfall conditions, the impact of grassland and *E. viminalis* trees in reducing ingress of water into the mine working, were similar.

Under hostile conditions as experienced at Secunda, however, the potential impact of *E. viminalis* trees could be optimised through successful tree establishment and by ensuring maximum leaf area (growth). This will require near ideal conditions for tree growth throughout the growing season, especially through soil water availability.

Although this study does not provide exact predictive knowledge in terms of water movement below the root-zone and into mine workings, it does increase our knowledge on the potential impact of afforestation with *Eucalyptus* species in reducing the ingress of water into mine workings.

## ACKNOWLEDGEMENTS

I wish to record my sincere gratitude to:

- Sasol Coal (Brandspruit Collieries) for funding the project
- My main supervisor, Professor M.J. Savage (University of Natal) for his time, guidance and valuable scientific inputs
- My other supervisors, Dr C.S. Everson (CSIR), Dr S.A. Lorentz (University of Natal), Professor J.G. Annandale (University of Pretoria), and the late Professor M.A. Johnston (University of Natal) for their scientific inputs
- The CSIR, and specifically Mr J.M. Bosch, for time made available to work on my thesis
- Dr P.J. Dye (CSIR) for valuable scientific inputs
- Institute for Commercial Forestry Research, and specifically Dr C. Smith for providing trial information for *E. viminalis* trees
- Mr E. Blaauw (Sasol Coal) and Dr C.S. Everson for logistical help during field visits
- My Heavenly Father for his love, grace and privilege to study
- My husband, Bryan Jarman, for his love and encouragement
- My pa en ma, Johan and Maryna Burger, en die res van my familie vir julle liefde en ondersteuning deur my jare van studie.

## TABLE OF CONTENTS

<b>LIST OF FIGURES .....</b>	<b>xiii</b>
<b>LIST OF TABLES .....</b>	<b>xvii</b>
<b>NOTATION LIST.....</b>	<b>xix</b>
<b>CHAPTER 1 INTRODUCTION.....</b>	<b>1</b>
1.1 <i>General problem statement .....</i>	<i>1</i>
1.2 <i>Background to the mine water problem .....</i>	<i>1</i>
1.2.1 <i>Effect of different mining methods on the water in mines.....</i>	<i>1</i>
1.2.2 <i>Extent of the mine water problem.....</i>	<i>3</i>
1.2.3 <i>Importance of solutions to the mine water problem.....</i>	<i>4</i>
1.2.4 <i>Solutions to the mine water problem .....</i>	<i>5</i>
1.3 <i>Solution developed for and tested in this research project .....</i>	<i>8</i>
1.4 <i>Potential of solution proposed in this research project.....</i>	<i>9</i>
1.5 <i>Hypothesis of this research project.....</i>	<i>11</i>
1.6 <i>Aims of this research project.....</i>	<i>11</i>
1.7 <i>Outline of document.....</i>	<i>11</i>
<b>CHAPTER 2 TECHNIQUES FOR ESTIMATING TOTAL EVAPORATION AND TRANSPIRATION.....</b>	<b>13</b>
2.1 <i>Introduction .....</i>	<i>13</i>
2.2 <i>Definitions .....</i>	<i>14</i>
2.2.1 <i>Evaporation .....</i>	<i>14</i>
2.2.2 <i>Transpiration .....</i>	<i>14</i>
2.2.3 <i>Total evaporation .....</i>	<i>14</i>
2.2.4 <i>Evaporation of intercepted water .....</i>	<i>15</i>
2.2.5 <i>Reference evaporation.....</i>	<i>15</i>
2.3 <i>A description of the Bowen ratio energy balance technique .....</i>	<i>15</i>
2.3.1 <i>Theory.....</i>	<i>15</i>
2.3.2 <i>A description of the Bowen ratio energy balance equipment ...</i>	<i>17</i>
2.3.3 <i>Assumptions of the Bowen ratio energy balance technique.....</i>	<i>20</i>
2.3.4 <i>Limitations of the Bowen ratio energy balance (BREB)         technique .....</i>	<i>22</i>
2.3.5 <i>Accuracy of the Bowen ratio energy balance technique and         rejection criteria used .....</i>	<i>25</i>
2.4 <i>A description of the heat pulse velocity technique .....</i>	<i>29</i>
2.4.1 <i>Theory of the heat pulse velocity technique .....</i>	<i>29</i>
2.4.2 <i>A description of the heat pulse velocity equipment .....</i>	<i>31</i>
2.4.3 <i>Advantages and disadvantages of the heat pulse velocity         technique .....</i>	<i>31</i>
2.4.4 <i>Accuracy of the heat pulse velocity technique .....</i>	<i>32</i>
2.4.5 <i>Patching of heat pulse velocity data.....</i>	<i>32</i>
2.5 <i>A description of the Penman-Monteith equation .....</i>	<i>33</i>

<b>CHAPTER 3</b>	<b><i>IN SITU</i> SOIL WATER CONTENT AND SOIL WATER POTENTIAL MEASUREMENT TECHNIQUES .....</b>	<b>37</b>
3.1	<i>Introduction</i> .....	37
3.2	<i>Definitions</i> .....	37
3.2.1	Gravimetric and volumetric soil water content.....	37
3.2.2	Soil water potential.....	38
3.2.3	Matric potential.....	39
3.2.4	Residual soil water content .....	39
3.2.5	Saturated soil water content.....	39
3.2.6	Water retention characteristics.....	40
3.2.7	Profile soil water content .....	40
3.2.8	Soil water storage change.....	41
3.2.9	Relative saturation .....	41
3.3	<i>Water content reflectometer technique</i> .....	42
3.3.1	A description of the technique used by the water content reflectometer .....	42
3.3.2	A description of the CS615 water content reflectometer .....	43
3.3.3	Accuracy of the CS615 water content reflectometer .....	43
3.3.4	Advantages and disadvantages of the CS615 water content reflectometer .....	45
3.4	<i>Heat dissipation technique</i> .....	45
3.4.1	A description of the heat dissipation technique .....	45
3.4.2	A description of the heat dissipation sensor.....	47
3.4.3	Accuracy of the heat dissipation sensor.....	47
3.4.4	Empirical relationships between matric potential and temperature change .....	48
3.4.5	Advantages and disadvantages of the heat dissipation sensor.....	49
3.5	<i>Thermocouple psychrometric technique</i> .....	50
3.5.1	A description of the thermocouple psychrometry technique.....	50
3.5.2	A description of the thermocouple psychrometer .....	52
3.5.3	Accuracy of the thermocouple psychrometer .....	53
3.5.4	Advantages and disadvantages of the thermocouple psychrometer .....	56
3.6	<i>Summary</i> .....	57
<b>CHAPTER 4</b>	<b>THE SOIL WATER ATMOSPHERE PLANT (SWAP) MODEL ... .....</b>	<b>58</b>
4.1	<i>Introduction</i> .....	58
4.2	<i>A description of the most important processes applied in SWAP</i> .....	59
4.2.1	Soil water flow .....	59
4.2.2	Daily evapotranspiration.....	60
4.2.3	Crop growth .....	63
4.2.4	Rainfall interception.....	63
4.2.5	Bottom boundary condition .....	64
4.3	<i>Sensitivity of soil water balances modelled with SWAP to different input parameters</i> .....	64
4.4	<i>Advantages and disadvantages of the SWAP model</i> .....	65
4.5	<i>Application of techniques</i> .....	66



<b>CHAPTER 5</b>	<b>MATERIALS AND METHODS</b>	<b>67</b>
5.1	<i>Introduction</i>	67
5.2	<i>Simplified soil water balance</i>	67
5.3	<i>Conditions of site</i>	68
5.3.1	General	68
5.3.2	Climate	68
5.3.2.1	Rainfall	68
5.3.2.2	Reference evaporation	70
5.3.3	Soil conditions	70
5.3.4	Vegetation	72
5.3.5	General	72
5.3.6	Methods for estimating total evaporation and transpiration	78
5.3.6.1	Method for estimating total evaporation	78
5.3.6.2	Method for determining transpiration	79
5.3.7	Methods for determining soil water content and soil water potential	80
5.3.8	Estimating climatic conditions	82
5.4	<i>Long-term soil water balance modelling</i>	83
5.4.1	General	83
5.4.2	Simulation of the soil water balances with the Soil Water Atmosphere Plant (SWAP) model	83
5.5	<i>Summary</i>	84
<b>CHAPTER 6</b>	<b>SOIL WATER CONTENT AND TOTAL EVAPORATION ESTIMATED AT A GRASSLAND AND AN <i>E. VIMINALIS</i> SITE</b>	<b>85</b>
6.1	<i>Introduction</i>	85
6.2	<i>General information</i>	86
6.2.1	Technique used for soil water content comparison	86
6.2.2	Patching of missing soil water content data	86
6.2.3	Seasonal changes in the total evaporation of grassland and transpiration of <i>E. viminalis</i> trees	87
6.3	<i>Relative saturation for grassland and <i>E. viminalis</i> sites</i>	88
6.3.1	Introduction	88
6.3.2	Seasonal differences in relative saturation at different soil depths	91
6.3.3	Cumulative effect of grassland and <i>E. viminalis</i> trees on the relative saturation at different soil depths under above-average rainfall conditions	93
6.4	<i>Profile soil water contents for a grassland and an <i>E. viminalis</i> site</i>	96
6.4.1	Introduction	96
6.4.2	Seasonal changes in the profile soil water contents	97
6.4.3	Cumulative profile soil water contents	98
6.5	<i>Total evaporation and soil water content relationships</i>	98
6.5.1	Introduction	98
6.5.2	Plant and soil water relationships during spring and summer	99
6.5.3	Plant and soil water relationships during autumn and winter	106
6.6	<i>Summary and conclusions</i>	107

<b>CHAPTER 7</b>	<b>SOIL WATER BALANCES FOR THE GRASSLAND AND <i>E. VIMINALIS</i> SITES ESTIMATED FROM THE FIELD EXPERIMENT RESULTS .....</b>	<b>110</b>
7.1	<i>Introduction .....</i>	110
7.2	<i>Relationship between the soil water storage reduction and total evaporation at a grassland site, and transpiration at an <i>E. viminalis</i> site .....</i>	111
7.3	<i>Comparison of soil water storage reduction at a grassland and an <i>E. viminalis</i> site .....</i>	113
7.4	<i>Summary and conclusions.....</i>	116
<b>CHAPTER 8</b>	<b>SOIL WATER BALANCES OF GRASSLAND AND <i>E. VIMINALIS</i> TREES MODELLED WITH THE SOIL WATER ATMOSPHERE PLANT (SWAP) MODEL.....</b>	<b>118</b>
8.1	<i>Introduction .....</i>	118
8.2	<i>Parameterisation of SWAP .....</i>	118
8.2.1	<i>General .....</i>	118
8.2.2	<i>Crop growth .....</i>	119
	8.2.2.1 <i>Grassland growth .....</i>	119
	8.2.2.2 <i><i>E. viminalis</i> tree growth .....</i>	120
8.2.3	<i>Soils information.....</i>	120
8.3	<i>Annual differences in the soil water balances simulated for grassland and for <i>E. viminalis</i> trees.....</i>	121
	8.3.1 <i>Rainfall and total evaporation.....</i>	121
	8.3.2 <i>Drainage .....</i>	124
	8.3.3 <i>Soil water storage change.....</i>	126
8.4	<i>Importance of the different soil water balance components in relation to rainfall.....</i>	127
8.5	<i>Seasonal differences in the soil water balances simulated for grassland and <i>E. viminalis</i> trees .....</i>	128
8.6	<i>Accumulated differences in the soil water balances simulated for grassland and <i>E. viminalis</i> trees for a tree rotation.....</i>	134
8.7	<i>Summary and conclusions.....</i>	137
<b>CHAPTER 9</b>	<b>CONCLUSIONS AND RECOMMENDATIONS .....</b>	<b>138</b>
9.1	<i>Conclusions .....</i>	138
9.2	<i>Recommendations relating to further research.....</i>	141
	9.2.1 <i>General .....</i>	141
	9.2.2 <i>Impact of trees on the regional water resources .....</i>	143
	9.2.3 <i>Research into the effectiveness of tree species other than <i>Eucalyptus</i>, other agricultural crops and agroforestry, in preventing and/or reducing drainage beyond the root-zone... </i>	144
	9.2.4 <i>Research into the increase of evaporation of trees (or high water use agricultural crops) to potential evaporation rates, through irrigation .....</i>	145
<b>REFERENCES</b>	<b>.....</b>	<b>146</b>

<b>APPENDIX A</b>	<b>SOIL DESCRIPTION FOR THE GRASSLAND AND E. VIMINALIS SITES .....</b>	<b>157</b>
A.1	<i>Introduction .....</i>	157
A.2	<i>Definitions .....</i>	157
A.2.1	Particle size distribution .....	157
A.2.2	Bulk density .....	157
A.2.3	Van-Genuchten parameters .....	157
A.2.4	Porosity .....	158
A.2.5	Electrical conductivity .....	158
A.2.6	Soil pH .....	158
A.2.7	Saturation extract .....	158
A.2.8	Sodium adsorption ratio .....	158
A.2.9	Colour .....	159
A.2.10	Structure .....	159
A.2.11	Consistence .....	159
A.2.12	Nodules .....	160
A.3	<i>Properties of soil layers at field research sites, and that of calibration soil samples .....</i>	160
A.4	<i>Description of soil profiles and diagnostic soil horizons at grassland and E. viminalis sites .....</i>	166
A.4.1	Description of the Rensburg soil profile at the grassland and E. viminalis sites .....	166
A.4.2	Description of the Arcadia soil profile at the E. viminalis site .....	169
<b>APPENDIX B</b>	<b>LABORATORY CALIBRATION OF SOIL SENSORS FOR SITE-SPECIFIC CONDITIONS .....</b>	<b>171</b>
B.1	<i>Introduction .....</i>	171
B.2	<i>Materials and methods .....</i>	172
B.3	<i>Results and discussion .....</i>	175
B.4	<i>Application of calibration results to field measurements .....</i>	178
B.5	<i>Conclusions .....</i>	182
<b>APPENDIX C</b>	<b>RELATIONSHIP BETWEEN THE SOIL WATER CONTENT AND THE SOIL WATER POTENTIAL .....</b>	<b>185</b>
C.1	<i>Introduction .....</i>	185
C.2	<i>Comparison of the soil water potentials estimated d with water content reflectometers, heat dissipation sensors and thermocouple psychrometers .....</i>	185
C.3	<i>Possible reasons for discrepancies between soil water potentials estimated with different soil water sensors .....</i>	189
C.3.1	Conversion of soil water content into soil water potential .....	189
C.3.2	Conversion equations (sensor output vs soil water potential) .....	189
C.3.3	Soil water potential vs soil matric potential .....	190
C.3.4	Disadvantages and limitations of, and damage to soil sensors 191	
C.4	<i>Summary .....</i>	191

<b>APPENDIX D</b>	<b>SEASONAL CHANGES IN THE TOTAL EVAPORATION OF GRASSLAND AND TRANSPIRATION OF <i>E. VIMINALIS</i> TREES</b>	<b>192</b>
D.1	<i>Introduction</i>	192
D.2	<i>Total evaporation for the grassland site</i>	192
	D.2.1 <i>Introduction</i>	192
	D.2.2 <i>Seasonal variation in total evaporation of a grassland</i>	193
D.3	<i>Transpiration by <i>E. viminalis</i> trees</i>	196
	D.3.1 <i>Introduction</i>	196
	D.3.2 <i>Seasonal variation in the transpiration of three <i>E. viminalis</i> trees</i>	197
D.4	<i>Summary</i>	200
<b>APPENDIX E</b>	<b>SEASONAL CHANGES IN THE ENERGY BALANCE COMPONENTS OF A GRASSLAND</b>	<b>201</b>
E.1	<i>Introduction</i>	201
E.2	<i>Estimation of the net irradiance as a function of solar irradiance</i>	201
	E.2.1 <i>Introduction</i>	201
	E.2.2 <i>Estimation of net irradiance using Eq. 2.25</i>	201
	E.2.3 <i>Estimation of net irradiance as a site-specific linear function of only solar irradiance</i>	203
	E.2.4 <i>Use of the estimated net irradiance</i>	205
E.3	<i>Changes in the partitioning of the available energy (<math>R_n-G</math>) into sensible and latent heat flux density at a grassland site</i>	205
E.4	<i>Summary</i>	209
<b>APPENDIX F</b>	<b>SWAP MODEL INPUT PARAMETERS FOR THE <i>E. VIMINALIS</i> AND GRASSLAND SITES</b>	<b>211</b>
F.1	<i>Introduction</i>	211
F.2	<i>General data inputs</i>	211
F.3	<i>Atmospheric data inputs</i>	213
F.4	<i>Plant data inputs</i>	213
	F.4.1 <i>Growth calendar</i>	214
	F.4.2 <i>Simple growth model data inputs</i>	214
F.5	<i>Soil data inputs</i>	
	F.5.1 <i>Profile description</i>	218
	F.5.2 <i>Layer property inputs</i>	219
F.6	<i>Water data inputs</i>	219

## LIST OF FIGURES

- Fig. 4.1 Hydrological processes used in the simulations with the Soil Water Atmosphere Plant (SWAP) model (SWAP, undated)
- Fig. 5.1 Location of research site: Secunda, South Africa (National Geographic, undated)
- Fig. 5.2 “Annual” (July to June) total rainfall at Secunda for the period 1 July 1964 to 30 June 2000. The dotted-line represents the long-term average annual rainfall.
- Fig. 5.3 From top to bottom: Summary of the monthly total rainfall, monthly average daily total reference evaporation calculated with the Penman-Monteith equation, monthly average air temperature and average daily radiant density for the period July 1998 to June 2000
- Fig. 5.4 Images of the *E. viminalis* experimental site and instrumentation used
- Fig. 5.5 Images of the grassland experimental site and instrumentation used
- Fig. 5.6 Schematic of the implantation of sets of probes at different depths below the cambium (d1 to d4), into the stem of an *E. viminalis* tree
- Fig. 5.7 Installation of soil water content reflectometers (CS615), heat dissipation sensors (229-L) and thermocouple psychrometers (TCP) into the soil at a grassland and an *E. viminalis* site, at 200 mm intervals
- Fig. 5.8 Images of the automatic weather station installed above a short, well watered grass surface approximately 5 km from the grassland and *E. viminalis* sites
- Fig. 6.1 Relative saturation (expressed as a percentage) for different soil depths at a grassland (grass) and a *E. viminalis* (trees) site for different days within the period 1 July 1998 to 30 June 2000
- Fig. 6.2 Soil water potentials as estimated with *in situ* soil thermocouple psychrometers installed at various soil depths (100 to 900 mm) below a grassland for the period 1 November 1998 to 10 April 1999
- Fig. 6.3 Soil water potential as estimated with *in situ* soil thermocouple psychrometers installed at various soil depths (100 to 900 mm) below *E. viminalis* trees for the period 28 October 1999 to 22 March 2000
- Fig. 6.4 Total profile soil water content at the grassland (grass) and *E. viminalis* (trees) sites over a 1000 mm soil profile for the period May 1998 to June 2000. grass (saturated) and trees (saturated) indicate the saturated profile soil water content for the grassland and *E. viminalis* sites.
- Fig. 6.5 Daily total rainfall (top), daily total evaporation of grassland (total evaporation\_grass) (middle) and daily total transpiration by three *E. viminalis* trees (transpiration\_Tree1, transpiration\_Tree2, transpiration\_Tree3) (bottom) from 1 July 1998 to 30 June 2000
- Fig. 6.6 Leaf area indices of grassland (grass\_) and *E. viminalis* trees (trees\_) during 1998/1999 (\_1998/1999) and 1999/2000 (\_1999/2000)
- Fig. 6.7 Daily total reference evaporation calculated with the Penman-Monteith equation, from 1 July 1998 to 30 June 2000
- Fig. 6.8 Daily total evaporation of grassland (grass) and daily total transpiration of three *E. viminalis* trees (Tree1, Tree2, Tree3) vs soil profile saturation (%)
- Fig. 6.9 Daily total evaporation (total evaporation) and relative saturation (%) at different soil depths (100 to 900 mm) below a grassland from 1 July 1998 to 30 June 2000

- Fig. 6.10 Daily total transpiration for three trees (Transpiration\_Tree1, \_Tree2, \_Tree3) and relative saturation (%) at different depths (100 to 900 mm) at an *E. viminalis* site from 1 July 1998 to 30 June 2000
- Fig. 6.11 Daily total evaporation and soil profile saturation at the grassland site from 1 July 1998 to 30 June 2000
- Fig. 6.12 Daily total transpiration of three *E. viminalis* trees (\_Tree1, \_Tree2, \_Tree3) and soil profile saturation at the *E. viminalis* site from 1 July 1998 to 30 June 2000
- Fig. 6.13 Actual total and saturated profile soil water content at the grassland (grass) and *E. viminalis* (trees) sites over a 1000 mm soil profile
- Fig. 7.1 Top: Differences between monthly total rainfall and monthly total long-term average rainfall at the research sites from July 1998 to June 2000. Bottom: Profile soil water storage reduction (grass\_dS) over a 1000 mm soil depth, and total evaporation of a grassland (grass\_et) on a daily basis. This dataset exclude days with rainfall exceeding 10 mm d<sup>-1</sup> or rainfall on the preceding day exceeding 10 mm d<sup>-1</sup>
- Fig. 7.2 Top: Differences between monthly total rainfall and monthly total long-term average rainfall at the research sites from July 1998 to June 2000. Bottom: Profile soil water storage reduction (trees\_dS) over a 1000 mm soil depth, and daily total transpiration of three trees (Tree1\_t, Tree2\_t and Tree3\_t). This dataset exclude days with rainfall exceeding 10 mm d<sup>-1</sup> or rainfall on the preceding day exceeding 10 mm d<sup>-1</sup>
- Fig. 7.3 Daily profile soil water storage reduction for a grassland (grass) and an *E. viminalis* site (trees) over a soil depth of 1000 mm for the period 8 September 1998 to 22 April 1999
- Fig. 7.4 Daily profile soil water storage reduction for a grassland (grass) and an *E. viminalis* site (trees) over a soil depth of 1000 mm for the period 17 September 1999 to 20 May 2000
- Fig. 7.5 Daily total evaporation for a grassland (grass) and daily total transpiration for three *E. viminalis* trees (Tree1, Tree2, Tree3) vs the daily profile soil water storage reduction over a soil depth of 1000 mm
- Fig. 8.1 Annual total rainfall (top) and simulations of annual total evaporation, annual drainage and annual soil water storage for the grassland (grass) and *E. viminalis* (trees) sites from 1 July 1964 to 30 June 1994, and the differences in annual total evaporation, annual total drainage and annual soil water storages between the grassland and *E. viminalis* sites (grass minus trees)
- Fig. 8.2 Annual total drainage at the grassland (grass) and *E. viminalis* (trees) sites, and annual total rainfall exceeding the annual long-term average rainfall (Rain-Rainlong) from 1 July 1964 to 30 June 1994
- Fig. 8.3 Simulated annual total evaporation (ET/rain), annual total drainage (BF/rain) and annual total soil water storage (dS/rain) as a percentage of the annual total rainfall, for the period 1 July 1964 to 30 June 1994 for the grassland (top) and *E. viminalis* (bottom) sites
- Fig. 8.4 Simulated daily total evaporation (top), daily soil water storage (middle) and daily total drainage for the grassland (grass) and *E. viminalis* (trees) sites (bottom) during an above-average rainfall year (1966/1967). Bars represent daily total rainfall.

- Fig. 8.5 Simulated daily total evaporation (top), daily soil water storage (middle) and daily total drainage for the grassland (grass) and *E. viminalis* (trees) sites (bottom) during a below-average rainfall year (1988/1989). Bars represent daily total rainfall.
- Fig. 8.6 Top: Accumulated simulated drainage at the grassland (grass\_D) and *E. viminalis* tree (trees\_D) sites, accumulated rainfall (rain) and accumulated total evaporation at the grassland (grass\_ET) and *E. viminalis* (trees\_ET) sites during an above-average (1966/1967 - left) and below-average rainfall year (1988/1989 - right). Bottom: Accumulated simulated soil water storage at the grassland (grass\_dS) and *E. viminalis* tree sites (trees\_dS) over the same period
- Fig. 8.7 Total annual (grass and trees) and accumulated (grass\_acc and trees\_acc) rainfall, and simulated total evaporation, soil water storage and drainage at the grassland (grass) and *E. viminalis* (trees) sites for the period 1 July 1972 to 30 June 1980 (years three to ten of a tree rotation)
- Fig. A.1 Top to bottom: Water retention functions (pressure head vs volumetric soil water content) for different soil depths at the grassland and *E. viminalis* sites, and for the soil samples used in the sensor calibration
- Fig. B.1 An example of one of the U-shaped metal frames used in the sampling of block soil samples at the grassland site, for the water content reflectometer calibration
- Fig. B.2 Horizontal installation of water content reflectometers, time domain reflectometers and heat dissipation sensors (top) in the block soil samples used in the sensor calibration, and the connections of the sensors to CR01X, CR23X and CR7 dataloggers (bottom)
- Fig. B.3 Daily measured volumetric soil water content (mass based) for four soil samples used in the sensor calibration, over a period of 170 days. 100, 300, 500 and 700 mm represent the depths at which the calibration soil samples were taken.
- Fig. B.4 Fractional relative saturation of the four soil samples used in the sensor calibration, over a period of 170 days. 100, 300, 500 and 700 mm represent the depths at which the calibration soil samples were taken.
- Fig. B.5 Relationship between the measured volumetric soil water content ( $x$ ) and the soil water content calculated using the manufacturers' polynomials ( $y$ ) for different soil samples (100, 300, 500 and 700 mm)
- Fig. B.6 Relationship between the output of the model CS615 water content reflectometer in ms for each soil layer, and the volumetric soil water content measured
- Fig. B.7 Relationship between the measured ( $x$ ) and calculated ( $y$ ) (based on new estimated polynomial functions) volumetric soil water content for each soil layer
- Fig. B.8 Relationship between combinations of newly calculated volumetric soil water content and measured soil water content. The newly estimated volumetric soil water content is based on polynomials derived for the data combinations collected during the calibration periods, and is indicated in the legend
- Fig. C.1 Daily soil water potentials for the 100-mm, 300-mm, 500-mm, 700-mm and 900-mm soil depths (top to bottom) at the *E. viminalis* site. Soil water potentials estimated with water content reflectometers measurements (tdr), heat dissipation sensors (229-L) and thermocouple psychrometers (tcp). Bars represent the daily rainfall
- Fig. D.1 Daily total evaporation of grassland measured with the Bowen ratio energy balance technique for the period 3 October 1998 to 30 May 1999

- Fig. D.2 Climatic conditions for the period 3 October 1998 to 30 May 1999: Accumulated rainfall (rain), daily minimum air temperature ( $T_{a\_min}$ ), daily solar radiant density ( $R_s$ ) and daily average water vapour pressure deficit ( $es-e$ )
- Fig. D.3 Leaf area index variations at the grassland site for the period December 1998 to June 2000
- Fig. D.4 Daily total evaporation of grassland estimated with the Bowen ratio energy balance technique ( $et$ ), solar radiant density ( $R_s$ ), average daily air temperature ( $T_a$ ) and daily total rainfall (rain) for the period 3 October 1998 to 14 November 1999
- Fig. D.5 Daily transpiration of three *E. viminalis* trees (Tree1, Tree2 and Tree3) representing different diameter classes for the period 1 September 1998 to 30 July 1999
- Fig. D.6 Leaf area index variation at the *E. viminalis* site for the period 1998 to 2000
- Fig. D.7 Daily total transpiration of Tree1, Tree2 and Tree3, and accumulated rainfall (rain) for the period April 1999 to April 2000
- Fig. E.1 Hourly measured ( $x$ ) vs estimated ( $y$ , simulated) net irradiance for grassland during January 1999. Note: The dotted line indicates the 1:1 relationship between the measured and estimated net irradiance, and the solid line the linear relationship between  $x$  and  $y$ . Each data point represents a 20-minute average
- Fig. E.2 Energy flux densities ( $R_n$ ,  $G$ ,  $LE$  and  $H$ ) for a grassland site during different times of the year (1998 to 1999).  $R_n$  represents net irradiance flux density,  $G$  soil heat flux density,  $LE$  latent heat flux density and  $H$  sensible heat flux density. From top to bottom: 3 October and 3 November 1998 (top); 13 January and 13 February 1999 (middle); 16 April and 3 May 1999 (bottom).
- Fig. E.3 Leaf area index at the grassland site for the period December 1998 to June 2000
- Fig. E.4 Air temperature ( $dT$ ) and water vapour pressure profile differences ( $de$ ) measured at the grassland site during spring (3 October 1998). Profile differences are measured between two sampling arms of the Bowen ratio energy balance system installed at different heights above the grassland. Note: The dotted lines indicate the air temperature and water vapour pressure rejection ranges
- Fig. E.5 Air temperature ( $dT$ ) and water vapour pressure profile differences ( $de$ ) measured at the grassland site during spring (13 January 1999). Profile differences are measured between two sampling arms of the Bowen ratio energy balance system installed at different heights above the grassland. Note: The dotted lines indicate the air temperature and water vapour pressure rejection ranges
- Fig. F.1 Average leaf area index ( $y$ ) as a function of the month of the year ( $x$ ) measured for grassland during the field experiment. Dotted line represents the third order polynomial fitted to the data
- Fig. F.2 Average canopy height ( $y$ ) over time ( $x$ ) measured for *E. viminalis* during field trials by the ICFR. Dotted line represents the second order polynomial fitted to the height data, as a function of time



## LIST OF TABLES

- Table 3.1 Relationship between the different units providing an estimate of soil water potential
- Table 5.1 A summary of the measurements made and methods and equipment used to estimate different parameters required during the field experiment
- Table 6.1 Relative saturation (expressed as a percentage) for different soil depths at a grassland (Grass) and *E. viminalis* (Trees) site from 1 July 1998 to 30 June 2000, and the rainfall between different time period
- Table 8.1 Total and annual average (ave), maximum (max) and minimum (min) rainfall, total evaporation, soil water storage and drainage simulated at a grassland (Grass) and *E. viminalis* (Trees) site over a 30-year period (1 July 1964 to 30 June 1994). G-T represents the difference in total evaporation, soil water storage and drainage between the grassland and *E. viminalis* sites
- Table 8.2 Total and annual average (ave), maximum (max) and minimum (min) rainfall, total evaporation, soil water storage and drainage simulated at a grassland (Grass) and *E. viminalis* (Trees) site over years three to ten of a tree rotation (e.g. 1 July 1972 to 30 June 1980). G-T represents the difference in total evaporation, soil water storage and drainage between the grassland and *E. viminalis* sites
- Table A.1 Particle size distribution, expressed as a percentage, for different soil depths at the grassland and *E. viminalis* sites studied, and for the soil samples used in the sensor calibration
- Table A.2 Bulk densities for different soil depths at the grassland and *E. viminalis* sites studied, and for the soil samples used in the sensor calibration
- Table A.3 Electrical conductivity for different soil depths at the grassland and *E. viminalis* sites, for the Rensburg and Arcadia soil forms
- Table A.4 Soil pH (H<sub>2</sub>O) for different soil depths at the grassland and *E. viminalis* sites, for both the Rensburg and Arcadia soil forms
- Table A.5 Na, Ca, Mg and K saturation extracts and sodium adsorption ratio (SAR) for different soil depths at the grassland and *E. viminalis* sites for both the Rensburg and Arcadia soil forms
- Table A.6 Van-Genuchten parameters estimated with RETC (Van Genuchten *et al.*, 1991) for different soil layers at the *E. viminalis* and grassland sites, and for the soil samples used in the sensor calibration
- Table A.7 Porosity for different soil depths at the grassland and *E. viminalis* sites, and for the soil samples used in the sensor calibration
- Table A.8 Soil profile description of the Rensburg form at the grassland site
- Table A.9 Soil profile description of the Rensburg form at the *E. viminalis* site
- Table A.10 Soil profile description of the Arcadia form at the tree site
- Table B.1 Van Genuchten water retention parameters (Eq. 3.4) for the calibration soil samples taken from different depths below the soil surface (100 to 700 mm)
- Table B.2 Statistical information on the relationship between the measured soil water content and the soil water contents estimated from CSI polynomials, presented in Fig. B.5
- Table B.3 Statistical information on the relationship between the CS615 output (ms) and the measured volumetric soil water content, presented in Fig. B.6

- Table B.4 Statistical information on the relationship between the measured soil water content and the volumetric soil water content calculated from the new polynomials, presented in Fig. B.7
- Table B.5 Regression coefficients of the fitted second-order polynomial for the estimation of volumetric soil water content. Second-order polynomials are based measured volumetric soil water content and CS615 sensor output period for different soil depths or soil depth combinations
- Table B.6 Statistical information on the relationship between the measured soil water content and the soil water content calculated from combined polynomials, presented in Fig. B.8
- Table E.1 Statistical information on the relationship between the measured ( $x$ ) and the estimated ( $y$ ) net irradiance, using different reflection coefficients where  $y = mx + c$  where  $m$  is the slope of the relationship and  $c$  is the offset
- Table E.2 Published surface reflection coefficients for grassland
- Table E.3 Statistical information on the relationship between solar irradiance ( $x$ ) and the net irradiance ( $y$ ) where  $y = mx + c$ ,  $m$  is the slope of the relationship,  $c$  is the offset of the relationship and  $R^2$  is the coefficient of determination, and the relationship between the measured net irradiance ( $x$ ) and the net irradiance calculated as a function of the solar irradiance ( $y$ )
- Table E.4 Relationship between the soil heat flux density and the net irradiance ( $G:R_n$ ) measured at the grassland site, where the soil heat flux density is a percentage of the net irradiance
- Table F.1 A summary of the SWAP model inputs
- Table F.2 A summary of the SWAP model outputs in  $\text{cm a}^{-1}$
- Table F.3 General information relating to the simulations for both the grassland and *E. viminalis* sites
- Table F.4 Information regarding the growth simulations used for both sites
- Table F.5 Growth information required in the simple model parameterisation
- Table F.6 Growth information required in the simple model parameterisation at the grassland site as a function of development stage
- Table F.7 Growth information required in the simple model parameterisation for the *E. viminalis* site as a function of development stage for a fixed maximum rooting depth of 1200 mm and a leaf area index of 2.6
- Table F.8 Profile description used for both the *E. viminalis* and grassland sites
- Table F.9 Soil layer properties at the *E. viminalis* and grassland sites

## NOTATION LIST

**Lower case**

$a$	Soil specific parameters of heat dissipation sensor	$^{\circ}\text{C}^{-1}$
$a$	Empirical coefficient	mm
$b$	Soil specific parameters of heat dissipation sensor	Unitless
$b_1$	Slope parameter of the relationship between the thermal conductivity and the matric potential	Unitless
$c$	Offset for linear relationship ( $y = mx + c$ ) between $x$ and $y$	Unitless
$c_{dsoil}$	Specific heat capacity of a dry soil	$\text{J kg}^{-1} \text{ }^{\circ}\text{C}^{-1}$
$c_{dw}$	Specific heat capacity of dry wood	$0.33 \text{ J kg}^{-1} \text{ }^{\circ}\text{C}^{-1}$
$c_p$	Specific heat capacity of air at constant pressure	$\text{J kg}^{-1} \text{ K}^{-1}$
$c_s$	Specific heat capacity of dry soil	$\text{J kg}^{-1} \text{ K}^{-1}$
$c_{soil}$	Specific heat capacity of the soil	$\text{J kg}^{-1} \text{ }^{\circ}\text{C}^{-1}$
$c_w$	Specific heat capacity of water	$\text{J kg}^{-1} \text{ K}^{-1}$
$d$	Solar declination angle	Degrees
$de$	True profile water vapour pressure difference	kPa
$dt$	time interval between datalogger output intervals	minutes
$dT$	True profile temperature difference	$^{\circ}\text{C}$ or $\text{K}$
$dT_{soil}$	Change in soil temperature between the 20 and 60 mm soil depths	$^{\circ}\text{C}$
$d\theta$	True profile equivalent temperature difference	$^{\circ}\text{C}$ or $\text{K}$
$e_1$	Water vapour pressure at $z_1$	kPa
$e_2$	Water vapour pressure at $z_2$	kPa
$e_a$	Atmospheric water vapour pressure	kPa
$e_{act}$	Atmospheric water vapour pressure	kPa
$e_s$	Saturated water vapour pressure	kPa
$e_{sat}$	Saturated water vapour pressure	kPa
$e/e_0$	Fractional relative humidity	Unitless
$es-e$	Water vapour pressure deficit	kPa
$et$	Total evaporation measured with the Bowen ratio energy balance system	$\text{mm d}^{-1}$
$h$	Soil water potential expressed as energy/weight	m
$i$	Soil layer number	Unitless
$j$	Day of year	Unitless
$k$	Thermal conductivity	$\text{J s}^{-1} \text{ m}^{-1} \text{ K}^{-1}$
$k_c$	Canopy factor	Unitless
$l$	Latitude at a site	$^{\circ}$
$m$	Slope of linear curve in relationship $y = mx + c$	Unitless
$m$	Shape factor for the relationship between the soil water content and soil water potential	Unitless
$m_c$	Fractional water content of the sapwood on a dry weight basis	Unitless
$n$	Shape factor for the relationship between the soil water content and soil water potential	Unitless
$n$	Number of soil layers	Unitless

$p$	Correction coefficients for the wound size	Unitless
$q$	Correction coefficients for the diameter of Teflon probes (thermistor probes)	Unitless
$q$	Heat dissipation sensor heat input per unit length of heater	$\text{W m}^{-1}$
$q$	Soil water flux density	$\text{mm d}^{-1}$
$r$	Correction coefficients for the probe separation distance	Unitless
$r_a$	Aerodynamic resistance	$\text{s m}^{-1}$
$r_c$	Canopy resistance	$\text{s m}^{-1}$
$r_v$	Combined canopy and aerodynamic resistance to water vapour	$\text{s m}^{-1}$
rain	Rainfall	mm per time unit
$t$	Time	s
$t_e$	Equation of time	day
$t_o$	Time of solar noon	h
$t_o$	Offset or correction time used by heat dissipation sensor	s
$u$	Windspeed	$\text{m s}^{-1}$
$u$	Velocity of the heat pulse	$\text{m s}^{-1}$
$u'$	Corrected heat pulse velocity	$\text{m s}^{-1}$
$v$	Sap flow	$\ell \text{d}^{-1}$
$x$	Fetch and roughness length for momentum transfer	m
$z$	Vertical coordinate	mm
$z_1$	Height of measurement at level 1	m
$z_2$	Height of measurement at level 2	m
$z_{om}$	Roughness length for momentum transfer	m

### Upper case

$C$	Specific heat capacity	$\text{J kg}^{-1} \text{K}^{-1}$
$C$	Differential soil water capacity	$\text{mm}^{-1}$
$C_{air}$	Heat capacity of moist air	$\text{J kg}^{-1} \text{K}^{-1}$
$Ca$	Calcium	$\text{me L}^{-1}$
$D$	Drainage beyond the root-zone	mm
$D_{root}$	Rooting depth	mm
$E(e)$	Resolution limit for water vapour pressure sensor	kPa
$E(T)$	Resolution limit for temperature sensor	$^{\circ}\text{C}$
$E(\theta)$	Resolution limit in terms of the equivalent temperature	K
$E_a$	Actual soil evaporation calculated using an empirical function in SWAP	mm
$E_{max}$	Maximum evaporation according to Darcy's equation	mm
$E_o$	Evaporation in Penman equation	mm
$E_p$	Potential evaporation	mm
$E_{p0}$	Potential evaporation of a wet bare soil	
$EC$	Electrical conductivity	$\text{S m}^{-1}$
$ET_{areo}$	Aerodynamic term of the Penman-Monteith equation	mm
$ET_B$	Bowen ratio total evaporation	mm
$ET_o$	Potential or reference Penman-Monteith evaporation	mm
$ET_{p0}$	Potential evapotranspiration of a dry canopy completely covering the soil	mm
$ET_{rad}$	Radiation term of the Penman-Monteith equation	mm

$ET_{ref}$	Reference potential evapotranspiration	mm
$ET_{w0}$	Potential evapotranspiration of a wet canopy completely covering the soil	mm
$F$	Soil heat flux density at 80 mm	$W m^{-2}$
$G$	Soil heat flux density	$W m^{-2}$
$G_s$	Simulated soil heat flux density	$W m^{-2}$
$H$	Sensible heat flux density	$W m^{-2}$
$K$	Thermal conductivity	$J s^{-1} m^{-1} K^{-1}$
$K_v$	Diffusivity coefficient for latent heat transfer	$m^2 s^{-1}$
$K_h$	Diffusivity coefficient for sensible heat transfer	$m^2 s^{-1}$
$K_m$	Diffusivity coefficient for momentum heat transfer	$m^2 s^{-1}$
$K(h)$	Hydraulic conductivity	$mm d^{-1}$
$L$	Longitude of site	°
$L_c$	Longitude correction	°
$L_{ni}$	Atmospheric radiant emittance minus the crop emittance at air temperature	$W m^{-2}$
$L_{nic}$	Atmospheric radiant emittance minus the crop emittance at air temperature under clear skies	$W m^{-2}$
$L_s$	Longitude of the standard meridian	°
$LAI$	Leaf area index	$m^2 m^{-2}$
$LE$	Latent heat flux density	$W m^{-2}$
$M_d$	Molecular mass of dry air	$kg mol^{-1}$
$Mg$	Magnesium	$me L^{-1}$
$M_w$	Molecular mass of water	$0.018 kg mol^{-1}$
$Na$	Sodium	$me L^{-1}$
$P$	Atmospheric pressure	kPa
$P$	Precipitation	mm
$P_{gross}$	Gross precipitation	mm
$P_i$	Rainfall interception by a canopy	mm
$P_o$	Sea level pressure	kPa
$Q$	Runoff	mm
$R$	Universal gas constant	$8.3143 \times 10^{-3} kJ mol^{-1} K^{-1}$
$R_n$	Net irradiance	$W m^{-2}$
$Rn$	Net irradiance	$W m^{-2}$
$R_{ns}$	Simulated net irradiance	$W m^{-2}$
$R_o$	Potential net irradiance	$W m^{-2}$
$R_s$	Solar irradiance	$W m^{-2}$
$Rs$	Solar irradiance	$W m^{-2}$
$S$	Average heat flux density stored in the soil	$W m^{-2}$
$S$	Seebeck coefficient	$\mu V ^\circ C^{-1}$
$S_a$	Actual soil water extraction rate by plant roots	$mm^3 mm^{-3} d^{-1}$
$S_a(z)$	Actual root water flux density	$d^{-1}$
$S_e$	Relative saturation	$m^3 m^{-3}$
$S_{initial}$	Initial stored soil water	mm
$S_{final}$	Final stored soil water	mm
$SAR$	Sodium adsorption ratio	$me L^{-1}$
$SC$	Soil cover fraction	Unitless
$T$	Heat dissipation sensor temperature	°C
$T$	Absolute temperature	K
$T_1$	Air temperature at $z_1$	°C or K

$T_2$	Air temperature at $z_2$	°C or K
$T_a$	Air temperature	°C or K
$T_{a\_min}$	Minimum air temperature	°C or K
$T_b$	Ambient temperature	°C or K
$T_j$	Thermocouple junction surface temperature of Psychrometer	°C or K
$T_o$	Surface air temperature	°C or K
$T_o$	Initial temperature	°C
$T_p$	Potential transpiration	mm
$V$	Voltage of psychrometer	$\mu\text{V}$
$V_w$	Partial molar volume of water	$18 \times 10^{-6} \text{ m}^3 \text{ mol}^{-1}$
$V_{25}$	Voltage output of psychrometer after correcting for 25 °C	$\mu\text{V}$
$X_d$	Distance downstream from the heater probe	mm
$X_u$	Distance upstream from the heater probe	mm

### Other

$\alpha$	Shape factor for the relationship between the soil water content and soil water potential	$\text{m}^{-1}$
$\alpha_{rs}$	Actual root water flux density reduction factor due to salinity stresses	Unitless
$\alpha_{rw}$	Actual root water flux density reduction factor due to water stresses	Unitless
$\alpha_s$	Crop reflection coefficient (albedo)	Unitless
$\beta$	Bowen ratio	Unitless
$\delta$	Equilibrium layer thickness	m
$\delta e$	Measured water vapour pressure profile difference	kPa
$\delta T$	Measured air temperature profile difference	°C or K
$\delta z$	Measured separation difference	m
$\Delta$	Slope of the saturation water vapour pressure vs air temperature	$\text{Pa } ^\circ\text{C}^{-1}$
$\Delta_v$	Slope of the saturation water vapour pressure vs air temperature	$\text{kPa K}^{-1}$
$\Delta S$	Change in the soil water storage	mm
$\Delta S_i$	Change in the soil water content in layer i over time	mm
$\Delta T$	Temperature difference	°C or K
$\Delta T$	Increase in temperature following a heat pulse	°C
$\Delta z$	Difference in height	m
$\Delta Z_i$	Thickness of soil layer i	m
$\varepsilon$	Ratio of the molecular mass of water to that of dry air	Unitless
$\gamma$	Thermodynamic psychrometer constant	$\text{kPa K}^{-1}$
$\gamma$	Thermodynamic psychrometer constant	$\text{kPa K}^{-1}$
$\gamma_{air}^*$	Thermodynamic psychrometer constant	$\text{kPa K}^{-1}$
$\gamma^*$	Apparent psychrometer constant	$\text{kPa K}^{-1}$
$\gamma_{air}^*$	Apparent psychrometer constant	$\text{kPa K}^{-1}$
$\phi$	Elevation angle of the sun	Degrees
$\kappa$	Sensor thermal diffusivity	$\text{m}^2 \text{ s}^{-1}$

$\kappa_{gr}$	Product of the extinction coefficient of diffuse and direct visible irradiance	Unitless
$\lambda$	Specific latent heat of vaporization	2450 kJ kg <sup>-1</sup>
$\lambda_w$	Specific latent heat of vaporization	J kg <sup>-1</sup>
$\lambda E$	Latent heat flux density	W m <sup>-2</sup>
$\mu$	Soil water potential expressed as energy/mass	J kg <sup>-1</sup>
$\pi_{root}$	Root length density	m m <sup>-3</sup>
$\theta_{final}$	Final volumetric soil water content	m <sup>3</sup> m <sup>-3</sup>
$\theta_i$	Soil water content of layer i with thickness $\Delta Z_i$ for n soil layers	m <sup>3</sup> m <sup>-3</sup>
$\theta_{initial}$	Initial volumetric soil water contents	m <sup>3</sup> m <sup>-3</sup>
$\theta_m$	Water content of the soil on a mass basis	kg kg <sup>-1</sup>
$\theta_{profile}$	Profile soil water content	m
$\theta_R$	Residual soil water content	m <sup>3</sup> m <sup>-3</sup>
$\theta_S$	Saturated soil water content	m <sup>3</sup> m <sup>-3</sup>
$\theta_v$	Volumetric soil water content	m <sup>3</sup> m <sup>-3</sup>
$\theta_{vs}$	Soil water content under completely water-saturated conditions	m <sup>3</sup> m <sup>-3</sup>
$\theta_w$	Gravimetric soil water content	kg kg <sup>-1</sup>
$\rho$	Density of air	kg m <sup>-3</sup>
$\rho$	Density of the sensor material	kg m <sup>-3</sup>
$\rho_b$	Dry wood density	kg m <sup>-3</sup>
$\rho_s$	Bulk density of soil	kg m <sup>-3</sup>
$\rho_{soil}$	Dry bulk density of soil	kg m <sup>-3</sup>
$\rho_w$	Density of water	1000 kg m <sup>-3</sup> at 20 °C
$\psi$	Soil water potential expressed as energy/volume	Pa
$\Psi_m$	Soil matric potential	Pa
$\Psi_m$	Soil matric potential	Pa

## CHAPTER 1

### INTRODUCTION

#### 1.1 General problem statement

Current mining methods used to extract coal from underground mine workings disturb the natural environment and the existing stable geological structures. As a result, the influx of water into mines increases and the quality of water passing through mine workings deteriorates, irrespective of the operational status of the mines.

The influx of water is generated by regional aquifers, local aquifers, recharge from the surface through rainfall, natural drainage paths on the surface, and surface water bodies. The quality of water in the mines deteriorates as a result of contact with the remaining coal in the mines. Mining can therefore cause an increased influx of water into a mine and the degradation of this water. The solution to reducing the impact of mines on the environment is to prevent, or at least reduce, the amount of water entering the mines, and to manage this water to prevent further degradation in water quality.

#### 1.2 Background to the mine water problem

##### 1.2.1 Effect of different mining methods on the water in mines

Intensive mining in South Africa started over 100 years ago (1870s), after the discovery of the richness of minerals in some parts of South Africa. These minerals occur mainly underground. Various mining methods are used to extract the minerals that are economical to mine. All of the mining methods impact the environment to some degree and therefore have the potential to pollute the surface and/or groundwater. The coal mining industry has an extensive impact on the environment and has a high potential impact on the landscape. However, this impact is less visible after mine rehabilitation (Hodgson and Krantz, 1998; Hodgson *et al.*, 2001).



Coal mining is done opencast or below ground. Underground mining methods include longwall mining, shortwall mining, bord-and-pillar mining, and stooping or pillar extraction. During underground coal mining, coal seams are removed. The removal of these strata results in or could potentially result in the subsidence or collapse of the soil surface overlaying the strata. The extent of the subsidence depends on the mining method and the associated depth of mining (Hodgson and Krantz, 1998; Hodgson *et al.*, 2001).

*Longwall* coal mining takes place at 50 to 200 m below the soil surface, and is seen as the most destructive underground coal mining method. It has the greatest impact of all mining methods on the surface and groundwater resources. Longwall mining is a very rigid method and results in severe collapse of material above the coal seam. It can affect the aquifers above and below the mine workings, and has the highest risk of dewatering the overlying aquifer. After the soil has collapsed, the longwall mining method leaves many cracks (fractures) that may extend to the soil surface. These cracks allow oxygen-rich water to flow into and fill the mine, and subsequently react with the pyrite in the remaining coal-bearing material to form sulphuric acid (Hodgson and Krantz, 1998).

*Shortwall* mining is very similar to longwall mining, but is slightly less destructive as a smaller area is mined at a time. However, this mining method also impacts water quality and quantity (Hodgson and Krantz, 1998).

*Bord-and-pillar* mining is seen as the most environmentally-friendly mining method, and generally does not result in subsidence of the surface. Bord-and-pillar mining occurs at least 100 m below the soil surface. *Stooping* or *pillar extraction* normally follows bord-and-pillar mining, and is less destructive than longwall mining (Hodgson and Krantz, 1998). Pillar crushing or pillar punching may result in gentle and gradual subsidence. Stooping potentially leave pathways for direct ingress of water into mines and the associated oxidization of pyrite.

When cracks or fractures are formed during or following mining, rainfall follows the paths into the mines and accumulates within the underground mine workings. The water that reacts with the pyrite through oxidization, forms sulphuric acid and this in

turn creates the *water quality* problem. This results in a change in the pH and chemical composition of the water, and causes some toxic metals to go into solution. The resulting polluted water resources are very difficult to manage because of their extent and their underground location. The impacted (polluted) mine water can also potentially contaminate adjacent aquifers (groundwater) or nearby streams directly. Therefore, mining methods create or could create a water quality that is unacceptable when the water is released into rivers with the result that the water needs to be contained or utilized in a different manner (Hodgson *et al.*, 2001). This water quality/quantity problem is sometimes extensive, and could to some extent affect mining operations or productivity.

### 1.2.2 Extent of the mine water problem

Coal is an important energy source in South Africa, and coal mining is therefore important to the South African economy. The coal reserves underlie 2.7 million ha of land of which 1 million ha could potentially be mined. This 1 million ha area contains 49 % of the total coal reserve and through high extraction mining methods, could potentially disturb 410000 ha of the Highveld (Versfeld *et al.*, 1998). Further, extensive areas are earmarked for mining in the future, with 40000 ha allocated for high extraction coal mining over the next 30 years (Hodgson *et al.*, 2001). Due to this planned increased mining activity, significant amounts of water can potentially accumulate within mines, be contaminated and potentially impact on surface and groundwater quality.

Hodgson *et al.* (2001) found that a large colliery which produces up to  $10 \times 10^9$  kg of coal per annum could create  $6.25 \times 10^6$  m<sup>3</sup> of underground space. If three quarters of this space collapsed, then  $10 \text{ M } \ell \text{ d}^{-1}$  of mine water could be accumulated. Then, over 40 years, a mine area of 12000 ha, could create  $120 \times 10^6$  m<sup>3</sup> of space. The potential influx (cumulative influx of  $100 \times 10^6$  m<sup>3</sup>) would equal the volume of the Witbank Dam (Hodgson *et al.*, 2001). Hodgson and Krantz (1998) also found differences in the influx of water in different coal mines. Water influx into a bord-and-pillar mine is often difficult to predict because of the irregularity of the cracks into the mines. In general a flux of  $0.5$  to  $1 \text{ M } \ell \text{ d}^{-1}$  during the first 2 to 4 years can be expected, escalating to 2 to

4 M  $\ell$  d<sup>-1</sup> for larger established mines. However, the influxes into high extraction mines are initially comparatively high (4000 to 13000 m<sup>3</sup> d<sup>-1</sup>) due to the dewatering of strata overlaying the mine. Water influx into high extraction mines will continue indefinitely while drainage out of the mine will occur at the same time (Hodgson and Krantz, 1998). Hodgson *et al.* (2001) found the influx into high extraction mines ranged between 1000 and 17000 M  $\ell$  d<sup>-1</sup> per area mined. However, Hodgson *et al.* (2001) suggested that through proper planning, mines would be able to cope with large volumes of water.

### 1.2.3 Importance of solutions to the mine water problem

The water resources of South Africa are scarce, and are insufficient for the growing industrial, human and agricultural water demand. Already in the 1970s, research predicted that by the turn of the century, South Africa would not meet its water requirements (Van der Riet, 1975; Merensky and Hopkins, 1979; Department of Water Affairs and Forestry, 1980; Res Nova, 1984; Tylcoat and Forster, 1987 all cited by Hodgson *et al.*, 2001). However, these authors explained that measures such as catchment water transfer schemes, indigenous water supplies and water restrictions in urban areas were put into place to delay the associated problems. These measures prevented water shortages and assured a sufficient supply of water to the most important sectors.

During the 1970s, a stronger focus was also placed on the importance of groundwater in order to meet the country's water needs as these resources were often close to the demand. At that stage, the groundwater contributed to only 3 % of the country's water requirement, compared to 13 % during the 1980s (Department of Water Affairs and Forestry, 1980 cited by Hodgson *et al.*, 2001). For many years, groundwater was seen as a cheap source of water that needed little management (Braune, 2000) and little attention was paid to the potential impact of different sectors, mining included, on the surface and groundwater resources. Unfortunately in some instances, groundwater was exploited and polluted.

Today, however, both surface and groundwater management is very important in South Africa and is managed through the National Water Act (NWA) (no. 36, 1998). While the previous focus was on finding additional water resources, the focus of the NWA is now on water resource management through demand management, and involves all of the available resources (Braune, 2000). Water management in South Africa is the result of many years (20 years) of research. Water-management-related research included catchment runoff field experiments and modelling exercises, and groundwater studies (geohydrological and water quality) (Hughes, 1985; Brown and Van Niekerk, 1991; Jakubczyk, 1991; Pitman and Kakabeeke, 1991 cited by Hodgson *et al.*, 2001). The NWA places the responsibility of water management of both surface and groundwater on the landowner or the responsible industry.

As mining and other industries are seen as important contributors to water quality and quantity problems (Van Niekerk, 1990 cited by Versfeld *et al.*, 1998), these industries have to comply with regulations relating to water management and mine rehabilitation (Environmental Conservation Act, 1989; Minerals Act, 1991; National Water Act, 1998). For example, mines have to submit closure plans to the Government Mining Engineer and obtain a closure certificate according to the Minerals Act (1991) (Sections 12, 39 and 54). These closure plans help identify and evaluate possible pollution risks and/or problems. The mines have to illustrate the long-term effect of a closed mine on the environment (in terms of water quality and quantity), within acceptable criteria (Hodgson *et al.*, 2001).

#### **1.2.4 Solutions to the mine water problem**

In order to reduce mine water ingress, a clear understanding of the impact of mining on water quality and quantity and the environment is necessary. This knowledge can assist mine management in managing the water from the design stage of the mine through to its closure.

Historically, insufficient attention was devoted to water management planning in advance, for mines applying high extraction underground and other mining methods. This was not done mainly because management did not foresee water shortages, and did

not anticipate the negative impact of mining on the environment, and specifically not on the water resources. Today, however, mine management is under much more pressure to improve water resources management. Management is also aware of the potential impacts and associated problems resulting from different mining methods. Salmon (2000) suggests that mine water management strategies for coal mines need to include preventative measures for water pollution, separation of clean and dirty water, maximum water reclamation, re-use of water, holistic mine planning, and treatment of water.

Over the past 20 years, South African mining houses have invested millions of Rands to investigate and gain a more complete understanding of the effect of different mining methods on the environment, including surface and groundwater resources. This research is ongoing. The research results are used to prevent current and potential future problems, and reduce the impact of these problems. Preconditions to these solutions or strategies are that they be environmentally friendly, cost-effective, and that they do not introduce new problems.

Strategies to control the influx of water into mines and utilize polluted water can be divided into three classes. Strategies include:

- Current and/or future water uses
  - underground water storage during mining (Hodgson *et al.*, 2001),
  - utilization of mine water after closure (e.g. for irrigation) (Barnard *et al.*, 1998),
  - utilization of best quality water,
  - dilution and mixing of disposed mine water (Hodgson *et al.*, 2001),
  - disposal into sea (Dumsday *et al.*, 1989; Hodgson *et al.*, 2001),
  - flood release of poor quality water into streams (Hodgson *et al.*, 2001),
  - pumping (Dumsday *et al.*, 1989) and desalination of water (Hodgson *et al.*, 2001; Kotze, 2001),
  - lime dosing (Maree *et al.*, 1996; Hodgson *et al.*, 2001), and
  - separation of clean and dirty water (Salmon, 2000).

- Mining technology or engineering changes
  - redesign of extraction panels so as to not collapse and fracture strata (Hodgson *et al.*, 2001),
  - re-evaluation of longwall high extraction mining as a mining method (Hodgson *et al.*, 2001),
  - limiting the size of the mines (Hodgson *et al.*, 2001),
  - use of vertical intrusions as barriers to water movement (Hodgson *et al.*, 2001),
  - minimization of water influx by not undermining high transmissive aquifers (Hodgson *et al.*, 2001),
  - changes in mining events (sequence) (bottom to top mining) (Hodgson *et al.*, 2001),
  - holistic mine planning (Salmon, 2000), and
  - installation of anoxic limestone drains (Hodgson *et al.*, 2001),
- Environmentally related solutions
  - rehabilitation of the surface (Hodgson *et al.*, 2001), and
  - reforestation, agroforestry or agronomic measures (Dumsday *et al.*, 1989; Versfeld *et al.*, 1998; Hodgson *et al.*, 2001; Jarman *et al.*, 2001).

Rehabilitation of the surface includes the rehabilitation of the areas above high extraction mining activities, the sealing of cracks/fractures where little vegetative cover exists, deep ploughing over high extraction areas to destroy cracks and drainage paths forming in subsiding areas and frequently (annually) inspecting the areas (Hodgson *et al.*, 2001). Reforestation, agroforestry or agronomic measures again include planting of *Eucalyptus* or other high water-using trees or vegetation upstream or downstream to decanting areas, or above high extraction panels (Dumsday *et al.*, 1989; Versfeld *et al.*, 1998; Hodgson *et al.*, 2001; Jarman *et al.*, 2001). The use of deep-rooted, perennial crops, e.g. lucerne, instead of seasonal shallow-rooted crops are suggested as well as intensive, continuous cropping with a decreased fallow period, minimum tillage, and an increased number of cultivations (Dumsday *et al.*, 1989).

### 1.3 Solution developed for and tested in this research project

A number of possible solutions to deal with water quality and quantity problems experienced by mines are mentioned above and address both the symptoms of the problem and the causes. This study focuses on afforestation with *Eucalyptus* species to manage or inhibit drainage of soil water into underground mine workings. This management option suggests a longer-term solution at a local and/or a catchment level.

The research site to investigate this possible solution was situated in Mpumalanga, one of South Africa's major coal bearing areas. Although the Secunda area is a treeless environment, it has the potential to grow high water users e.g. *Eucalyptus* species, suited for conditions (frost and periodic droughts) encountered in this area. Mining houses in this area (e.g. Sasol Collieries) have recognized the potential of trees to minimize the negative effect introduced by mining on the hydrological system. Sasol Collieries has already planted a variety of *Eucalyptus* species suited to this area, and other mines are also planning to do so.

Since 1990 Sasol Coal has undertaken various projects to investigate afforestation as a potential solution to their problem of increased influx of water into mines (Button *et al.*, 1993). Projects include:

- investigations on the survival and growth of the existing afforestation areas (Du Toit and Basson, 1993),
- field trials to identify tree species suited to different site types, and to identify site-specific soil preparation guidelines (Du Toit, 1993; Du Toit and Mostert, 1993; Cunningham, 1995, 1996), and
- quantification of the water use by trees at various espacements (Olbrich and Poulter, 1992; Olbrich *et al.*, 1994; Versfeld *et al.*, 1998).

A site-based management plan was also devised in 1992 for Brandspruit Collieries, but with the option to include the greater Sasol Mines. In 2000, Sasol Collieries structured an intensive research plan to “*refine the understanding of factors and parameters involved in the prediction of water and salt balances at mine compartment level*” in order to develop a set of “*tools or rules for optimal water management orientated design of new mining operations*” (Kotze, 2001).

Fast-growing and potentially high water-using trees like *Eucalyptus* can potentially modify site and catchment soil water balances and address the water quality and quantity problems experienced by mines. The components of the soil water balance mostly affected by a change in vegetation include soil water storage and total evaporation. However, fast growing, high water-using *Eucalyptus* species, if planted at a large scale (catchment scale), could have a negative effect on the water availability in those areas (Le Maitre *et al.*, 2000). Nambiar (2000) and Sikka *et al.* (2003) also expressed concern that the planting of trees on a large scale, in some instances, will reduce the available water of downstream users, and that it is therefore important to understand the full hydrological impact of *Eucalyptus* trees or other high water-users.

#### 1.4 Potential of solution proposed in this research project

Examples exist that illustrate the effect of a change in vegetation (afforestation or deforestation) at a catchment level on the water balance through streamflow modification (Le Maitre and Scott, 1997; Allen and Chapman, 2000; Gush *et al.*, 2002). In South Africa, the catchment water yield decreased by up to 100 % following afforestation with *Eucalyptus* species (Van Lill *et al.*, 1980; Van Wyk, 1987; Bosch and Smith, 1989; Lesch and Scott, 1993 cited by Versfeld *et al.*, 1998). Other South African examples showed that the water use (transpiration) of *Eucalyptus* could exceed rainfall by  $1200 \text{ mm a}^{-1}$ , where the trees have direct access to groundwater (and soil water stored) (Dye, 1987). However, these high decreases in catchment water yield were estimated under ideal (optimal) forestry conditions.

International examples, like one in Western Australia, also show the effect of *Eucalyptus* trees on the soil water balance. Trees in the Mediterranean parts of Australia are referred to as “biological wicks”, drawing water from the water table throughout the year. After the removal of indigenous deep-rooted *Eucalyptus* species for agricultural and mining purposes, groundwater tables rose, flushing salts through the soil profile to the soil surface, and increasing the salinity levels in the streams. This resulted in less arable land (Peck, 1983; Dumsday *et al.*, 1989; Bell *et al.*, 1990; Leuning *et al.*, 1991; Morris, 1991; Schofield, 1991; Ward, 1991 cited by Versfeld *et al.*, 1998; Raper, 2000). Legislative and other measures are now in place to restrict land clearing. The re-establishment of vegetation in Western Australia is also a



precondition to e.g. extensive bauxite mining. The clearing of *Eucalyptus* forests for bauxite strip mining is only allowed if the new trees or vegetation prove to have the ability to use equivalent or higher amounts of water than the original vegetation. In Western Australia, reforestation of areas with risen groundwater tables, where pasture previously existed, showed relationships between groundwater table reduction and the area reforested.

Other international examples illustrate the impact of *Eucalyptus* species on the water resources (Lima, 1984; Raper, 2000; Sikka *et al.*, 2003). These include India, where three *Eucalyptus* species were used to drain marshes (Shiva and Bandyopadhyay, 1983), to reclaim water logged areas in Punjab and Haryana (Gupta, 1979), and dried up burrow pits on the road sides (Gupta, 1979). Sikka *et al.* (2003) suggested that caution needs to be exercised when large scale conversions of natural grassland into *E. globulus* plantations, are planned. Sikka *et al.* (2003) showed how a conversion from grassland to *E. globulus* decreases the low flow and peak flow, and increases soil moisture losses in South India. These changes were more pronounced during the second rotation.

However, at the proposed research site in the Mpumalanga mining area (South Africa), conditions are less favourable for forestry than other forestry areas in South Africa. Unfavourable conditions include an average annual rainfall of 680 mm a<sup>-1</sup>, frost, shallow soil depths in some areas (less than 500 mm), and the swelling and shrinking characteristics of some soil forms. The effectiveness of *Eucalyptus* species on the soil water balance under these conditions will therefore depend largely on the tree species selected, effectiveness of tree establishment, climatic conditions, position in the landscape, planting density, topography, underground mining method, soil properties, depth of groundwater table and water quality. Raper (2000) found that despite hostile environments in which trees like *Eucalyptus* are sometimes planted, the trees can still lower the water table significantly. Raper (2000) also pointed out that the impact of trees will depend on plantation design, and the species selected. Therefore, it is believed that *Eucalyptus* species still have the potential to decrease the drainage of water into mine workings.

## 1.5 Hypothesis of this research project

The hypothesis of this study is that a change in vegetation, from grassland to *E. viminalis*, will increase the total evaporation and decreases the soil water storage. It is hypothesised that a change in vegetation from grassland to *E. viminalis* trees will reduce the drainage of water beyond the root-zone and into the mine workings, over the short- and long-term.

## 1.6 Aims of this research project

This project compared the soil water balance of a grassland site to that of *E. viminalis* trees. Through this it is possible to infer the impact of a change in vegetation from grassland to *E. viminalis* trees on the drainage beyond the root-zone. In order to achieve these aims, the total evaporation and soil water storage at a grassland and an *E. viminalis* site were estimated during a field experiment over a period of two years. The plant soil water relations at a grassland and a *Eucalyptus* site were modelled on a field scale over an extended period. The results from the modelling were used to illustrate the accumulated differences in the soil water balance components between a grassland and an *E. viminalis* site over a period of 30 years.

## 1.7 Outline of document

The underlying theory of the techniques used in the measurements are discussed in *Chapter 2* (total evaporation and transpiration) and *Chapter 3* (soil water content and soil water potential). *Chapter 4* includes a brief discussion of the Soil Water Atmosphere Plant (SWAP) model used in the simulations.

The layout of the experiment (field measurements and modelling) is discussed in *Chapter 5*.

The soil water balance results are subsequently discussed in *Chapters 6 to 8*. The seasonal changes in the soil water and total evaporation estimated from measurements at the grassland and *E. viminalis* sites are discussed in *Chapter 6*. The soil water balances estimated from measurements at the grassland and *E. viminalis* sites are discussed in

*Chapter 7.* The results of the long-term simulations of the soil water balances at the grassland and *E. viminalis* sites are presented in *Chapter 8.*

The document is concluded in *Chapter 9*, and includes recommendations relating to future research.

## CHAPTER 2

### TECHNIQUES FOR ESTIMATING TOTAL EVAPORATION AND TRANSPIRATION

#### 2.1 Introduction

Total evaporation and crop water use (transpiration) can be determined by different techniques. Each technique applies to a specific spatial and temporal scale, and some are therefore more suitable than others under specific conditions. No single technique is ideal, and it is sometimes best to use a combination of techniques to complement each other. Some techniques measure total evaporation whereas others only measure a component of total evaporation and include:

- energy balance and micrometeorological (Rosenberg *et al.*, 1983; Kite and Droogers, 2000),
- climatological (Rosenberg *et al.*, 1983),
- plant physiological (Rana and Katerji, 2000; Wilson *et al.*, 2001),
- water balance, hydrological or agro-hydrological (Allen *et al.*, 1989; Kite and Droogers, 2000; Wilson *et al.*, 2001), and
- remote sensing techniques (Kite and Droogers, 2000), and
- the use of lysimeters (Allen *et al.*, 1998; Wilson *et al.*, 2001).

Energy balance and micrometeorological techniques include the *mass transport, aerodynamic, Bowen ratio energy balance, resistance, eddy covariance* and *infra-red thermometry* techniques and *large aperture* and *laser scintillometry* (Rosenberg *et al.*, 1983 and Kite and Droogers, 2000).

Climatological techniques include *air temperature based formulas* (the Thornthwaite, Blaney-Criddle, Hargreaves and Linacre techniques), *solar radiation formulas* (regression techniques and the Makkink, Jensen-Haise and solar thermal unit techniques), *solar and thermal radiation techniques* and *combination formulas* (the Penman, Penman-Monteith, Slatyer and McIlroy and Priestley-Taylor model techniques) (Rosenberg *et al.*, 1983).

Plant physiological techniques include sapflow methods and plant chambers (Rana and Katerji, 2000; Wilson *et al.*, 2001).

In this study, the total evaporation of a grassland was measured using the Bowen ratio energy balance (BREB) technique. However, as the *E. viminalis* research plot was small and the canopy fetch to height ratio at this site insufficient for the application of the Bowen ratio energy balance technique, the transpiration of *E. viminalis* trees was measured with a plant physiological method, namely the heat pulse velocity (HPV) technique. The theory underlying these two techniques will be discussed below.

## **2.2 Definitions**

### **2.2.1 Evaporation**

Evaporation is the “*physical process by which a liquid or solid is transferred to the gaseous state*” (Huschke, 1959).

### **2.2.2 Transpiration**

Transpiration can be defined as evaporation of water that has passed through the plant. Transpiration therefore consists of vaporization of liquid water contained in the plant tissues and vapour removal to the atmosphere (Allen *et al.*, 1998).

### **2.2.3 Total evaporation**

Total evaporation ( $ET$ ) can be defined as the total process of water movement into the atmosphere. Soil evaporation ( $E$ ) and transpiration ( $T$ ) occur simultaneously and are determined by the atmospheric evaporative demand (available energy and water vapour pressure deficit), soil (soil water availability) and canopy characteristics (canopy resistances) (Rosenberg *et al.*, 1983). Others (Kite and Droogers, 2000) refer to total evaporation as evapotranspiration.

In this experiment *total evaporation* refers to the sum of:

- evaporation from the soil surface,
- transpiration by vegetation, and
- evaporation of water intercepted by vegetation.

#### **2.2.4 Evaporation of intercepted water**

Plants intercept precipitation (rainfall, dew, irrigation) and therefore prevent a fraction of the precipitation from reaching the soil surface. A fraction of the precipitation that remains intercepted by the canopy is removed by evaporation. This involves the physical change of water from liquid to gas.

#### **2.2.5 Reference evaporation**

Allen *et al.* (1998) defines reference evaporation ( $ET_o$ ) as “*The evaporation from a reference surface, not short of water ... The reference surface is a hypothetical grass reference crop with specific characteristics... The only factors affecting  $ET_o$  are climatic parameters. Consequently,  $ET_o$  is a climatic parameter and can be computed from weather data.  $ET_o$  expresses the evaporating power of the atmosphere at a specific location and time of the year and does not consider the crop characteristics and soil factors.*” Other definitions specify that the reference surface should fully cover the soil surface.

### **2.3 A description of the Bowen ratio energy balance technique**

#### **2.3.1 Theory**

The shortened canopy surface energy balance equation,

$$R_n - G - \lambda E - H = 0 \quad 2.1$$

consists of the net irradiance ( $R_n$ ) (incoming irradiance minus outgoing irradiance of all wave lengths), the soil heat flux density ( $G$ ), the latent heat flux density ( $\lambda E$ ) and the sensible heat flux density ( $H$ ) (Oke, 1978; Rosenberg *et al.*, 1983; Monteith and Unsworth, 1990). The sign convention used is  $R_n$  positive when directed towards the surface and  $G$ ,  $\lambda E$  and  $H$  positive when directed away from the surface. This shortened form of the energy balance ignores stored heat in the canopy and the influence of advection.

Finite water vapour pressure and air temperature profile differences are measured over a vertical distance in the atmosphere and an effective eddy diffusivity assumed to calculate the latent ( $\lambda E$ ) and sensible heat flux densities ( $H$ ):

$$\lambda E = \frac{\lambda \rho \epsilon K_v (\bar{e}_1 - \bar{e}_2)}{P (z_1 - z_2)} \quad 2.2$$

$$H = \frac{\rho c_p K_h (\bar{T}_1 - \bar{T}_2)}{(z_1 - z_2)} \quad 2.3$$

with the diffusivity coefficient for latent ( $K_v$ ) and sensible heat transfer ( $K_h$ ), the density of the air ( $\rho$ ), the ratio of the molecular mass of water ( $M_w$ ) to that of dry air ( $M_d$ ) ( $\epsilon = M_w / M_d$ ), atmospheric pressure ( $P$ ), the specific heat capacity of dry air at constant pressure ( $c_p$ ) and the water vapour pressure  $(\bar{e}_1 - \bar{e}_2) / (z_1 - z_2)$  and air temperature gradients  $(\bar{T}_1 - \bar{T}_2) / (z_1 - z_2)$ .

Assuming that the diffusivity coefficients ( $K_v$  and  $K_h$ ) are equal, the Bowen ratio ( $\beta$ ) is given by:

$$\beta = H / \lambda E \quad 2.4$$

$$\beta = (P c_p / \lambda \epsilon) \frac{\bar{T}_1 - \bar{T}_2}{\bar{e}_1 - \bar{e}_2} \quad 2.5$$

$$\beta = \gamma \frac{\bar{T}_1 - \bar{T}_2}{\bar{e}_1 - \bar{e}_2}$$

where  $\gamma$  (kPa °C<sup>-1</sup>) is the psychrometric constant (Campbell Scientific, Inc., 1998).

Using the shortened surface energy balance (Eq. 2.1) and the computed Bowen ratio (Eq. 2.4), Bowen (1926) showed the sensible (Eq. 2.6) and latent heat flux densities (Eq. 2.7) to be:

$$H = \frac{\beta (R_n - G)}{\beta + 1} \quad 2.6$$

and

$$\lambda E = \frac{R_n - G}{\beta + 1} \quad 2.7$$

respectively, where  $\beta \neq -1$  (Sinclair *et al.*, 1975; Spittlehouse and Black, 1980; Ohmura, 1982).

The total evaporation ( $ET_B$ ) as estimated with the Bowen ratio energy balance technique is solved as:

$$ET_B = \frac{R_n - G}{\lambda(\beta + 1)} \quad 2.8$$

where  $\lambda$  is the latent heat of vaporization (Angus and Watts, 1984).

## 2.3.2 A description of the Bowen ratio energy balance equipment

### 2.3.2.1 Introduction

The Bowen ratio energy balance method requires measurements of net irradiance ( $R_n$ ), soil heat flux density ( $G$ ) and the mean air temperature and water vapour pressure profile differences over 20 minute intervals. The net irradiance and soil heat flux density are used to establish the available energy flux density ( $R_n - G$ ). The available energy flux density is partitioned between the sensible ( $H$ ) and latent heat flux densities ( $\lambda E$ ) (Monteith and Unsworth, 1990; Malek and Bingham, 1993).



### 2.3.2.2 Net irradiance

The net irradiance (the difference between the total incoming and outgoing irradiance fluxes at all wavelengths) is measured every 10 seconds with a net radiometer and averaged over 20 minute periods.

### 2.3.2.3 Soil heat flux density

Two soil heat flux plates, together with four averaging thermocouples are generally used to calculate the soil heat flux density ( $G$ ) at the soil surface:

$$G = F + S \quad 2.9$$

where  $F$  is the soil heat flux density at 80 mm and  $S$  the heat stored above the soil heat flux plates. These sensors are installed to represent the average soil conditions (Campbell Scientific, Inc., 1998).

The buried soil heat flux plates sense the soil heat flux density at 80 mm ( $F$ ). This depth is chosen to exclude errors due to water vapour transport of heat if the plates are placed near the surface.

The two pairs of averaging thermocouples, buried at 20 and 60 mm, are used to calculate the heat stored above the soil heat flux plates ( $S$ ):

$$S = \frac{\rho_{soil} \Delta z dT_{soil} c_{soil}}{dt} \quad 2.10$$

where  $\rho_{soil}$  is the bulk density of the soil,  $\Delta z$  the soil depth (0.08 m),  $dT_{soil}$  the change in soil temperature between the 20 and 60 mm soil depths ( $^{\circ}\text{C}$ ),  $c_{soil}$  the specific heat capacity of the soil ( $\text{J kg}^{-1} \text{ }^{\circ}\text{C}^{-1}$ ) and  $dt$  the time interval between datalogger output intervals (20 minutes) (Savage *et al.*, 1997). The specific heat capacity of the soil ( $c_{soil}$ ) ( $\text{J kg}^{-1} \text{ }^{\circ}\text{C}^{-1}$ ) is calculated as:

$$c_{soil} = c_{dsoil} + \theta_w c_w \quad 2.11$$

where  $c_{dsoil}$  is the specific heat capacity of a dry soil ( $\text{J kg}^{-1} \text{ }^\circ\text{C}^{-1}$ ),  $\theta_w$  the soil water content on a mass basis ( $\text{kg kg}^{-1}$ ) and  $c_w$  the specific heat capacity of water ( $4190 \text{ J kg}^{-1} \text{ }^\circ\text{C}^{-1}$ ) (Savage *et al.*, 1997).

#### 2.3.2.4 Air temperature profile differences

Lower ( $T_1$ ) and upper air temperatures ( $T_2$ ) are measured at heights  $z_1$  and  $z_2$  respectively utilising chromel-constantan (type-E) thermocouples with diameter of  $75 \mu\text{m}$ . The air temperatures are used in the sensible heat flux density (Eq. 2.3) and Bowen ratio (Eq. 2.5) calculations. A differential voltage (mV) is measured due to a temperature difference between  $T_1$  and  $T_2$  and converted into a temperature difference by multiplying by a conversion factor ( $0.06 \text{ mV } ^\circ\text{C}^{-1}$  for type-E thermocouples). The resolution of the datalogger is  $0.006 \text{ }^\circ\text{C}$  with a  $0.1 \mu\text{V}$  root mean square noise (Campbell Scientific, Inc., 1998).

Differences in the radiative heating of the two thermocouples may cause errors in the gradient measurements, but since only the air temperature difference is required, the errors are minimized. The Bowen ratio system uses two sets of thermocouples on each Bowen ratio system: one set of  $25 \mu\text{m}$  (less prone to solar radiant heating) and one set of  $76 \mu\text{m}$  diameter (less prone to breakage). The use of two parallel junctions at each height acts as a back up against breakage (Beringer and Tapper, 1996; Campbell Scientific, Inc., 1998).

#### 2.3.2.5 Water vapour pressure profile differences

The Campbell Scientific Inc. Bowen ratio system utilizes a single cooled-mirror dew point hygrometer to measure the water vapour pressure difference. Air samples are drawn into the system at two heights ( $z_1$  and  $z_2$ ) through  $25 \text{ mm}$  diameter filter containers attached to the arms. The attached containers are fitted with teflon filters with a  $1 \mu\text{m}$  pore size to prevent the entry of dust and liquid water. Air samples drawn

into the system are routed through mixing bottles (2 ℓ) to the cooled mirror. The flow is switched between the two levels every two minutes, using a solenoid valve. Forty seconds are allowed for the system to stabilise and 80 seconds for measurements during a two minute cycle. The water vapour pressure is averaged every 20 minutes for each height and is calculated from the measured dew point temperature. The dew point hygrometer yields a water vapour pressure resolution of  $\pm 0.01$  kPa (Cellier and Olioso, 1993; Campbell Scientific, Inc., 1998).

### 2.3.3 Assumptions of the Bowen ratio energy balance technique

The Bowen ratio energy balance technique assumes a shortened energy balance, finite air temperature and water vapour pressure differences and similarity of the diffusivity coefficients.

#### 2.3.3.1 Assumption of a shortened energy balance

The Bowen ratio energy balance technique utilizes a shortened energy balance equation (Eq. 2.1), which neglects advection and physically and photosynthetically stored energy in the canopy, as they are considered negligible (Thom, 1975; Savage *et al.*, 1997).

#### 2.3.3.2 Assumption of finite differences to measure the air temperature and water vapour pressure gradients

The Bowen ratio energy balance technique assumes finite differences as being an adequate indication of gradients in air temperature  $\delta\bar{T}/\delta z$  and vapour pressure  $\delta\bar{e}/\delta z$

$$\left[ \frac{\delta\bar{T}/\delta z}{\delta\bar{e}/\delta z} \right] \approx \frac{\Delta\bar{T}}{\Delta\bar{e}}$$

with  $\Delta z$  for small values of  $\delta z$  ( $\delta z \approx 1$  to 3 m) (Savage *et al.*, 1997).

The Bowen ratio energy balance technique further assumes that the two levels, at which the air temperature and water vapour pressure measurements are made, are within the boundary layer of air flow (Angus and Watts, 1984; Nie *et al.*, 1992; Beringer and Tapper, 1996).

### 2.3.3.3 Assumption of similarity of the diffusivity coefficients

Under conditions of neutral stability, the diffusivity coefficients for momentum ( $K_m$ ), sensible heat ( $K_h$ ) and water vapour ( $K_v$ ) are assumed to be the same ( $K_m = K_h = K_v$ ) (Metelerkamp, 1993; Savage *et al.*, 1997).

The processes involved occur across the *same* interface and concerns the *same* set of vapours in the *same* atmospheric layer moving in the *same* direction. This however, is not always the case (Pieri and Fuchs, 1990; Metelerkamp, 1993; Savage *et al.*, 1997).

#### 2.3.3.3.1 Stability aspects of the similarity assumption

During unstable conditions  $K_h$  exceeds  $K_v$ , because of the preferential upward transport of heat (Monteith, 1963; Metelerkamp, 1993). Therefore, under conditions of high evaporative flux levels ( $\beta$  small) and an assumption of  $K_h = K_v$  (where  $K_h$  and  $K_v$  are not markedly different), no serious errors in the  $\lambda E$  estimates may result. During dry conditions when  $\lambda E$  is small ( $\beta$  large) and  $K_h \neq K_v$ , conditions can lead to errors of the same magnitude of  $\lambda E$  (Denmead and McIlroy, 1970; Metelerkamp, 1993; Savage *et al.*, 1997).

#### 2.3.3.3.2 The effects of advection on the similarity assumption

The application of the Bowen ratio energy balance technique in semi-arid conditions, leads to the inadequate performance of this technique (Angus and Watts, 1984; Metelerkamp, 1993; Unland *et al.*, 1998). Blad and Rosenberg (1974) questioned the use of the assumption of similarity under these advective conditions. The erroneous

assumption of similarity can lead to an underestimation of  $\lambda E$  under advective conditions (Blad and Rosenberg, 1974; Metelerkamp, 1993).

### 2.3.4 Limitations of the Bowen ratio energy balance (BREB) technique

The application of the BREB technique is limited by theoretical, practical and boundary layer limitations. These limitations can invalidate the Bowen ratio energy balance technique (Barr *et al.*, 1994).

#### 2.3.4.1 Theoretical limitations

Examining the denominator  $(1+\beta)$  in the calculation of the latent heat flux density (Eq. 2.7) (which may not become zero), the calculation of  $\lambda E$  tends to infinity or minus infinity as the Bowen ratio approaches -1. The Bowen ratio often tends to -1 during early morning and late afternoon periods when the available energy ( $R_n - G$ ) approaches zero. Rainfall events also cause  $\beta$  to approach -1 (Savage *et al.*, 1997). The latent heat flux density during these periods is low and can therefore be ignored. For Bowen ratio values ranging between -1.25 and -0.75, the latent heat flux densities are assumed to be negligible and are not calculated or included in evaporative totals (Ohmura, 1982; Savage, *et al.*, 1997; Campbell Scientific, Inc., 1998).

#### 2.3.4.2 Practical limitations

##### 2.3.4.2.1 Measurement limitations

Sustained operation of the Bowen ratio instrumentation for long periods is technically difficult (Pieri and Fuchs, 1990). Continuous and accurate measurement of water vapour pressure at two levels is a particular limitation (Lukangu, 1998). Accurate net irradiance and soil heat flux density measurements could also be a major measurement limitation (Savage *et al.*, 1997).

#### 2.3.4.2.2 *Resolution limitations*

A major difficulty associated with the Bowen ratio energy balance technique is the instrumentation. Instrumentation must detect air temperature and water vapour pressure differences of the same magnitude as the bias of the sensors (Pieri and Fuchs, 1990). The measured air temperature and water vapour pressure differences across a vertical distance must therefore be larger than the resolution of the individual sensors for meaningful results to be obtained (Savage *et al.*, 1997). If the air temperature and water vapour pressure differences approach the resolution limits of the different sensors, the measured differences tend to zero.

When resolution limits are approached, the sensor separation should be increased so as to increase the air temperature and water vapour pressure differences (Cellier and Olioso, 1993; Savage *et al.*, 1997). This approach assumes that there is a constant water vapour pressure and air temperature gradient in the equilibrium layer

#### 2.3.4.2.3 *Condensation limitations*

Dew condensation on thermocouples, air intakes and net radiometer domes precludes any meaningful measurement of flux densities. Dew condensation occurs during periods when the Bowen ratio approaches -1 (early morning and late afternoon) and the evaporation rates are low. Data recorded under these conditions need to be rejected (Cellier and Olioso, 1993; Savage *et al.*, 1997) since, for example, dew often occurs on the top net radiometer dome only. Mainly, this would alter the exchange of long wave radiation between the sky and the upper net radiometer sensor.

#### 2.3.4.3 *Boundary layer/fetch limitations*

The BREB technique is theoretically restricted to ideal sites which require an infinite, homogenous canopy and flat terrain (Businger, 1986). Only when there is horizontal uniformity can the vertical fluxes be considered to be similar in form (Angus and Watts, 1984). In order to overcome the lack of heterogeneity of the canopy caused by the

horizontal distribution of foliage, the measurements must be made sufficiently high above the canopy layer (Brutsaert, 1982).

Fetch requirements relate to the boundary layer requirements (Heilman and Brittin, 1989). Ideally measurements should be made within the equilibrium sub-layer (Savage *et al.*, 1996). The internal equilibrium layer ( $\delta$ ) is the lower portion of the boundary layer, which has reached water vapour pressure, air temperature and momentum equilibrium with the surface. Brutsaert (1982) defined this layer as the region where the momentum flux density is within 10 % of the value at the surface. The thickness of the internal equilibrium layer is calculated using the Munro and Oke (1975) equation for stable conditions:

$$\delta = x^{0.8} z_{om}^{0.2} \quad 2.12$$

with  $x$  equal to the fetch and roughness length (m) for momentum transfer ( $z_{om}$ ) (Heilman and Brittin, 1989).

Practically, fetch is often limited. The necessary fetch required to establish equilibrium conditions has often been assumed to be 100 times the maximum measurement height above the ground (Blad and Rosenberg, 1974; Angus and Watts, 1984). If the fetch is very large, the location of the sensors within the equilibrium sub-layer (while still maintaining detectable air temperature and water vapour pressure differences between the two levels) is relatively easy (Stannard, 1997). Fetch-to-height ratios ranging from 10:1 to 200:1 have been recommended with 100:1 considered adequate for most measurements (Heilman and Brittin, 1989; Nie *et al.*, 1992). Practical limitations result in measured  $\delta T$  and  $\delta e$  values affected by an upwind surface and some measurements made above the equilibrium layer (Stannard, 1997).

Heilman and Brittin (1989) evaluated the effect of fetch and measurement height, on the Bowen ratio estimation of sensible and latent heat flux densities (Heilman and Brittin, 1989). The variability of the Bowen ratio tends to increase with measurement height because of the departure from the ideal site with uniform fetch (Heilman and Brittin, 1989).

Yeh and Brutsaert (1971) indicated that the Bowen ratio method may be less sensitive to imperfect fetch conditions when  $\beta$  is small (Heilman and Brittin, 1989) and can be successfully used at fetch-to-height ratios as low as 20:1 (Heilman and Brittin, 1989). Hanks *et al.* (1971) found that under advective conditions changes in air temperature and water vapour pressure were still evident at fetch-to-height ratios of 105:1 (Hanks *et al.*, 1971). The Bowen ratio energy balance fetch requirements can be reduced significantly by lowering the lower as well as the upper sensor (Stannard, 1997).

### 2.3.5 Accuracy of the Bowen ratio energy balance technique and rejection criteria used

#### 2.3.5.1 Accuracy of the Bowen ratio energy balance technique

The BREB technique has been thoroughly tested in the past and its validity as a standard for evaporation measurement has been well established (Fritschen, 1966; Fuchs and Tanner, 1970; Sinclair *et al.*, 1975).

The BREB technique has proved to be most appropriate on extensive homogenous surfaces (Malek, 1993). The majority of the studies utilizing the BREB method have been concerned with irrigated pastures and crops or other types of vegetation (e.g. forests) (Angus and Watts, 1984). Malek (1993) indicated that the BREB technique provided accurate estimates of evaporation over any agricultural and non-agricultural ecosystems. Spittlehouse and Black (1980) indicated that the application of the BREB technique over forests is more difficult but still suitable.

Ohmura (1982) stresses the importance of checking the Bowen ratio flux calculation to see whether it is close to reality or in error due to measurement error or instrumentation resolution limits.

The BREB estimate of latent heat flux density ( $\lambda E$ ) is directly proportional to the available energy flux density  $R_n - G$  and inversely proportional to  $1 + \beta$ . If  $R_n$  or  $G$  is underestimated,  $\lambda E$  will be underestimated. Accurate estimates of net irradiance are therefore critical for reliable  $\lambda E$  estimates. Soil heat flux density measurements are less



critical since for complete cover situations  $G$  is very small in comparison to  $R_n$  (Blad and Rosenberg, 1974). The accuracy of the calibration of net radiometers is stated to be 5 % and 5 % for the soil heat flux plates. If sampling problems and spatial variability of soils are included, a combined error of up to 20 % for soil heat flux is possible (Angus and Watts, 1984). Errors in the latent and soil heat flux densities depend on the sign of the Bowen ratio. When  $\beta$  is positive and large, a large relative error in the latent heat flux density exists (after Fuchs and Tanner, 1970). For  $-0.6 < \beta < 2$ , the error in the available energy flux density  $R_n - G$  is a major contributor to the error in the latent heat flux density. For conditions where  $\beta$  exceeds 2, the accuracy to which the water vapour pressure differences are measured, is important (Spittlehouse and Black, 1980).

From a modelling point of view, however, the absolute error in the latent heat flux density is usually more important than the relative error (Angus and Watts, 1984). The accuracy of the computed latent heat flux density is strongly dependent on the accuracy of  $\beta$  (Angus and Watts, 1984). When evaporation is close to potential rates ( $-0.2 < \beta < 0.2$ ), relative errors of approximately 30 % in  $\beta$  produce errors of less than 5 % in the latent heat flux density. If the errors in  $R_n$  and  $G$  are included, the error in  $\lambda E$  increases to 9 %. During periods of high evaporation rates, the relative accuracy of the computed latent heat flux density is increased even if the Bowen ratio is poorly measured (Angus and Watts, 1984). For  $\beta \rightarrow -1$  (such as at sunrise and sunset), the relative error in  $\lambda E$  becomes infinite ( $\delta T$  approaches 0 and  $R_n - G \approx 0$ ) as it occurs over short periods and the error introduced into the daily evaporation totals is insignificant.

The relative error in the latent heat flux density is increased, due to the errors in  $\beta$  when water becomes less available and the Bowen ratio increases (Angus and Watts, 1984).

### 2.3.5.2 Rejection criteria

A rejection scheme is important to prevent the acceptance of physically inconsistent or inaccurate flux values (Ohmura, 1982). Ohmura (1982) stresses the importance of judging whether the results are close to reality or not.

Various data rejection criteria exist which need to be used with discretion so as not to exclude data unnecessarily. Five rejection criteria were adopted in this study. It was decided to reject all Bowen ratio data for periods when any of conditions 1 to 5 were met.

### 2.3.5.2.1 Condition 1

Following Ohmura (1982), the Bowen ratio rejection criteria, for  $\beta \rightarrow -1$  are derived. Savage *et al.* (1997) shows a much more elegant method of obtaining the rejection criteria in terms of the equivalent temperature or the resolution limits of the air temperature and water vapour pressure sensors.

If

$$\beta = \gamma dT/de = -1$$

then

$$d\theta = 0.$$

Within experimental limits then,

$$|d\theta| < 2 E(\theta)$$

or

$$-2E(\theta) < \delta e/\gamma + \delta T < 2E(\theta) \quad 2.13$$

or

$$-\delta e/\gamma - 2E(\theta) < \delta T < -\delta e/\gamma + 2E(\theta) \quad 2.14$$

(Ohmura, 1982; Savage *et al.*, 1997).

### 2.3.5.2.2 Condition 2

Where  $\beta$  approaches -1 (at sunrise and sunset), numerically meaningless fluxes are calculated and the data points should be excluded from further data analysis (Cellier and Olioso, 1993; Metelerkamp, 1993; Ortega-Farias, 1996). Frequently the equation

$$-1.25 < \beta < -0.75 \quad 2.15$$

has been employed to reject data.

### 2.3.5.2.3 Condition 3

Data suggesting periods where the mean water vapour pressure ( $\bar{e}_1$  or  $\bar{e}_2$ , in kPa) exceeds the saturation water vapour pressure ( $e_s$ ), must be excluded from further data analysis (Metelerkamp, 1993; Savage *et al.*, 1997), using the criterion:

$$\bar{e}_1 \text{ or } \bar{e}_2 > e_s + 0.01. \quad 2.16$$

### 2.3.5.2.4 Condition 4

If the absolute profile air temperature difference  $|\delta T|$  decreases below the thermocouple sensor resolution  $E(T)$  (0.006 °C), the data should be rejected and considered unsuitable for processing (Savage *et al.*, 1997), using the criterion:

$$|\delta T| < \text{resolution limit of temperature sensor, or}$$

$$|\delta T| < 0.006 \text{ °C.}$$

### 2.3.5.2.5 Condition 5

When the absolute profile water vapour pressure difference  $|\delta e|$  decreases below the dewpoint hygrometer sensor resolution  $E(e)$  (0.01 kPa), the data for that period are inconclusive and should be rejected (Savage *et al.*, 1997), using the criterion:

$$|\delta e| < \text{resolution limits of vapour pressure sensor, or}$$

$$|\delta e| < 0.01 \text{ kPa.}$$

## 2.4 A description of the heat pulse velocity technique

### 2.4.1 Theory of the heat pulse velocity technique

The heat pulse velocity (HPV) technique measures the velocity of a heat pulse propagating through a tree using the compensation technique (Huber and Schmidt, 1937; Swanson, 1974 cited by Dye *et al.*, 1992). The temperature rise in the thermistor probe as a result of the application of a heat pulse is measured at a distance  $X_u$  upstream and  $X_d$  downstream from the heater probe. According to Swanson (1983) (cited by Olbrich, 1994), the velocity of the heat pulse ( $u$  in  $\text{m s}^{-1}$ ) is calculated as:

$$u = \frac{(X_u + X_d)}{2t} \quad 2.17$$

where  $t$  (in second) is the time it takes for the temperature at  $X_u$  and  $X_d$  to become equal (Dye *et al.*, 1992) or for the Wheatstone bridge voltage to return to the initial balance point after the heater is pulsed (Olbrich, 1994), where  $(X_u + X_d)/2$  refers to the probe separation (Olbrich, 1994). Both  $X_u$  and  $X_d$  are regarded as positive quantities.

The heat pulse velocity is corrected for wound size or width according to Swanson and Whitfield (1981):

$$u' = p + qu + ru^2 \quad 2.18$$

where  $p$ ,  $q$  and  $r$  are correction coefficients derived for the wound size, diameter of Teflon probes (thermistor probes) and probe separation distance.

Finally, the sap flow ( $v$ ), is calculated from the corrected heat pulse velocity ( $u'$ ) (Marshall, 1958):

$$v = \rho_b (m_c + c_{dw}) u' \quad 2.19$$

where  $\rho_b$  is the dry wood density ( $\text{kg m}^{-3}$ ),  $m_c$  the fractional water content of the sapwood on a dry weight basis (unitless), and  $c_{dw}$  the specific heat capacity of dry wood ( $0.33 \text{ J kg}^{-1} \text{ }^\circ\text{C}^{-1}$ ) (Dunlap, 1912 cited by Dye *et al.*, 1992).

The various sap fluxes ( $v$ ) measured at different depths below the bark of a tree, are regarded as representative of a ring of sapwood centred at the probe depth. The total sap flux per tree is therefore calculated as the sum of the partial areas (a concentric ring area with limits mid-way between successive thermistors) multiplied by their associated sap fluxes. The sap flux per tree can be converted into sap flux per unit area, using the tree espacement.

The wound size for each set of probes is measured at the end of the experiment. The sections of the tree trunk containing the probe implantation holes are cut out. Then each block containing the probe implant holes is cut longitudinally at the depth at which the thermistors were implanted. The area is then shaved smoothly with a microtome after which the wound width is identified by discolourization, and measured to the nearest 0.1 mm. Measurements are taken midway between the position of the heater probe and the two thermistor probes. From these measurements, the average wound width is calculated for each tree. The assumption is generally that the same wound size existed for the duration of the experiment. The wood density is also calculated at the end of the experiment, using a fresh sample of sapwood.

### 2.4.2 A description of the heat pulse velocity equipment

The heat pulse velocity system consists of a datalogger (a custom made heat pulse velocity recorder) and sets of probes. A set of probes consist of two thermistor probes and one heater probe.

Teflon probes, each with a thermistor imbedded, are connected in a Wheatstone bridge configuration by using the datalogger. A heat pulse is generated when a current is supplied for 0.5 to 1 s to the heater probes. The data recorder then estimates the time it takes for the bridge to return to the initial balance point, following the heat pulse.

### 2.4.3 Advantages and disadvantages of the heat pulse velocity technique

Advantages of the heat pulse velocity technique include:

- suitability of the technique for transpiration measurements in even-aged forests (Dye *et al.*, 1992),
- reliability and inexpensiveness of technique,
- automation of the data collection and storage,
- sequential and simultaneous measurement of the sapflow of numerous trees,
- estimation of tree transpiration for a complete stand,
- higher accuracy in sapflow rates than with the heat balance technique (Cohen *et al.*, 1981), and
- minimal tree destruction.

Disadvantages include:

- sensitivity of sapflux estimates to wound width where the sapflow is interrupted i.e. where the probes were implanted (Swanson and Whitfield, 1981),
- sensitivity of technique to errors in the measurement of probe separation and the sapwood water content,
- reduced accuracy for low to moderate sap fluxes compared to the heat balance method (Cohen *et al.*, 1981),

- violation of the idealized heat transport and interference with sapflux by probes implanted into sapwood (Swanson and Whitfield, 1981),
- difficulty in scaling measurements up for uneven stands,
- invasion of probes and typically bulkiness (Bauerle *et al.*, 2002),
- poor temperature control by probes,
- lengthy response times, and the inability to measure short-term transients, and
- the assumption of the same wound size for the duration of the experiment.

#### 2.4.4 Accuracy of the heat pulse velocity technique

Swanson and Whitfield (1981) noted that the heat pulse velocity technique is an accurate technique to estimate transpiration, when the correction factor for wound size measured at the completion of an experiment, is used. Olbrich (1994) also found good agreement between the transpiration estimates obtained from the heat pulse velocity method and that obtained in a cut tree experiment. Olbrich (1994) also found that the accuracy of the transpiration is sensitive to the wound size correction. Dye *et al.* (1992) further noted that the heat pulse velocity technique is a reliable method to estimate the water use, especially for stands of even-aged trees.

#### 2.4.5 Patching of heat pulse velocity data

Tree transpiration data loss during a field experiment can result from low battery voltages, corrosion of heater probes, and cracks around heater and thermistor probes and subsequent large wound widths.

Dye *et al.* (2001) found good agreement between daily sapflow (total transpiration) measured with the HPV technique and the product of the average daily water vapour pressure deficits  $e_s - e$  and the daylight hours, for a number of tree species. This relationship has been used by Dye *et al.* (2001) to accurately patch missing sap flow data.

## 2.5 A description of the Penman-Monteith equation

Penman (1948) derived a formula to account for the energy required to sustain evaporation and a mechanism to remove water vapour. The original Penman equation for reference evaporation ( $E_o$ ) over a open water surface is given as:

$$E_o = (\Delta R_n + \gamma E_a) / (\Delta + \gamma) \quad 2.20$$

where  $R_n$  is the net irradiance,  $\Delta$  ( $\text{kPa } ^\circ\text{C}^{-1}$ ) is the slope of the saturation water vapour pressure vs temperature curve at the surface temperature ( $T_o$ ),  $\gamma$  is the psychrometric constant ( $\text{kPa } ^\circ\text{C}^{-1}$ ) and

$$E_a = f(u)(e_s - e_a) \quad 2.21$$

where  $e_s - e_a$  is the daily averaged water vapour pressure deficit ( $\text{kPa}$ ) and the wind function,  $f(u)$ , given by:

$$f(u) = 0.27 (1 + u/100) \quad 2.22$$

where  $u$  is the daily averaged windspeed ( $\text{m s}^{-1}$ ) (Rosenberg, *et al.*, 1983).

The Penman equation was later modified by Monteith (1963, 1964) to give the Penman-Monteith combination equation. The Penman-Monteith equation combines a "radiative" and "aerodynamic" component to calculate the Penman-Monteith reference evaporation ( $ET_o$ ):

$$ET_o = \frac{\Delta (R_{ns} - G_s)}{\lambda (\Delta + \gamma)} + \frac{\gamma^* M_w (e_s - e_a)}{R (T_a + 273.15) r_v (\Delta + \gamma)} \quad 2.23$$

$ET_o = \text{"radiative" component} + \text{"aerodynamic" component}$

where  $R_{ns}$  is the calculated daily radiant density,  $G_s$  the calculated daily soil heat flux density,  $\gamma^*$  is the apparent psychrometric constant,  $M_w$  the molar mass of water,  $R$  the



universal gas constant,  $T_a$  the daily average air temperature and  $r_v$  the combined aerodynamic and canopy resistance to water vapour:

$$r_v = r_a + r_c \quad 2.24$$

where  $r_a$  is the aerodynamic resistance for heat transfer and  $r_c$  the canopy resistance (Campbell; undated; Oke, 1978; Allen *et al.*, 1998; Monteith and Unsworth, 1990; Metelerkamp, 1993).

The net radiant density ( $R_{ns}$ ) is estimated from the solar radiant density ( $R_s$ )

$$R_{ns} = (1 - \alpha_s) R_s + L_{ni} \quad 2.25$$

where the net radiant density,  $R_n$ , is the sum of the net radiant density and the net long-wave radiant density, where  $\alpha_s$  is the reflection coefficient of the crop and  $L_{ni}$  the atmospheric radiant emittance minus the crop emittance at daily average air temperature. Under clear skies,  $L_{ni}$  ( $\text{kW m}^{-2}$ ) is given by:

$$L_{nic} = 0.0003 T_a - 0.107 \quad 2.26$$

with  $T_a$  as the daily average air temperature ( $^{\circ}\text{C}$ ). Under cloudy skies  $L_{ni}$  approaches zero. Cloudiness is estimated from the ratio of measured to potential daily total solar radiant density during daylight hours ( $R_s/R_o$ ). A cloudiness function,  $f(R_s/R_o)$  is computed:

$$f(R_s/R_o) = 1 - \frac{1}{[1 + 0.034 \exp(7.9 R_s/R_o)]} \quad 2.27$$

The daily net isothermal long-wave radiant density ( $L_{ni}$ ) is then calculated as:

$$L_{ni} = f(R_s/R_o) L_{nic} \quad 2.28$$

The cloudiness function (Eq. 2.27) requires the computation of the potential solar radiant density on a horizontal surface outside the earth's atmosphere,  $R_o$ :

$$R_o = 1.36 \sin \varphi \quad 2.29$$

where  $1.36 \text{ kW m}^{-2}$  is the solar constant, and  $\varphi$  the solar elevation:

$$\sin \varphi = \sin d \sin l + \cos d \cos l \cos [15(t - t_o)] \quad 2.30$$

where  $d$  is the solar declination angle,  $l$  the latitude at the site,  $t$  the local time and  $t_o$  the time of solar noon. A polynomial is used for  $\sin d$ :

$$\sin d = -0.37726 - 0.105564j + 1.2458j^2 - 0.75478j^3 + 0.13627j^4 - 0.00572j^5 \quad 2.31$$

where  $j$  is the day of the year (DOY) divided by 100 (DOY/100) and  $d$  is the declination. The cosine of  $d$  is computed from the trigonometric identity:

$$\cos d = (1 - \sin^2 d)^{0.5} \quad 2.32$$

The time  $t$  is the datalogger local time less half the time increment from the last  $ET_o$  computation. The time of solar noon,  $t_o$ , is given by:

$$t_o = 12.5 - L_c - t_e \quad 2.33$$

with  $L_c$  the longitude correction and  $t_e$  the "equation of time". The longitude correction is calculated by determining the difference between the longitude of the site and the longitude of the standard meridian. The longitude correction is given as:

$$L_c = (L_s - L)/15 \quad 2.34$$

The “equation of time” is an additional correction to the time of solar noon that depends on the day of year. Two equations are used to calculate  $t_e$ : one for the first half of the year (for  $\text{DOY} \leq 180$ , where  $j = \text{DOY}/100$ ):

$$t_e = -0.04056 - 0.74503j + 0.08823j^2 + 2.0515j^3 - 1.8111j^4 + 0.42832j^5 \quad 2.35$$

and one for the second half of the year (for  $\text{DOY} > 180$ , where  $j = (\text{DOY}-180)/100$ ):

$$t_e = -0.05039 - 0.33954j + 0.04084j^2 + 1.8928j^3 - 1.7619j^4 + 0.4224j^5 \quad 2.36$$

Evaporation occurs mainly during daylight hours when the net irradiance is the main driving force of the evaporation and is positive. The soil heat flux density can be estimated as a fraction of the net irradiance. For a complete canopy cover,  $G_s$  is assumed to be approximately 10 % of the net radiant density.

$$G_s = 0.1R_n \quad 2.37$$

During the night  $R_s = 0$  and  $G_s$  is assumed to be 50 % of the net irradiance.

$$G_s = 0.5R_n \quad 2.38$$

The Penman-Monteith equation has been applied successfully over different surfaces (crops and forests) of optimal or limited water supply where the resistance required, is known (Campbell, undated; Rosenberg *et al.*, 1983).

## CHAPTER 3

### **IN SITU SOIL WATER CONTENT AND SOIL WATER POTENTIAL MEASUREMENT TECHNIQUES**

#### **3.1 Introduction**

Several techniques exist to measure *in situ* soil water content and soil water potential. These techniques include gravimetric, nuclear, electromagnetic, tensiometric, hygrometric and remote sensing techniques (Zazueta and Xin, undated). Some sensors allow long-term monitoring of soil water content or soil water potential through the availability of dataloggers and electronic equipment. These sensors and microprocessor systems can be left unattended to do numerous measurements per day, and collect data automatically. These sensing techniques have a distinct advantage over the widely used neutron probe technique (Herkeleath and Delin, undated) which requires the presence of an operator. However, of all these techniques, none is completely satisfactory.

Most of the techniques relate more easily measured soil properties to the water content or the water potential of the soil. For example, the water content reflectometer technique relates the dielectric constant of the soil to the soil water content, whereas the heat dissipation technique relates the thermal conductivity and heat capacity (temperature change) to the soil water potential, and the thermocouple psychrometric technique relates the soil humidity to the soil water potential. The three techniques mentioned here will be discussed in more detail below.

#### **3.2 Definitions**

##### **3.2.1 Gravimetric and volumetric soil water content**

Gravimetric soil water content ( $\theta_m$ ) is the water content of the soil expressed relative to the mass of oven dry soil ( $\text{kg kg}^{-1}$  or other mass unit):

$$\theta_m = \frac{\text{mass of wet soil} - \text{mass of oven dry soil}}{\text{mass of oven dry soil}} = \frac{\text{mass of water}}{\text{mass of dry soil}} \quad 3.1$$

The gravimetric soil water content can be converted to volumetric water content ( $\theta_v$ ) using the dry bulk density of soil ( $\rho_{soil}$ ):

$$\theta_v = \theta_m \left( \frac{\rho_{soil}}{\rho_w} \right) \quad 3.2$$

where  $\rho_w$  is the density of water ( $1000 \text{ kg m}^{-3}$  at  $20 \text{ }^\circ\text{C}$ ) (Sumner, 2000).

The volumetric soil water content ( $\theta_v$ ) is defined as the water content on a volume basis, the volume of water per volume of soil, or the depth of water per unit depth of soil (Sumner, 2000):

$$\theta_v = \frac{\text{mass of water} / \text{density of water}}{\text{sample volume}} = \frac{\text{volume of water}}{\text{bulk volume of soil}} \quad 3.3$$

### 3.2.2 Soil water potential

Soil water potential can be defined as the difference between the free energy per unit of volume of soil water and that of pure water in a reference state. Free energy characterises the energy status of water and involves all other forms of energy available to move the water and is therefore a measure of the tendency of that substance to move. The reference state is pure free water at atmospheric pressure and at the same temperature as the soil. The soil water potential consists of gravitational potential, matric potential and osmotic potential. These potentials act simultaneously but result from different forces. The combined effect caused by the different potentials influence soil water movement and behaviour (Brady, 1990).

Soil water potential can be expressed in different units: energy/mass ( $\mu$  in  $\text{J kg}^{-1}$ ), energy/volume ( $\psi$  in Pa) or energy/weight ( $h$  in m) (Sumner, 2000). The relationships between these units are given in Table 3.1.

Table 3.1 Relationship between the different units providing an estimate of soil water potential

Energy/mass ( $\mu$ )	Energy/volume ( $\psi$ )	Energy/weight ( $h$ )
1 J kg <sup>-1</sup>	1 kPa = 0.001 MPa = 10 mbar = 0.01 bar = 0.0099 atm = 0.145 psi	10 cm = 0.1 m

### 3.2.3 Matric potential

Soil matric potential ( $\psi_m$ ) results from water adsorption and capillary water. Water adsorption and the capillary water reduce the free energy of the soil water compared to that of un-adsorbed pure water. Consequently, matric potentials are always negative. The matric potential exerts its effect on soil water retention and soil water movement (Brady, 1990).

### 3.2.4 Residual soil water content

The residual soil water content ( $\theta_r$ ) is can be defined as the minimum (Vertessy and Elsenbeer, 1999) or irreducible water content of a soil.

### 3.2.5 Saturated soil water content

The saturated soil water content ( $\theta_s$ ) can be defined as the maximum amount of water in the soil when all the pores are filled with water. It is therefore the ratio of the mass of water to the dry mass of the soil, for a soil completely saturated with water (Van der Watt and Van Rooyen, 1990).

### 3.2.6 Water retention characteristics

An inverse relationship exists between the volumetric soil water content ( $\theta_v$ ) and the soil water potential or soil water pressure head (Brady, 1990). This relationship is influenced mainly by soil texture, soil structure and organic matter (Sumner, 2000).

Soil water pressure heads can be related to volumetric soil water content ( $\theta_v$ ) through the Van Genuchten (1980) relationship:

$$\theta_v = \theta_R + \frac{\theta_S - \theta_R}{\left(1 + |\alpha h|^n\right)^{\frac{n-1}{n}}} \quad 3.4$$

where  $\theta_R$  is the residual soil water content ( $\text{m}^3 \text{m}^{-3}$ ),  $\theta_S$  the saturated soil water content ( $\text{m}^3 \text{m}^{-3}$ ),  $h$  the soil water pressure head (m), and  $\alpha$  ( $\text{m}^{-1}$ ) and  $n$  are shape factors for the relationship between the soil water content and soil water potential (Van Dam, 2000).

### 3.2.7 Profile soil water content

The profile soil water content ( $\theta_{profile}$ , m) is calculated as:

$$\theta_{profile} = \sum_{i=1}^n \theta_i \Delta Z_i \quad 3.5$$

where  $\theta_i$  is the soil water content ( $\text{m}^3 \text{m}^{-3}$ ) of layer  $i$  with thickness  $\Delta Z_i$  (m) for  $n$  soil layers.

### 3.2.8 Soil water storage change

The change in the soil water storage ( $\Delta S$ ) at a specific point is calculated as:

$$\Delta S = S_{Initial} - S_{Final} \quad 3.6$$

or within a layer  $i$ , as:

$$\Delta S_i = (\theta_{final} - \theta_{initial}) \cdot \Delta Z_i \quad 3.7$$

where  $S_{initial}$  and  $S_{final}$  are the initial and final stored soil water,  $\Delta S_i$  the change in the soil water content in layer  $i$  over time,  $\theta_{final}$  and  $\theta_{initial}$  the final and initial volumetric soil water contents and  $\Delta Z_i$  the thickness of the soil layer  $i$  (Sumner, 2000).

### 3.2.9 Relative saturation

The relative saturation ( $S_e$ ) of a soil is an indication of the wetness of the soil. The relative saturation is a function of the volumetric soil water content ( $\theta_v$ ), residual soil water content ( $\theta_R$ ) and saturated soil water content ( $\theta_s$ ):

$$S_e = \frac{\text{volume of water filled pore space}}{\text{total volume of soil pore space}} = \frac{\theta_v}{\theta_{vs}} = \frac{\theta_v - \theta_R}{\theta_s - \theta_R} \quad 3.8$$

where  $\theta_{vs}$  is the soil water content under completely water-saturated conditions (Van Dam *et al.*, 1997; Sumner, 2000).



### **3.3 Water content reflectometer technique**

The Campbell Scientific model CS615 water content reflectometer provides a measure of the volumetric soil water content. When this sensor is used under standard conditions (electrical conductivity  $EC$  less than  $0.1 \text{ S m}^{-1}$  and clay content less than 30 %), the volumetric soil water content can be calculated directly using the calibration polynomials provided by the manufacturer (Campbell Scientific, Inc., 1996). However, if used under non-standard conditions, e.g. in soils with a clay content greater than 30 %, these sensors need to be calibrated individually for specific field conditions. Herkelrath and Delin (undated) found that laboratory calibrations differed significantly from that specified by the manufacturer. This was mainly because of the application of this technique under non-standard conditions.

#### **3.3.1 A description of the technique used by the water content reflectometer**

The technique used by the CS615 water content reflectometer sensor relies on the fact that each material has a unique dielectric constant. Different dielectric constants result in different propagation times of an electromagnetic wave from a sensing rod, or different oscillation frequencies of a sensor. For example, a wave will move slowly through a medium with a high dielectric constant like water (Campbell Scientific, Inc., 1996).

The dielectric constant of soil is the weighted sum of the dielectric constants of the soil constituents. The propagation time of a wave through a dry soil (low dielectric constant) will be higher than that of a wet soil (high dielectric constant). The water content reflectometer therefore relates the dielectric constant to the volumetric soil water content (Campbell Scientific, Inc., 1996).

### **3.3.2 A description of the CS615 water content reflectometer**

The CS615 water content reflectometer consists of two stainless steel rods of fixed length (300 mm), a built-in circuit board and a coaxial four core insulated cable. The circuit board consists of high-speed electronic components. This circuit board controls the power supply, enables the measurements, and outputs the measuring period (propagation time). The circuit board is configured as a multi-vibrator and the outputs of this multi-vibrator are connected to the sensing rods and acts as a wave-guide. This multi-vibrator oscillates at a frequency dependent on the dielectric constant of the soil. Therefore, any change in the volumetric soil water content or the associated dielectric constant, will translate into a change or shift in the oscillation frequency. The CS615 water content reflectometer outputs a square wave with a specific amplitude and shape. The voltage amplitude ranges between 0 and 2.5 V and the output period (propagation time) between 0.7 and 1.6 ms (Campbell Scientific, Inc., 1996).

### **3.3.3 Accuracy of the CS615 water content reflectometer**

The accuracy of the volumetric soil water content measured with the CS615 water content reflectometer depends on the conditions under which the sensor is applied. Where site-specific calibration functions are used, errors of only approximately 2 % were found in the soil water content estimates (Campbell Scientific, Inc., 1996). However, where the manufacturers' polynomials are applied but the sensor is used under non-standard conditions, the accuracy of the volumetric soil water content will depend on the air temperature, electrical conductivity (mineral composition) of the soil, and clay and organic matter contents (texture) (Campbell Scientific, Inc., 1996). Herkelrath and Delin (undated) found significant differences between the soil water content calculated with the polynomials supplied by the manufacturer and polynomials derived from laboratory calibrations under non-standard conditions.

### 3.3.3.1 Electrical conductivity influence

The electrical conductivity (*EC*) of the soil water affects the accuracy and the quality of the volumetric soil water content measurement. The propagation time of the electromagnetic wave along the sensing rods, is a function of the dielectric constant. However, the propagation time is also a function of the electrical conductivity. If the electrical conductivity exceeds  $0.1 \text{ S m}^{-1}$ , the slope of the standard calibration function changes (Campbell Scientific, Inc., 1996). The slope will decrease with increased electrical conductivity. For an *EC* between  $0.1$  and  $0.5 \text{ S m}^{-1}$ , the sensor detects changes in the dielectric constant under stable conditions. But, for *EC* greater than  $0.5 \text{ S m}^{-1}$ , the sensor output is unstable and the technique or measurements are no longer reliable (Campbell Scientific, Inc., 1996).

### 3.3.3.2 Clay and organic matter content influence

Both the clay and organic matter contents in the soil have strong polarities and affect the dielectric constant. The electromagnetic energy from the wave propagating through soil may polarize the polar water molecules. If other forces act on these water molecules, the electromagnetic energy may not polarize the water molecules. Then the propagation time or oscillation frequency is not representative of the real soil water content (Campbell Scientific, Inc., 1996).

### 3.3.3.3 Air temperature influence

The water content reflectometer is sensitive to changes in air temperature. A correction function, based on the volumetric soil water content, slightly improves the accuracy of the soil water content measurements (Campbell Scientific, Inc., 1996). After applying the correction function, the maximum difference between the corrected and uncorrected soil water contents is 1.6 % (Campbell Scientific, Inc., 1996).

### 3.3.4 Advantages and disadvantages of the CS615 water content reflectometer

Advantages of the water content reflectometer include:

- CS615 provides estimates of volumetric soil water content,
- unattended, reliable and accurate measurements over long time periods (Herkelrath and Delin, undated), and
- soil water content representative of a larger soil volume compared to other sensors such as the thermocouple psychrometer and heat dissipation sensor.

Disadvantages include:

- high temperature dependency,
- sensitivity to electrical surges and lightning,
- sensitivity of manufacturers calibration polynomials to clay content,
- required individual calibrations for non-standard conditions ( $EC$  less than  $0.1 \text{ S m}^{-1}$  and clay content less than 30%), and
- necessity for soil-sensor contact.

## 3.4 Heat dissipation technique

The heat dissipation technique relies on the relationship between the matric potential ( $\Psi_m$ ) of the soil and its thermal conductivity and heat capacity. The heat dissipation sensor does not measure the matric potential directly, but requires an empirical relationship to convert a change in temperature, before and after an imposed pulse of heat, to matric potential (Jovanovic and Annandale, 1997).

### 3.4.1 A description of the heat dissipation technique

The porous ceramic material of the heat dissipation sensor equilibrates hydraulically with the surrounding porous media (soil) after the sensor is installed. Under conditions of a water potential gradient between the ceramic and soil, water will move to or from the sensor to equilibrate the soil water potential gradient. The time to reach equilibrium depends on the magnitude of the water potential gradient and the hydraulic

conductivity. For equilibration to take place and to be representative of the soil conditions, and real time changes in the soil water content/potential, good contact between the sensor and the soil is required.

When power or a heat pulse is applied to the heat dissipation sensor the temperature around the heating element will increase. The increase in temperature ( $\Delta T$ ) following the heat pulse is estimated as the difference between the temperature within the sensor just before heating or 1 s after heating, and 16 to 30 s after heating. The rate of heat dissipation away from the heater and the associated temperature rise ( $\Delta T$ ) within the soil sensor is dependent on sensor thermal diffusivity, which in turn depends on the amount of soil water present (Phene *et al.*, 1971; Campbell Scientific, Inc., 1995; Reece, 1996). The sensor thermal diffusivity ( $\kappa$ ,  $\text{m}^2 \text{s}^{-1}$ ) is a function of the thermal conductivity ( $K$ ,  $\text{J s}^{-1} \text{m}^{-1} \text{K}^{-1}$ ), specific heat capacity ( $C$ ,  $\text{J kg}^{-1} \text{K}^{-1}$ ) and density of the sensor material ( $\rho$ ,  $\text{kg m}^{-3}$ ) through:

$$\kappa = K / \rho C \quad 3.9$$

The thermal conductivity of the porous material depends on the thermal conductivity of the matrix, the proportion of pore spaces filled with water, and the proportion of the material that is pore space (Phene *et al.*, 1971). The thermal conductivity increases exponentially with increase in soil water content and the specific heat capacity increases almost linearly with increase in soil water content (Phene *et al.*, 1971).

Air is a better thermal insulator than water. As the soil dries, water is replaced with air in the soil (and sensor) and thinner water films cover the soil particles. This creates an increased path length for heat conduction and requires an increased temperature gradient to dissipate a given amount of water.

The relationship between the change in temperature,  $T - T_o$ , ( $^{\circ}\text{C}$ ) and the thermal conductivity,  $k$ , is given by the equation for time dependence,  $t - t_o$ , of temperature in a line heat source (Campbell *et al.*, undated):

$$T - T_0 = \left( \frac{q}{4\pi k} \right) \ln (t - t_0) \quad 3.10$$

where  $T$  is the sensor temperature related to time ( $t$ ),  $T_0$  the initial temperature,  $q$  the heat input per unit length of heater ( $\text{W m}^{-1}$ ), and  $t_0$  is the offset or correction time (s) (Reece, 1996). This relationship is used to calculate the matric potential ( $\psi_m$ ) (Reece, 1996) and only holds if  $t_0$  and  $q$ , do not vary from measurement to measurement (Campbell *et al.*, undated and Shiozawa and Campbell, 1990 cited by Campbell *et al.*, undated; Reece, 1996):

$$\psi_m = \exp \left[ \left( k^{-1} - 0.134 \right) / b_1 \right] \quad 3.11$$

where  $b_1$  is the slope parameter of the relationship between the thermal conductivity and the matric potential (Reece, 1996).

Since the sensor and soil need to be in thermal equilibrium before a measurement, the interval between subsequent heat dissipation measurements of a block should be sufficient so as to permit the previously applied heat pulse to dissipate without affecting the next measurement. Bristow *et al.* (1993) suggest a maximum of 20 minutes for re-equilibrium for a coarse loamy soil.

### 3.4.2 A description of the heat dissipation sensor

The heat dissipation sensor consists of a porous ceramic cylinder with a fine wire heating element centred in the block and a copper-constantan thermocouple (type-T) located next to this heating element (Campbell Scientific, Inc., undated; Reece, 1996).

### 3.4.3 Accuracy of the heat dissipation sensor

Scanlon *et al.* (1999) noted that the accurate operating range for the heat dissipation sensor is  $-500$  to  $-10 \text{ J kg}^{-1}$ . Scanlon *et al.* (1999) further noted that outside this range, the sensor become increasingly insensitive to decreasing matric potentials and predict

matric potentials greater than the actual potentials. Reece (1996) also found that the accuracy of matric potential, measured with the heat dissipation sensor, decreases beyond  $-1200 \text{ J kg}^{-1}$ . Within the range  $-1200$  to  $-10 \text{ J kg}^{-1}$ , Reece (1996) showed that the matric potentials estimated with the heat dissipation sensors were within 20 % of independently measured matric potentials. Reece (1996) further showed that the heat dissipation sensor slightly over-predicts the matric potential for the range  $-1200$  to  $-400 \text{ J kg}^{-1}$ , when compared to thermocouple psychrometers. Jovanovic and Annandale (1997) found that the accuracy of the matric potential measurements beyond  $-100$  to  $0 \text{ J kg}^{-1}$  decreases, especially when an exponential calibration function between matric potential ( $\psi_m$ ) and the soil temperature change ( $\Delta T$ ) was used.

#### **3.4.4 Empirical relationships between matric potential and temperature change**

Good results can be obtained with heat dissipation sensors. However, calibrations are required to establish the relationship between matric potential and the corresponding temperature change (Campbell Scientific, Inc., 1995).

The relationship between the matric potential ( $\Psi_m$ ) and the change in temperature following heating ( $\Delta T$ ) can be used for probe calibration. This relationship however, is an empirical calibration relationship and can take different forms.

Calibration functions for the heat dissipation sensors vary with soil type. Additionally, the variation in the hydraulic and thermal conductivity properties between probes is great enough to reduce the measurement accuracy if the same calibration function is applied to more than one probe. However, the required matric potential resolution (or accuracy) will determine whether individual sensor calibration is necessary (Campbell Scientific, Inc., 1995).

The matric potential is related to the thermal conductivity of the soil water solution, equilibrated in the ceramic block. The matric potential ( $\psi_m, \text{ J kg}^{-1}$ ) can be related to the change in temperature using a power function:

$$\psi_m = a \Delta T^b \quad 3.12$$

where  $a$  and  $b$  are soil specific parameters (Campbell Scientific, Inc., 1995). For example, Jovanovic and Annandale (1997) found  $a$  and  $b$  to be  $-2.55 \text{ }^\circ\text{C}^{-1}$  and  $10.53$  respectively, within the optimal range of  $-100$  to  $0 \text{ J kg}^{-1}$ .

### 3.4.5 Advantages and disadvantages of the heat dissipation sensor

The advantages of the heat dissipation sensor outweigh the disadvantages.

Advantages include:

- a matric potential range of  $-10000$  to  $-10 \text{ J kg}^{-1}$  (Campbell *et al.*, undated), and an accurate operating range of  $-500$  to  $-10 \text{ J kg}^{-1}$  according to Scanlon *et al.* (1999),  $-1200$  to  $-10 \text{ J kg}^{-1}$  according to Reece (1996) and  $-1500$  to  $0 \text{ J kg}^{-1}$  according to Phene *et al.* (1971),
- long-term use of the sensor (Phene *et al.*, 1971),
- reliability in sensor outputs (Phene *et al.*, 1971),
- independency of sensor to salinity (Phene *et al.*, 1971; Jovanovic and Annandale, 1997),
- estimated temperature and matric potential (Phene *et al.*, 1971)
- ease of construction of sensor (Phene *et al.*, 1971),
- moderate cost of sensor (Phene *et al.*, 1971),
- simplicity of sensor (Phene *et al.*, 1971),
- possible linear relationship between  $\Psi_m$  and  $T - T_o$  for the  $\Psi_m$  range  $-1500$  to  $0 \text{ J kg}^{-1}$  (Phene *et al.*, 1971), and
- a single calibration curve for sensors through normalising for thermal conductivity (Reece, 1996).

Disadvantages of the sensor include:

- a decrease in the accuracy of matric potential beyond the  $-100$  to  $0 \text{ J kg}^{-1}$  range, especially when applying an exponential function (Jovanovic and Annandale, 1997),



- a smaller sensitivity to decreasing matric potentials less than  $-500$  to  $-10 \text{ J kg}^{-1}$  resulting in predicted soil water potentials greater than actual potentials (Scanlon *et al.*, 1999) as suggested by Reece (1996) and Jovanovic and Annandale (1997) for soil water potentials below  $-1200 \text{ J kg}^{-1}$  and
- a slight over-prediction of matric potential for range  $-1200$  to  $-400 \text{ J kg}^{-1}$  when compared to soil water potentials measured with thermocouple psychrometers (Reece, 1996),
- large power requirements for frequent measurements (SOWACS, undated),
- required initial equilibrium time in soil before measurements,
- required measurement separation time, to allow heat from previous pulse to dissipate before next measurement,
- cracking of the sensor ceramic installed in swelling and shrinking soils, and
- required contact between soil and sensor.

### **3.5 Thermocouple psychrometric technique**

The free energy difference between soil water and pure water per unit volume of water determines the soil water potential. Water moves from higher to lower potential areas and requires energy. The larger the difference in the water potential between two points, the more energy will be exchanged whilst moving the water. Thermocouple psychrometers measure the total soil water potential based on the energy exchange that result from the water potential differences. The thermocouple psychrometric technique is a highly specialised technique and requires instruments of extreme accuracy (Brown and Oosterhuis, 1992; Jovanovic and Annandale, 1997; Wescor Inc., 1998).

#### **3.5.1 A description of the thermocouple psychrometry technique**

Soil psychrometers or hygrometers measure the total water potential of a soil. This measurement is based on energy exchange to move water reversibly and isothermally from the soil under consideration to a reference state. The soil psychrometer or hygrometer measures the relative humidity of a soil air sample that has equilibrated with the soil. The water potential ( $\psi$ , in Pa) of a soil is related to the relative humidity through the Kelvin equation:

$$\psi = \frac{RT}{V_w} \ln e/e_0 \quad 3.13$$

where  $R$  is the universal gas constant ( $8.3123 \text{ J mol}^{-1} \text{ K}^{-1}$ ),  $T$  the absolute temperature in K,  $e/e_0$  the fractional relative humidity, and  $V_w$  the partial molar volume of water ( $18 \times 10^{-6} \text{ m}^3 \text{ mol}^{-1}$ ) (Savage *et al.*, 1981; Wescor Inc., 1998).

Soil psychrometers or hygrometers employ one of two methods (SOWACS, undated; Wescor Inc., 1998):

- psychrometry through the wet bulb technique, or
- hygrometry through the dewpoint technique.

Of these, Baughn (1974) (cited by Savage *et al.*, 1981) noted that psychrometry (wet bulb) is more popular than hygrometry (dewpoint). The dewpoint hygrometer is less sensitive to temperature changes and gradients than wet bulb psychrometer (Savage *et al.*, 1981). The hygrometer is also much more sensitive to voltage changes than the psychrometer ( $-7.0 \times 10^{-3} \mu\text{V kPa}^{-1}$  vs  $3.7 \times 10^{-3} \mu\text{V kPa}^{-1}$  at  $25^\circ\text{C}$ ). However, the accuracy of the hygrometer is highly dependent on the correct dewpoint cooling coefficient, especially at temperatures of less than about  $15^\circ\text{C}$  (Savage *et al.*, 1981).

In the *psychrometric* method, the total soil water potential is related to the wet bulb depression temperature of the thermocouple junction minus the ambient temperature. Peltier cooling (with a current of between about 5 and 8 mA) is used to cool the thermocouple below the dewpoint. Different cooling times can be used ranging between 60 s under dry conditions and 15 s under wet conditions. During this process very small droplets of water are condensed on the thermocouple junction surface. These small droplets are allowed to evaporate, and this evaporation process (cooling or release of latent heat) causes the temperature of the thermocouple junction to be reduced below the ambient temperature. The wet bulb depression continues until all the small water droplets have been evaporated. After this, the thermocouple junction temperature returns to ambient or the block temperature (Wescor Inc., 1998). Any temperature difference ( $\Delta T$ ), between the ambient temperature ( $T_b$ ) and the thermocouple junction

surface temperature ( $T_j$ ), results in a voltage ( $V$ ) as given by the Seebeck effect (Savage *et al.*, 1981)

$$V = S(T_b - T_j) \quad 3.14$$

where  $S$  is Seebeck coefficient in  $\mu\text{V } ^\circ\text{C}^{-1}$  ( $S = 58.62 + 0.09 T$  for psychrometer temperatures  $T$  between 0 and 50  $^\circ\text{C}$ ).<sup>1</sup>

When evaporation eases, the voltage corresponding to the wet bulb temperature (or endpoint) is measured. After evaporation, the voltages decrease rapidly, or slow or stop at a plateau, and then decrease further to a reference voltage level. For high water potentials or long Peltier cooling times, the plateau is horizontal. However, for low water potentials (dry samples) or short cooling periods, the endpoint is less clear and can be quite subjective (Savage and Wiebe, 1987).

However, in the *hygrometric* method the total soil water potential is related to the dewpoint depression. In this method too, the thermocouple is cooled below the dewpoint. Here the thermocouple temperature is controlled by the heat of the condensing water. The thermocouple temperature converges to the dewpoint and remains there with a static amount of water (Wescor Inc., 1998). Therefore, if a wet thermocouple junction is held at dewpoint temperature, water will not be lost (through evaporation) or gained (by condensation) (Savage *et al.*, 1981). This technique is found to be relatively unrelated to the wetting characteristics of the thermocouple junction and the size and shape of the water droplets formed on the junction (Neumann and Thurtell, 1972 cited by Savage and Cass, 1984).

### 3.5.2 A description of the thermocouple psychrometer

The thermocouple psychrometer and dewpoint hygrometer sensors use identical sensors, but with different voltmeter circuitry (Savage *et al.*, 1981).

---

<sup>1</sup> 1  $\mu\text{V}$  is equivalent to approximately -250 kPa at 25  $^\circ\text{C}$ .

The thermocouple psychrometer sensing head has a lead wire running through it and consists of two copper wires, and one constantan wire. The electrical circuit has a chromel-constantan thermocouple junction. This sensing wire pair is attached to the copper lead wires to form two reference junctions, a copper-chromel and a copper-constantan junction. The reference junctions are normally at the end of the two copper wires (lead-wire) and extend from the sensing body to the datalogger measuring the micro-voltage output. The additional copper wire provides a measure of temperature at the copper constantan junction. The protective cover covers the sensing head up to the lead wire (Brown and Oosterhuis, 1992).

The material of which the thermocouple psychrometer sensing head is made should not absorb large quantities of water. The porous material (screen cage), covering the sensing head should protect the sensor from contamination with soil particles, and provide for an effective path for equilibration between the sensor and the soil. The diffusion resistance of the mesh covering the sensor will affect the response time of the hygrometer. This resistance can be increased where poor contact exists between the soil and the psychrometer (Merrill and Rawlings, 1972 cited by SOWACS, undated).

### **3.5.3 Accuracy of the thermocouple psychrometer**

Thermocouple psychrometers are generally regarded as very accurate and consistent instruments. These sensors are, however, temperature sensitive and require great care to ensure accurate and routine measurements (Brown and Oosterhuis, 1992; Jovanovic and Annandale, 1997).

The accuracy of the water potentials measured with the thermocouple psychrometric technique depends on the extent to which the operational theory is understood and the sensors are calibrated and cleaned (Brown and Oosterhuis, 1992). In addition to this, the accuracy of the technique is also dependent on water vapour pressure equilibrium between the sensor and soil prior to the measurement, data interpretation, and detection and correction for temperature gradients (Brown and Oosterhuis, 1992).

### 3.5.3.1 Accuracy of *in situ* measurements of soil water potential with thermocouple psychrometer

The accuracy of *in situ* soil water potential measurements with the thermocouple psychrometer can be improved by the correct or optimal measurement times, field installation, choice of construction material and thermocouple junction, and hygrometer shape and size (SOWACS, undated).

Firstly, the soil water potential should be measured at the time of day when the soil heat flux density is close to zero or the net irradiance flux density is very small, e.g. at sunrise or sunset (Wiebe and Brown, 1979 cited by SOWACS, undated). At these times, the zero offsets will be comparatively small.

Secondly, the psychrometer or hygrometer should be installed horizontally into the soil as this will reduce the effect of the temperature gradients. Care should be taken to disturb the soil as little as possible. The lead wire should also be buried close to the sensor (Merrill and Rawlins, 1972 cited by SOWACS, undated).

Thirdly, a hygrometer should be constructed of low-conductivity material for the body, with a cylindrical stainless steel mesh to detect quick changes in the soil water potential (Campbell, 1972 cited by SOWACS, undated and Wiebe *et al.*, 1977). The hygrometer should have a single thermocouple junction to allow temperature measurement along the sensor, and should be constructed of fine wire. The hygrometer should be small (Wiebe and Brown, 1979 cited on SOWACS, undated) and the shape of the hygrometers should be concentric with the thermocouple sensor placed centrally in the chamber (Rawlins and Dalton, 1967; Campbell, 1972 and Wiebe *et al.*, 1977).

Lastly, following the installation of the sensor, it is advisable to wait a day or more before performing soil water potential measurements. This will allow the soil to return to thermal and water potential equilibrium, and to reach equilibrium with the sensor (Lawrence Berkeley National Laboratory, 2000).

### 3.5.3.2 Sensitivity of soil water potential measurements to temperature

The measured voltage-soil water potential relationship, through either the dewpoint (hygrometric) or wet bulb (psychrometric) methods is sensitive to temperature. However, if used correctly, the dewpoint hygrometer needs no temperature correction (Savage *et al.*, 1981; Savage and Cass, 1984). The wet bulb method (psychrometers) is highly dependent on temperature and all measurements (calibration or *in situ*) need to be corrected for the temperature according to Wiebe *et al.* (1977):

$$V_{25} = \frac{V}{a + bT} \quad 3.15$$

where  $V$  is the output voltage in  $\mu\text{V}$ , and  $V_{25}$  the voltage output ( $\mu\text{V}$ ) after correcting for 25 °C,  $T$  is psychrometer block temperature (°C) at which the reading was made, and  $a$  and  $b$  empirical constants determined during sensor calibration (P55 series psychrometers notes, undated; Savage *et al.*, 1981). For example, Brown (1970) (cited by Savage *et al.*, 1981) determined  $a$  and  $b$  to be 0.325 and 0.027 °C<sup>-1</sup> respectively. Savage and Cass (1984) reviewed psychrometer and hygrometer calibration data and the calculated  $a$  and  $b$  values for a number of leaf and soil psychrometers. From the differing  $a$  and  $b$  values found by different authors, it is clear that each sensor possesses a unique set of  $a$  and  $b$  values. Any of these sets ( $a$  and  $b$ ) will therefore not directly apply to all psychrometers.

### 3.5.3.3 Sensitivity of soil water potential measurements to temperature gradients

The derivation of the Kelvin equation (Eq. 3.13) assumes iso-thermality (Rawlins and Dalton, 1967 cited by Savage and Cass, 1984). The test for this is the measurement of the zero offset. This measurement involves measuring the thermojunction voltage when the psychrometer lead wires are shorted, corresponding to a base-line and then measuring the voltage with the lead wires not shorted just prior to cooling (Savage *et al.*, 1983). The difference between this voltage relative to the base-line, is a measure of the iso-thermality of the system.

### 3.5.4 Advantages and disadvantages of the thermocouple psychrometer

One major disadvantage of the soil psychrometer is the possibility of condensation or the drying of soil water in the area surrounding the sensor, or where temperature gradients exist. This will lead to either over- or under-estimations of water potentials (Savage and Cass, 1984).

Advantages of the thermocouple psychrometer include:

- measurements over a wide range of matric potentials (Zazueta and Xin, undated),
- low maintenance (Zazueta and Xin, undated),
- suitability for automatic measurements,
- soil water potential measurements obtained rather than soil water content measurement (SOWACS, undated),
- independency of calibration to soil type or particle sizes (SOWACS, undated),
- accuracy of measurements of soil water potential within the range -500 to -90 J kg<sup>-1</sup> (Reece, 1996).

Disadvantages of the thermocouple psychrometer include:

- high contact resistance and measurement error in swelling and shrinking soils if the soil draws away from the hygrometer (Merrill and Rawlins, 1972 cited by SOWACS, undated), where direct contact is not necessary but will accelerate the equilibration process (Lawrence Berkeley National Laboratory, 2000)
- inability of *in situ* calibration of soil psychrometers (SOWACS, undated) if individual psychrometers calibration is required (Zazueta and Xin, undated; Savage *et al.*, 1981),
- sensitivity to large and continual temperature gradients, especially in the wet bulb mode (SOWACS, undated; Zazueta and Xin, undated),
- dependency of the measurement accuracy to the similarity between the calibration and field conditions; therefore field measurements are only as accurate as their calibration demonstrates (Savage and Cass, 1984),
- the small soil volume sensed (SOWACS, undated),
- same cooling times required for both field measurements and calibration (Savage and Cass, 1984),

- time consuming data analysis, and
- required specialised equipment for excitation and measurements (SOWACS, undated).

### **3.6 Summary**

*Chapter 3* concludes the discussion of the techniques used in the short-term, site-specific field experiment. The following chapter (*Chapter 4*) describes the theory behind the Soil Water Atmosphere Plant model applied in the long-term soil water balance modelling.



## CHAPTER 4

### THE SOIL WATER ATMOSPHERE PLANT (SWAP) MODEL

#### 4.1 Introduction

SWAP, the Soil Water Atmosphere Plant model, simulates the hydrological processes at a field scale (Fig. 4.1). The water flow and solute transport processes in the vadoze zone are influenced by plant growth during the season. Van Dam *et al.* (1997) and Van Dam (2000) describe the processes applied in SWAP in detail. These processes include: soil water flow, solute transport, soil heat flow, daily evapotranspiration, crop growth, field irrigation and drainage, surface water and multilevel drainage at a sub-regional scale and discharge in a regional system.

The processes used in our simulations (soil water flow, daily evapotranspiration and crop growth) will be described briefly.

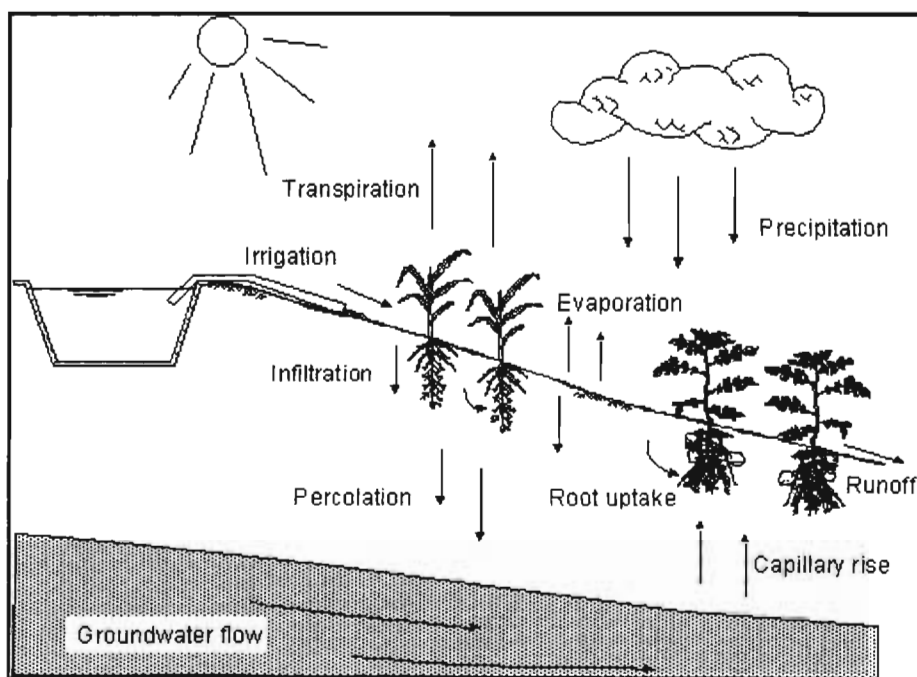


Fig. 4.1 Hydrological processes used in the simulations with the Soil Water Atmosphere Plant (SWAP) model (SWAP, undated)

## 4.2 A description of the most important processes applied in SWAP

### 4.2.1 Soil water flow

Soil water flows as a result of differences in pressure heads ( $h$ ) within the soil. The one dimensional flow of soil water in the vertical direction can be described by Darcy's equation:

$$q = -K(h) \frac{\partial(h+z)}{\partial z} \quad 4.1$$

where  $q$  is the soil water flux density ( $\text{mm d}^{-1}$ ),  $K(h)$  the hydraulic conductivity ( $\text{mm d}^{-1}$ ) which is dependent on soil water pressure head  $h$  (mm), and  $z$  the vertical coordinate (mm).

Darcy's equation is subsequently combined with the continuity equation for soil water:

$$\frac{\partial \theta_v}{\partial t} = -\frac{\partial q}{\partial z} - S_a(z) \quad 4.2$$

where  $\theta_v$  is the volumetric soil water content ( $\text{mm}^3 \text{mm}^{-3}$ ),  $t$  is the time (d) and  $S_a$  is the actual soil water extraction rate by plant roots ( $\text{mm}^3 \text{mm}^{-3} \text{d}^{-1}$ ). Invoking the chain rule of calculus we have:

$$\frac{\partial \theta_v}{\partial t} = \frac{\partial \theta_v}{\partial h} \frac{\partial h}{\partial t}$$

and combining equations 4.1 and 4.2, yields:

$$\frac{\partial \theta_v}{\partial t} = C(h) \frac{\partial h}{\partial t} = \frac{\partial \left[ K(h) \left( \frac{\partial h}{\partial z} + 1 \right) \right]}{\partial z} - S_a(z) \quad 4.3$$

<sup>2</sup> The outputs by the SWAP model in  $\text{cm d}^{-1}$  were converted to  $\text{mm d}^{-1}$ .

where  $C$  is the differential soil water capacity ( $d\theta/dh$ ) ( $\text{mm}^{-1}$ ). Eq. 4.3 is Richards' equation, which simulates vertical soil water movement in the soil profile using soil hydraulic functions.

## 4.2.2 Daily evapotranspiration

### 4.2.2.1 Introduction

SWAP uses a two-step approach to estimate potential evapotranspiration. Firstly, the potential evapotranspiration<sup>3</sup> is estimated with the Penman-Monteith equation for a daily time step:

$$ET_p = \frac{10^{-4} \Delta (R_n - G)}{\lambda_w (\Delta_v + \gamma_{air}^*)} + \frac{8.64 \times 10^6 \rho_{air} C_{air} (e_{sat} - e_{act})}{\lambda_w (\Delta_v + \gamma_{air}^*) r_{air}} \quad 4.4$$

$$= ET_{rad} + ET_{aero}$$

where  $ET_{rad}$  and  $ET_{aero}$  refer to the radiation and aerodynamic terms of the Penman-Monteith equation and is also described in Section 2.5.

Secondly, the actual evapotranspiration is calculated and includes the reduction of the rootwater uptake due to water and salt stress.

#### 4.2.2.2 Potential transpiration of a fully covered soil and the potential evaporation of a bare soil

SWAP uses the Penman-Monteith equation to calculate the:

- potential evapotranspiration of a wet canopy completely covering the soil ( $ET_{w0}$ ),
  - potential evapotranspiration of a dry canopy completely covering the soil ( $ET_{p0}$ ),
- and

<sup>3</sup>The Penman-Monteith evapotranspiration refers to the evapotranspiration from a dry, extensive, uniform canopy, optimally supplied by water as defined by Allen *et al.* (1998) and in section 2.2.5.

- potential evaporation of a wet bare soil ( $E_{p0}$ ).

SWAP also allows for the calculation of reference potential evapotranspiration ( $ET_{ref}$ ) using methods other than the Penman-Monteith method. This reference evapotranspiration is converted into potential evapotranspiration of a dry canopy using a canopy factor ( $k_c$ ):

$$ET_{p0} = k_c ET_{ref} \quad 4.5$$

Here, however, SWAP equates the potential evapotranspiration for a dry crop, wet crop or wet soil. SWAP assumes that the potential evapotranspiration of a wet ( $ET_{w0}$ ) and a dry ( $ET_{p0}$ ) canopy completely covering the soil is equal, and that the potential evaporation of a wet, bare soil ( $E_{p0}$ ) is equal to the potential evapotranspiration of a dry canopy completely covering the soil.

#### 4.2.2.3 Potential transpiration and evaporation of a partially covered soil

SWAP separates potential evapotranspiration into evaporation and transpiration, and uses a physically-based approach to estimate the reduction in the potential transpiration and the potential evaporation. The potential evapotranspiration is partitioned into evaporation and transpiration using either the leaf area index or the soil cover fraction as a function of the crop development stage.

The potential soil evaporation under a crop is calculated using the Penman-Monteith equation, neglecting the aerodynamic term (Eq. 4.4). Neglecting the soil heat flux density, and assuming an exponential decrease in net irradiance below the crop, this potential evaporation ( $E_p$ ) is given as a function of the leaf area index ( $LAI$ ) as used by Ritchie (1972):

$$E_p = ET_p e^{-k_g LAI} \quad 4.6$$

where  $-\kappa_{gr}$  is the product of the extinction coefficient of diffuse and direct visible irradiance, or alternatively  $E_p$  is given as a function of the soil cover fraction ( $SC$ ):

$$E_p = (1 - SC) ET_p \quad 4.7$$

The potential transpiration rate ( $T_p$ ) is given by:

$$T_p = ET_p \left( 1 - \frac{P_i}{ET_{po}} \right) - E_p \quad 4.8$$

where  $P_i$  is the rainfall interception by a canopy.

#### 4.2.2.4 Actual soil evaporation

The soil evaporation of a wet soil equals the potential soil evaporation ( $E_p$ ) and is determined by the atmospheric demand. For a drying soil, with a decreasing hydraulic conductivity, the potential soil evaporation is reduced to actual soil evaporation.

The actual soil evaporation is determined as the minimum of the potential soil evaporation ( $E_p$ ), the maximum evaporation according to Darcy's equation ( $E_{max}$ ), or the actual soil evaporation calculated using an empirical function ( $E_a$ ) of Black (1969) or Boesten and Stroosnijder (1986) (cited by Van Dam *et al.*, 1997).

#### 4.2.2.5 Actual plant transpiration

The maximum root water extraction rate over the rooting depth is equal to the potential transpiration rate ( $T_p$ ). The potential root water extraction rate  $S_p$  ( $d^{-1}$ ) at a certain soil depth  $z$  is:

$$S_p(z) = \frac{\pi_{root}(z)}{\int_{-Droot}^0 \pi_{root}(z) dz} T_p \quad 4.9$$

where  $\pi_{root}$  is the root length density ( $\text{m m}^{-3}$ ),  $Droot$  (mm) is the rooting depth, and where the potential transpiration rate  $T_p$  is reduced through stresses (water or salinity) to the actual root water flux density  $S_a(z)$  ( $\text{d}^{-1}$ ):

$$S_a(z) = \alpha_{rw} \alpha_{rs} S_p(z) \quad 4.10$$

where  $\alpha_{rw}$  is the reduction factor due to water stresses, and  $\alpha_{rs}$  is the reduction factor due to salinity stresses.

### 4.2.3 Crop growth

SWAP contains three crop growth routines: a detailed crop growth model (WOFOST), a detailed grass growth model (modified WOFOST) and a simple crop growth model.

The simple crop growth model is applied when crop growth simulations are not required, or when insufficient data exists. The simple model is based on a big leaf (green canopy), that intercepts rainfall, transpires and covers the ground. Inputs to this model include leaf area index or soil cover fraction, crop height, and rooting depth as a function of development stage. The development stage can be linear or a function of the air temperature sum.

This simple crop growth model can simulate up to three crops per year, and does not calculate the crop potential or actual yield.

### 4.2.4 Rainfall interception

SWAP utilizes a general formula for canopy interception proposed by Von Hoyningen-Hüne (1983) and Braden (1985) (cited by Van Dam *et al.*, 1997 and Van Dam, 2000).

This equation relates the intercepted precipitation  $P_i$  (mm), the leaf area index  $LAI$  ( $\text{m}^2 \text{m}^{-2}$ ), the gross precipitation  $P_{gross}$  (mm), an empirical coefficient  $a$  (mm) and the soil cover fraction  $SC$ :

$$P_i = a LAI \left( 1 - \frac{1}{1 + \frac{SC P_{gross}}{a LAI}} \right) \quad 4.11$$

#### 4.2.5 Bottom boundary condition

Whilst in the unsaturated zone, water flow occurs mainly in the vertical direction. However, in the saturated zone, water moves in a three-dimensional pattern, according to the hydraulic head gradients. The bottom boundary of the one-dimensional SWAP model is either the bottom of the unsaturated zone or the upper part of the saturated zone, and can be described by the:

- groundwater level or soil water pressure head as a function of time,
- specific bottom flux as a function of time, or
- bottom flux as a function of groundwater level (Van Dam *et al.*, 1997).

#### 4.3 Sensitivity of soil water balances modelled with SWAP to different input parameters

Wesseling *et al.* (1998) quantified the sensitivity of the SWAP model outputs to the changes in the process parameters for different scenarios. The results of the sensitivity analysis showed that 95 % of the variance of all the outputs could be explained by variance of the bottom flux. In general the influence of the crop factors used in the simulations and the preferential flow on the outputs were surprisingly low, whereas the upper and lower boundary layers were very important. The leaf area indices strongly determined the soil evaporation and crop transpiration whereas the lateral drainage was sensitive to the surface water levels. The effect of the secondary channels in the drainage systems is negligible compared with the influence of the primary channels. In terms of the soil water, the CPU time requirement for SWAP execution is insufficient to

complete simulations with low saturated hydraulic conductivities. The maximum groundwater level is strongly related to the surface water level, the minimum groundwater levels to the leaf area indices, soil physical properties and surface water levels, whereas the average groundwater level is strongly dependent on the primary drainage system.

Van Dam (2000) also performed a sensitivity analysis with SWAP but focussed on the relative transpiration<sup>4</sup> and relative salt storage changes<sup>5</sup>. Van Dam (2000) found that the relative transpiration and relative salt storage changes were less sensitive to a change in the rooting depth, than the crop factor. A 50 % reduction in the rooting depth caused the relative transpiration to change from 0.93 to 0.89 and relative salt storage to change from 0.14 to 0.10. However, a change in the crop factor of only 25 % increased the relative transpiration by 0.06, and changed the relative salt storage from 0.14 to -0.48. The effect of a 33 % and a 16 % decrease in the Boesten and Stroosnijder soil parameter and saturated soil water content respectively, lead to an increase of 0.02 and decrease of 0.02 in the relative transpiration respectively. Some of the conclusions by Van Dam (2000) were that accurate data on crop factors and soil hydraulic functions are needed for reliable water and salt balances, and that the stress due to water shortage is affecting plant growth more than stress due to high salinity. However, the results suggested that for the specific research area no accurate rooting depth data were required.

#### **4.4 Advantages and disadvantages of the SWAP model**

SWAP can be used for investigating a range of different conditions, from alternative flow and transport concepts, laboratory and field experimental analysis and evaluation of management options with respect to field scale water and solute movement (Van Dam, 2000). Applications of SWAP includes the fields of ecology, desalinisation, design of drainage systems, irrigation scheduling, hydrological base for nutrient and pesticide transport, estimation of crop yield, analysis of surface water management to

---

<sup>4</sup> The relative transpiration can be defined as the ratio of the cumulative actual crop transpiration to the cumulative potential crop transpiration.

<sup>5</sup> The relative salt storage change can be defined as the ratio of the change in salt storage of the soil profile over a certain time span to the initial salt storage of the soil profile.



determine soil water flow, evaporation, crop growth, drainage, heat transport and/or solute transport and more (Wesseling *et al.*, 1998; Van Dam, 2000).

Disadvantages of SWAP identified during this modelling exercise included the inability to model overlapping growing seasons, and simulate understorey evaporation. The model further requires the use of high speed computers and even then cannot perform simulations for soils with low saturated hydraulic conductivities.

#### **4.5 Application of techniques**

This chapter concludes the description of the theory on the techniques (*Chapters 2 and 3*) and model (*Chapter 4*) applied in the research to determine the impact of different vegetation types on the soil water balance. The following chapter describes the research sites and the application of the techniques and model discussed in *Chapters 2 to 4*, to the research sites. That is followed (*Chapters 6 to 8*) by a presentation of the results on the application of these techniques and model to a grassland and an *E. viminalis* site.

## CHAPTER 5

### MATERIALS AND METHODS

#### 5.1 Introduction

The soil water balance approach was used to test the hypothesis of the study: whether a change in vegetation, from grassland to *E. viminalis*, will increase the total evaporation and decreases the soil water storage. It is hypothesised that a change in vegetation from grassland to *E. viminalis* trees will reduce the drainage of water beyond the root-zone and into the mine workings, over the short- and long-term.

#### 5.2 Simplified soil water balance

The simplified soil water balance at a field scale is given by:

$$P = ET \pm \Delta S + Q + D \quad 5.1$$

where  $P$  is the precipitation,  $ET$  the evaporation (the sum of soil evaporation, transpiration and interception),  $\Delta S$  the change in the soil water storage,  $Q$  the runoff and  $D^6$  the drainage beyond the root-zone, all components having the unit mm.

The soil water balance equation (Eq. 5.1) can be re-arranged to solve for the drainage term:

$$D = P - ET \pm \Delta S - Q \quad 5.2$$

Assuming the precipitation<sup>7</sup> at two sites with different vegetation types is the same, the difference in the soil water movement below the root-zone ( $D$ ) at the two sites can be attributed to the differences in the total evaporation (or the components therefore), soil water storage and runoff. Therefore, on a surface with a gentle slope and negligible

<sup>6</sup> The drainage below the root-zone refers mainly to soil water movement below the root-zone due to gravity.

<sup>7</sup> The precipitation is assumed to be equal to the rainfall for the grassland and *E. viminalis* sites.

runoff, differences in the drainage beyond the root-zones of grassland and *E. viminalis* trees are assumed to be due to differences in the plant soil water relations (total evaporation, soil water storage).

$$D = -ET \pm \Delta S \quad 5.3$$

### 5.3 Conditions of site

#### 5.3.1 General

The site soil water balances of a grassland and of *E. viminalis* trees were studied within the Brandspruit Management Unit, Sasol Collieries, Secunda, South Africa (26° 36' S and 29° 08' E, 1650 m above mean sea level) (Fig. 5.1) for the period 1 July 1998 to 30 June 2000. The natural grassland and *E. viminalis* sites selected for the soil water balance field experiment were adjacent and in close proximity to exclude differences in local climate and soils.

#### 5.3.2 Climate

##### 5.3.2.1 Rainfall

Rainfall recorded during the field experiment (1110 mm and 1218 mm during 1998/1999 and 1999/2000 respectively) exceeded the long-term average rainfall (680.2 mm a<sup>-1</sup>) by 430 and 538 mm a<sup>-1</sup> respectively (Fig. 5.2). The rainfall during the years immediately prior to the study period (1995 to 1998) also exceeded the long-term rainfall by about 30 % (or 202 mm a<sup>-1</sup>). The study period (1998 to 2000) therefore falls within a wet period, and the soil water balance results should be seen in this context.

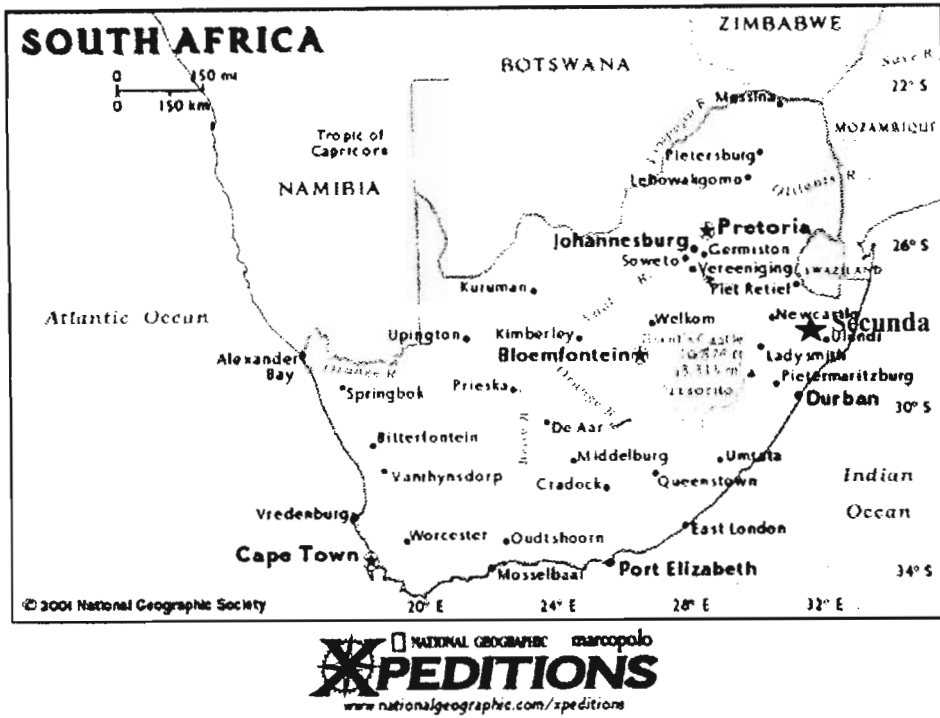


Fig. 5.1 Location of research site: Secunda, South Africa (National Geographic, undated)

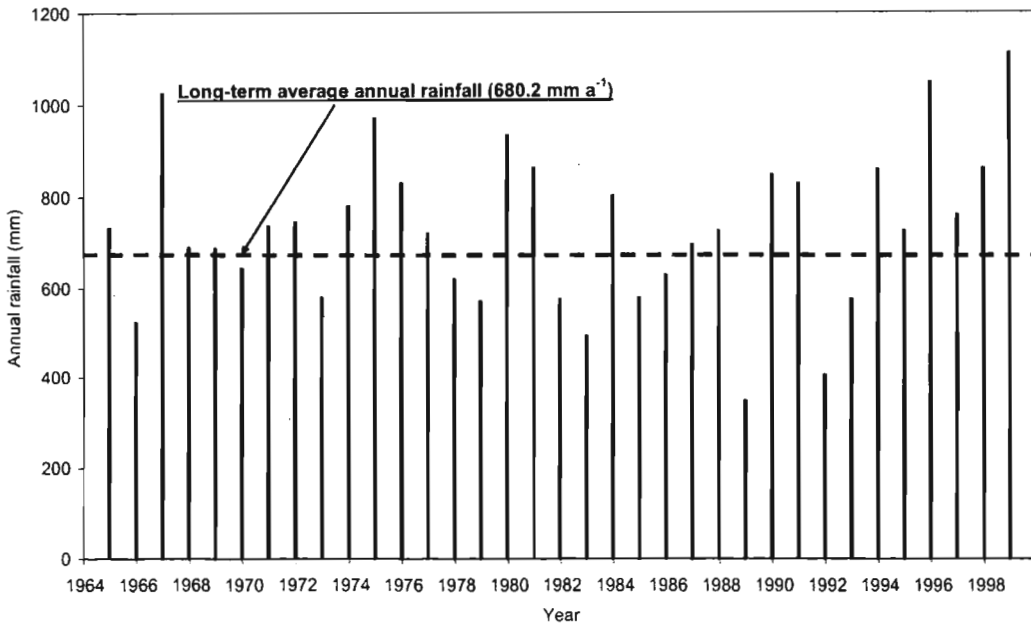


Fig. 5.2 “Annual” (July to June) total rainfall at Secunda for the period 1 July 1964 to 30 June 2000. The dotted-line represents the long-term average annual rainfall.

### 5.3.2.2 Reference evaporation

Daily total reference evaporation ( $ET_o$ )<sup>8</sup> was calculated with the Penman-Monteith equation. During 1998/1999  $ET_o$  was 1134 mm and exceeded the reference evaporation during 1999/2000 (1060 mm a<sup>-1</sup>) by 74 mm (6.5 %). The lower reference evaporation during 1999/2000 compared to 1998/1999, resulted from a higher rainfall (1218 vs 1110 mm a<sup>-1</sup>), lower average daily air temperature (10.9 vs 12.2 °C), and lower average daily solar radiant density (16.4 to 18.5 MJ m<sup>-2</sup>) during 1999/2000 (Fig. 5.3).

Monthly average daily reference evaporation ranged between 4.2 mm d<sup>-1</sup> during summer (e.g. November 1999) and 1.6 mm d<sup>-1</sup> during winter (e.g. June 2000) (Fig. 5.3). However, maximum daily reference evaporation of up to 6 mm d<sup>-1</sup> was estimated for summer, and a minimum reference evaporation of 1.4 mm d<sup>-1</sup> during winter.

### 5.3.3 Soil conditions

The soil forms identified at the research sites include the Arcadia (Vertic A-horizon overlaying Sandstone) and Rensburg (Vertic A-horizon overlying G-horizon overlaying weathering dolorite) soil forms (Soil Classification Working Group, 1991). A number of other soil forms also occur in the area. Du Toit (1993) studied the soil forms within the Brandspruit Management Unit and found ten different soil forms including the Rensburg and Arcadia forms.

The Rensburg and Arcadia soil forms consist of material with an expansive nature, which could potentially hamper root development, especially under extremely dry conditions when root pruning can occur. These soils exhibit shallow soil depths of 600 mm and 1500 mm for the Arcadia and Rensburg soil forms respectively. Due to high clay contents (up to 56 %) in some of the soils layers, these soils are generally prone to water logging during summer. Appendix A provides a detailed description of the Rensburg and Arcadia soil forms.

---

<sup>8</sup> Reference evaporation can be defined as the evaporation above a short, well watered grass surface that fully covers the soil, is not limited by water or nutrients, and is equivalent to class A-pan evaporation (Allen *et al.*, 1998).

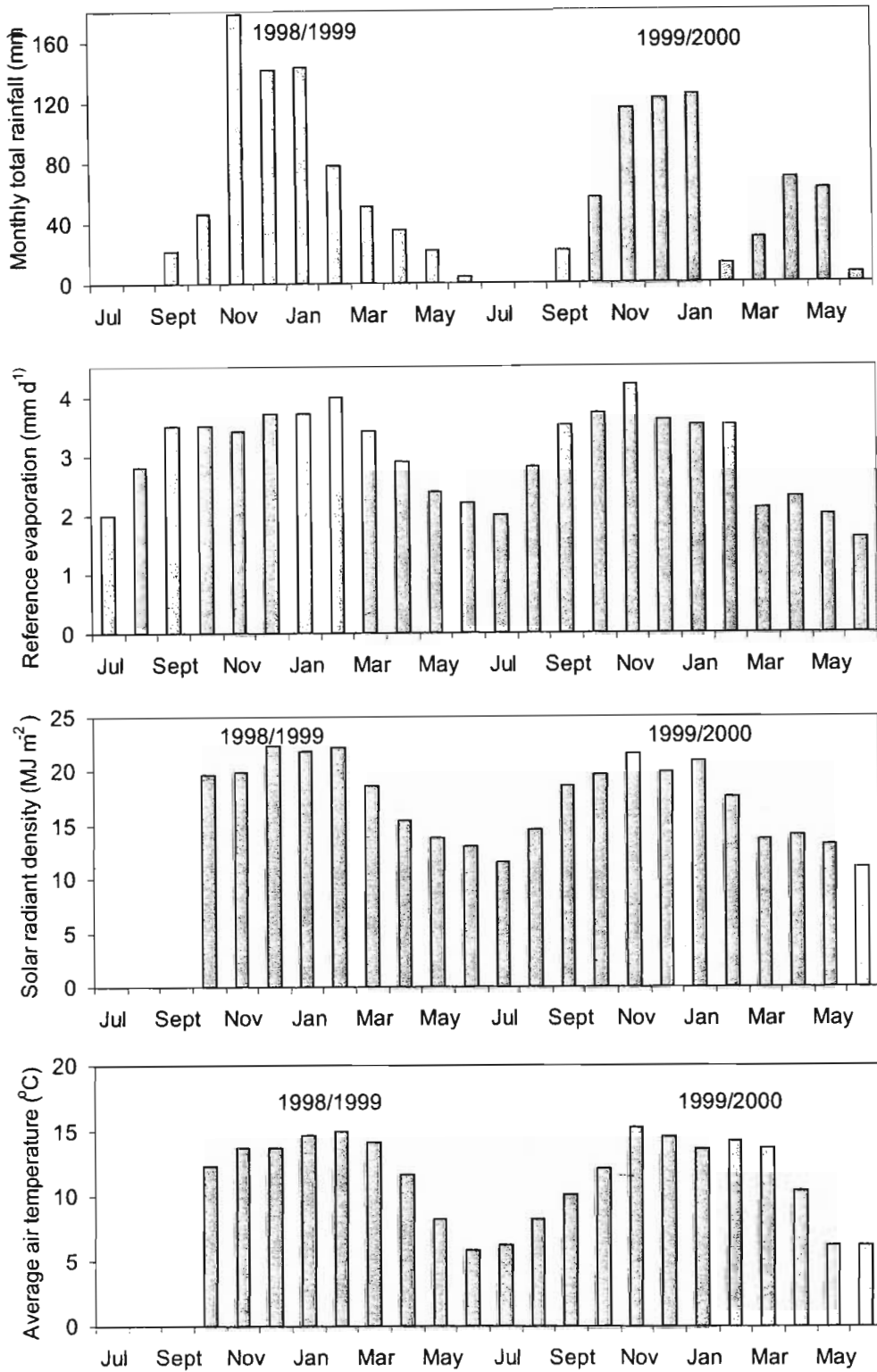


Fig. 5.3 From top to bottom: Summary of the monthly total rainfall, monthly average daily total reference evaporation calculated with the Penman-Monteith equation, monthly average air temperature and average daily radiant density for the period July 1998 to June 2000

### 5.3.4 Vegetation

The tree site consisted of *E. viminalis* trees with a grassland understorey. Blocks (area of 50 m<sup>2</sup>) of *E. viminalis* and other *Eucalyptus* species were planted in 1990 at Brandspruit Collieries, and were successfully established over some areas. The *E. viminalis* trees at the research site were planted at an espacement of 2 m x 3 m, but tree deaths have left some gaps. The *Eucalyptus* species planted and ideal soil preparation and espacement used was the result of extensive research on survival of different trees under non-ideal conditions (droughts, frost, swelling and shrinking soils) (Du Toit and Basson, 1993), and research of the optimum water use of different tree species under different espacements (Olbrich and Poulter, 1992; Versfeld *et al.*, 1998) and ideal soil preparations (Cunningham, 1995, 1996). The height and diameters (at breast height) of the trees at the start of the experiment ranged between 8 and 10 m and between 90 and 150 mm respectively.

The natural grassland site was generally dominated by *Cymbopogon* and *Eragrostis* species. However, towards the end of summer and during autumn 1999 and 2000, Cosmos weeds growing in-between these species were dominating. The site is not formally managed, but is frequently burnt by veld fires, as was the case during August 1999. The grassland canopy is uniform, with a fetch distance of 80 to 100 m in all directions. The canopy reached a height of at least 1000 mm during summer.

### 5.3.5 General

The field experiment was conducted over a period of two years (1 July 1998 until 30 June 2000). This period was divided into two 12-month periods: (i) 1 July 1998 to 30 June 1999 and (ii) 1 July 1999 to 30 June 2000, and are hereafter referred to as 1998/1999 and 1999/2000.

The components of the simplified soil water balance (Eq. 5.1) were estimated from *in situ* measurements (Table 5.1, Figs 5.4 to 5.8). These soil water balances will illustrate the potential impact of grassland and *E. viminalis* trees on the total evaporation and soil water storage relationship of a site.

Table 5.1 A summary of the measurements made and methods and equipment used to estimate different parameters required during the field experiment

<b>Parameter</b>	<b>Method</b>	<b>Measurements</b>	<b>Equipment</b>	<b>Manufacturer</b>
<b><u>Total evaporation</u></b> (Fig. 5.4)	Bowen ratio energy balance	Net irradiance	Net radiometer	Q*6, REBS, Seattle, USA
		Air temperature	Chromel-constantan thermocouples	N/a
		Water vapour pressure	Dew-10 hygrometer	N/a
		Soil temperature	Copper-constantan thermocouple	N/a
		Soil heat flux	Soil heat flux plates	N/a
		Output period	Water content reflectometer	Campbell Scientific CS615 probe
<b><u>Transpiration</u></b> (Figs 5.5 and 5.6)	Heat pulse velocity	Velocity of a heat pulses	Thermistors, Heaters	Custom made
<b><u>Soil water content</u></b> (Figs 5.4 and 5.5)	Water content reflectometer	Output period	Water content reflectometer model CS615	Campbell Scientific
<b><u>Soil water potential</u></b> (Figs 5.4 and 5.5)	Heat dissipation	Change in temperature	Heat dissipation sensor model 229-L	Campbell Scientific
	Soil psychrometry	Relative humidity	Soil psychrometer model PCT-55	Wescor
<b><u>Rainfall</u></b> (Fig. 5.8)	Automatic weather station	Rainfall	Tipping bucket	OSK Ogawa Seiki Co. Ltd.
<b><u>Other climatic</u></b> (Fig. 5.8)	Automatic weather station	Air temperature	Vaisala air temperature and humidity probe model CS500	Campbell Scientific
		Relative humidity		
		Solar irradiance	Pyranometer model LI-200	Li-Cor
		Wind speed	Three cup anemometer model 03001	RM Young
		Wind direction		
Barometric pressure	Barometric pressure sensor model CS105	Campbell Scientific		



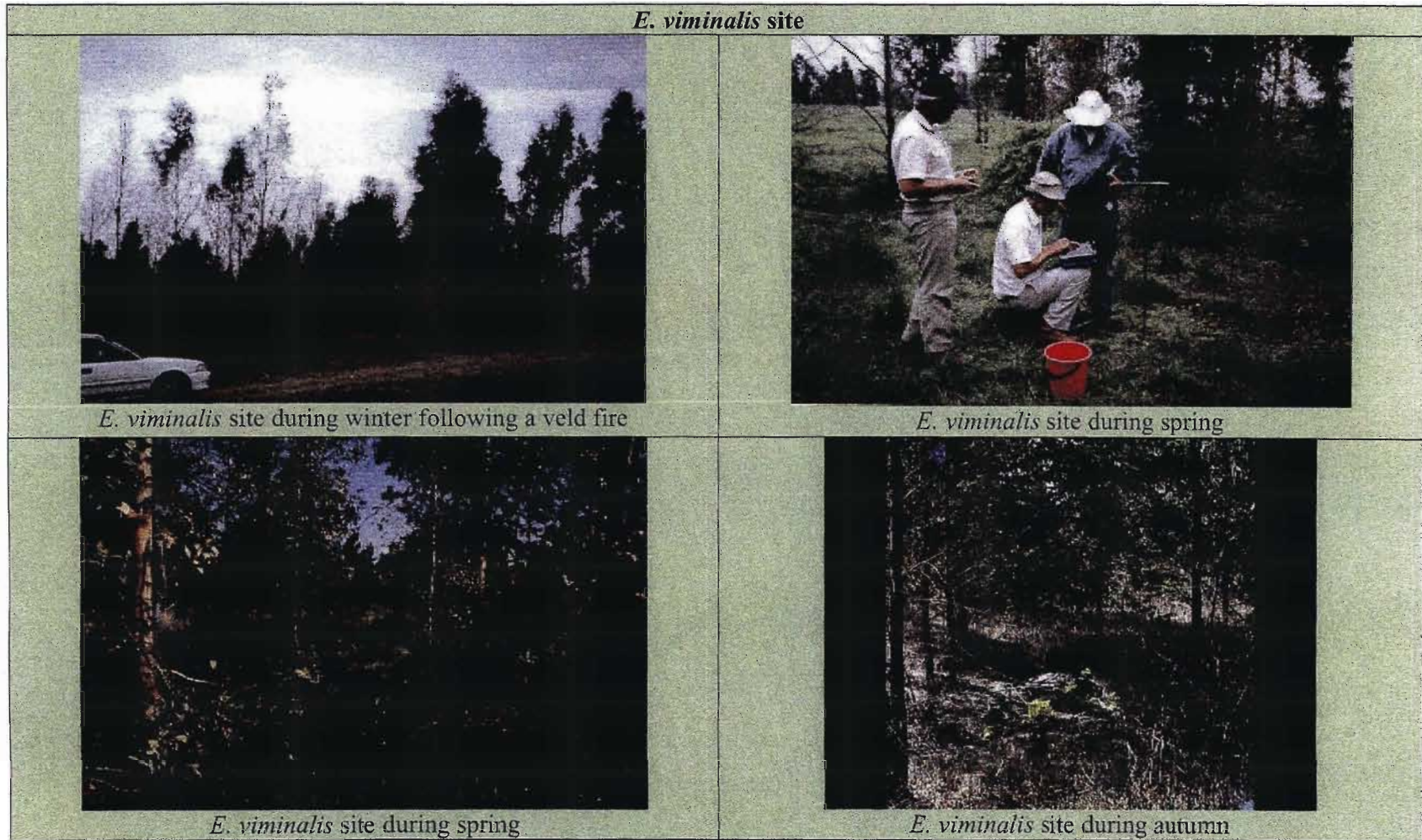


Fig. 5.4 (a) Images of the *E. viminalis* experimental site and instrumentation used

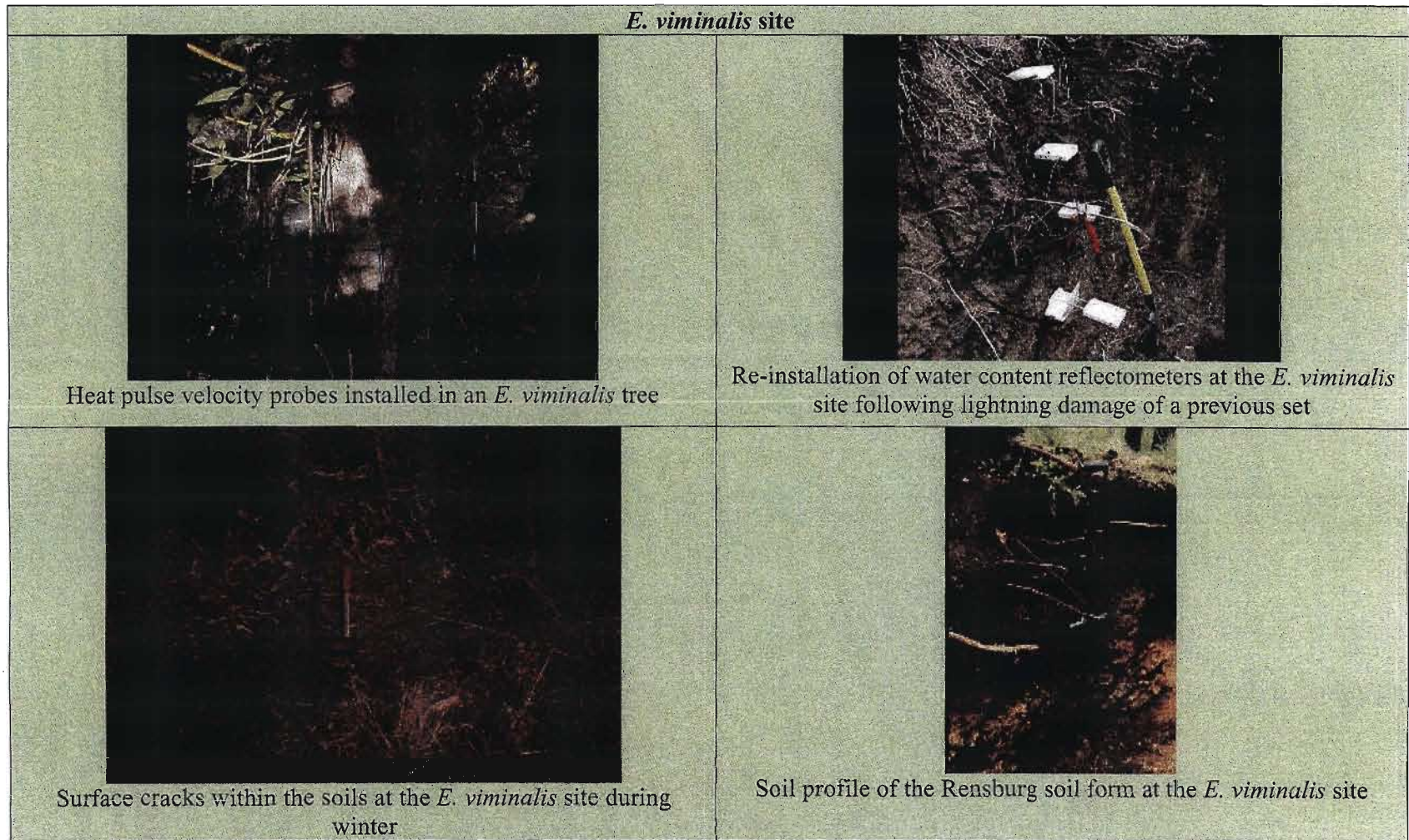


Fig. 5.4 (b) Images of the *E. viminalis* experimental site and instrumentation used

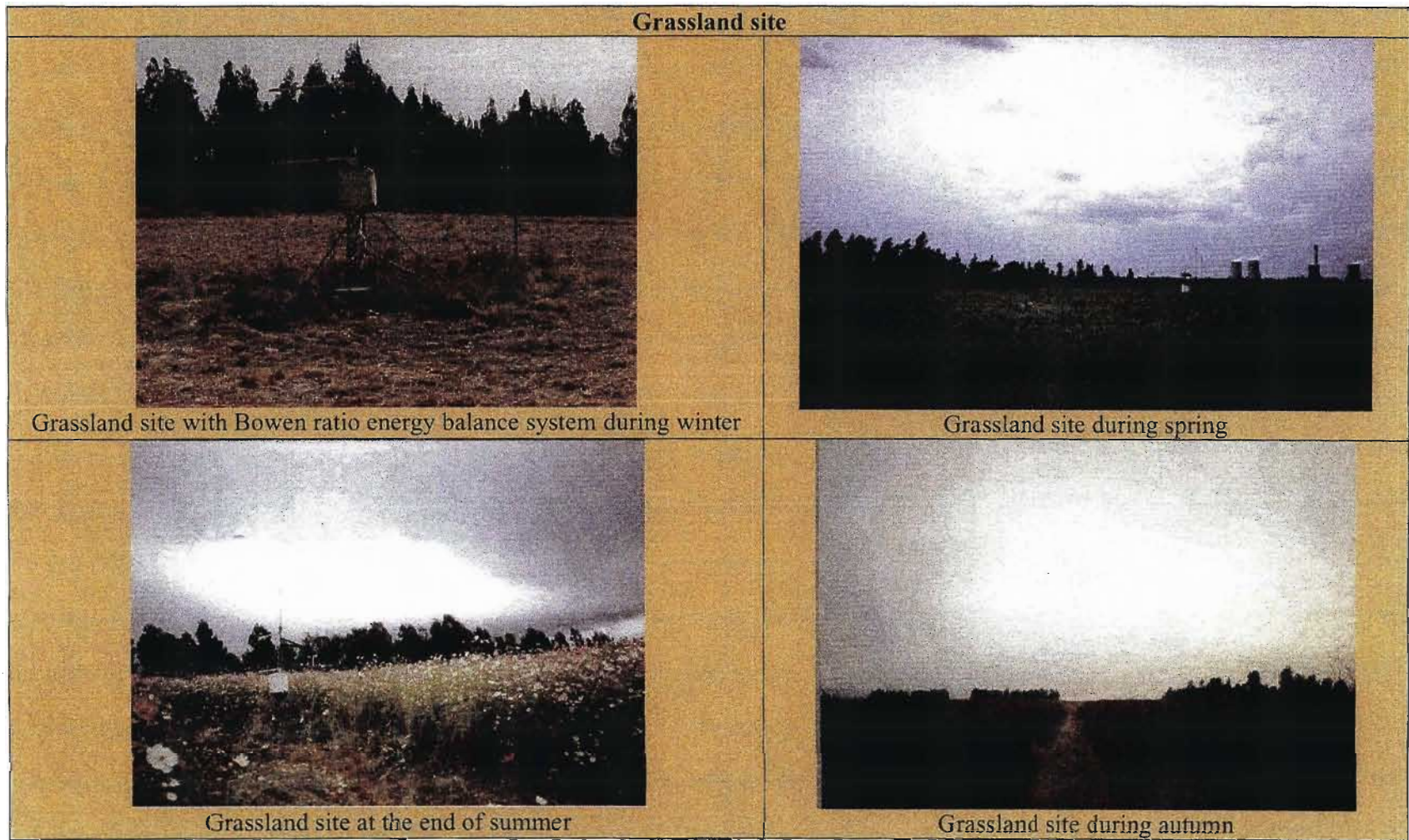


Fig. 5.5 (a) Images of the grassland experimental site and instrumentation used

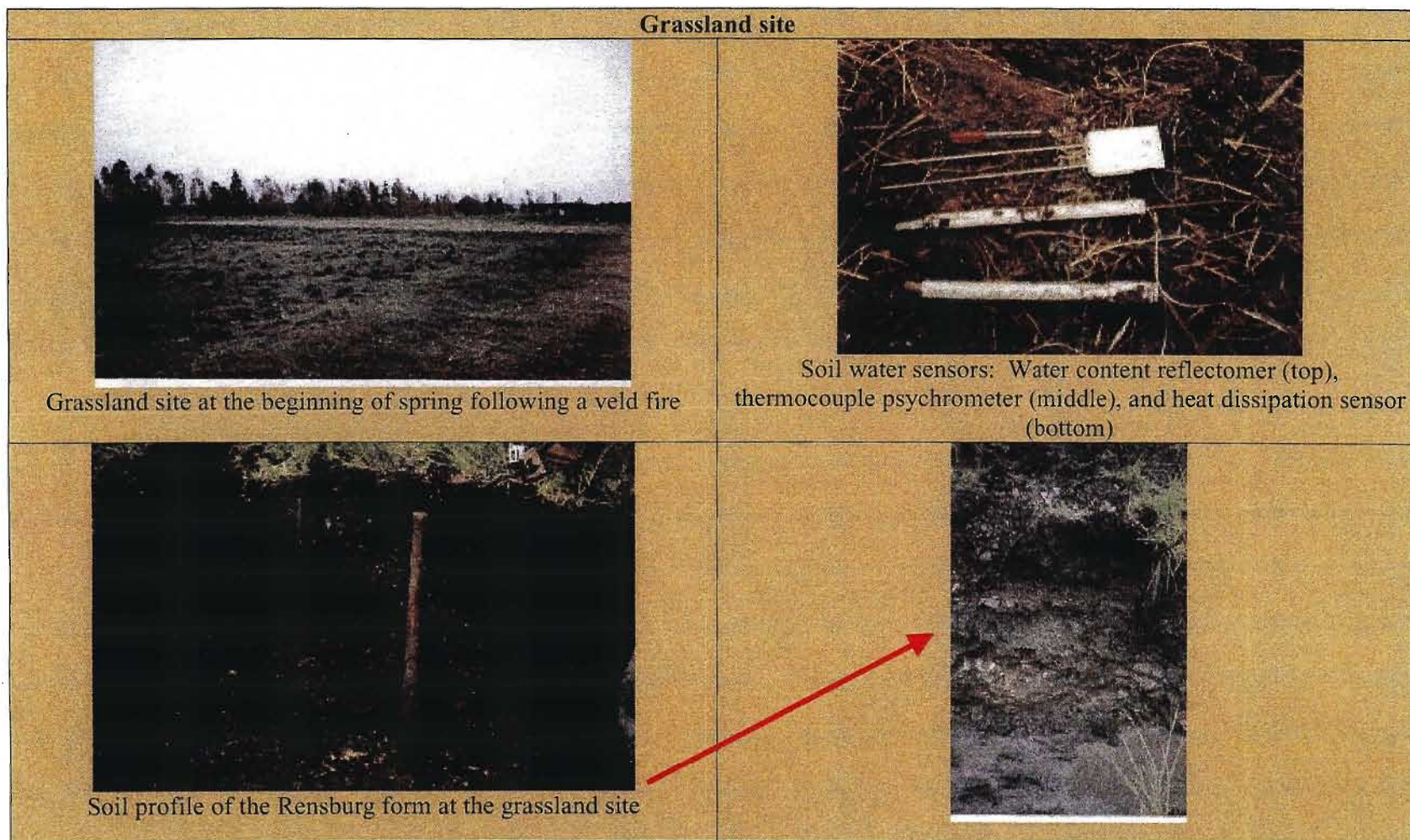


Fig. 5.5 (b) Images of the grassland experimental site and instrumentation used

### 5.3.6 Methods for estimating total evaporation and transpiration

#### 5.3.6.1 Method for estimating total evaporation<sup>9</sup>

The Bowen ratio energy balance technique (Campbell Scientific, Inc., Logan, USA) was used to estimate the total evaporation of grassland (Fig. 5.4). The Bowen ratio energy balance method requires measurements of net irradiance, air temperature and water vapour pressure vertical profile differences, soil heat flux density, soil temperature and soil water content. A Campbell Scientific CR23X datalogger was used to record the measurements. Measurement intervals were 1 s for the air temperature and water vapour pressure profile differences, and 10 s for the net irradiance, soil heat flux density, soil temperature and soil water content. Measurements were averaged at 20 minute intervals.

The Bowen ratio sampling arms and net radiometer (Q\*6, REBS, Seattle, USA) were mounted on a tripod and pole respectively. The sampling arms of the Bowen ratio energy balance system were orientated due north to avoid partial shading of the thermocouples on the arms, while the net radiometer was positioned north to prevent sensor shading. The air sensed by sensors mounted on these arms should be representative of the surface studied (Campbell Scientific, Inc., 1998). The lower arm should be installed low enough for the bulk crop surface environment not to be sensed, whereas the upper arm should be installed low enough in order to not sense a different environment upwind. The measurement of the air temperature and water vapour profile differences should be within the resolution of the sensors. A separation distance between the Bowen ratio sampling arms of 0.5 to 3 m is suggested in the Bowen ratio users' manual (Campbell Scientific Inc., 1998). With an increased distance between the arms, the water vapour pressure and air temperature differences are increased. A separation distance of at least 0.5 to 1 m between the sampling arms was therefore maintained throughout the experiment, with the height of the lower Bowen ratio arms at approximately 1 m above the vegetation (Fig. 5.5).

---

<sup>9</sup> Total evaporation (ET) can be defined as the total process of water movement into the atmosphere. In this experiment total evaporation refers to the sum of evaporation from the soil surface, transpiration by vegetation, and evaporation of water intercepted by vegetation (Rosenberg *et al.*, 1983).

The soil heat flux density at the surface was estimated using measurements of soil heat flux density, soil temperature and soil water content for the upper 80 mm soil depth. As the grassland surface was uniform, only two heat flux plates and four averaging thermocouples were used. As the groundcover did not vary considerably, it was not considered necessary to include additional sensors. The soil heat flux plates were installed at 80 mm below the soil surface, the averaging thermocouples were installed at 20 mm and 60 mm below the surface, and the soil water content reflectometer was installed at an angle over the upper 80 mm of the soil. Initially, the soil water content was estimated gravimetrically. Later, a water content reflectometer (Campbell Scientific CS615 probe) was used to estimate volumetric soil water content at 20 minute intervals.

#### 5.3.6.2 Method for determining transpiration<sup>10</sup>

The heat pulse velocity technique (Huber and Schmidt, 1937; Swanson, 1974 cited by Dye *et al.*, 1992) was used to calculate the transpiration (sapflux) of six representative trees within an *E. viminalis* tree stand. Four 12-channel heat pulse dataloggers (custom made) were used to measure the velocity at which a heat pulse moves through a tree stem at different depths below the cambium. Measurements were made at hourly intervals. Swanson (1983) found that radial differences in the sapflux occur, and suggested that sets of probes be implanted to different depths within the sapwood (e.g. d1 to d4) (Fig. 5.6) (cited by Olbrich, 1994). Four sets of probes (a set consisting of a heater probe and two thermistor probes) were therefore installed at different depths (9, 14, 21, 28 mm) below the cambium of each *E. viminalis* tree studied. This ensured that the variation in sapflux over the sapwood was covered and reflected in the tree transpiration estimated.

---

<sup>10</sup> Transpiration can be defined as evaporation of water that has passed through the plant. Transpiration therefore consists of vaporization of liquid water contained in the plant tissues and vapour removal to the atmosphere (Allen *et al.*, 1998).

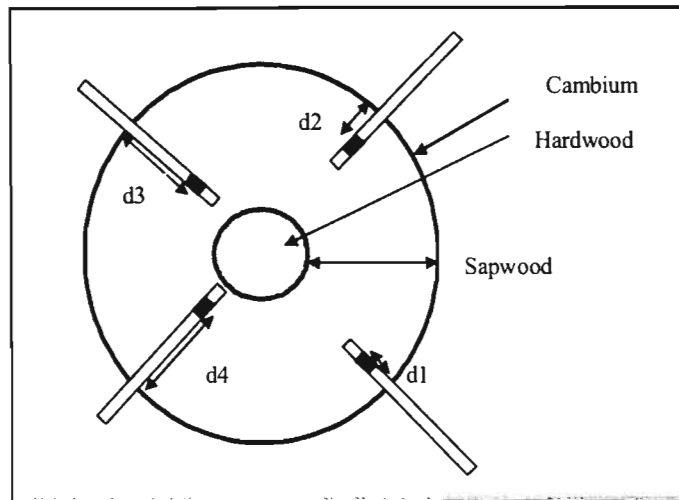


Fig. 5.6 Schematic of the implantation of sets of probes at different depths below the cambium (d1 to d4), into the stem of an *E. viminalis* tree

As the accuracy of the sapflux measurements and heat pulse velocity depends on the distance between the probes, a drill jig with three aligned holes was used to install the probes accurately and parallel to each other. The heater probe was installed in the centre hole, and the two thermistor probes were installed at 5 mm below and 10 mm above the heater probe (Fig. 5.4).

### 5.3.7 Methods for determining soil water content<sup>11</sup> and soil water potential<sup>12</sup>

Soil water content and soil water potential were estimated at different depths below the soil surface at both the grassland and the *E. viminalis* sites (Figs 5.4 and 5.5). The soil water content was estimated with Campbell Scientific model 615 water content reflectometers. The soil water potential was estimated with Campbell Scientific 229-L heat dissipation sensors and Wescor PCT-55 thermocouple psychrometers.

<sup>11</sup> Volumetric soil water content can be defined as the water content on a volume basis (Sumner, 2000).

<sup>12</sup> Soil water potential can be defined as the differences between the free energy per unit of volume of soil water and that of pure water in a reference state (Brady, 1990).

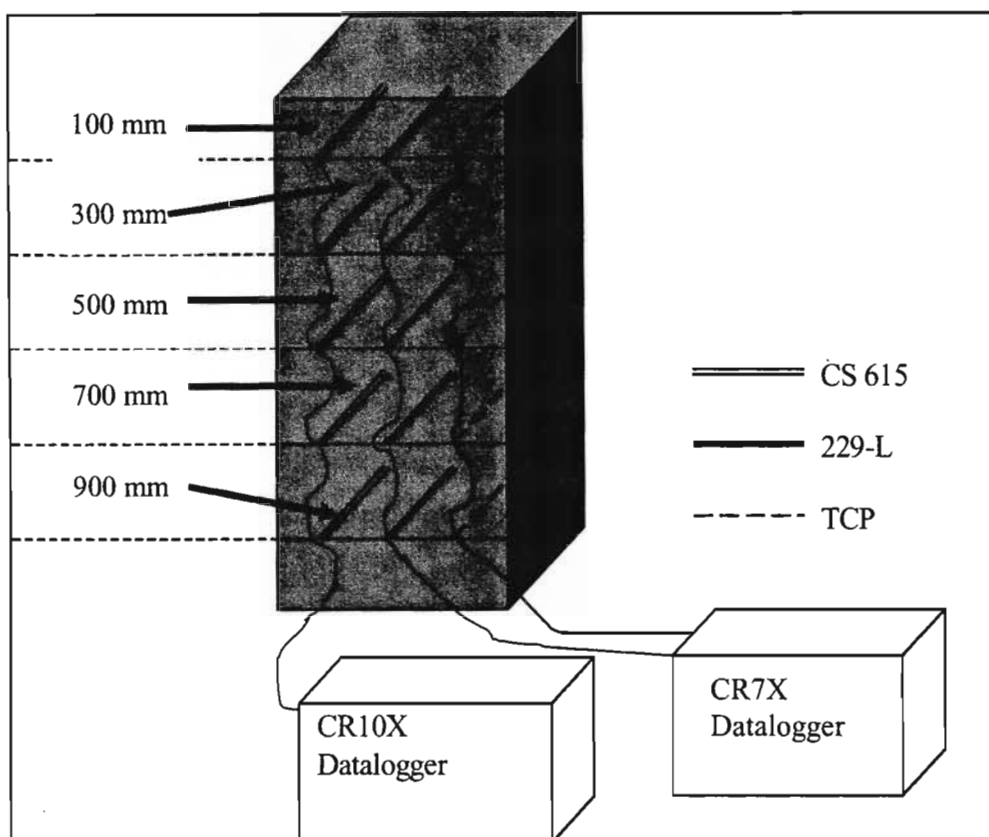


Fig. 5.7 Installation of soil water content reflectometers (CS615), heat dissipation sensors (229-L) and thermocouple psychrometers (TCP) into the soil at a grassland and an *E. viminalis* site, at 200-mm depth intervals

During May 1998, trenches were opened at the grassland and *E. viminalis* sites to a depth of between 0.5 and 1.2 m. Sets of sensors (a set of sensors consist of a water content reflectometer, a heat dissipation sensor and a thermocouple psychrometer) were subsequently installed at 200-mm depth intervals and up to 900 mm below the soil surface at each site (Fig. 5.7), with the first set installed at a soil depth of 100 mm. The sensors were installed horizontally into the soil and adjacent to each other, but approximately 150 mm apart. The trenches were then filled with the excavated soil. The additional lead wire was buried close to the sensors at a depth of approximately 500 mm, to prevent large temperature variations.

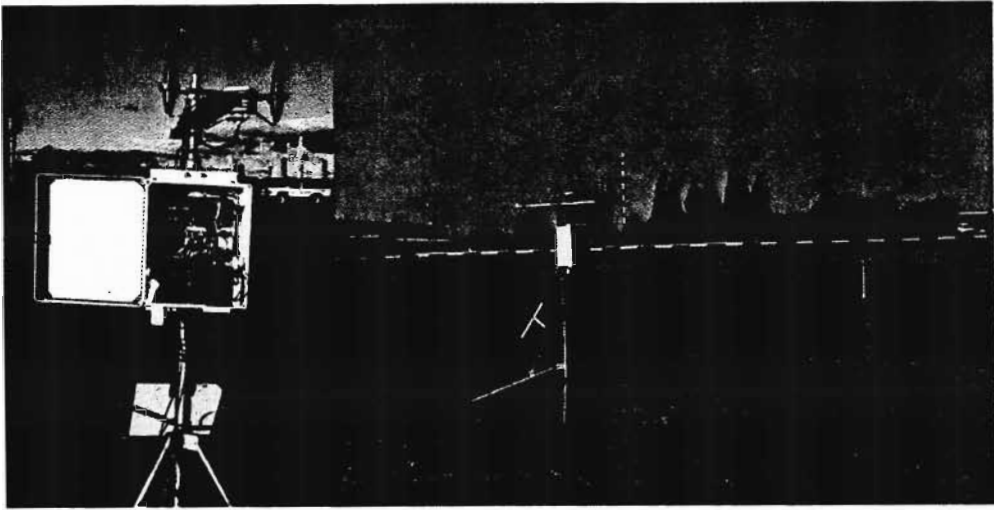


Five water content reflectometers per site were connected to a CR10X Campbell Scientific datalogger, and five thermocouple psychrometers and five heat dissipation sensors of each site were connected to a Campbell Scientific CR7X datalogger. Two different dataloggers were used as the sensors had different datalogging requirements. Measurements were made at four-hourly intervals. Measurements with the heat dissipation sensor involved a 20-s excitation with a constant current interface providing a consistent heating input whilst the temperature was collected at 1 s intervals during the heating. The temperature difference was calculated as the difference between the temperatures 1 s and 20 s after heating. During thermocouple psychrometer measurements, a cooling current of 5 mA at the thermocouple junction was maintained, using a cooling interface for 30 s under wet conditions and 60 s under dry conditions. Twenty nine wet bulb measurements were made over this period in addition to the measurement of the zero offset voltage and psychrometer block temperature (Savage *et al.*, 1981).

### 5.3.8 Estimating climatic conditions

Rainfall, solar irradiance, air temperature, relative humidity, wind speed, wind direction, and atmospheric pressure were measured from October 1998 to June 2000 above a short grass surface (Fig. 5.8). This site was situated approximately 5 km from the grassland and *E. viminalis* sites.

Rainfall was measured using a tipping bucket raingauge (Ota Keiki Seisakusho, OSK Ogawa Seiki Co. Ltd.) with a 0.2-mm resolution. The raingauge was installed at a height of 0.5 m above the soil surface. Solar irradiance was measured using a Li-Cor LI-200 pyranometer and the air temperature and relative humidity with a Vaisala CS500 temperature and humidity probe (Campbell Scientific, Inc., Logan, USA). The wind speed and the wind direction were measured with a three cup anemometer and a windvane (RM Young model 03001) and the atmospheric pressure with a barometric pressure sensor model CS105 (Campbell Scientific, Inc., Logan, USA). These sensors were installed at a height of 2 m above the grass surface.



---

Fig. 5.8 Images of the automatic weather station installed above a short, well watered grass surface approximately 5 km from the grassland and *E. viminalis* sites

---

## **5.4 Long-term soil water balance modelling**

### **5.4.1 General**

During the field experiment, components of the soil water balances of a grassland and of *E. viminalis* trees were measured. The two years studied represented above-average rainfall years. The results of this experiment are therefore very specific to the conditions encountered during these two years, and reflect the above-average rainfall conditions. The soil water balance simulations were therefore extended for another 30 years, through the simulation of the soil water balances to reflect the changes in climatic conditions and plant growth on the soil water balances.

### **5.4.2 Simulation of the soil water balances with the Soil Water Atmosphere Plant (SWAP) model**

The Soil Water Atmosphere Plant (SWAP) model (Van Dam *et al.*, 1997), a site soil water balance model was parameterised for a grassland and an *E. viminalis* site. The soil water balances were simulated from 1 July 1964 to 30 June 1994.

The soil water balance simulations for both the grassland and *E. viminalis* sites utilized the same long-term climatic information, and the same soil parameters. The required climatic information was obtained from long-term climatic data sets for the Bethal region, and by data generated with CLIMGEN (undated)<sup>13</sup>. The soil parameters required within SWAP for both sites were obtained from an analysis of the Rensburg soil form at the grassland site, and up to a depth of 1 m. The simple crop growth model was used because of limited crop growth information available for both the grassland and *E. viminalis* sites. The growth model within SWAP was parameterised for the grassland site so as to represent the growth conditions generally experienced within that area. The growth model for the *E. viminalis* site was however parameterised to represent an idealised, closed canopy for tree rotation years three to ten.

## 5.5 Summary

The design of the soil water balance experiment was presented in *Chapter 5*. The theory of the techniques used in the field experiment and mentioned in Section 5.4, were discussed in detail in *Chapters 2 and 3*. The underlying theory of the soil water balance model (Section 5.5) was discussed in *Chapter 4*.

The results of the application of the different techniques and the soil water balance model to the grassland and *E. viminalis* sites are presented in *Chapters 6 to 8*.

---

<sup>13</sup> CLIMGEN is a weather generator. CLIMGEN uses site specific information and different climatic data combinations to generate climatic data over a specified period. CLIMGEN also perform statistical analysis on the data generated to determine the significance of this data set (CLIMGEN, undated). Available from: <http://www.bsyse.wsu.edu/climgen>.

## CHAPTER 6

### SOIL WATER CONTENT AND TOTAL EVAPORATION ESTIMATED AT A GRASSLAND AND AN *E. VIMINALIS* SITE

#### 6.1 Introduction

The hypothesis of this study is that a change in vegetation, from grassland to *E. viminalis* trees, will potentially reduce the drainage of water beyond the root-zone over the short- and long-term. This reduction in drainage is achieved through an increase in the total evaporation and the associated decrease in the soil water storage. Therefore, from the differences in the plant soil water relationships for a grassland and an *E. viminalis* site, it should be possible to infer the potential impact of a change in vegetation on the drainage beyond the root-zone.

Calder (1986) lists factors determining transpiration of *Eucalyptus spp.* and most other vegetation types as: climatic demand, physiological mechanisms, canopy structure and the soil water availability to root water uptake. Under the same climatic and soil conditions, differences in the total evaporation (and drainage beyond the root-zone) of grassland (and other short vegetation types) and *Eucalyptus spp.* can therefore be attributed to differences in the leaf area index (Greenwood *et al.*, 1985; Dunin, 2002), tree height (Greenwood *et al.*, 1985; Le Maitre and Scott, 1997; Dunin, 2002), the length of the growing season or seasonality (Greenwood *et al.*, 1985; Dunin, 2002), soil water availability (Sharma, 1984; Olbrich *et al.*, 1994; Calder, 1998; Silberstein *et al.*, 2001; Dunin, 2002), rooting depth and the depth of soil water extraction (Greenwood *et al.*, 1985; Dunin, 2002).

A number of studies have showed that the water use of *Eucalyptus* species exceeds that of grassland and other short crops (e.g. Sharma, 1984; Greenwood *et al.*, 1985; Le Maitre and Scott, 1997; Versfeld *et al.*, 1998; Dunin, 2002; Sikka *et al.*, 2003). Other studies showed that soil water storage is depleted more by *Eucalyptus* and other trees compared to grassland and crops (e.g. Holmes and Wronski, 1971 cited by Lima, 1984; Sharma, 1984). These studies all suggest that the proposed hypothesis, that a change in

vegetation from grassland to *E. viminalis* trees will cause a reduction in the drainage below the root-zone, is possibly true.

## **6.2 General information**

### **6.2.1 Technique used for soil water content comparison**

Three different types of soil sensors, water content reflectometers, heat dissipation sensors and soil psychrometers, were used to cover the possible range of soil water contents and soil water potentials expected within the soils, ranging from periodically saturated conditions to very dry soils. Details on the calibration of the soil sensors and a comparison of soil water potentials calculated from each method, are given in Appendices B and C.

Of the three techniques applied in the field experiment, only the water content reflectometers estimated the soil water content, and were calibrated in the laboratory following the field experiment (Appendix B). Second-order polynomials derived for the different soil depths (and the associated clay contents) during the calibration process were used to convert water content reflectometer period output to soil water content (Appendix B, Table B.5). The soil water content results for the water content reflectometer will therefore be used in the discussion below. The soil water content for different soil depths was integrated to provide a single estimate of the profile soil water content at a particular time.

General equations provided by Jovanovic and Annandale (1997), and Wiebe *et al.* (1977) and Brown (1970) respectively were used to convert the output of heat dissipation sensors and thermocouple psychrometers, into soil water potential. The soil water potential results for these sensors are compared in Appendix C.

### **6.2.2 Patching of missing soil water content data**

At the grassland site, the water content reflectometers installed at the 300- and 500-mm soil depths were malfunctioning from the end of December 1998 until the end of the field experiment. As this was only detected towards the end of the field experiment,

these sensors were not replaced during the field experiment. This malfunction of the sensors followed a large rainfall event (71.8 mm) and possible lightning damage to the sensors on 27 December 1998. Linear relationships (data not shown) existed between the soil water contents estimated for the 300- and 700-mm soil depths and the 500- and 700-mm soil depths, during the period preceding the malfunctioning (1 July to 26 December 1998). These linear relationships were used to estimate the soil water content for the 300- and 500-mm soil depths for the period 27 December 1998 to 30 June 2000.

At the *E. viminalis* site, soil water content and soil water potential data for all soil depths were missing from 20 April to 13 September 1999 and from 19 May to 30 June 2000. This was the result of lightning damage to the dataloggers and sensors, and theft of the dataloggers respectively. Since a small change in profile soil water storage was expected during this period, due to low transpiration rates (1 to 3 mm d<sup>-1</sup>), the soil water contents were estimated as a linear function of time. The soil water contents at the 100-, 700- and 900-mm soil depths decreased over time but increased slightly at the 300- and 500-mm soil depths.

### **6.2.3 Seasonal changes in the total evaporation of grassland and transpiration of *E. viminalis* trees**

The seasonal changes in the total evaporation component of a grassland and *E. viminalis* trees observed during the field experiment, and the climatic conditions experienced during the field experiment, are presented in Appendix D. These seasonal changes in the total evaporation and transpiration are related to changes in climatic conditions (and atmospheric demand), plant growth (leaf area index, root density distribution) and soil water availability experienced during the field experiment. The energy flux densities determining the total evaporation at the grassland site are also presented in Appendix E.

### 6.3 Relative saturation<sup>14</sup> for grassland and *E. viminalis* sites

#### 6.3.1 Introduction

The water retention characteristics (Eq. 3.4) for different soil layers of the grassland and *E. viminalis* tree sites were different (Table A.6, Fig. A.1). Therefore, to compare the effect of grassland and *E. viminalis* trees on the soil wetness throughout the season, the relative saturation (Eq. 3.8) of the soil depths, were used for comparison rather than the actual soil water contents. Relative saturation is expressed as a percentage.

The relative saturation for different soil depths at both sites changed over the season and differences existed between the grassland and the *E. viminalis* sites (Fig. 6.1). In general, the relative saturation for the grassland site soil depths below was greater than those of the *E. viminalis* tree site throughout the field experiment (Fig. 6.1).

The exceptions were periods during spring 1998 (September to November 1998), where the 100-, 300- and 500-mm soil depths at the grassland site were periodically drier than that at the *E. viminalis* site. The drier 100- to 500-mm soil depths at the grassland site during this period were the result of the higher grassland total evaporation (3 to 6 mm d<sup>-1</sup>) (Fig. D.1), compared to the tree transpiration (Fig. D.5). At this time, most of the *E. viminalis* trees were in a poor condition due to frost and a pathogen infestation (Roux, 1998) and transpired at low rates (less than 1 to 3 mm d<sup>-1</sup>) (Fig. D.5).

Throughout the experiment, the deeper depths (700 and 900 mm) at the *E. viminalis* site were drier (lower relative saturation) than at the grassland site. At the grassland site, these depths were saturated for extended periods during summer (Fig. 6.1, Table 6.1). By comparison with the deeper soil depths, the soil surface depths (100 mm) at both sites showed large variations in the relative saturations due to responses to changes in the climatic conditions.

---

<sup>14</sup> The relative saturation of a soil is an indication of the wetness of the soil, and is expressed as a function of volumetric soil water content, residual soil water content and saturated soil water content (Sumner, 2000).

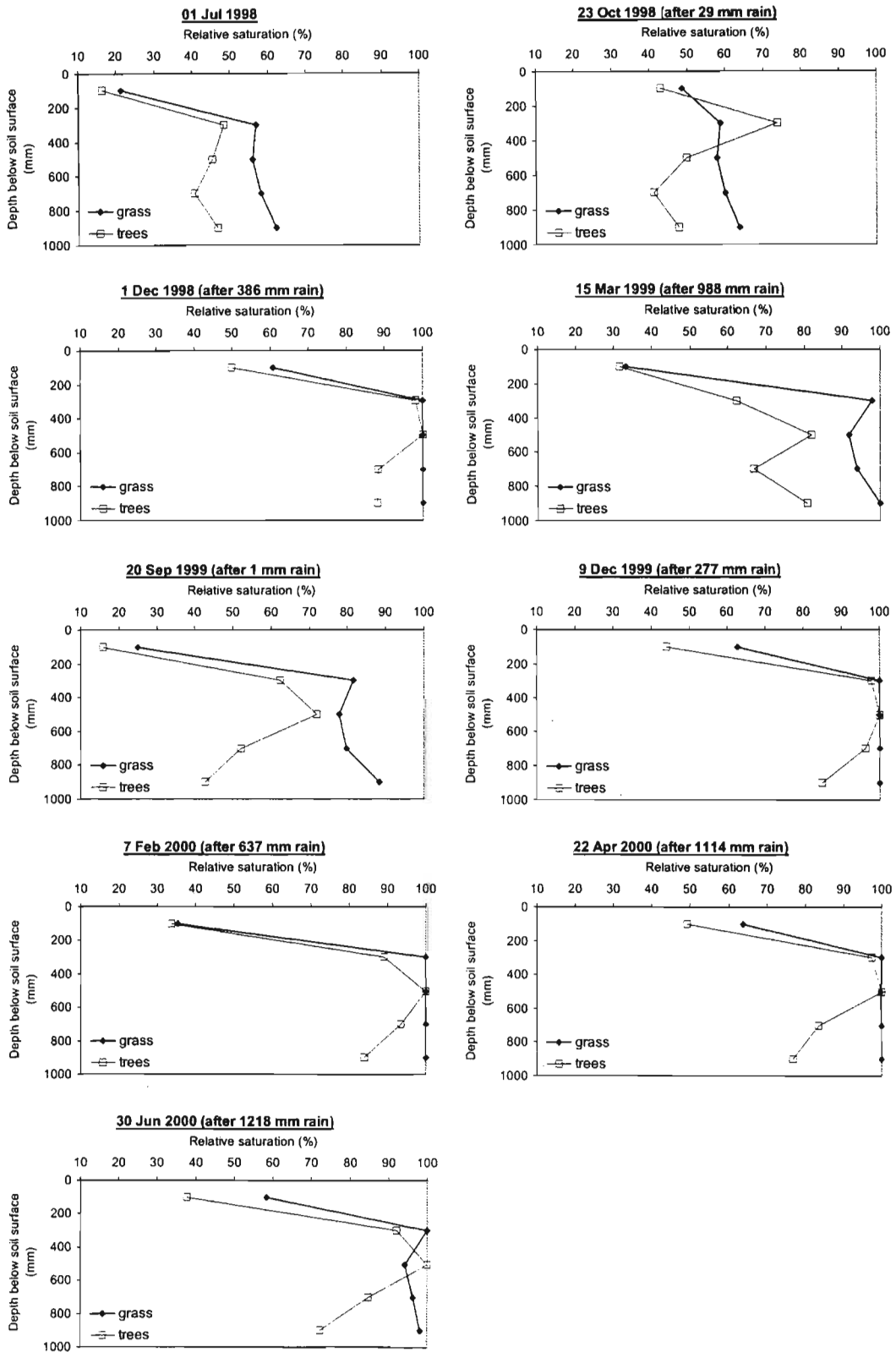


Fig. 6.1 Relative saturation (expressed as a percentage) for different soil depths at a grassland (grass) and a *E. viminalis* (trees) site for different days within the period 1 July 1998 to 30 June 2000. Rainfall in brackets represents the accumulated rainfall for the year (July to June).



Table 6.1 Relative saturation (expressed as a percentage) for different soil depths at a grassland (Grass) and *E. viminalis* (Trees) site from 1 July 1998 to 30 June 2000, and the rainfall between different time period

Date	Relative saturation (%)										Rainfall <i>between</i> measurements (mm)
	Soil depths (mm)										
	100		300		500		700		900		
	Grass	Trees	Grass	Trees	Grass	Trees	Grass	Trees	Grass	Trees	
1: 1 Jul 1998	21	16	57	49	56	45	58	41	62	47	0
2: 23 Oct 1998	49	43	59	74	58	50	60	41	64	48	29
3: 1 Dec 1998	60	49	100	97	100	100	100	88	100	88	357
4: 15 Mar 1999	33	32	98	62	92	82	94	67	100	81	602
5: 20 Sep 1999	25	16	82	62	78	72	80	52	88	43	123
6: 9 Dec 1999	63	44	100	97	100	100	100	96	100	85	276
7: 7 Feb 2000	35	34	100	89	100	100	100	94	100	84	360
8: 22 Apr 2000	64	49	100	97	100	100	100	84	100	77	477
9: 30 Jun 2000	58	41	100	90	94	100	96	86	98	78	104

### 6.3.2 Seasonal differences in relative saturation at different soil depths

At the start of the research (1 July 1998), the soil surface depths (100 mm) at both sites were dry (21 and 16 % relative saturation respectively) and the relative saturations differed by only 5 % (Fig. 6.1). All the other depths (300, 500, 700 and 900 mm) at both sites had higher relative saturations ranging from 57 to 62 % (grassland) and 41 to 49 % (*E. viminalis*) (Fig. 6.1, Table 6.1).

After the first rainfall of the season (29 mm) (23 October 1998), the relative saturations of the surface depths (100 mm) of both sites, increased by similar amounts (28 and 27 % respectively) (Fig. 6.1, Table 6.1). However, large differences existed in the increases in relative saturations for the 300-mm soil depths. At the grassland site, the relative saturation for this depth increased by only 2 % whereas that at the *E. viminalis* site increased by 25 %. The lower relative soil saturation increase at this depth at the grassland site suggested water extraction by the grass roots and higher total evaporation rates compared to that at the *E. viminalis* site (Figs D.1 and D.5). According to Versfeld *et al.* (1998), 80 % of the grass roots of a site similar to the one studied, occurred in the upper 400 mm of the soil profile with 1000 mm depth.

In contrast, sixty percent of the roots of the *E. viminalis* trees occur within the upper 400 mm of soil, with the remainder up to a depth of 3000 mm (Versfeld *et al.*, 1998). The higher relative saturation at the 300-mm soil depth of the *E. viminalis* site compared to the grassland site further suggest that little water is extracted from this depth by the *E. viminalis* tree roots. The rest of the soil depths (500 to 900 mm) at both sites remained at similar relative saturations on 23 October 1998 when compared to 1 July 1998. This suggests that the wetting front following the 29 mm of rainfall did not reach the soil depths below 300 mm.

After 357 mm of rainfall (1 December 1998), the relative saturation at all depths for both sites increased (Fig. 6.1). At the grassland site, all soil depths except those near the soil surface (100 mm) reached saturation. The 300- to 900-mm soil depths at the *E. viminalis* site were as much as 12 % drier than at the grassland site (Fig. 6.1, Table 6.1). The drier greater depths (700 and 900 mm) at the *E. viminalis* site,

compared to the grassland site (Fig. 6.1, Table 6.1), suggest that the *E. viminalis* trees were extracting water from these depths and/or that the wetting front did not reach these soil depths. The high relative saturations for both sites shows that there was water available within the soil profiles to sustain high transpiration and total evaporation rates exceeding  $6 \text{ mm d}^{-1}$  (Figs D.1 and D.5).

Over the next three and a half months (1 December 1998 to 15 March 1999) with 602 mm of rainfall, all the soil depths at the grassland site, with the exception of the 100-mm depth near the surface, remained within 8 % of soil saturation (Fig. 6.1, Table 6.1). The high relative saturations within the 300- to 900-mm soil depths suggest that the grass was unable to utilize the available soil water within these soil depths. The high soil water potentials associated with the high relative saturations further suggest a downward flux of water through and below the soil profile (Fig. 6.2). Since water flow from soil depths with a high soil water potential (wet soil) to those with a lower soil water potential (drier soil depths), the water will move downward from the 100-, 300- and 500-mm soil depths to the 700-mm soil depth. Although, only a few soil water potential data points are available for the 900-mm soil depth, it is expected that the downward flux further extends from the 700-mm soil depth to the 900-mm soil depth at the grassland site.

During the same period (15 March 1999), the 300- to 700-mm soil depths below the *E. viminalis* canopy were up to 35 % drier than on 1 December 1998. The 300- and 700-mm soil depths were also 15 to 20 % drier than the 500- and 900-mm soil depths (Fig. 6.1, Table 6.1). The drier 300-mm soil depth at the *E. viminalis* site is to some extent the result of the effect of the atmospheric conditions on the shallower soil depths, but also due to the movement of soil water out of this soil layer and to some extent transpiration from grass in the understorey layer. The soil water therefore moves from the wetter 500-mm soil depth to the drier 700-mm soil depth. This downward movement of soil water will continue towards the 900-mm depth where the water will either be utilized by tree roots or move beyond the root-zone.

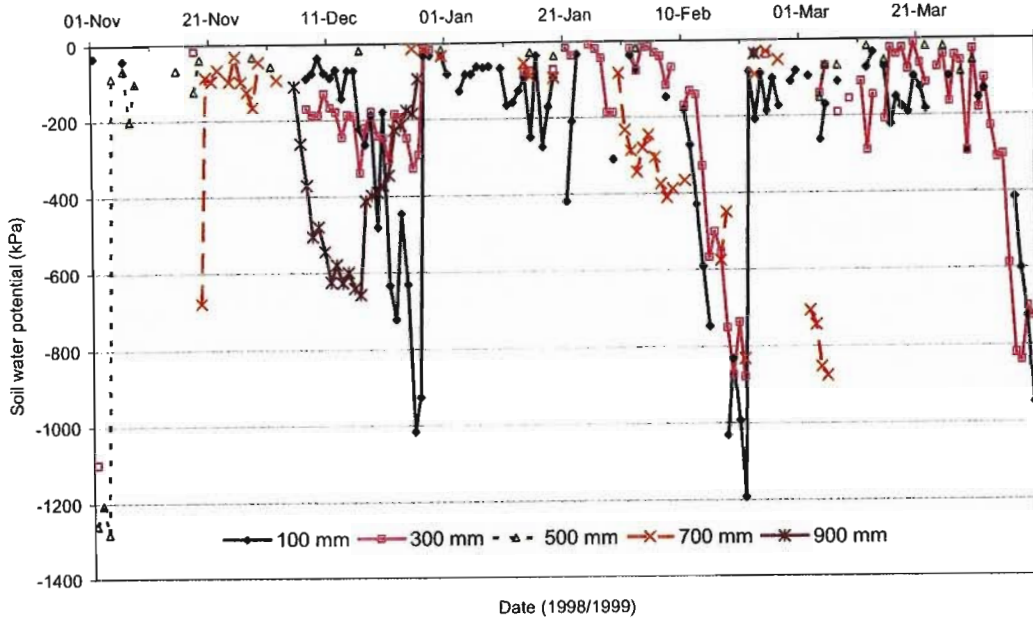


Fig. 6.2 Soil water potentials as estimated with *in situ* soil thermocouple psychrometers installed at various soil depths (100 to 900 mm) below a grassland for the period 1 November 1998 to 10 April 1999

### 6.3.3 Cumulative effect of grassland and *E. viminalis* trees on the relative saturation at different soil depths under above-average rainfall conditions

During spring of the second year of measurements (20 September 1999) and just before the onset of the new rainy season, all soil depths at both sites with the exception of the 300-mm soil depth at the *E. viminalis* site were drier than on 15 March 1999 (Fig. 6.1, Table 6.1). The constant relative saturation at the 300-mm soil depth at this site suggests that little or no soil water extraction or movement from this depth took place during this period. At the start of the 1999/2000 season (20 September 1999), all soil depths at the grassland site were also wetter (higher relative saturation) than at the start of the previous year (1998/1999). The grassland was therefore unable to utilize all of the rainfall (1110 mm) during the previous year, which resulted in an increase in soil water storage. This was also the case at the *E. viminalis* site. The 300-mm to 700-mm soil depths of the *E. viminalis* site were 11 to 27 % wetter at the start of the 1999/2000 season (20 September 1999) than at the start of the 1998/1999 season (1 July 1998).

Only the 100-mm and the 900-mm soil depths had similar relative saturation values at the start of the 1998/1999 season (16 and 47 in the 100- and 900-mm soil depths respectively) and the start of the 1999/2000 season (16 and 43 % in the 100- and 900-mm soil depths respectively).

After 276 mm of rainfall during 1999/2000 (9 December 1999), all the soil depths at the grassland site, with the exception of the depth near the surface (100 mm) were saturated (Fig. 6.1, Table 6.1). The rapid saturation of these soil depths following only 276 mm of rainfall during 1999/2000 was the result of a build-up of soil water over time. At the *E. viminalis* site the 300- to 900-mm depths were 85 to 100 % saturated. The wettest depths at this site were the 300- and 500-mm soil depths, where little soil water extraction occurred. It is assumed that none or few of the *E. viminalis* tree roots exist at these depths. The increased relative saturation for the 700- and 900-mm soil depths also suggest that tree roots were unable to utilize all of the available soil water at these depths and that the soil wetting front has reached these soil depths. This is illustrated by the higher soil water potentials at the 300-mm soil depth, compared to that of the 500- and 900-mm soil depths (Fig. 6.3). Water will therefore move from the 300-mm soil depth downward.

Towards the end of summer (7 February 2000), after a further 360 mm of rainfall, there was little change in the relative saturation at the 300- to 900-mm soil depths for the grassland site. These depths remained saturated. It is therefore predicted that the water will move downwards, through and below the grassland soil profile. Only the depth near the surface (100 mm) was 28 % drier than on 1 December 1999. The lower relative saturation of the soil depth near the surface at the grassland site was the result of water extraction by the grass roots to maintain transpiration, and soil evaporation.

The relative saturation of all the soil depths at the *E. viminalis* site also remained similar during this period (1 December 1999 to 7 February 2000). At the *E. viminalis* site, the relative saturations of the soil depths were less than 10 % drier than on 1 December 1999. The soil water potentials estimated with the *in situ* soil psychrometers also indicated very low soil water potentials. It is expected that the soil water within this profile too will also move downwards and possibly below the soil profile (Fig. 6.3).

Finally, after more rainfall during autumn (581 mm) (7 February 2000 to 30 June 2000), the relative saturations of the 300- to 900-mm soil depths at the grassland site remained similar whilst the depth closest to the surface showed a further increase in the saturation until the end of the experiment (Fig. 6.1, Table 6.1). However, between 7 February 2000 and 30 June 2000, the relative saturations of the 100- and 300-mm soil depths at the *E. viminalis* site increased slightly (7 and 1 % respectively), the relative saturation of the 500-mm depth remained the same at saturation. The relative saturations of only the 700- and 900-mm soil depths, decreased (by 8 and 6 % respectively). This suggests that the *E. viminalis* trees were utilizing some of the available soil water from the 700- to 900-mm soil depths during this period, and/or that a downward flux of soil water below the profile occur.

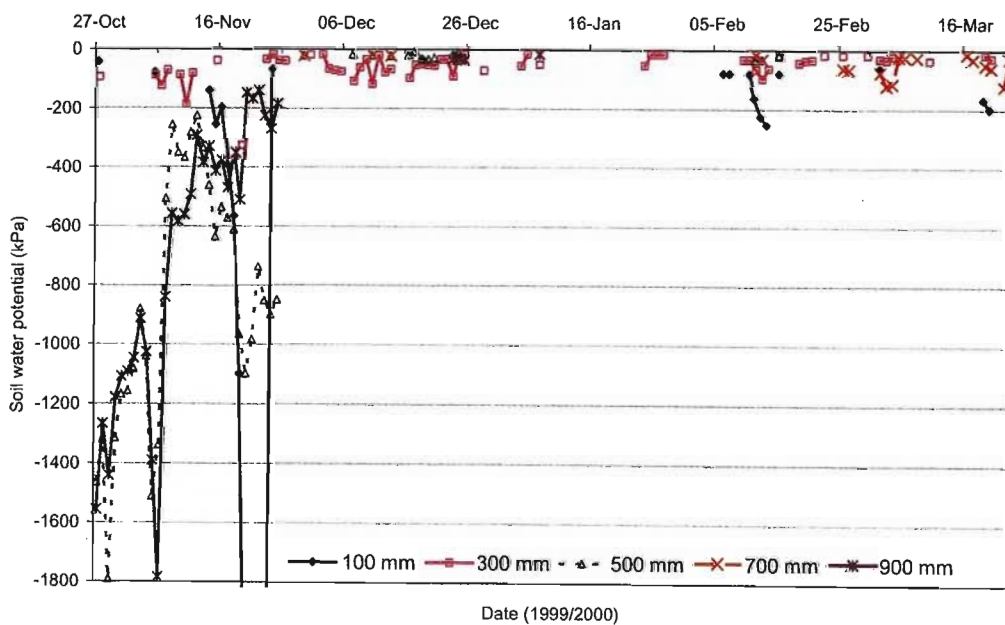


Fig. 6.3 Soil water potential as estimated with *in situ* soil thermocouple psychrometers installed at various soil depths (100 to 900 mm) below *E. viminalis* trees for the period 28 October 1999 to 22 March 2000

## 6.4 Profile soil water contents for a grassland and an *E. viminalis* site

### 6.4.1 Introduction

The profile soil water contents at both sites were calculated over a depth of 1000 mm using Eq. 3.5. The profile soil water content illustrates the cumulative effect of the soil water content within the soil layers.

In general, the profile soil water content at the grassland site exceeded that at the *E. viminalis* site (Fig. 6.4). The exceptions were from 3 to 18 November 1998. The lower profile soil water content at the grassland site during this period was the result of the high total evaporation rates (up to  $7.8 \text{ mm d}^{-1}$ ) (Fig. D.1) at the grassland site at the start of the new growing season. During this period, the *E. viminalis* trees were in a poor condition due to a pathogen infestation and severe frost during the previous winter, and transpired at low rates ( $1 \text{ to } 3 \text{ mm d}^{-1}$ ) (Fig. D.5).

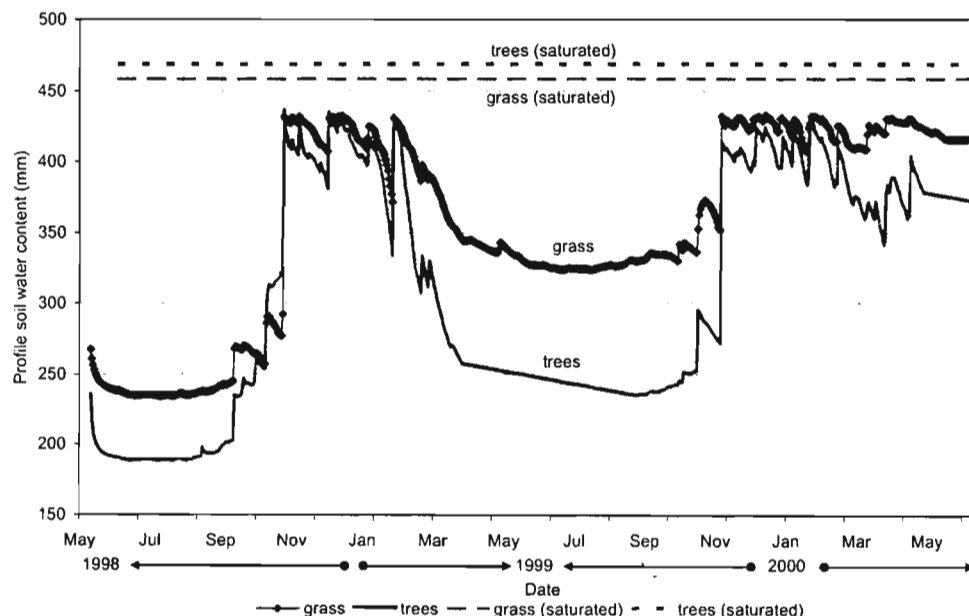


Fig. 6.4 Total profile soil water content at the grassland (grass) and *E. viminalis* (trees) sites over a 1000 mm soil profile for the period May 1998 to June 2000. grass (saturated) and trees (saturated) indicate the saturated profile soil water content for the grassland and *E. viminalis* sites.

### 6.4.2 Seasonal changes in the profile soil water contents

The largest differences (up to 98 mm d<sup>-1</sup>) in the profile soil water contents between the two sites occurred during autumn, winter and early spring (Fig. 6.4). These differences existed after the occurrence of frost during autumn and winter, and the senescence of the grass during autumn. These large differences lasted until after the onset of the new rain season and the associated new growth of the grass. During this period (autumn to early spring), the total evaporation at the grassland site was possibly less than 0.5 mm d<sup>-1</sup> (Fig. D.1), similar to the minimum total evaporation suggested by Everson *et al.* (1998) and Versfeld *et al.* (1998) for grassland. The profile soil water content remained fairly constant (Fig. 6.4). Since little rainfall occurred during this period, any change in the profile soil water content was the result of soil evaporation. However, during the corresponding period at the *E. viminalis* site, the *E. viminalis* trees maintained transpiration rates of 1 to 3 mm d<sup>-1</sup> (Fig. D.5). The continued transpiration during autumn, winter and spring by *E. viminalis* trees, resulted in a steady decrease in the profile soil water content at the *E. viminalis* site until the beginning of the new rain season (Fig. 6.4). The continued transpiration of *E. viminalis* trees resulted in an increased difference between the profile soil water content at the sites (Fig. 6.4).

In contrast, during summer (December to February), a much smaller difference existed between the profile soil water contents at the two sites (1 to 38 mm d<sup>-1</sup>) (Fig. 6.4). Both the grassland and *E. viminalis* soil profiles responded to rainfall events through increased profile soil water content. However, the profile soil water content decreased more at the *E. viminalis* site following a rainfall event than at the grassland site (Fig. 6.4). This suggests that when soil water is available the transpiration rates of *E. viminalis* trees exceed the total evaporation rates of the grassland when soil water is available.



### 6.4.3 Cumulative profile soil water contents

The effect of different vegetation on profile soil water contents over a period of two years (1 July 1998 to 30 June 2000) with above-average rainfall, is the gradual increase in the profile soil water contents (175 and 181 mm at the grassland and *E. viminalis* sites respectively) from 1 July 1998 to 30 June 2000 (Fig. 6.4). These increases suggest that both vegetation types, grassland and *E. viminalis* trees, were unable to utilize the available soil water. The *E. viminalis* trees were, however, slightly more effective in utilizing the available soil water during the first year (1998/1999) compared to the grass. During 1998/1999, the profile soil water content (soil water storage) for *E. viminalis* trees increased by 32 mm less than at the grassland site (56 mm and 88 mm at the *E. viminalis* and grassland sites respectively) (Fig. 6.4). However, during the second year, the profile soil water content at the *E. viminalis* site increased by 126 mm whereas that at the grassland site increased by 88 mm (Fig. 6.4).

## 6.5 Total evaporation and soil water content relationships

### 6.5.1 Introduction

The total evaporation of grassland and transpiration of *E. viminalis* trees are discussed in Appendix D. From this dataset it is clear that maximum total evaporation of grassland and transpiration of *E. viminalis* trees were reached during summer when the leaf area indices, reference evaporation and profile soil water content were at a maximum. However, the potential total evaporation of grassland and transpiration rates of trees (during both summer and winter), were affected by occasional unfavourable conditions which affected both grassland and *E. viminalis* trees: frost, fire and pathogens. Minimum total evaporation and transpiration were reached during winter, following frost (senescence of grassland) and a veld fire, and when the leaf area indices and reference evaporation were a minimum. The maximum and minimum total evaporation (and transpiration) rates estimated during the field experiment were further dependent on the soil water content (or relative saturation) of individual soil depths.

## 6.5.2 Plant and soil water relationships during spring and summer

Following the onset of rainfall, for example on 14 October 1998 (18 mm), the total evaporation of grassland increased from winter minimum to summer maximum rates ranging between 6.0 and 7.8 mm d<sup>-1</sup> (Fig. 6.5). Maximum total evaporation rates were maintained from November 1998 until February 1999. However, the transpiration of three *E. viminalis* trees increased from less than 1.0 mm d<sup>-1</sup> (prior to or directly following rainfall), to 3.0 mm d<sup>-1</sup> (August and September 1998) and 1.8 mm d<sup>-1</sup> respectively (August and September 1999) (Fig. 6.5). Maximum transpiration rates for *E. viminalis* trees (6.0 and 9.0 mm d<sup>-1</sup>), similar to or higher than the grassland total evaporation rates, were only reached from December to February (Fig. 6.5). Everson (1993) also found similar and high total evaporation of grassland and *Eucalyptus* plantations during dry summers (5.0 mm d<sup>-1</sup>). These maximum rates of total evaporation for grassland and transpiration of *E. viminalis* trees coincided with maximum leaf area indices (3.5 to 6.0 and 1.8 to 4.0 at the grassland and *E. viminalis* sites respectively) (Fig. 6.6), daily reference evaporation (as high as 6.0 mm d<sup>-1</sup>) (Fig. 6.7) and monthly rainfall ranging between 12.8 and 178.0 mm (Fig. 5.3).

The maximum total evaporation estimated in this study was higher than that recorded for other grassland sites. Versfeld *et al.* (1998) measured total evaporation for grassland in the Secunda area over a short period in summer of 1 and 3 mm d<sup>-1</sup>. Wever *et al.* (2002) found the total evaporation of a northern temperate grassland to reach a maximum of 4.5 mm d<sup>-1</sup>, whereas Everson *et al.* (1998) found total evaporation for moist upland grassland during summer to be between 3 and 7 mm d<sup>-1</sup>. The high total grassland evaporation estimated in this study can be attributed to the high leaf area index<sup>15</sup> (up to 6) and the consistently high soil profile saturation during summer.

However, the maximum transpiration rates of up to 9 mm d<sup>-1</sup> calculated for *E. viminalis* trees were in accordance with transpiration of *E. viminalis* and other *Eucalyptus* tree species within the study area and other areas.

---

<sup>15</sup> The leaf area indices represent the total leaf area of the vegetation as measured with a LI-COR canopy analyzer.

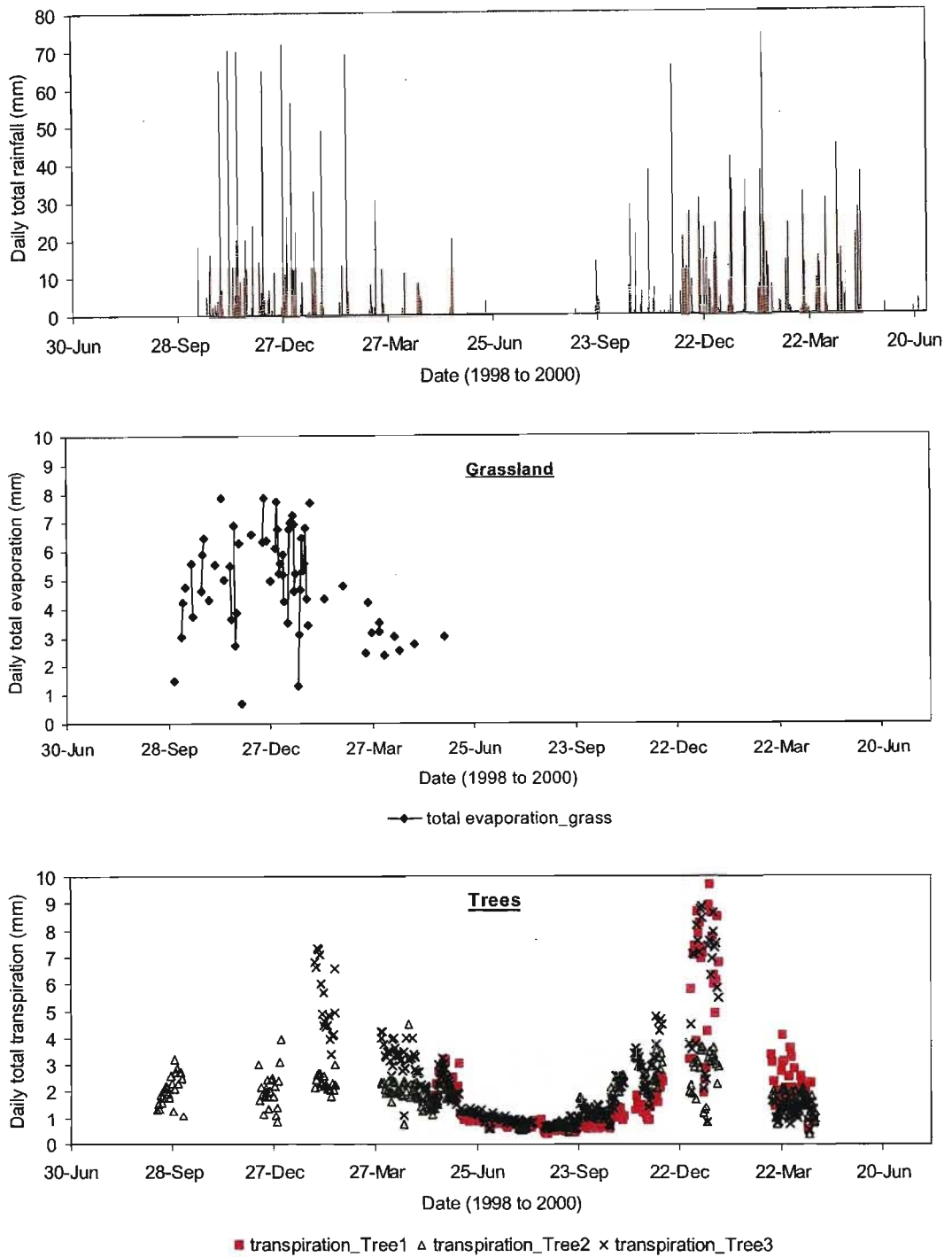


Fig. 6.5 Daily total rainfall (top), daily total evaporation of grassland (total evaporation\_grass) (middle) and daily total transpiration by three *E. viminalis* trees (transpiration\_Tree1, transpiration\_Tree2, transpiration\_Tree3) (bottom) from 1 July 1998 to 30 June 2000

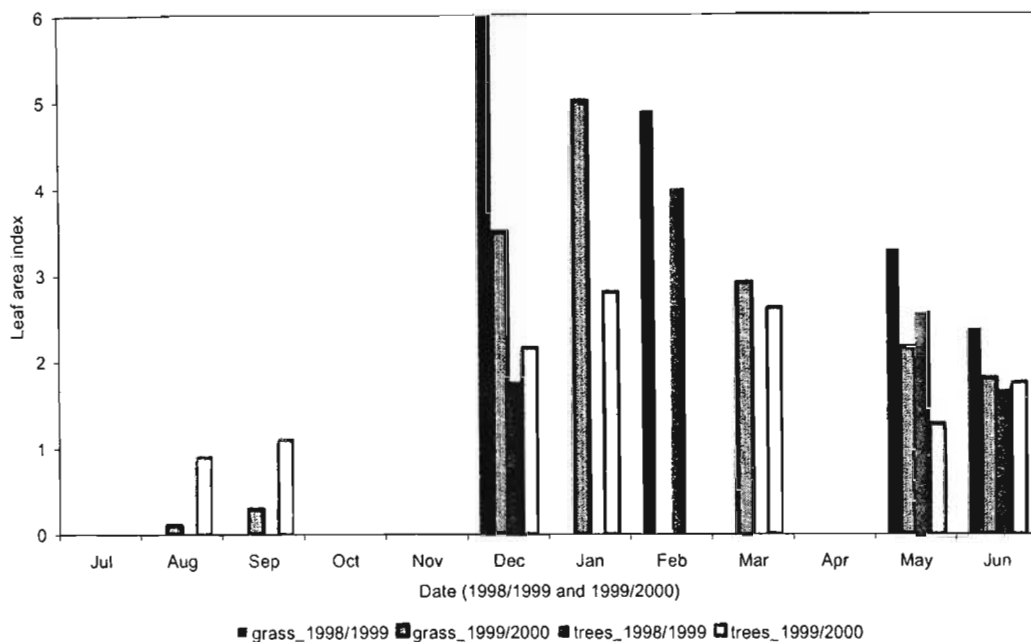


Fig. 6.6 Leaf area indices of grassland (grass\_) and *E. viminalis* trees (trees\_) during 1998/1999 (\_1998/1999) and 1999/2000 (\_1999/2000)

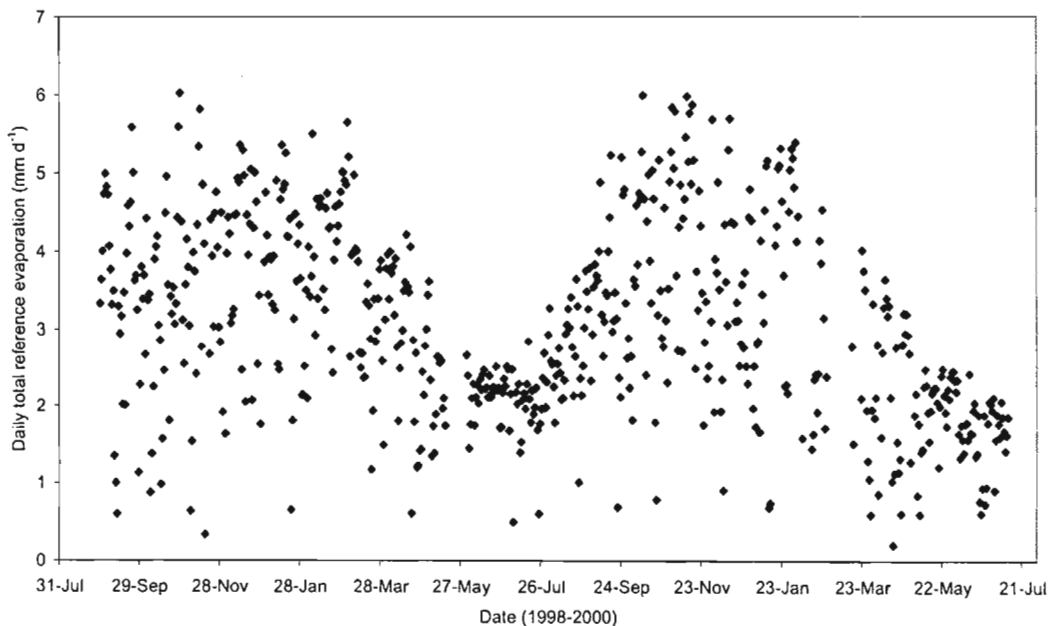


Fig. 6.7 Daily total reference evaporation calculated with the Penman-Monteith equation, from 1 July 1998 to 30 June 2000

Olbrich *et al.* (1994) found maximum summer transpiration by *E. viminalis* trees in the Secunda area of  $6 \text{ mm d}^{-1}$ . Versfeld *et al.* (1998) reported maximum transpiration rates by *Eucalyptus* species in the Secunda area to be as high as  $12 \text{ mm d}^{-1}$ . Other examples of high maximum total evaporation and transpiration rates by *Eucalyptus* species are given by Lima (1984) ( $6 \text{ mm d}^{-1}$ ), Honeysett *et al.* (1992) (5 to  $6 \text{ mm d}^{-1}$ ) (cited by Hunt and Beadle, 1998) and Zohar and Schiller (1998) ( $5.1 \text{ mm d}^{-1}$ ) and Jarmain and Everson (2002) ( $9 \text{ mm d}^{-1}$ ).

The maximum grassland total evaporation rates occurred at profile saturations of 55 to 60 %, and at profile saturation exceeding 90 % (Fig. 6.8). The lower grassland total evaporation rates estimated at soil profile saturations of 60 to 90 % suggest lower atmospheric demand, or the occurrence of cloud cover. However, maximum transpiration rates of *E. viminalis* trees only occurred at profile saturations exceeding 85 % (Fig. 6.8). *E. viminalis* trees therefore required higher profile soil saturations to reach transpiration rates exceeding  $5.0 \text{ mm d}^{-1}$ . Differences in the relationship between the total evaporation (and transpiration) and the soil profile saturation of the two sites (Figs 6.8 to 6.12) suggest differences in root distribution between the grassland and *E. viminalis* trees, and subsequent differences in the depth of soil water extraction. Figs 6.9 and 6.10 suggest soil water extraction by *E. viminalis* roots at greater depths compared to grassland.

According to Versfeld *et al.* (1998) approximately 60 % of the roots of an *E. viminalis* tree in a vertisol occur within the upper 400 mm of a soil (maximum rooting depth 3 m). Knight (1999) suggested that 84 % of the *Eucalyptus* species roots occur in the upper 40 % of a soil profile. For a grassland, however, Versfeld *et al.* (1998) found that 80 % of grass roots occurred in the upper 400 mm of a 1000 mm soil profile. These rooting differences possibly suggest that the *E. viminalis* trees required a more saturated soil profile, and movement of the soil water to greater depths (700 to 900 mm) before transpiration rates exceeding  $5.0 \text{ mm d}^{-1}$  could occur (Figs 6.8 and 6.10). By contrast, high total evaporation of grassland (greater than  $5.0 \text{ mm d}^{-1}$ ) will occur when only the upper layers (100 to 300 mm) are wet, and therefore under low or higher profile saturations (Fig 6.9 and 6.11).

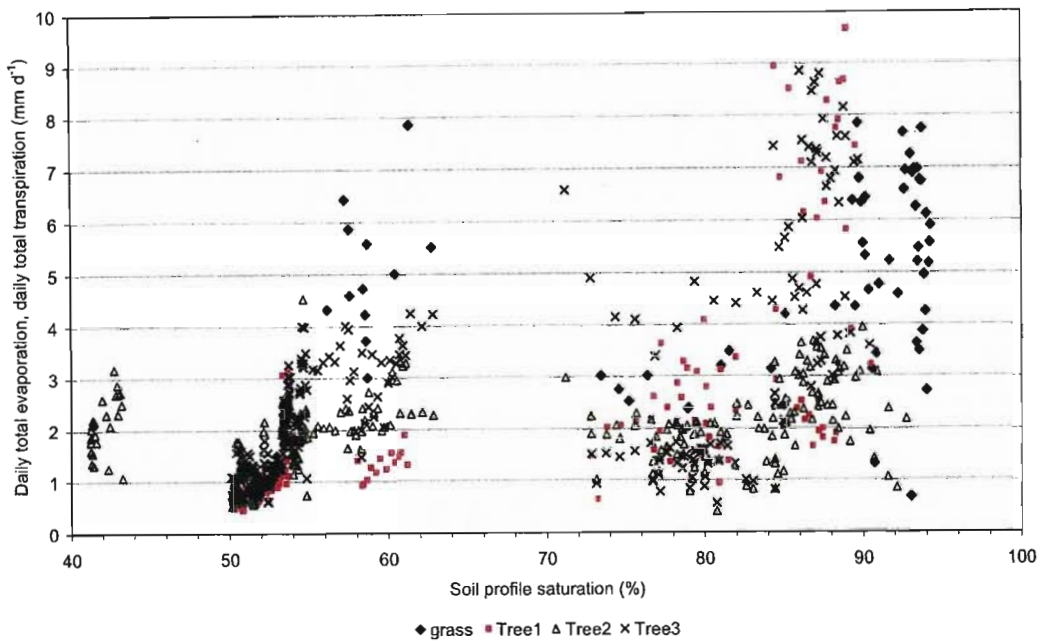


Fig. 6.8 Daily total evaporation of grassland (grass) and daily total transpiration of three *E. viminalis* trees (Tree1, Tree2, Tree3) vs soil profile saturation (%)<sup>16</sup>

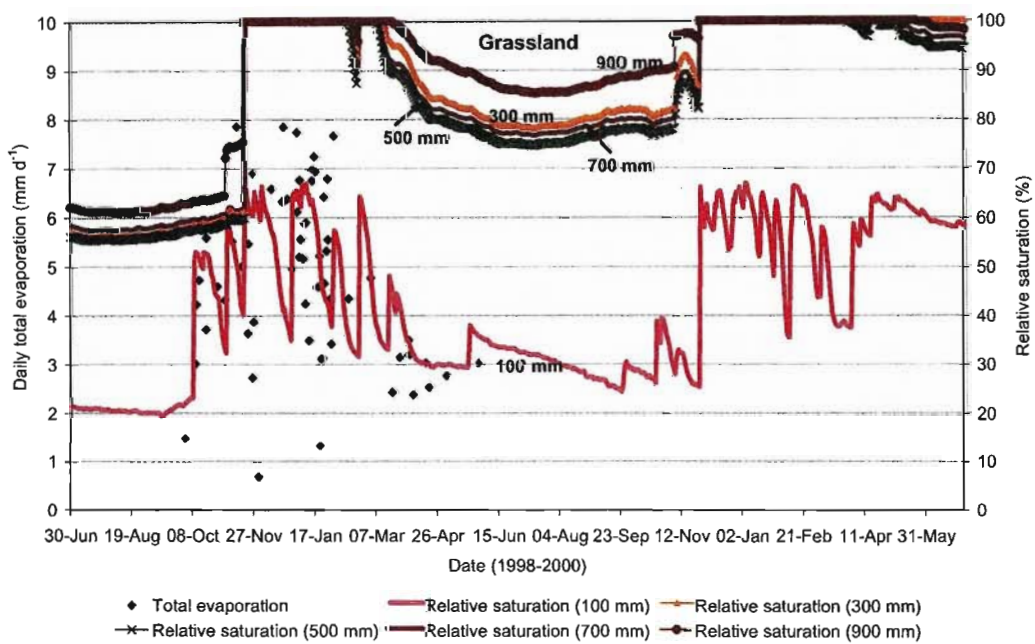


Fig. 6.9 Daily total evaporation (total evaporation) and relative saturation (%) at different soil depths (100 to 900 mm) below a grassland from 1 July 1998 to 30 June 2000

<sup>16</sup> The soil *profile* saturation is defined as the percentage of actual *profile* soil water content to saturated *profile* soil water content.

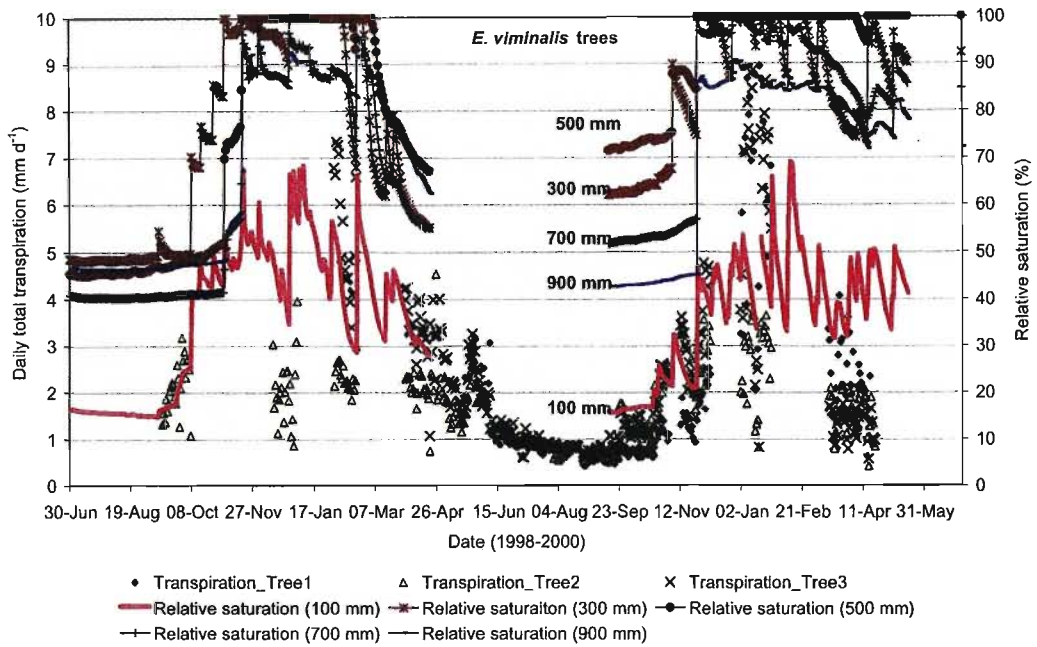


Fig. 6.10 Daily total transpiration for three trees (Transpiration\_Tree1, \_Tree2, \_Tree3) and relative saturation (%) at different depths (100 to 900 mm) at an *E. viminalis* site from 1 July 1998 to 30 June 2000

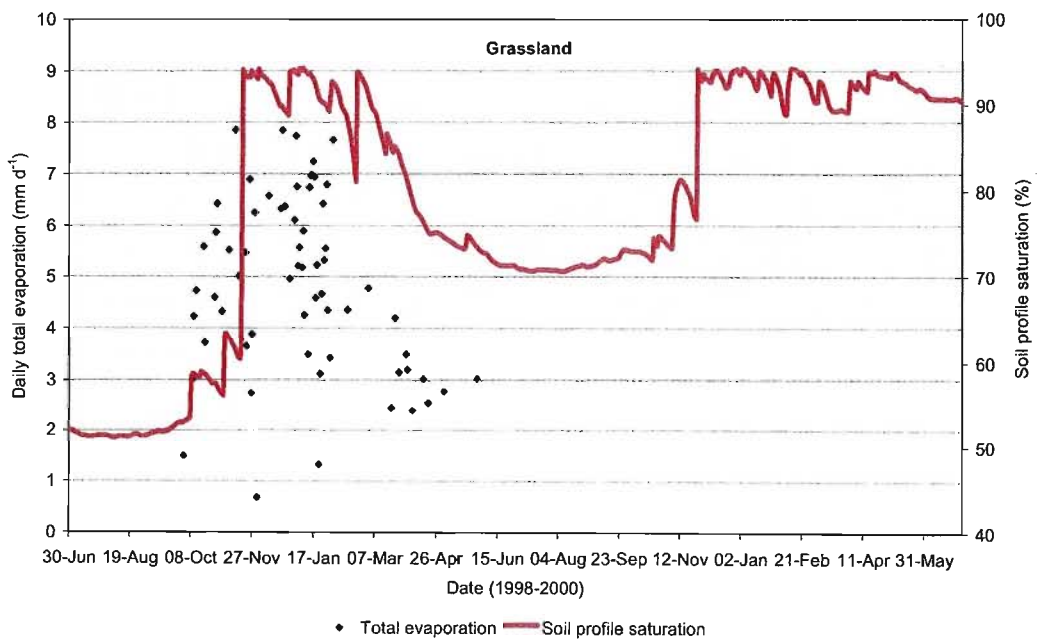


Fig. 6.11 Daily total evaporation and soil *profile* saturation at the grassland site from 1 July 1998 to 30 June 2000

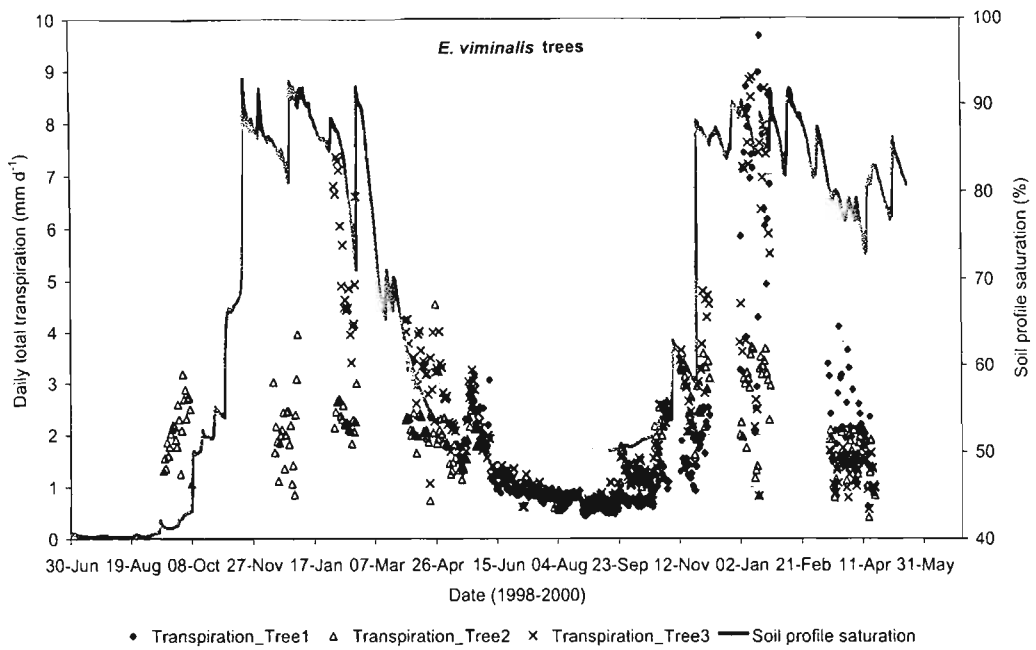


Fig. 6.12 Daily total transpiration of three *E. viminalis* trees (\_Tree1, \_Tree2, \_Tree3) and soil profile saturation at the *E. viminalis* site from 1 July 1998 to 30 June 2000

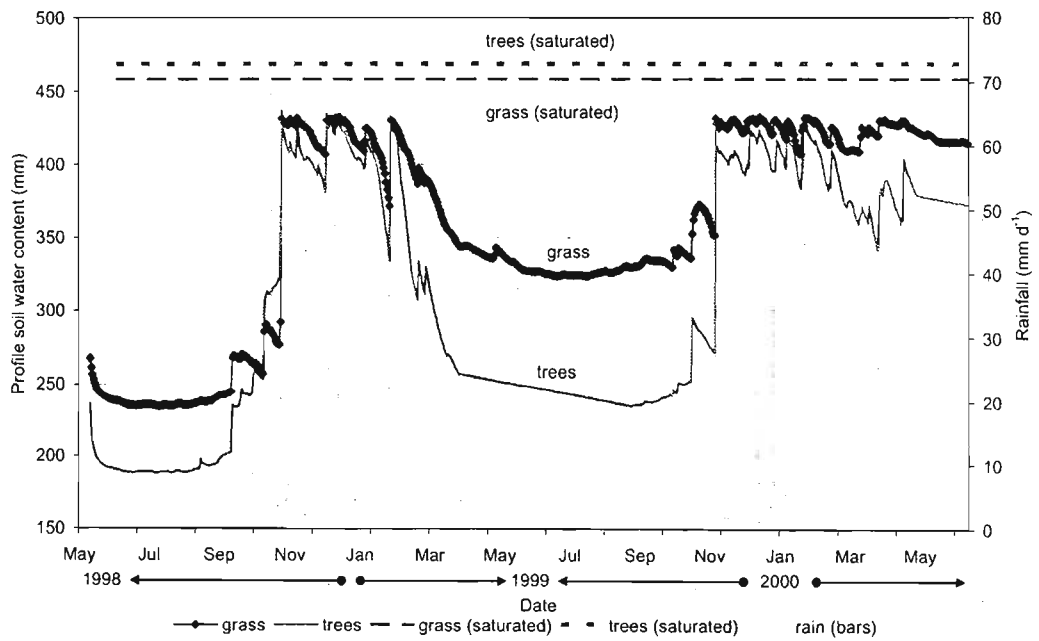


Fig. 6.13 Actual total and saturated profile soil water content at the grassland (grass) and *E. viminalis* (trees) sites over a 1000 mm soil profile



High total evaporation rates by grassland under high or low profile saturation are therefore possible as the grass roots are concentrated close to the surface and would be able to extract soil water under both conditions (Figs 6.8, 6.9 and 6.11).

The higher grassland total evaporation during spring and early summer and the rapid increase in the total evaporation to maximum rates compared to the transpiration by *E. viminalis* trees, was therefore partially the result of the earlier availability of soil water to the shallow grassland roots and partially due to differences in physiological responses (leaf area indices) and the poor quality of the *E. viminalis* trees. The grassland responded to the increased soil water availability within the 100- to 300-mm soil depths, through increased growth. Maximum leaf area indices of up to 6 were reached (Fig. 6.6). Here, the relative saturation at the 100-mm soil depth increased from 20 to 30 % (during winter), to 40 to 50 % (following the first rainfall) (Fig. 6.9).

### 6.5.3 Plant and soil water relationships during autumn and winter

During autumn, total evaporation of grassland and transpiration of *E. viminalis* trees were similar (Fig. 6.5), while soil water was available from the previous rain season and before the first frost. Autumn transpiration for *E. viminalis* trees ranged between 0.4 mm d<sup>-1</sup> (rainy days) and 4.5 mm d<sup>-1</sup> (sunny days), while the total grass evaporation ranged between 2.4 mm d<sup>-1</sup> and 4.8 mm d<sup>-1</sup> (sunny days).

Following the first light frost of autumn (minimum air temperature,  $T_{min}$ , of -0.01 and -0.9 °C during 1998/1999 and 1999/2000 respectively), the transpiration of all three *E. viminalis* trees decreased to less than 1.0 mm d<sup>-1</sup> (e.g. Figs. 6.5). But, following light frost and e.g. 30.4 mm of rainfall on 16 March 1999 and the subsequent increase in soil profile saturation (66 to 71 %) (Fig. 6.12), the transpiration of *E. viminalis* trees again increased to between 2.1 to 3.2 mm d<sup>-1</sup>. However, following more severe frost ( $T_{min}$  of -1.1 and -1.3 °C during 1998/1999 and 1999/2000 respectively), the *E. viminalis* transpiration decreased from 3.2 mm d<sup>-1</sup> to about 1.0 mm d<sup>-1</sup>. Although no autumn total evaporation data were available for the grassland site following the more severe frost, it is expected that the total evaporation of grassland would decrease to values similar to that quoted by other authors (about 0.5 mm d<sup>-1</sup>). Examples of minimum total

evaporation of grassland include that by Wever *et al.* (2002) (less than  $0.5 \text{ mm d}^{-1}$ ), Versfeld *et al.* (1998) ( $0.5 \text{ mm d}^{-1}$ ) and Everson *et al.* (1998) (less than  $1 \text{ mm d}^{-1}$ ). Lima (1984) found the minimum transpiration of *Eucalyptus* spp. to be  $1.5 \text{ mm d}^{-1}$ , slightly higher than that calculated here, whereas Olbrich *et al.* (1994) and Versfeld *et al.* (1998) found transpiration of *E. viminalis* trees within the same range of that calculated in this experiment:  $0.42 \text{ mm d}^{-1}$  and  $0.5 \text{ mm d}^{-1}$  respectively.

During autumn and winter, the minimum total evaporation of grassland and transpiration by *E. viminalis* trees coincided with the minimum reference evaporation (about  $2.0 \text{ mm d}^{-1}$ ) (Fig. 6.7), minimum leaf area indices (0.1 and 0.9 for grassland and *E. viminalis* respectively) following frost and fire (Fig. 6.6), and minimum profile soil water contents (324 and 415 mm for grassland, and 235 and 372 mm for *E. viminalis* during winter 1999 and winter 2000 respectively) (Fig. 6.13). The grassland and *E. viminalis* soil profiles were saturated to 71 and 91 % and 50 and 80 % during winter 1999 and winter 2000 respectively. However, the upper 300-mm soil depth at the grassland site was saturated to 55 (winter 1999) and 80 % (winter 2000), while the 700- to 900-mm soil depth at the *E. viminalis* site was saturated to 47 (winter 1999) and 80 % (winter 2000). Therefore, soil water was available for continued transpiration by *E. viminalis* trees during winter. However, as the grass reached senescence following the first frost in autumn, no water was extracted by the grass roots within the upper 300-mm soil depth during winter and the total evaporation of grassland is expected to consist mainly of soil evaporation. Only the *E. viminalis* tree roots will continue to utilize the available soil water, specifically within the 700- to 900-mm soil depths.

## 6.6 Summary and conclusions

The hypothesis of this study is that a change in vegetation, from grassland to *E. viminalis* trees, will potentially increase the total evaporation and decrease the associated soil water storage. In this chapter, the results from the field experiment, to test this hypothesis, are presented. This chapter showed the effect of grassland and *E. viminalis* trees on the profile soil water content (Section 6.4) and relative saturation for the different soil layers (Section 6.3). It further combined the results of the field experiment (total evaporation, transpiration and soil water content) and compared the plant and soil water relationships for a grassland and *E. viminalis* trees (Section 6.5).

Differences in the total evaporation and profile soil water content between the grassland and *E. viminalis* trees are evident. These differences were mainly the result of depth of soil water extraction (and root distribution), and the seasonality of grassland (senescence). It can be concluded that the *E. viminalis* trees impact more on the soil water content (relative saturation and profile soil water content) than the grassland.

From the differences in the relative saturations of the soil layers at the grassland and *E. viminalis* sites, it can be concluded that differences exist in the depth of soil water extraction by roots and suggested differences in the root distribution. During summer, major changes in relative saturations of the different soil layers at the grassland site were only visible in the upper 300-mm soil depth, whereas the most important relative saturation changes at the *E. viminalis* site occurred at the 700- and 900-mm soil depths. This suggests that most of the soil water extracting roots are situated within these soil layers and it can be concluded that the relative saturation changes within the associated layers can be translated into soil water extraction by the roots. It can further be concluded that the largest differences in the profile soil water content of the grassland and *E. viminalis* sites occur during autumn and winter when the grassland has reached senescence.

At the start of the growing season in spring, the total evaporation of grassland exceeded the transpiration of *E. viminalis* trees because of physiological differences, the availability of soil water to the shallow grass roots and a pathogen infection at the tree site. However, maximum transpiration rates of *E. viminalis* trees (up to 9 mm d<sup>-1</sup>) were reached towards the end of spring and during summer, and exceeded the maximum total evaporation of grassland (6 to 8 mm d<sup>-1</sup>). It can be concluded that since the *E. viminalis* tree transpiration excludes evaporation of intercepted water or transpiration of the understorey, it is expected that the total evaporation of *E. viminalis* trees will exceed that at the grassland site even more. This higher maximum transpiration of *E. viminalis* trees could be attributed to the recovery of the *E. viminalis* trees and the availability of soil water to the greater depth within the soil profile. It can therefore be concluded that frost, fire and pathogens affect the state of the *E. viminalis* trees, the transpiration of *E. viminalis* trees and the possible impact of a change in vegetation on the soil water balance.

From the relationship between the soil saturation (profile and individual soil layers) and the transpiration, it can be concluded that the maximum transpiration rates by *E. viminalis* trees were dependent on the availability of soil water. High transpiration rates (greater than  $5 \text{ mm d}^{-1}$ ) only occurred at high profile soil saturations (greater than 85 %). By contrast, maximum total evaporation of grassland (more than  $5 \text{ mm d}^{-1}$ ) were only dependent on the saturation of the 0- to 300-mm soil layers containing the grassland roots.

From the differences in the plant soil water relationships for a grassland and an *E. viminalis* site, it should be possible to infer the potential impact of a change in vegetation on the drainage beyond the root-zone. *Chapter 7* infers the potential impact of a change in vegetation on the drainage beyond the root-zone.

## CHAPTER 7

### SOIL WATER BALANCES FOR THE GRASSLAND AND *E. VIMINALIS* SITES ESTIMATED FROM THE FIELD EXPERIMENT RESULTS

#### 7.1 Introduction

In the soil water balance field experiment, the total evaporation (and transpiration) and soil water storage changes were calculated, but not the drainage beyond the root-zone. However, an estimate of drainage beyond the root-zone is important in terms of mine water management.

According to the simplified soil water balance equation (Eq. 5.1), if the precipitation and runoff is 0, then Eq. 5.1 is reduced to:

$$ET = D \pm \Delta S \quad 7.1$$

Then, if the total evaporation is equal to the soil water storage change, can it be hypothesised that the drainage beyond the root-zone is 0? Further, if the total evaporation exceeds the soil water storage change, can one assume that this difference is equal to the drainage beyond the root-zone?

Therefore, if this is possible, a comparison can be made of the soil water storage change (reduction<sup>17</sup>) and the total evaporation on a daily basis, in relation to the amount by which the measured rainfall exceeds the long-term average rainfall on a monthly basis. This comparison could potentially illustrate whether drainage beyond the root-zone occurs. This could further illustrate how effective the grassland and *E. viminalis* trees are in removing soil water from the profile in the absence of precipitation and runoff, and subsequently reducing or preventing drainage beyond the root-zone.

---

<sup>17</sup> A reduction in the soil water storage change over a period of time refers to the removal of water from the soil profile in consideration. This could be through drainage out of the profile, soil water extraction by roots (transpiration) or soil evaporation.

The relationships between the soil water storage reduction, and the total evaporation (and transpiration) of a grassland and of *E. viminalis* trees will therefore be discussed further (Figs 7.1 and 7.2). The soil water storage reductions at the grassland and *E. viminalis* sites are also compared (Figs 7.3 and 7.4).

## **7.2 Relationship between the soil water storage reduction and total evaporation at a grassland site, and transpiration at an *E. viminalis* site**

From the available data sets there are only a few days where the absolute profile soil water storage reduction at the grassland site and the total evaporation of grassland are similar (Fig. 7.1). Most of the corresponding data points occur at rates of less than  $4.0 \text{ mm d}^{-1}$ , and mainly during autumn 1998 (Fig. 7.1). For the remaining period the total evaporation of the grassland exceeds the absolute profile soil water storage reduction by between 1 and  $6 \text{ mm d}^{-1}$ . However, the absolute profile soil water storage reduction for the *E. viminalis* site and transpiration by the *E. viminalis* trees are more often similar, compared to that at the grassland site (Fig. 7.2). Corresponding absolute soil water storage reduction and transpiration values occur during spring, autumn and summer and range between less than  $1 \text{ mm d}^{-1}$  and  $8 \text{ mm d}^{-1}$  (Fig. 7.2). Therefore, for both sites where the absolute profile soil water storage reduction and the total evaporation (or transpiration) were different (mainly during summer), on days with rainfall not exceeding  $10 \text{ mm d}^{-1}$ , or where the rainfall on the preceding day did not exceed  $10 \text{ mm d}^{-1}$ , it could be that drainage beyond the root-zone occurred. Under these conditions, it could be argued that the higher total evaporation of grassland (Fig. 7.1) and transpiration of *E. viminalis* trees (Fig. 7.2) when compared to the absolute profile soil water storage reduction (e.g. during the summers of 1998/1999 and 1999/2000), suggests the occurrence of drainage beyond the root-zone<sup>18</sup>.

The more improved relationship (more similarities) between the transpiration and soil water storage reduction at the *E. viminalis* site (Fig. 7.2), compared to that at the grassland site (Fig. 7.1) can possibly be attributed to differences in the soil volume utilized for soil water extraction. The grassland utilizes a small soil volume compared

---

<sup>18</sup> This assumption can only be made if it is assumed that the total evaporation, transpiration and soil water storage estimates are correct.

to the *E. viminalis* trees, as a result of root distribution differences. Further, the soil water storage reduction at the grassland site is compared to the total evaporation of grassland, which not only consists of soil water extraction (transpiration) but also includes soil evaporation and evaporation of water intercepted by the grass canopy.

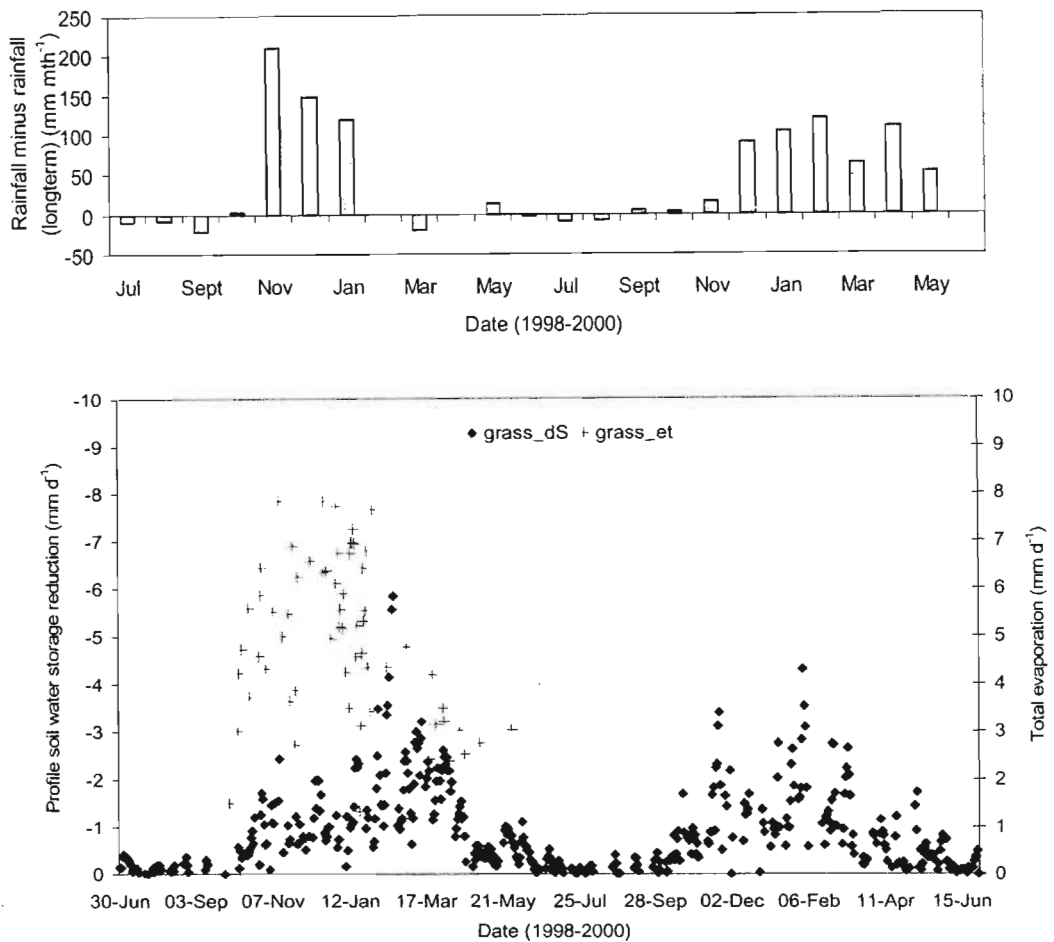


Fig. 7.1 Top: Differences between monthly total rainfall and monthly total long-term average rainfall at the research sites from July 1998 to June 2000. Bottom: Profile soil water storage reduction (grass\_dS) over a 1000 mm soil depth, and daily total evaporation of a grassland (grass\_et). This dataset exclude days with rainfall exceeding  $10 \text{ mm d}^{-1}$  or rainfall on the preceding day exceeding  $10 \text{ mm d}^{-1}$

### 7.3 Comparison of soil water storage reduction at a grassland and an *E. viminalis* site

The profile soil water storage reductions at the grassland and the *E. viminalis* sites reflect the soil water extraction by grass roots and *E. viminalis* tree roots, and possibly the drainage below the root-zones. These profile soil water content reductions between the sites were different (Figs 7.3 and 7.4).

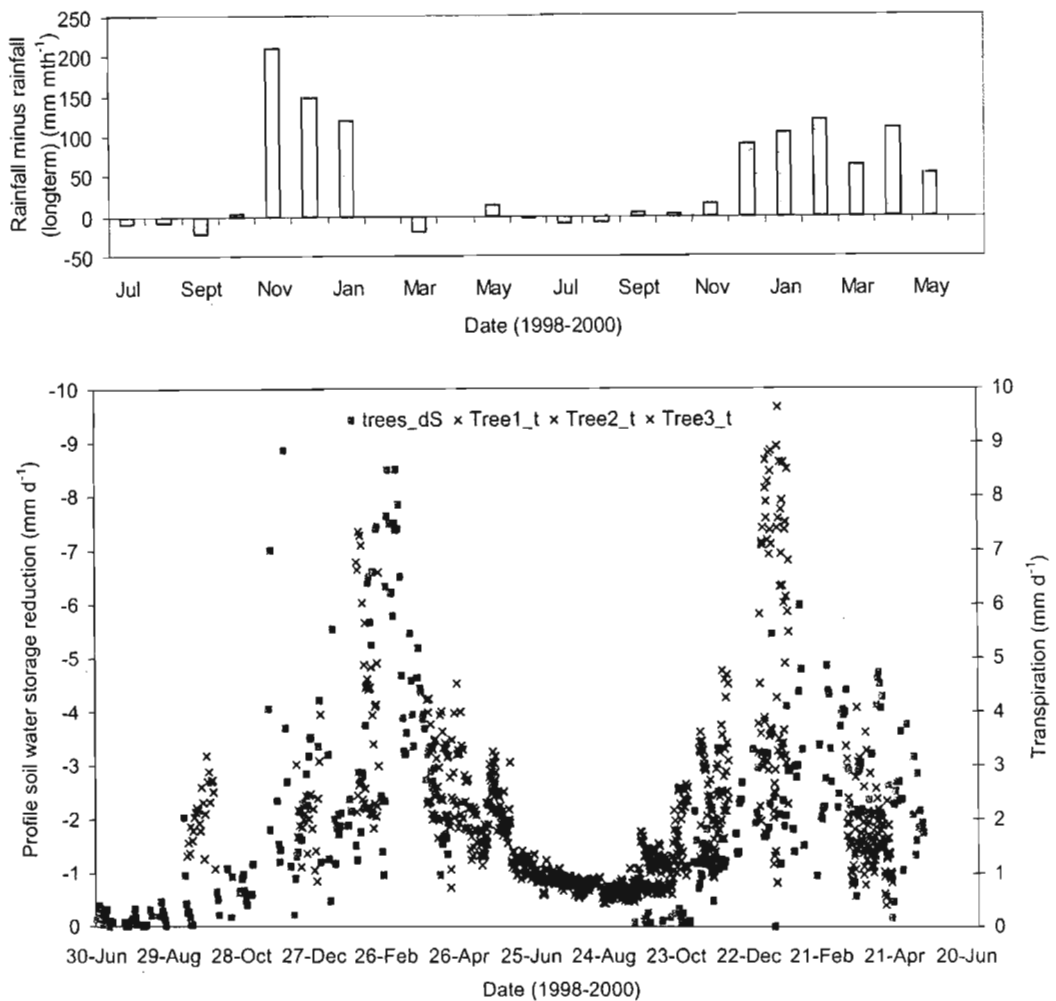


Fig. 7.2 Top: Differences between monthly total rainfall and monthly total long-term average rainfall at the research sites from July 1998 to June 2000.

Bottom: Profile soil water storage reduction ( $\text{trees\_dS}$ ) over a 1000 mm soil depth, and daily total transpiration of three trees ( $\text{Tree1\_t}$ ,  $\text{Tree2\_t}$  and  $\text{Tree3\_t}$ ). This dataset exclude days with rainfall exceeding  $10 \text{ mm d}^{-1}$  or rainfall on the preceding day exceeding  $10 \text{ mm d}^{-1}$



The largest differences in the profile soil water storage reductions between the two sites occurred during periods of summer when no significant rainfall ( $> 10 \text{ mm d}^{-1}$ ) events occurred, and during autumn (Figs 7.3 and 7.4). With the exceptions of short periods during spring (1998/1999 and 1999/2000), the profile soil water storage reductions at the *E. viminalis* site always exceeded that at the grassland site (Figs 7.3 and 7.4).

During spring, the soil water storage reduction at the grassland site exceeded that at the *E. viminalis* site generally by less than  $1.0 \text{ mm d}^{-1}$  and coincided with periods of higher total evaporation at the grassland site compared to the *E. viminalis* site (Fig. 7.1). During summer, the soil water storage reduction at the grassland site was between approximately  $0.5$  and  $10.0 \text{ mm d}^{-1}$  less than at the *E. viminalis* site. However, during autumn, this reduction at the grassland site was approximately  $1.0$  to  $6.0 \text{ mm d}^{-1}$  less than at the *E. viminalis* site.

During periods in summer, and especially during autumn and winter, the profile soil water storage reduction possibly indicates root water extraction or transpiration. From summer to autumn (1998/1999 and 1999/2000) it is clear that the daily profile soil water reduction at the *E. viminalis* site decreased over time from more than  $8.0 \text{ mm d}^{-1}$  (1998/1999 and 1999/2000) during summer to  $2.0 \text{ mm d}^{-1}$  (1998/1999) and  $4.0 \text{ mm d}^{-1}$  (1999/2000) during winter and autumn (Figs 7.3 and 7.4). However, the profile soil storage reduction over this period at the grassland site was less and decreased from approximately  $6.0 \text{ mm d}^{-1}$  (summer) to less than  $1.0 \text{ mm d}^{-1}$  (winter) (Figs 7.3 and 7.4). The trends in the profile soil water storage reductions towards the end of summer and during autumn compares well with the total evaporation (and transpiration) during these periods (Figs 7.1 and 7.2).

However, although some relationship existed between the trends in the reduction in the soil water storage at both the grassland and *E. viminalis* sites and the total evaporation, no linear relationships were found between the daily profile soil water storage reductions and total evaporation (and transpiration) for these sites (Fig. 7.5). This was mainly because of a lag in the soil water movement and the differences in the grassland and *E. viminalis* trees response to changes in soil water availability.

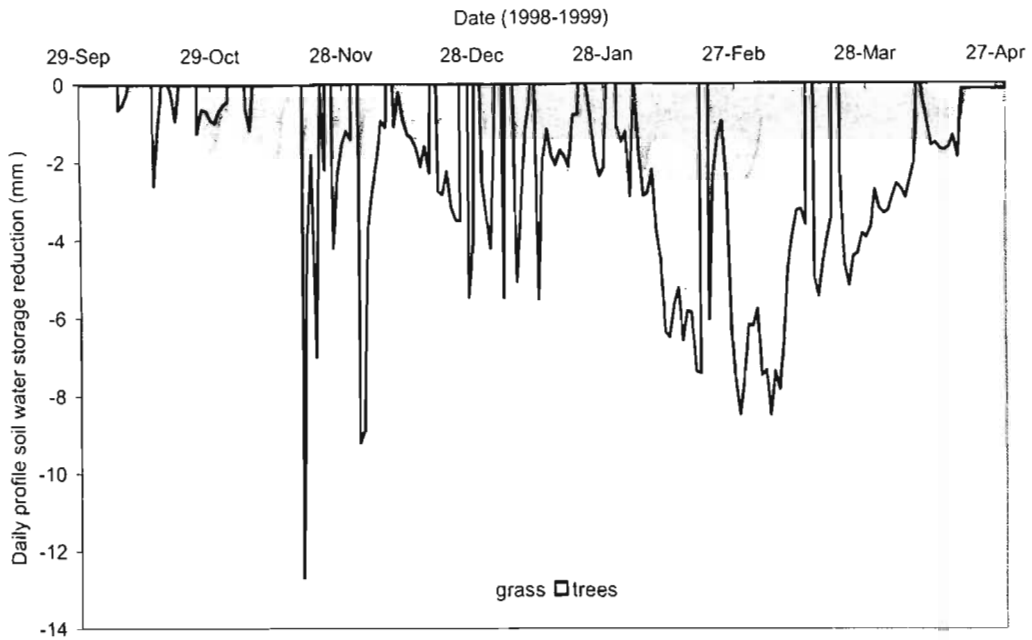


Fig. 7.3 Daily profile soil water storage reduction for a grassland (grass) and an *E. viminalis* site (trees) over a soil depth of 1000 mm for the period 8 September 1998 to 22 April 1999

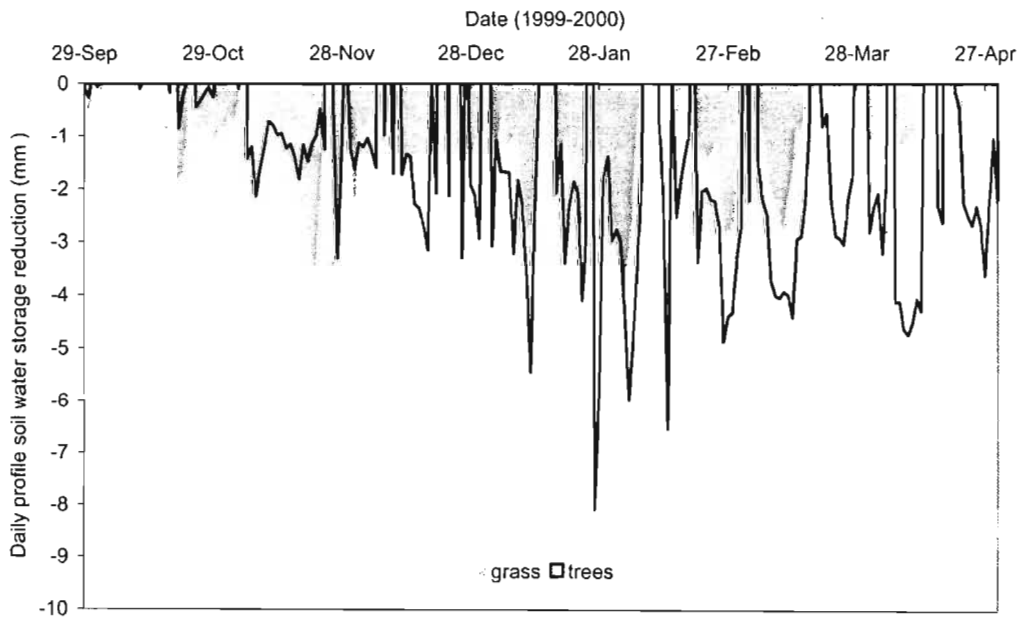


Fig. 7.4 Daily profile soil water storage reduction for a grassland (grass) and an *E. viminalis* site (trees) over a soil depth of 1000 mm for the period 17 September 1999 to 20 May 2000

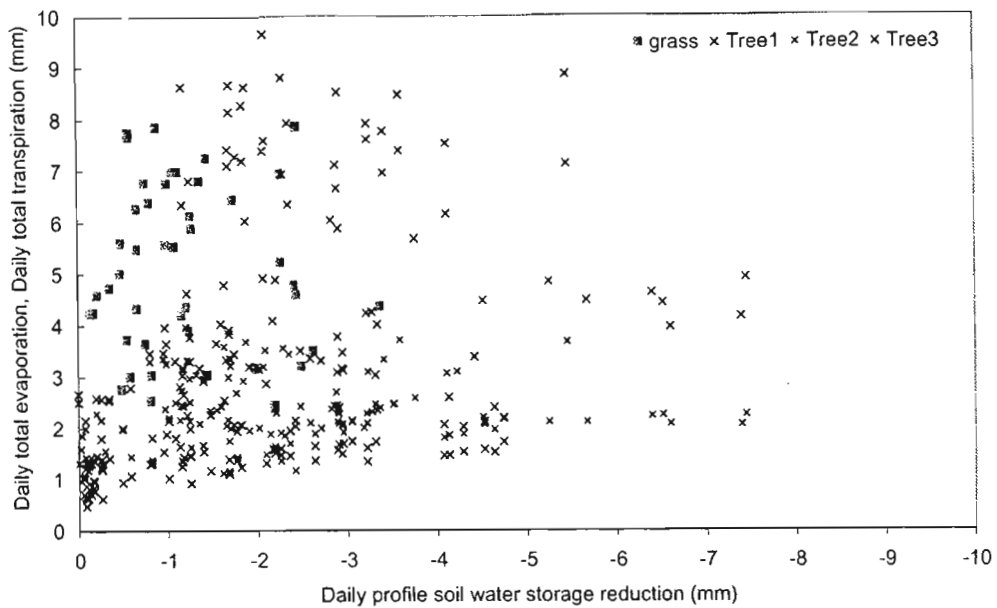


Fig. 7.5 Daily total evaporation for a grassland (grass) and daily total transpiration for three *E. viminalis* trees (Tree1, Tree2, Tree3) vs the daily profile soil water storage reduction over a soil depth of 1000 mm

#### 7.4 Summary and conclusions

The relationships between the soil water storage reduction, and the total evaporation (and transpiration) of a grassland and of *E. viminalis* trees were discussed in Chapter 7. The similar transpiration rates and soil water storage change rates at the *E. viminalis* site during periods of no significant rainfall, suggest no or little drainage beyond the root-zone. It was concluded that the reduction in the soil water storage at this site can be translated into the transpiration by the *E. viminalis* trees. It was also concluded that the differences between the soil water storage reduction and the total evaporation of the grassland, will translate into the occurrence of drainage beyond the root-zone.

The results from the field experiment presented in Chapters 6 and 7 are very specific to the conditions experienced during the field experiment (climatic, soil and plant) as described in Chapter 5. It gives a window period (1998-2000) of potential differences in the total evaporation and soil water storage of grassland and *E. viminalis* trees over the short-term. Because of this time limitation, the soil water balances of the grassland

---

and *E. viminalis* trees were simulated over the long-term to test the hypothesis of this study under different climatic and plant growth conditions. The results of these simulations are presented in *Chapter 8*.

## CHAPTER 8

### SOIL WATER BALANCES OF GRASSLAND AND *E. VIMINALIS* TREES MODELLED WITH THE SOIL WATER ATMOSPHERE PLANT (SWAP) MODEL

#### 8.1 Introduction

Chapters 6 and 7 investigated the effect of different vegetation types (grassland and *E. viminalis* trees) on the total evaporation and soil water storage relationships, through *in situ* measurements. From these results it is possible to test the hypothesis of the study (Section 1.5), and therefore to deduce the effect of grassland and *E. viminalis* trees on the drainage beyond the root-zone under the conditions experienced at this research site.

SWAP, the Soil Water Atmosphere Plant model (Van Dam *et al.*, 1997), was parameterised for the grassland and *E. viminalis* sites (Appendix F), and the soil water balances simulated over 30 years<sup>19</sup> (1 July 1964 to 30 June 1994). The results from these simulations allowed a comparison of the effect of different vegetation types (grassland *vs* *E. viminalis* trees) or the potential effect of a change in vegetation, on the soil water balances over the long-term. These simulations also enabled a comparison of the annual, seasonal and cumulative differences in the various components of the soil water balances for the two sites.

#### 8.2 Parameterisation of SWAP

##### 8.2.1 General

The soil water balances of a grassland and an *E. viminalis* site were separately simulated over a 30-year period (1 July 1964 to 30 June 1994) using SWAP. Long-term climatic data (rainfall, minimum and maximum air temperature) for a daily time step were available for the Secunda region from the South African Weather Bureau (undated) and Blaauw (2000). These data, together with climatic data (daily) collected during the field experiment (solar radiant density, minimum and maximum air temperature, relative

---

<sup>19</sup> A year refers to a 12 month period starting on 1 July and ending on 30 June the following year.

humidity, rainfall, wind speed, wind direction) (*Chapter 5*) were used with CLIMGEN (undated)<sup>20</sup>, a climatic generator programme to obtain the daily data required in SWAP. The required climatic data set consisted of daily total solar radiant density, relative humidity, minimum and maximum air temperature and wind speed. SWAP subsequently used the Penman-Monteith equation and the climatic input data to calculate the daily total reference evaporation.

## 8.2.2 Crop growth

The simple crop growth model, one of the three crop growth models within SWAP, was used in the soil water balance simulations at both the grassland and *E. viminalis* sites. The simple crop growth model represents a big leaf that intercepts water, transpires and shades the ground. The model requires leaf area index (or soil cover fraction), crop height (or crop factor) and rooting depth as a function of development stage, and is either controlled by air temperature or is linear in time.

### 8.2.2.1 Grassland growth

At the grassland site, the leaf area index (Fig. D. 3) and canopy height data collected during the field experiment (1 July 1998 to 30 June 2000) were used in the simulations (Table F.6). A third order polynomial, as a function of time, was fitted through the available leaf area index measurements (Fig. F.1). This provided leaf area indices that included both mowing and burning before the start of the new growing season. The rooting depth vs root density relationship used for the grassland site is that of Versfeld *et al.* (1998) (Tables F.5 and F.6). These root density data were obtained from a grassland site within the Secunda region with the same grassland species and on the same soil form (Rensburg as classified by the Soils Classification Working Group, 1991) used in these simulations (Versfeld *et al.*, 1998).

---

<sup>20</sup> CLIMGEN is a weather generator. CLIMGEN uses site specific information and different climatic data combinations to generate climatic data over a specified period. CLIMGEN also perform statistical analysis on the data generated to determine the significance of this data set. CLIMGEN programme available from: <http://www.bsyse.wsu.edu/climgen>.

### 8.2.2.2 *E. viminalis* tree growth

It was assumed that the largest differences in the soil water balances between the two sites would occur after the *E. viminalis* trees reached complete canopy cover, or behaved like a big leaf. Therefore, simulations at this site were for years three to ten of the suggested 10-year tree rotation (Smith, 2003). For these simulations (years three to ten) at the *E. viminalis* site a constant leaf area index of 2.6 (Dye, 2003), reflecting a complete canopy cover, was used. The canopy height data used in the simulations were based on *E. viminalis* trial data collected by the Institute of Commercial Forestry, Pietermaritzburg, South Africa (Smith, 2003). A second order polynomial (tree height as a function of time) was fitted to the tree height data (Fig. F.2). A combination of the rooting depth and density relationships (Tables F.5 and F.7) as estimated by Versfeld *et al.* (1998) for *E. viminalis* in the Secunda area, on a Rensburg soil form (Soil Classification Working Group, 1991), and that suggested by Knight (1999) for *Eucalyptus* were used at this site.

### 8.2.3 Soils information

The soil parameters used in the simulations at the grassland and *E. viminalis* sites were identical. The soil parameters determined *in situ* and in the laboratory for the grassland site (Tables A.1 and A.6), were used (Table F.9). These included the saturated hydraulic conductivity, particle size distribution and water retention characteristics (Table F.9). However, due to some limitations in the SWAP model execution, the low saturated hydraulic conductivity for the sites (Tables F.9) had to be adjusted to the lower end of the range ( $0.1 \text{ mm d}^{-1}$ ) accepted in SWAP. The observed maximum soil profile depth at the experimental site (1200 mm), were used in the parameterisation<sup>21</sup>. The bottom boundary condition of SWAP was set to allow free vertical drainage from the soil profile.

---

<sup>21</sup> Parameters for the 700-mm soil depth were used up to a depth of 1200 mm.

### 8.3 Annual differences in the soil water balances simulated for grassland and for *E. viminalis* trees

#### 8.3.1 Rainfall and total evaporation

During the 30-year simulation period, the annual rainfall ranged between 347 mm (1988/1989) and 1024 mm (1966/1967) representing a wide range of climatic conditions. During this period, the annual total evaporation<sup>22</sup> at the *E. viminalis* site (362 to 645 mm a<sup>-1</sup>) consistently exceeded that at the grassland site (283 to 467 mm a<sup>-1</sup>) by 26 to 223 mm a<sup>-1</sup> (Fig. 8.1, Table 8.1). The lowest annual total evaporation at both sites and the smallest differences in the total evaporation between the two sites (79, 32 and 26 mm a<sup>-1</sup> during 1988/1989, 1991/1992 and 1992/1992 respectively) was simulated during low rainfall years (e.g. 1988/1989 and 1991/1992), or, following a year with low rainfall (e.g. 1992/1993).

The differences in the total evaporation of the grassland and transpiration of *E. viminalis* trees were attributed to differences in the leaf area index, plant canopy height and rooting depth, length of growing season, soil water availability, soil water movement and depth of soil water extraction. Greenwood *et al.* (1985) and Dunin (2002) also attributed total evaporation differences between grassland (and pastures) and *E. viminalis* trees to differences in the depth of soil water uptake (or rooting), seasonality, leaf area index and canopy height. Silberstein *et al.* (2001) noted the importance of a deep soil profile at a *Eucalyptus* forest in retaining soil water from the preceding rainfall season, in order to supply adequate soil water to maintain high evaporation rates during long dry summers. Dunin (2002) also noted that the relative soil water content at which the soil water limits the potential total evaporation varies with the leaf area index. Calder (1998), using a limits concept, suggests that soil water and physiological controls are the principle limits to evaporation of both tall and short crops grown under dry temperate climates.

---

<sup>22</sup> Total evaporation includes transpiration, soil evaporation and evaporation of intercepted water.



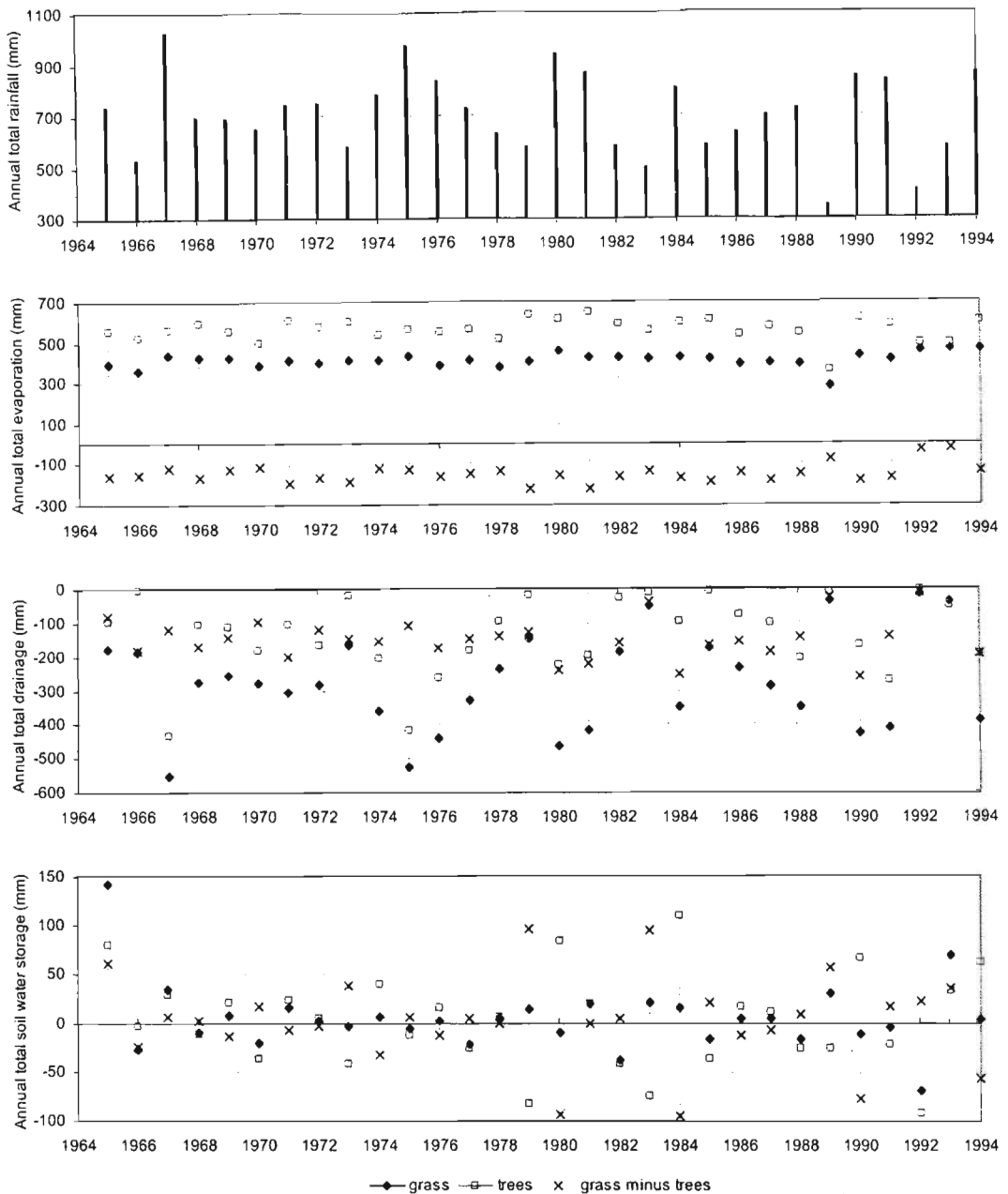


Fig. 8.1 Annual total rainfall (top) and simulations of annual total evaporation, annual drainage<sup>23</sup> and annual soil water storage for the grassland (grass) and *E. viminalis* (trees) sites from 1 July 1964 to 30 June 1994, and the differences in annual total evaporation, annual total drainage and annual soil water storages between the grassland and *E. viminalis* sites (grass minus trees)

<sup>23</sup> The drainage presented in *Chapter 9* is the bottom fluxes simulated with SWAP.

Table 8.1 Total and annual average (ave), maximum (max) and minimum (min) rainfall, total evaporation, soil water storage and drainage simulated at a grassland (Grass) and *E. viminalis* (Trees) site over a 30-year period (1 July 1964 to 30 June 1994). G-T represents the difference in total evaporation, soil water storage and drainage between the grassland and *E. viminalis* sites

Date	Rainfall (mm)	Total evaporation (mm)			Soil water storage (mm)			Drainage (mm)		
		Grass	Trees	G-T	Grass	Trees	G-T	Grass	Trees	G-T
Total	20961	12353	16814	-4461	141	90	51	-8330	-4045	-4285
Ave	699	412	561	-149	5	3	2	-278	-135	-143
Max	1024	467	645	-178	141	110	31	-15	-4	-11
Min	347	283	362	-79	-69	-92	23	-553	-432	-121

Everson *et al.* (1998) found the total evaporation of grassland to range between 651 and 752 mm a<sup>-1</sup>, whereas Greenwood *et al.* (1985) found the total evaporation of grazed pasture to be approximately 400 mm a<sup>-1</sup>. By contrast with the lower total evaporation for grassland, Greenwood *et al.* (1985) estimated total evaporation by *Eucalyptus* plantations, with phreatophytic root systems to be between 1600 and 2700 mm a<sup>-1</sup>. Kallarackal and Somen (1997) found that the transpiration of *E. tereticornis* was 853 and 1563 mm a<sup>-1</sup> for the rain-free days of two sites, whereas Soares and Almeida (2001) found the total evaporation of a *Eucalyptus* plantation to be 1345 mm a<sup>-1</sup>. Shiva and Banyopadhyay (1983) found annual total evaporation for *Eucalyptus* to be 1200 mm a<sup>-1</sup>, whereas Raper (2000) quoted values between 182 mm a<sup>-1</sup> (Hookey *et al.*, 1987) and 2690 mm a<sup>-1</sup> (Greenwood *et al.*, 1985). Differences in the annual total evaporation therefore exist between the various *Eucalyptus* species grown under different conditions.

### 8.3.2 Drainage

The consistently greater total evaporation at the *E. viminalis* site throughout the simulation period, resulted in consistently lower (11 to 121 mm a<sup>-1</sup> lower) drainage<sup>24</sup> at the *E. viminalis* site, compared to the grassland site (Fig. 8.1, Table 8.1). The drainage at the grassland site ranged between 15 and 553 mm a<sup>-1</sup> and between 4 and 432 mm a<sup>-1</sup> at the *E. viminalis* site. During a number of years, the drainage at the *E. viminalis* site was less than 50 mm a<sup>-1</sup> (1965/1966, 1972/1973, 1978/1979, 1981 to 1985, 1988/1989 and 1991 to 1993). During these years the annual rainfall was close to or less than the long-term average rainfall (Fig. 8.2). However, the simulation for the grassland site showed that drainage less than 50 mm a<sup>-1</sup> occurred only during 1982/1983, 1988/1989 and 1991 to 1993.

Jenkin and Irwin (1975) (cited by Dumsday *et al.*, 1989) found that in catchments under complete forest cover, recharge (and therefore drainage) was negligible. Raper (2000) also found that groundwater levels of pasture areas continued to increase whereas that under tree plantations declined.

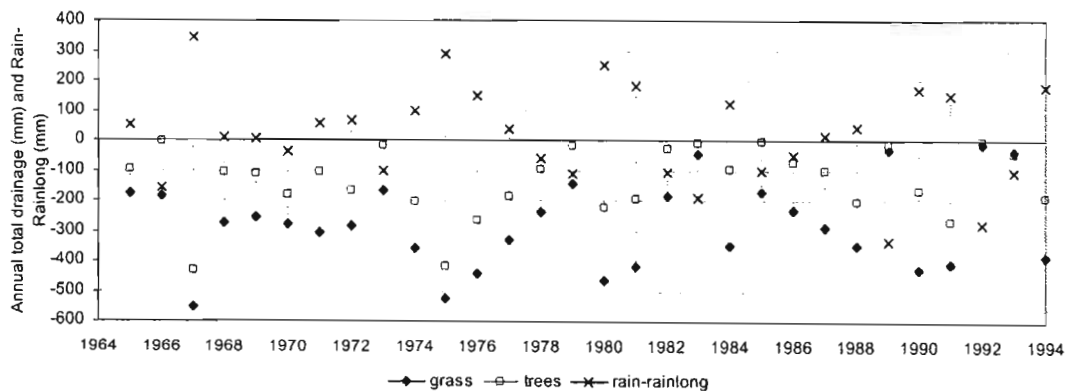


Fig. 8.2 Annual total drainage at the grassland (grass) and *E. viminalis* (trees) sites, and annual total rainfall exceeding the annual long-term average rainfall (Rain-Rainlong) from 1 July 1964 to 30 June 1994

<sup>24</sup> The bottom flux refers to the vertical flux of water out of the soil profile, and is generally drainage beyond the rooting zone.

Le Maitre and Scott (1997), Allen and Chapman (2000) and Gush *et al.* (2002) also illustrated how afforestation or deforestation at a catchment level changed the streamflow. Van Lill *et al.* (1980), Van Wyk (1987), Bosch and Smith (1989), Lesch and Scott (1993) (cited by Versfeld *et al.*, 1998) found that the catchment water yield decreased by up to 100 % following afforestation with *Eucalyptus* species. Dunin (2002) found that the recharge to the groundwater of three communities studied (*Eucalyptus* trees, lucerne, and annual crop and pasture), was approximately equal to the difference between annual rainfall and total evaporation.

In Western Australia, the effect of *Eucalyptus* trees on the soil water balance was also shown. Trees in the Mediterranean Australia are referred to as “biological wicks”, drawing water from the water table throughout the year. After the removal of the indigenous deep-rooted *Eucalyptus* species for agricultural and mining purposes, the level of the groundwater tables increased, flushing salts to the surface, increasing the salinity levels in the streams. The result is less arable land (Peck, 1983; Dumsday *et al.*, 1989; Bell *et al.*, 1990; Leuning *et al.*, 1991; Morris, 1991; Schofield, 1991; Ward, 1991 cited by Versfeld *et al.*, 1998; Raper, 2000; Dunin, 2002). In Western Australia, reforestation of areas with higher groundwater levels, where pasture previously existed, showed relationships between groundwater table reduction and the area reforested. Sikka *et al.* (2003) illustrated how a conversion from grassland to *E. globulus* decreases the low flow, peak flow and soil moisture losses in South India. These changes were more pronounced during the second rotation.

For above-average rainfall conditions, the drainage at both sites was directly related to the rainfall and the amount by which the rainfall exceeded the long-term average rainfall (Fig. 8.2). Where the rainfall exceeded the long-term average by more than 300 mm a<sup>-1</sup>, the drainage reached maximum values exceeding 400 mm a<sup>-1</sup> and 500 mm a<sup>-1</sup> at the *E. viminalis* and grassland sites respectively. Hodgson *et al.* (2001) also suggested that during a single high rainfall year, up to three times more recharge is likely than during a normal year.

### 8.3.3 Soil water storage change

The changes in the soil water storage simulated for grassland and *E. viminalis* trees, were small at both sites. In the simulations, the bottom boundary conditions at both sites were set to be free drainage out of the soil profile. This resulted in a small increase in profile soil water content or soil water storage from year-to-year and over the 30-year simulation period. Under those conditions nearly all the excess rainfall (i.e. not evaporated) exited the soil profile as drainage. Therefore, the soil water storage at both the grassland and *E. viminalis* sites remained fairly constant over the 30-year simulation period (Fig. 8.1). Differences in the vegetation type did therefore not affect the soil water storage in the long-term, and the long-term average soil water storage at the grassland and *E. viminalis* sites were only  $5 \text{ mm a}^{-1}$  and  $3 \text{ mm a}^{-1}$  respectively. Therefore, there were only a few years during which the soil water storage changed by more than  $50 \text{ mm a}^{-1}$  (Fig. 8.1). In general, nearly all of the soil water as a result of rainfall was utilized or removed from the soil profile by either total evaporation or drainage. The maximum annual increase in soil water storage at the grassland ( $141 \text{ mm a}^{-1}$ ) and *E. viminalis* sites ( $110 \text{ mm a}^{-1}$ ) occurred during 1964/1965 and 1983/1984 respectively with respective annual rainfalls of 730 and 800 mm. The maximum annual soil water depletion ( $69$  and  $92 \text{ mm a}^{-1}$  at the grassland and *E. viminalis* sites respectively) occurred during 1991/1992 for which the rainfall was  $403 \text{ mm a}^{-1}$  (Fig. 8.1).

Holmes and Wronski (1981) (quoted by Lima, 1984) found much larger differences in the soil water storage between a *Eucalyptus* forest (up to  $250 \text{ mm a}^{-1}$ ) and annual crops ( $180 \text{ mm a}^{-1}$ ). Lima (1984) also quoted Nicolls *et al.* (1982) who found an increase in the soil water depletion over time, after planting. During the first year, the soil water was not depleted, but during the second year, the soil water depletions were  $80 \text{ mm}$  over a 2-m soil depth, compared to  $230 \text{ mm}$  for mature trees. Sharma (1984) found under soil conditions without the effect of a water table, the soil water deficit under *Eucalyptus* forest was about three times larger than that under pasture. Sharma (1984), in a study on the total evaporation of *E. marginata* and *E. calophylla*, found that water was extracted from depths up to 6 m, creating a soil water deficit of up to  $450 \text{ mm}$ , compared to less than  $150 \text{ mm}$  under annual pastures.

#### **8.4 Importance of the different soil water balance components in relation to rainfall**

The magnitude (and therefore the importance) of total evaporation, soil water storage and drainage<sup>25</sup>, in relation to rainfall is shown (Fig. 8.3). Over the 30-year simulation period, the largest soil water balance component next to rainfall was total evaporation (Fig. 8.3). At the grassland and *E. viminalis* sites the total evaporation as a percentage of rainfall (total evaporation/rainfall) ranged between 43 and 86 %, and 55 and 121 % at the grassland and *E. viminalis* sites respectively. The exception at the grassland site was during 1991/1992 where the total evaporation exceeded the annual rainfall (403 mm a<sup>-1</sup>) by 14 %. Sharma (1984) and Dunin (2002) found that the total evaporation of a *Eucalyptus* catchment was more than 70 % and 80 % of the annual rainfall respectively. Soares and Almeida (2001) found that the total evaporation of *Eucalyptus* was 96 % of the rainfall.

The drainage was also a significant proportion of the rainfall, especially at the grassland site. In some instances the absolute magnitude of the drainage and total evaporation was similar (e.g. 1979 to 1981). At this site the magnitude of the drainage ranged between 10 and 54 % of the rainfall, but was lower at the *E. viminalis* site and ranged between 1 and 43 % (Fig. 8.3). Therefore, up to 54 and 43 % of the rainfall can potentially result in drainage at the grassland and *E. viminalis* sites respectively.

The soil water storage was a small proportion of the water balance and the annual rainfall (Fig. 8.3). The fractional soil water storages (soil water storage/rainfall) were similar for both sites, and ranged between 0 and 20 % for the grassland site and 0 and 22 % for the *E. viminalis* site (Fig. 8.3). The highest soil water storage fraction at the *E. viminalis* site was simulated during a dry year, when the soil water storage was depleted by 22 %. However, the highest value (soil water storage/rainfall) for the grassland was during a wet year, when the soil profile was recharged by 20 % through rainfall.

---

<sup>25</sup> The bottom fluxes discussed here refer to an absolute bottom flux.

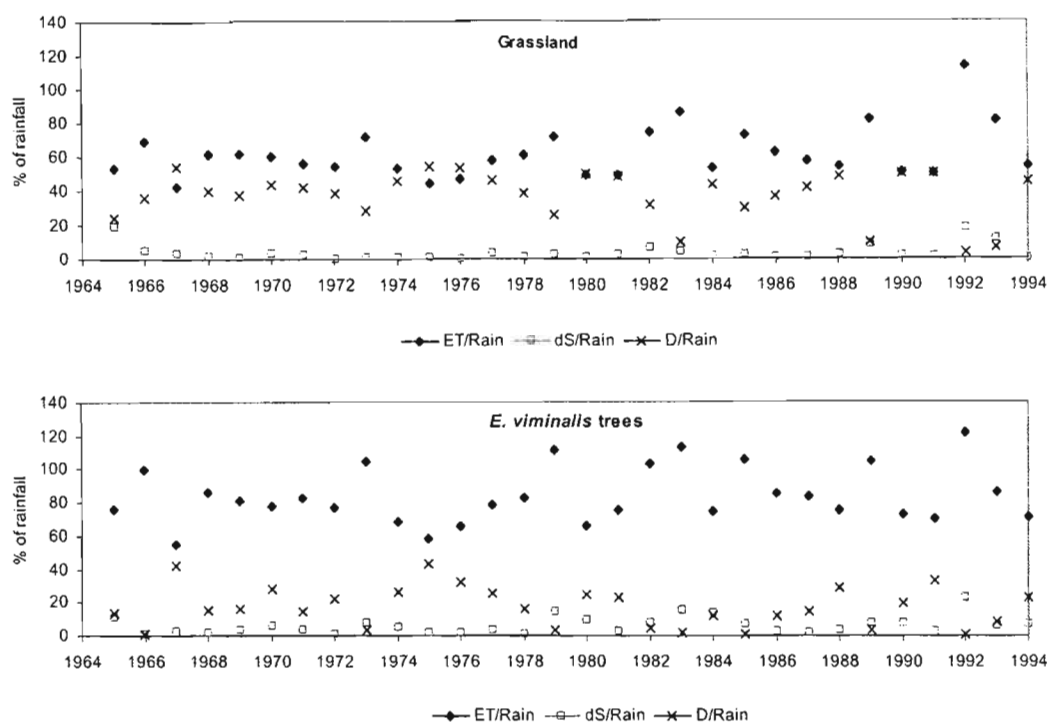


Fig. 8.3 Simulated annual total evaporation (ET/rain), annual total drainage (BF/rain) and annual total soil water storage (dS/rain) as a percentage of the annual total rainfall, for the period 1 July 1964 to 30 June 1994 for the grassland (top) and *E. viminalis* (bottom) sites

The results from the measurements confirm the simulations. The soil water balance results presented above are therefore likely to represent what happens in the long-term if the vegetation is changed from grassland to *E. viminalis*. The results from both the measurements and soil water balance simulations showed that the total evaporation is increased when grassland is replaced by *E. viminalis* trees.

### 8.5 Seasonal differences in the soil water balances simulated for grassland and *E. viminalis* trees

The lower annual drainage for the *E. viminalis* site, compared to that for the grassland site (Fig. 8.1), was mainly the result of the greater annual total evaporation for the *E. viminalis* site. The differences in the annual drainage for the two sites were the result of the seasonal differences in the drainage caused by seasonal differences in total evaporation. The daily (Figs 8.4 and 8.5) and accumulated (Fig. 8.6) total evaporation

and soil water storage illustrate the effect of different vegetation types on the drainage under different climatic conditions.

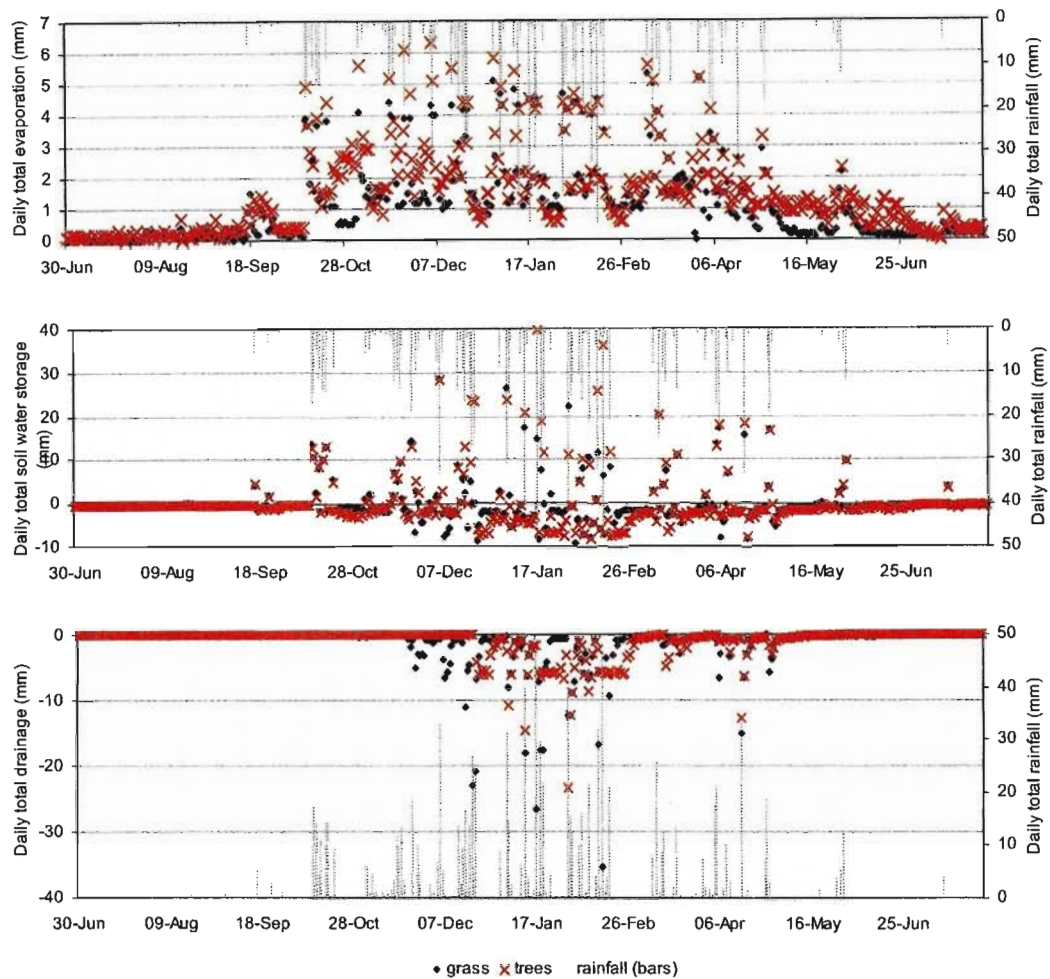


Fig. 8.4 Simulated daily total evaporation (top), daily soil water storage (middle) and daily total drainage for the grassland (grass) and *E. viminalis* (trees) sites (bottom) during an above-average rainfall year (1966/1967). Bars represent daily total rainfall.



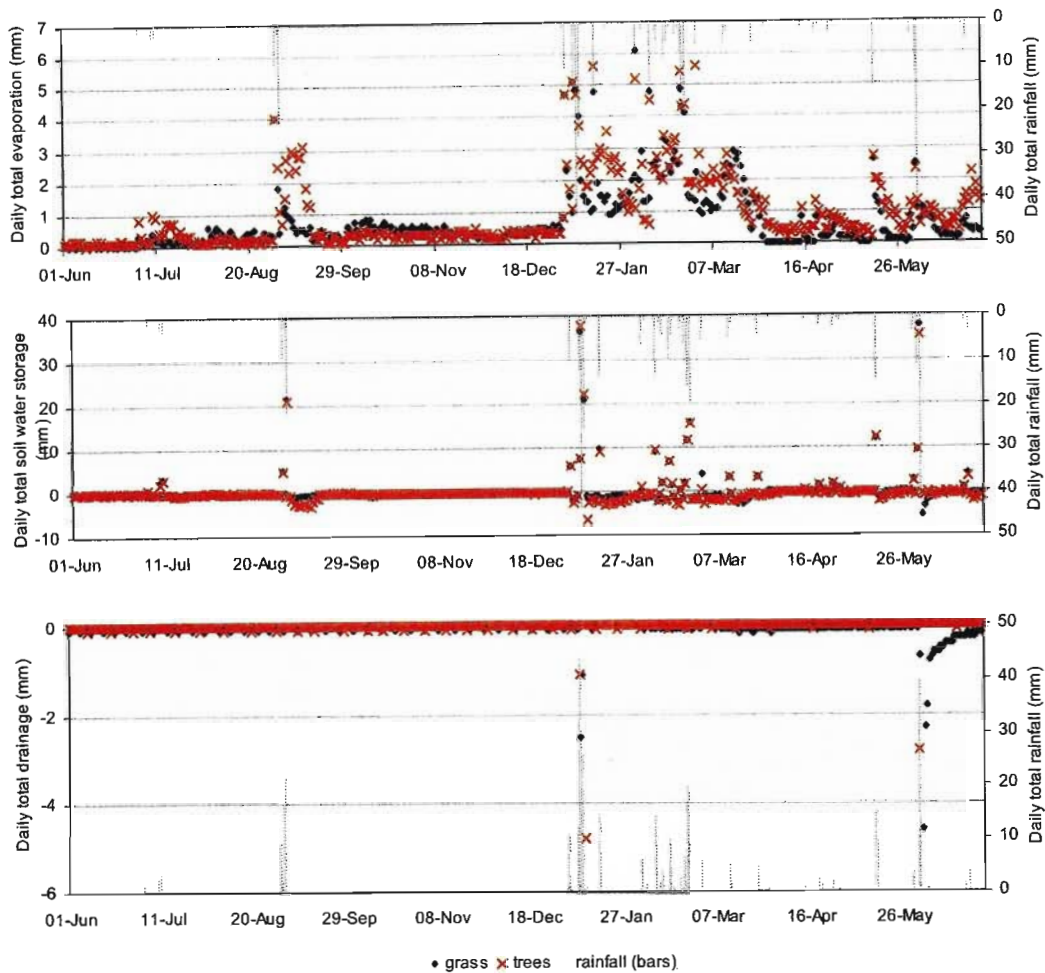


Fig. 8.5 Simulated daily total evaporation (top), daily soil water storage (middle) and daily total drainage for the grassland (grass) and *E. viminalis* (trees) sites (bottom) during a below-average rainfall year (1988/1989). Bars represent daily total rainfall.

Drainage occurs at both sites during the rainy season and normally follow large rainfall events (Figs 8.4 and 8.5). But, for below-average rainfall conditions (e.g. 1988/1989), drainage are limited to large rainfall events (Fig. 8.5). Also, drainage at both sites is smaller in magnitude for below-average rainfall years (0 to 4.8 mm d<sup>-1</sup>) than during above-average rainfall years (0 to 35.3 mm d<sup>-1</sup>) (Fig. 8.5). During an above-average rainfall year (e.g. 1966/1967), the daily drainage at the grassland site (up to 35.3 mm d<sup>-1</sup>) exceeded that at the *E. viminalis* site (up to 23.4 mm d<sup>-1</sup>) (Fig. 8.4), whereas fluxes for a below-average rainfall year are similar (4.6 and 4.8 mm d<sup>-1</sup> in magnitude at the grassland and *E. viminalis* sites respectively) (Fig. 8.5).

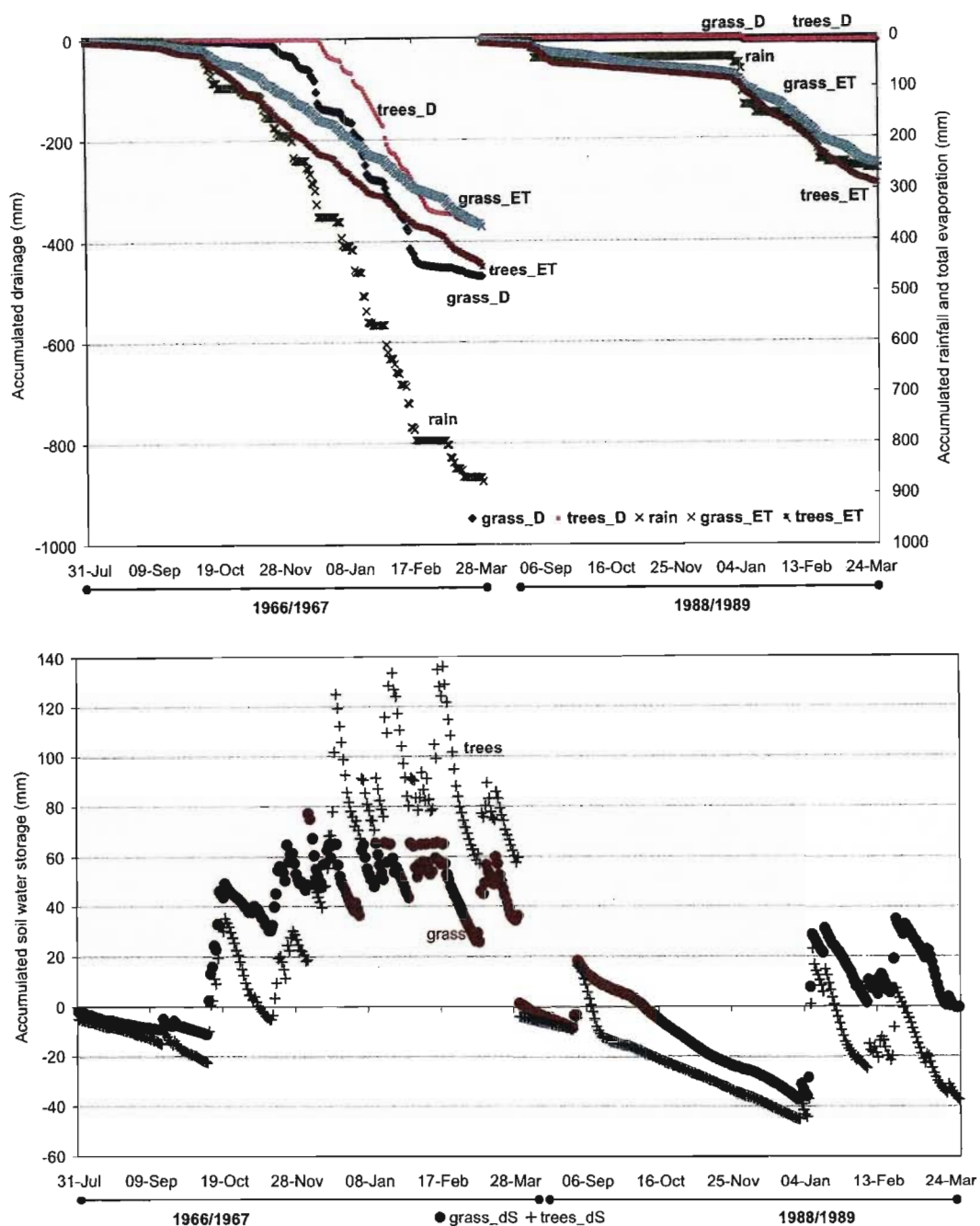


Fig. 8.6 Top: Accumulated simulated drainage at the grassland (grass\_D) and *E. viminalis* tree (trees\_D) sites, accumulated rainfall (rain) and accumulated total evaporation at the grassland (grass\_ET) and *E. viminalis* (trees\_ET) sites during an above-average (1966/1967 - left) and below-average rainfall year (1988/1989 - right). Bottom: Accumulated simulated soil water storage at the grassland (grass\_dS) and *E. viminalis* tree sites (trees\_dS) over the same period

Although the daily drainage shows an immediate response to individual rainfall events (Figs 8.4 and 8.5), the accumulative rainfall, soil water storage and total evaporation show the net effect of both immediate and lagged changes in the soil water balance components for both grassland and *E. viminalis* sites, on the drainage over the season (Fig. 8.6).

For example, following the start of the rainy season of an above-average rainfall year, drainage at the grassland site occurred earlier than that at the *E. viminalis* site (Fig. 8.6). At the grassland site, the accumulated drainage exceeded 20 mm after 185 mm of rainfall (26 November 1966), whereas the drainage at the *E. viminalis* site only exceeded 20 mm in magnitude a month later on 25 December 1966, after 352 mm of rainfall. The lower and lagged drainage at the *E. viminalis* site was the result of greater accumulated total evaporation (103 mm vs 232 mm at the grassland and *E. viminalis* sites respectively) and soil water storage (61 mm vs 99 mm at the grassland and *E. viminalis* sites respectively) (Fig. 8.6).

Very little drainage occurred during below-average rainfall years (e.g. 1988/1989) and depended on large rainfall events (Figs 8.5 and 8.6). Under these conditions, the accumulated rainfall was less than the total evaporation at both grassland and *E. viminalis* sites from July 1988 until January 1989; no drainage occurred whilst the soil water storage was slowly depleted at both sites. Furthermore, during this period, the accumulated total evaporation at both sites was very similar (Fig. 8.6).

The greater annual and accumulated total evaporation at the *E. viminalis* site especially during above-average rainfall years, and the associated lower soil water storage and drainage compared to the grassland site, was the result of the lower total evaporation and the lag in the start of the total evaporation (specifically transpiration) at the grassland site (Figs 8.4 to 8.6). These transpiration differences simulated are the result of differences in the seasonality of the grass and *E. viminalis* trees. The *E. viminalis* trees grow for the entire year, and therefore the total evaporation (and specifically the transpiration) will be maintained throughout this period, but will depend on the soil water availability (and rainfall) and the energy available to drive evaporation. However, the grass grows for only a limited number of months of the year and total

evaporation and the start of total evaporation (and transpiration) is dependent on physiological factors as well as climatic conditions.

The trends in the daily total evaporation at both sites were similar under both above and below-average rainfall years (e.g. 1966/1967 and 1988/1989). During above-average rainfall years, maximum total evaporation was reached during summer (6.3 and 5.2 mm d<sup>-1</sup> at the *E. viminalis* and grassland sites respectively), and minimum total evaporation during winter (less than 0.5 mm d<sup>-1</sup> at both sites) (Fig. 8.4). The largest differences in total evaporation between the two sites occurred at the start of summer, and during autumn and winter following rainfall events. During these periods, the total evaporation at the *E. viminalis* site exceeded that at the grassland site by as much as 2 mm d<sup>-1</sup> (Fig. 8.4). The greater total evaporation at the *E. viminalis* site during these periods is therefore dependent on rainfall events and soil water availability<sup>26</sup>. The increase in soil water storage at the *E. viminalis* site following a rainfall event was quickly depleted by the increased total evaporation by the *E. viminalis* trees (Fig. 8.4).

However, under below-average rainfall conditions, the period with total evaporation exceeding 0.5 mm d<sup>-1</sup> was much shorter than that of an above-average rainfall year (Fig. 8.5). Here, significant total evaporation occurred only following rainfall events (Fig. 8.5), but reached maximum values of up to 5.6 and 6.4 mm d<sup>-1</sup> at the *E. viminalis* and grassland sites respectively. The periodically greater total evaporation at the grassland site compared to the *E. viminalis* site suggests soil water stress experienced by the trees resulting in lower total evaporation. As the soil water storage was more depleted at the *E. viminalis* site than that at the grassland site, less soil water was available to drive total evaporation at the *E. viminalis* site (Fig. 8.5).

---

<sup>26</sup> SWAP, used for the soil water balance simulation, is a supply demand limited model, and the total evaporation is therefore directly related to the soil water availability.

### 8.6 Accumulated differences in the soil water balances simulated for grassland and *E. viminalis* trees for a tree rotation

The effect of the different vegetation types, grassland vs *E. viminalis*, on the drainage beyond the root-zone and the other soil water balance components over an extended period, is clearly illustrated through the accumulated differences in the drainage for years three to ten of a tree rotation (Fig. 8.7, Table 8.2). The grassland and *E. viminalis* tree site soil water balances (Fig. 8.7) are for the period 1 July 1972 to 30 June 1980, from the time the trees reached complete canopy cover (year three of the tree rotation) until maturity (year ten of the tree rotation).

During years three to ten of a tree rotation (e.g. 1 July 1972 to 30 June 1980), the rainfall differed by  $400 \text{ mm a}^{-1}$ , with five out of the eight years being above-average rainfall years, and exceeding the long-term average rainfall by up to  $289 \text{ mm a}^{-1}$  (Fig. 8.7, Table 8.2). The rainfall increased from  $578 \text{ mm a}^{-1}$  during the first year (1972/1973) to a maximum of  $969 \text{ mm a}^{-1}$  during the 3<sup>rd</sup> year, where after it decreased again over the next four years to reach  $569 \text{ mm a}^{-1}$ . The last year (1979/1980) was again an above-average rainfall year ( $933 \text{ mm a}^{-1}$ ). The rainfall over this eight year period accumulated to  $5995 \text{ mm}$ .

From the start of this simulation period (1972/1973), the total evaporation at the grassland was less than that at the *E. viminalis* site (Fig. 8.7). The difference in total evaporation increased over the eight years to a total of  $1268 \text{ mm}$ . The greatest difference in the total evaporation between the two sites, and the highest total evaporation at the *E. viminalis* site occurred during the lowest rainfall years (1972/1973 and 1978/1979). The trees depleted the soil water storage by  $42$  and  $102 \text{ mm a}^{-1}$  respectively during these two years. During 1972/1973 and 1978/1979 the drainage at both sites were also the lowest ( $-18$  and  $-19 \text{ mm a}^{-1}$  at the *E. viminalis* site and  $-164$  and  $-146 \text{ mm a}^{-1}$  at the grassland site) of all eight years (Fig. 8.7). During the other years, the total evaporation at the grassland site was consistently lower (by  $121$  to  $157 \text{ mm a}^{-1}$ ), than that at the *E. viminalis* site (Fig. 8.7, Table 8.2).

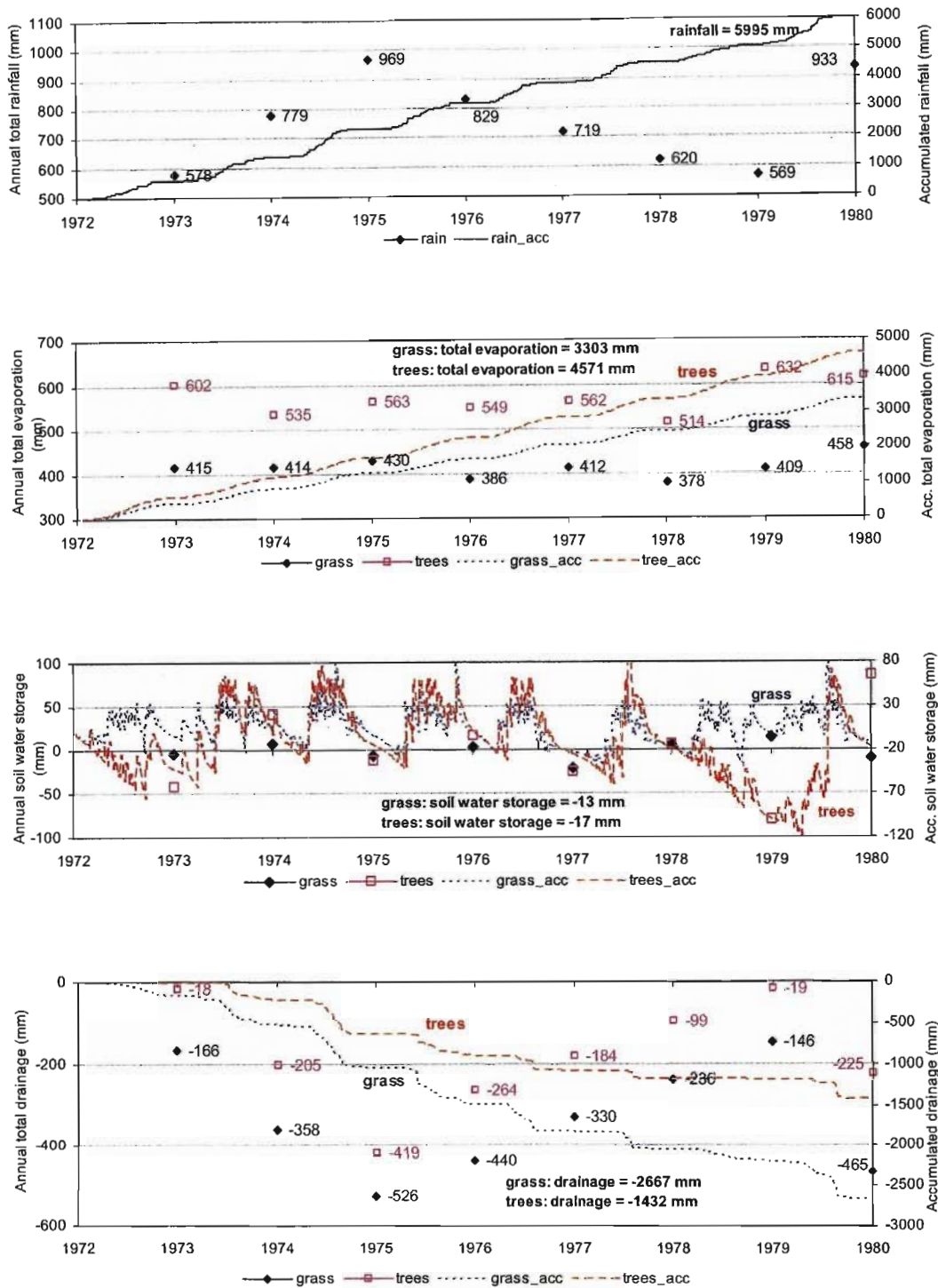


Fig. 8.7 Total annual (grass and trees) and accumulated (grass\_acc and trees\_acc) rainfall, and simulated total evaporation, soil water storage and drainage at the grassland (grass) and *E. viminalis* (trees) sites for the period 1 July 1972 to 30 June 1980 (years three to ten of a tree rotation)

Table 8.2 Total and annual average (ave), maximum (max) and minimum (min) rainfall, total evaporation, soil water storage and drainage simulated at a grassland (Grass) and *E. viminalis* (Trees) site over years three to ten of a tree rotation (e.g. 1 July 1972 to 30 June 1980). G-T represents the difference in total evaporation, soil water storage and drainage between the grassland and *E. viminalis* sites

Date	Rainfall (mm)	Total evaporation (mm)			Soil water storage (mm)			Drainage (mm)		
		Grass	Trees	G-T	Grass	Trees	G-T	Grass	Trees	G-T
Total	5995	3303	4571	-1268	-13	-17	4	-2667	-1432	-1235
Max	969	458	632	-	-22	-82	-	-526	-419	-
Min	569	378	514	-	-4	84	-	-146	-18	-

The total evaporation difference of 1268 mm between the two sites over the eight year period (or average  $0.43 \text{ mm d}^{-1}$ ), was directly translated into a difference of 1235 mm in the drainage (or average of  $0.42 \text{ mm d}^{-1}$ ) with the lower drainage occurring at the *E. viminalis* site (Fig. 8.7). The similar total evaporation and drainage differences were the result of the small changes in and similar soil water storages at the grassland (-13 mm) and *E. viminalis* (-17 mm) sites over the eight year period (Fig. 8.7, Table 8.2).

Therefore, for this site with a rainfall of 5995 mm over eight years, a rotation of trees instead of grassland, could increase the total evaporation by 1268 mm (or average  $159 \text{ mm a}^{-1}$ ). This increase in total evaporation could subsequently reduce the drainage beyond the root-zone by 1235 mm more than a grassland over eight years (or average  $154 \text{ mm a}^{-1}$ ). This decrease is equivalent to  $1540 \text{ m}^3 \text{ ha}^{-1} \text{ a}^{-1}$  or  $1.54 \text{ M} \ell \text{ ha}^{-1} \text{ a}^{-1}$ .

## 8.7 Summary and conclusions

The results from the modelling exercise illustrated the effect of different vegetation types (grassland and *E. viminalis* trees) on all the soil water balance components (total evaporation, soil water storage, runoff and drainage) in the short- and long-term, and not only on the total evaporation (and transpiration) and the profile soil water storage in the short-term as described in *Chapters 6 to 7*.

The results from the long-term simulations showed a higher total evaporation at the *E. viminalis* site, compared to the grassland site as suggested by other authors. It confirmed the hypothesis that afforestation with *E. viminalis* trees will cause a reduction in the drainage beyond the root-zone. From the results it can be concluded that a stand of *E. viminalis* trees with a closed canopy not only reduce the drainage below the root-zone, but also delay the occurrence of the drainage, especially under above-average rainfall conditions. The results further showed that a stand of *E. viminalis* trees has the potential to reduce the drainage by 1235 mm more than grassland over a period of eight years (or average 154 mm a<sup>-1</sup>). This decrease is equivalent to 1540 m<sup>3</sup> ha<sup>-1</sup> a<sup>-1</sup> or 1.54 Mℓ ha<sup>-1</sup> a<sup>-1</sup>. The annual average reduction in drainage below the root-zone caused by *E. viminalis* trees (1.79 Mℓ ha<sup>-1</sup> a<sup>-1</sup>), is a small reduction when compared to the influx of water into mineworkings. E.g. the influx of water into a bord-and-pillar mine range between 0.5 and 4 Mℓ d<sup>-1</sup> per area mined and up to 17000 Mℓ d<sup>-1</sup> per area mined under high extraction mining (Hodgson and Krantz, 1998; Hodgson *et al.*, 2001). It can also be concluded that under conditions of above-average rainfall, drainage will occur when the rainfall exceeds the long-term average rainfall, irrespective of the existing vegetation. Hodgson *et al.* (2001) also suggested that during a single high rainfall year, up to three times more recharge is likely than during a normal year.



## CHAPTER 9

### CONCLUSIONS AND RECOMMENDATIONS

#### 9.1 Conclusions

This study focused on afforestation with *Eucalyptus viminalis* trees to limit the ingress of water into mine workings. The hypothesis of this study was that a change in vegetation, from grassland to fast-growing and potentially high water-using trees like *Eucalyptus*, could potentially reduce the drainage of water below the root-zone and into the mine workings.

The results from this study showed the differences in the soil water balance of a grassland and an *E. viminalis* site. The results from both the field measurements and the modelling show the lower profile soil water content at the *E. viminalis* site, compared to the grassland site, and the associated higher total evaporation at the *E. viminalis* site, compared to the grassland site. These results are in accordance with that found by other authors (e.g. Greenwood *et al.*, 1985). From the higher total evaporation and lower profile soil water content calculated at the *E. viminalis* site, it is possible to conclude that the drainage beyond the *E. viminalis* site would be lower than at the grassland site. The results from the 30-year soil water balance modelling, supported the assumption that *E. viminalis* trees could potentially reduce the drainage below the root-zone. The modelling results further showed that the onset of drainage is delayed at the *E. viminalis* site, compared to the grassland site.

The total evaporation and associated profile soil water content differences calculated between the grassland and *E. viminalis* sites during the season were mainly the result of differences in the depth of soil water extraction, associated root distribution and plant physiological differences (including senescence). At the start of the growing season in spring, the total evaporation of grassland exceeded the transpiration of *E. viminalis* trees because of physiological differences, the availability of soil water to roots and a pathogen infection at the tree site. However, maximum transpiration rates of *E. viminalis* trees (up to 9 mm d<sup>-1</sup>) were reached towards the end of spring and during

summer, and exceeded the maximum total evaporation of grassland (6 to 8 mm d<sup>-1</sup>). However, since the *E. viminalis* tree transpiration excludes evaporation of intercepted water or transpiration of the understorey, it is expected that the total evaporation of *E. viminalis* trees will exceed that at the grassland site even more. This higher transpiration of *E. viminalis* trees could be attributed to the recovery of the *E. viminalis* trees and the availability of soil water to the greater depth within the soil profile. It was concluded that frost, fire and pathogens affect the state of *E. viminalis* trees, their transpiration and their possible impact of a change in vegetation on the soil water balance. However, minimum total evaporation of grassland occurs from autumn to spring. During the winter period, the total evaporation of the grassland was expected to be less than 0.5 mm d<sup>-1</sup>, whereas the *E. viminalis* trees maintained transpiration rates of 1 to 3 mm d<sup>-1</sup>.

The relationship between the soil saturation (profile and individual soil layers) and the transpiration, showed the dependence of *E. viminalis* trees on the availability of soil water for maximum transpiration rates to be achieved. High transpiration rates (> 5 mm d<sup>-1</sup>) only occurred at high profile soil saturations (> 85 %). By contrast, maximum total evaporation of grassland (> 5 mm d<sup>-1</sup>) was reached under low (55 to 60 %) and higher (> 90 %) profile saturation. However, the soil layers (0 to 300 mm) containing the grassland roots had high saturations.

From the differences in the relative saturations of the soil layers at the grassland and *E. viminalis* sites, it can be concluded that differences exist in the depth of soil water extraction by roots and the associated root distribution. At the grassland site, major changes in soil layer relative saturations during summer were only visible in the upper 300-mm soil depth. This is the result of water extraction by grassland roots during summer. In contrast, no major changes in the relative saturations were observed within the 500- to 900-mm soil depths, as no grassroots are generally situated at these depths. However, at the *E. viminalis* site, the most important relative saturation changes occurred at the 700- and 900-mm soil depths, where it is assumed that most of the tree roots occur.

The impact of *E. viminalis* trees on the site soil water balance, compared to the grassland site, was illustrated in the differences in the profile soil water content and the soil water storage changes. It can be concluded that the *E. viminalis* trees impact more on the profile soil water content and the soil water storage changes than the grassland. Throughout the experiment, the profile soil water content at the grassland site exceeded that at the *E. viminalis* site. The largest differences occurred following frost (autumn) and the senescence of the grassland, until the new growing season (spring). The reduction in the soil water storage (1000 mm soil depth) at the grassland site was also less than that at the *E. viminalis* site, throughout the season. The similar transpiration rates and soil water storage change rates at the *E. viminalis* site, during periods of no significant rainfall, suggest no or little drainage beyond the root-zone. It was concluded that this reduction in the soil water storage can be translated into the transpiration by the *E. viminalis* trees. However, it was concluded that the differences between the soil water storage reduction at the grassland site and the total evaporation of the grassland, will translate into the occurrence of drainage beyond the root-zone.

The results from the long-term simulations showed the higher total evaporation of *E. viminalis* trees, compared to grassland and support the observations by other authors. It confirmed the hypothesis that afforestation with *E. viminalis* trees will result in a reduction in the drainage beyond the root-zone, compared at the grassland site. The results showed how the *E. viminalis* trees with a closed canopy not only reduce the drainage beyond the root-zone, but also delay the occurrence of the drainage, especially under above-average rainfall conditions. Over a period of eight years, a stand of *E. viminalis* trees with a closed canopy has the potential to reduce the drainage by 1432 mm (or average 179 mm a<sup>-1</sup>). This decrease is equivalent to 1790 m<sup>3</sup> ha<sup>-1</sup> a<sup>-1</sup> or 1.79 Mℓ ha<sup>-1</sup> a<sup>-1</sup>. This is a small reduction when compared to e.g. the influx of water into a bord-and-pillar mine where the influx of water range between 0.5 and 4 Mℓ d<sup>-1</sup> per area mined and up to 17000 Mℓ d<sup>-1</sup> per area mined under high extraction mining (Hodgson and Krantz, 1998; Hodgson *et al.*, 2001). However, the simulation results illustrated that under conditions of above-average rainfall, drainage will occur when the rainfall exceeds the long-term average rainfall, irrespective of the existing vegetation. Hodgson *et al.* (2001) also suggested that during a single high rainfall year, up to three times more recharge is likely than during a normal year.

A change in vegetation from grassland to *E. viminalis* (or from a vegetation type with a short growing season, and a lower annual total evaporation, to a vegetation type with an all year growing season and therefore a higher annual total evaporation), will reduce and delay the drainage of water below the soil profile and therefore possibly into the mine workings, especially under above-average rainfall years. However, where the rainfall exceeds the long-term average rainfall, the type of vegetation will possibly not influence the occurrence of drainage.

This work gave a comprehensive account of the differences in the soil water relations of grassland and *E. viminalis* trees overlying coal mine working. Few other studies in South Africa compared the total evaporation and soil water relations of grassland and *E. viminalis* trees in so much detail. State of the art monitoring techniques were used and produced valuable comparison of their use in expansive clay profiles. The work should contribute to management decisions focussed on limiting ingress of water into mine workings.

## **9.2 Recommendations relating to further research**

### **9.2.1 General**

Section 1.2.4 provides possible solutions to reduce the ingress of water into the mine workings, and to manage the quality of this water. These include environmentally related solutions, of which this study focussed on the effect of afforestation with *E. viminalis* trees to prevent or manage drainage into mine workings. This study showed the differences in the impact of grassland and *E. viminalis* trees on the site soil water balance. The environmentally related solutions also include agroforestry or agronomic measures. Afforestation (or reforestation), agroforestry or agronomic measures therefore involve the planting of *Eucalyptus* or other high water-using trees or vegetation upstream or downstream to decanting areas, or above high extraction panels (Dumsday *et al.*, 1989; Versfeld *et al.*, 1998; Hodgson *et al.*, 2001; Jarman *et al.*, 2001). The use of deep-rooted, perennial crops, e.g. lucerne, instead of seasonal shallow-rooted crops are suggested as well as intensive, continuous cropping with a

decreased fallow period, minimum tillage, and an increased number of cultivations (Dumsday *et al.*, 1989).

The effectiveness of afforestation with *Eucalyptus* species or re-vegetation with other high water using vegetation in reducing drainage, compared to grassland in the Highveld area of South Africa, will depend on the success of the establishment of the vegetation (trees and other), and the cover (leaf area) reached (e.g. Versfeld *et al.*, 1998), as conditions in the Mpumalanga mining area are less favorable for forestry than other forestry areas in South Africa. Unfavourable conditions include an average annual rainfall of 680 mm a<sup>-1</sup>, frost, shallow soil depths in some areas (less than 500 mm), and the swelling and shrinking characteristics of some soil forms. Other factors that will influence the effectiveness of these trees include tree species selected, position in the landscape, planting density, topography, underground mining method, soil properties, depth of groundwater table and water quality.

As in the study by Versfeld *et al.* (1998) on the water use of different vegetation types in the mining environments, this study does not provide “exact predictive knowledge” (Versfeld *et al.*, 1998) in terms of water use or drainage into mine workings. However, the current study does increase our knowledge on the possible impacts of a change in vegetation on the soil water balance. Therefore, additional research is required, to provide predictive tools in terms of water management and vegetation changes. Versfeld *et al.* (1998) discuss research requirements in terms of hydrology and silviculture and relating to afforestation, in detail. Hydrological requirements include:

- site water use,
- species water use,
- relationships between age class and water use,
- grassland water use vs grassland management,
- effectiveness of afforestation,
- extrapolation of results to quaternary and primary catchment scale, and
- effect of afforestation to manage water quality, on the water supply (Versfeld *et al.*, 1998).

Important silvicultural and site research requirements include:

- genetic selection and clonal propagation,
- root studies,
- forest management practices including species selection, method of establishment, espacement, fertilization, length of rotation cycle and regeneration methods,
- agroforestry,
- irrigation with waste water, and
- sustainability (Versfeld *et al.*, 1998).

Recommendations relating to regional water resources, the use of alternative vegetation types, and the increase of total evaporation to potential rates, will be discussed below.

### **9.2.2 Impact of trees on the regional water resources**

Although advocating the growing of trees may be a solution for helping to prevent the ingress of excess water into mines, the extensive planting of trees could have negative impacts on the regional water resources of the Vaalriver catchment. This may conflict with the allocatable water rights within the catchment. Since commercial forestry has been declared a streamflow reduction activity in terms of the new National Water Act (Act No. 36, 1998), licensing for afforestation would need to be considered. This would have to be seen in the context of the total amount of afforestation planned and its impact on reducing the catchment water resources.

However, in the context of the Mpumalanga coal mining area and other mining areas, the issues of water quality may far outweigh those of water quantity, and some form of trade-off may be necessary. The economic implications of these issues would also need to be studied. Thus, the impact of increasing the area planted with potentially high water-using trees such as *Eucalyptus* species on the Vaalriver catchment needs to be investigated.

### 9.2.3 Research into the effectiveness of tree species other than *Eucalyptus*, other agricultural crops and agroforestry, in preventing and/or reducing drainage beyond the root-zone

A number of research projects have been concerned with the water use of grasslands and *Eucalyptus* trees within the Highveld mining environment (Versfeld *et al.*, 1998; Jarmain *et al.*, 2001). Recommendations have been made on potentially high water using *Eucalyptus* species suited to the Mpumalanga area (Versfeld *et al.*, 1998). These include *E. viminalis*, *E. macarthurri*, *E. camaldulensis*, *E. smitthi* and *E. nitens*. Local and international research on catchment hydrology has also been concerned with the effect of afforestation with *Eucalyptus* trees on the water balance.

Versfeld *et al.* (1998) also suggested the use of *Acacia mearnsii*, mulberries (*Morus spp.*) and willows (*Salix spp.*). However, in South Africa, little is known about the water use of these species, other potentially high water using indigenous trees and agroforestry combinations. Weiersbye (2002) is involved in trials testing the potential impact of woody, semi-woody vegetation (indigenous and exotic/invasive) and other vegetation (e.g. reeds) in containing pollution. These options need to be investigated further.

Other important options that need to be investigated, include agroforestry systems (Versfeld *et al.*, 1998; Dumsday *et al.*, 1989), deep rooted perennial grasses (Versfeld *et al.*, 1998) and legumes (Dunin, 2002), multi-cropping systems (Dunin, 2002), and strip planting (White *et al.*, 2002).

Although, *Eucalyptus* has been used to drain marshes, and manage waterlogging and salinity, White (2000) and Dunin (2002) suggested that mixed plantings (*Eucalyptus* species, perennial, woody, herbaceous species, lucerne), may result in a significant change in the drainage as the soil water of a larger portion of the profile will be utilized. Dunin (2002) found that a combination of 12 % mixed tree cover, 30 % lucerne and 58 % agricultural crops or pasture, will also control the drainage to within 5 mm a<sup>-1</sup>. White *et al.* (2002) confirmed that where groundwater is accessible, contour-planted belts comprising four *Eucalyptus* species are effective in reducing groundwater recharge, with minimum tree-crop competition for water.

#### **9.2.4 Research into the increase of evaporation of trees (or high water use agricultural crops) to potential evaporation rates, through irrigation**

If trees or grasses were transpiring at potential rates, a larger fraction of the rainfall would be evaporated back into the atmosphere and even less water would be available to drain beyond the root-zone. Evaporation rates equal to or exceeding potential rates, occur when enough energy is available to drive evaporation and when enough soil water is available to avoid any possible drought (soil water) stress conditions. For trees, drought stress generally occurs during winter and parts of autumn and spring. Irrigating trees during these periods could therefore result in maximum evaporation being maintained for a longer time period. It may also present a way of reducing excess water in storage dams. Research into ways of increasing transpiration by trees, deep-rooted perennial crops and agroforestry combinations to potential levels, through irrigation could therefore be valuable. Barnard *et al.* (1998) has been involved in screening crops, pastures and wetland species for tolerance of polluted water originating in coal mines.



## REFERENCES

- Allen R.G., Jensen M.E., Wright J.L., Burnman R.D., 1989. Operational estimates of reference evapotranspiration. *Agron. J.* 81, 650-662.
- Allen R.G., Pereira L.S., Raes D., Smith M. 1998. Crop evaporation: Guidelines for computing crop water requirements. *FAO Irrigation and Drainage Paper no. 56*, 300 pp.
- Allen A.R., Chapman D.V., 2000. A review of impacts of forestry on groundwater and implications for forestry management. In: Sililo, O. *et al.* (Editors) *Proceedings of the XXX IAH congress on Groundwater: Groundwater: Past achievements and future challenges Cape Town/South Africa, 26 November to 1 December 2000*, AA Balkema, Rotterdam, pp 863-868.
- Angus D.E., Watts P.J., 1984. Evapotranspiration - how good is the Bowen ratio method? *Agric. Water Manage.* 8, 133-150.
- Barnard R.O., Rethman N.F.G., Annandale J.G., Mentz W.H., Jovanovic N.Z., 1998. The screening of crop, pasture and wetland species for tolerance of polluted water originating in coal mines. *WRC Report no. 582/1/98*, ISBN no. 1 86845 433 9, 337 pp.
- Barr A.G., King K.M., Gillespie T.J., Den Hartog G.D., Neumann H.H., 1994. A comparison of Bowen ratio and eddy correlation sensible and latent heat flux measurements above deciduous forest *Boundary Layer Meteorol.* 71, 21-40.
- Bauerle W.L., Whitlow T.H., Pollock C.R., Frongillo E.A., 2002. A laser-diode-based system for measuring sap flow by the heat-pulse method. *Agric. Forest Meteorol.* 110, 275-285.
- Beringer J., Tapper N., 1996. Evapotranspiration measurements using the Campbell Scientific Bowen ratio system. *Conf. Proc. 2<sup>nd</sup> Austr. Conf. Agric. Meteorol.*, Oct 1-4, pp 264-296.
- Blaauw E., 2000 Long-term rainfall data for Secunda. Unpublished e-mail to Jarman, C.
- Blad B.L., Rosenberg N.J., 1974. Lysimetric calibration of the Bowen ratio-energy balance method for evapotranspiration estimation in the Central Great Plains. *J. Appl. Meteorol.* 13, 227-236.
- Bowen I.S., 1926. The ratio of heat losses by conduction and by evaporation from any water surface. *Phys. Rev.* 27, 779-787.
- Brady N.C., 1990. *The Nature and Properties of Soils*. 10<sup>th</sup> Edition, Macmillan Publishing Company, New York, 621 pp.
- Braune E., 2000. Towards comprehensive groundwater resource management in South Africa. In: Sililo, O. *et al.* (Editors). *Proceedings of the XXX IAH congress on*

- Groundwater: Groundwater: Past achievements and future challenges Cape Town/South Africa, 26 November to 1 December 2000, AA Balkema, Rotterdam, pp 7-16.
- Bristow K.L., Campbell G.S., Calissendorff K., 1993. Test of a heat-pulse probe for measuring changes in soil water content. *Soil Sci. Soc. Am. J.* 57, 930-934.
- Brown R.W., 1970. Measurement of water potential with thermocouple psychrometers: Construction and applications. *US For. Serv. Res. Pap. INT 80*, 29 pp.
- Brown R.W., Oosterhuis D.M., 1992. Measuring plant and soil water potentials with thermocouple psychrometers: Some concerns. *Agron. J.* 84, 78-86.
- Brutseart W., 1982. *Evaporation into the Atmosphere*. Reidel. Dordrecht, 299 pp.
- Businger J.A., 1986. Evaluation of the accuracy with which dry deposition can be measured with current meteorological techniques. *J. Clim. Appl. Meteorol.* 25, 1100-1124.
- Button S., Christie S., Du Toit B., Freimond S., Olbrich B.W., MacHutchon M., Olbrich K., 1993. Need analysis. CSIR Report no. FOR-I 349.
- Calder I.R., 1986. Water use of Eucalypts – a review with special reference to South India. *Agric. Water Manage.*, 11 33-342.
- Calder I.R., 1998. Water use by forests, limits and controls. *Tree Physiol.* 18, 625-631.
- Campbell G.C., 1972. Vapour sink and thermal gradient effects on psychrometer calibration. In: Brown R.W., Van Haveren B.P. (Editors). *Psychrometry in water relations research*, Utah State University, Utah, pp 94-97.
- Campbell G.S., undated. On-line measurement of potential evapotranspiration with the Campbell Scientific automated weather station. Application note by Campbell Scientific Inc., Department of Crop and Soil Sciences, Washington State University.
- Campbell G.S., Flint A.L., Bilskie J., Calissendorff C., undated. Calibration and temperature correction of heat dissipation matric potential sensor.
- Campbell Scientific, Inc., 1992. TDR soil moisture measurement system. Revision 2/92, Campbell Scientific, Inc.
- Campbell Scientific, Inc., 1995. 229-L Heat dissipation soil water potential probe, Campbell Scientific, Inc.
- Campbell Scientific, Inc., 1996. CS615 Water content reflectometer. Instruction manual. Version 8221-07, Revision 10/96, Campbell Scientific, Inc.
- Campbell Scientific, Inc., 1998. Instruction manual CSI Bowen ratio. Revision 1/98, Campbell Scientific, Inc.

- Campbell Scientific, Inc., undated. 229-L Heat dissipation matric potential sensor, Campbell Scientific, Inc.
- Cellier P., Olioso A., 1993. A simple system for automated long-term Bowen ratio measurement. *Agric. Forest Meteorol.* 66, 81-92.
- CLIMGEN, undated. ClimGen weather generator. Version 4.1.05. Stöckle C.O. (Model developer), Nelson R. (Programmer), Campbell G.S., Washington State University Biological Systems Engineering Department, Pullman WA 99164-6120. Available from: <http://www.bsyse.wsu.edu/climgen>.
- Cohen Y., Fuchs M., Green G.C., 1981. Improvement of the heat pulse method for determining sap flow in trees. *Plant Cell Environ.* 4, 391-397.
- Cunningham L., 1995. The one-year results of a series of land preparation trials at Brandspruit Colliery, Secunda. CSIR Report no. FOR-C 271.
- Cunningham L., 1996. The two year results of a series of land preparation trails at Brandspruit Colliery, Secunda. CSIR Report no. FOR-C 321.
- Dane, J.H. and Hopmans, J.W. 2002. Pressure plate extractor. In: Dane, J.H. and Topp, G.C. (Editors) *Methods of Soil Analysis, Part 4, Physical Methods*, Soil Science Society of America, Madison. WI., USA.
- Denmead O.T., McIlroy I.C., 1970. Measurements of non-potential evaporation from wheat. *Agric. Meteorol.* 7, 285-302.
- Du Toit B., 1993. Site types of the Brandspruit Management Unit: Secunda Collieries, Sasol Mining (Pty) Ltd. CSIR Report no. FOR-C 209.
- Du Toit B., Basson W., 1993. Assessment and evaluation report of the existing plantation areas at Secunda Collieries, Sasol Mining (Pty) Ltd. CSIR Report no. FOR-C 164.
- Du Toit B., Mostert G., 1993. Soil preparation and tree planting guidelines for the South-western shaft area, Secunda Collieries, Sasol mining (Pty) Ltd. CSIR report no. FOR-C 182.
- Dumsday R.G., Pegler R., Oram D.A., 1989. Is broad scale re-vegetation economic and practical as a groundwater and salinity management tool in the Murray-Darling Basin? *BMR. J. of Aust. Geol. and Geop.* 11, 209-218.
- Dunin F.X., 2002. Integrating agroforestry and perennial pastures to mitigate water logging and secondary salinity. *Agric. Water Manage.* 53, 259-270.
- Dye P.J., 1987. Estimating water use for *Eucalyptus grandis* using the Penman-Monteith equation. *IAHS Publ.* 167, 329-337.

Dye P.J., 1 July 2003. Leaf area index of *Eucalyptus* species growing on the Highveld, South Africa. Personal interview.

Dye P.J., Olbrich B.W., Calder I.R., 1992. A comparison of the heat pulse method and deuterium tracing method for measuring transpiration from *Eucalyptus grandis*. J. Exp. Bot. 43, 337-343.

Dye P.J., Moses G., Vilakazi P., Ndlela R., Royappen M., 2001. A comparison of the water use of wattle-invaded and indigenous riparian plant communities. WRC Report no. K5/808, ISBN no. 1 86845 793 1, 37 pp.

Environmental Conservation Act no. 54, 1989.

Everson C.S., 1993. Report on the development of a project for the determination of transpiration from plantation canopy surfaces through transition from grassland to *Eucalyptus* plantations in the Natal Midland. CSIR Report no. FOR-DEA 669, 18 pp.

Everson C.S., Molefe G.L., Everson T.M., 1998. Monitoring and modelling components of the water balance in a grassland catchment in the summer rainfall area of South Africa. WRC Report no. 493/1/98, ISBN no. 1 86845 520 3, 138 pp.

Fritschen L.J., 1966. Evapotranspiration rates of field crops determined by the Bowen ratio method. Agron. J. 58, 339-342.

Fuchs M., Tanner C.B., 1970. Error analysis of Bowen ratios measured by differential psychrometry. Agric. Meteorol. 7, 329-334.

Greenwood E.A.N., Klein L., Beresford J.D., Watson G.D., 1985. Differences in annual evaporation between grazed pasture and *Eucalyptus* species in plantation on a saline farm catchment. J. Hydrol. 78, 261-278.

Gupta R.K., 1979. Plants for Environmental Conservation. Bishen Singh Publishers, Dehradun.

Gush M.B., Scott D.F., Jewitt G.P.W., Schulze R.E., Lumsden T.G., Hallows L.A., Gorgens A.H.M., 2002. Estimation of streamflow reductions resulting from commercial afforestation in South Africa. WRC Report no. TT 173/02, ISBN no. 1 86845 845 8.

Hanks R.J., Allen L.H., Gardner R.H., 1971. Advection and evapotranspiration in wide-row sorghum in the Central Great Plains. Agron. J. 63, 520-527.

Heilman J.L., Brittin C.L., 1989. Fetch requirements for Bowen ratio measurements of latent and sensible heat fluxes. Agric. Forest Meteorol. 44, 261-273.

Herkelrath W.N., Delin G.N., undated. Long-term monitoring of soil-moisture in a harsh climate using reflectometer and tdr probes.  
<http://wwwmn.cr.usgs.gov/bemidji/results/Herkelrath-Delin%20paper.htm> (Accessed on 11/03/2003).

- Hodgson F.D.I., Krantz R.M., 1998. Investigation into groundwater quality deterioration in the Olifants river catchment above the Loskop Witbank dam Sub-catchment. WRC Report no. 291/1/98, ISBN no. 1 86845 701 X.
- Hodgson F.D.I., Usher B.H., Scott R., Zeelie S., Cruywagen L-M., De Necker E., 2001. Prediction techniques and preventative measures relating to the post operational impact of underground mines on the quality and quantity of groundwater resources. WRC Report no. 699/1/01, ISBN no. 1 86845 182 8, 272 pp.
- Hunt M.A., Beadle C.L., 1998. Whole-tree transpiration and water-use partitioning between *Eucalyptus nitens* and *Acacia dealbata* weeds in a short-rotation plantation in northern Tasmania. *Plant Physiol.* 18, 557-563.
- Huschke R.E., 1959 (Editor). Glossary of Meteorology, American Meteorological Society, Boston, Massachusetts, 638 pp.
- Jarmain C., Everson C.S., 2002. Comparative evaporation measurements above commercial forestry and sugarcane canopies in the KwaZulu-Natal Midlands. CSIR Report no. ENV-C-S 2002 005.
- Jarmain C., Everson C.S., Savage M.J., 2001. The impact of *Eucalyptus* on inhibiting the drainage of soil water into underground mine workings. CSIR Report no. ENV-S-C 2001-030.
- Jovanovic N.Z., Annandale J.G., 1997. A laboratory evaluation of Watermark electrical resistance and Campbell Scientific 229 heat dissipation matric potential sensors. *Water S.A.* 23, 227-232.
- Kallarackal J., Somen C.K., 1997. Water use by *Eucalyptus tereticornis* stands of differing density in southern India. *Tree Physiol.* 17, 195-203.
- Kalma J.D., Badham R., 1972. The radiation balance of a tropical pasture. I. The reflection of short wave radiation. *Agric. Meteorol.* 10, 251-259.
- Kite G., Droogers P., 2000. Comparing estimates of actual evapotranspiration from satellites, hydrological models, and field data: A case study from Western Turkey. International Water Management Institute Research Report no. 42, 32 pp.
- Knight J.H., 1999. Root distribution and water uptake patterns in *Eucalyptus* and other species. Paper no. 4. In: The ways trees use water – Four review papers. Landsberg J. (Editor). Produced as part of the Joint venture agroforestry program. 'Agroforestry to balance catchment health and primary production' project. Water and Salinity Issues in Agroforestry no. 5 RIRDC. Publication no. 99/37. RIRDC Project no. CSM-4A.
- Kotze A., 2001. Project plan for the development of a water management mine planning tool. Sasol Coal Report no. 3722/2358/12/W.
- Lawrence Berkeley National Laboratory, 2000. Psychrometer measurement. YMP-LBNL-TIP/AFT 6.0. Revision 2. <http://www-esd.lbl.gov/NW/tips/tipaft6r2m0.pdf>, (Effective date 25/08/2003).

- Le Maitre D., Scott D., 1997. Afforestation and water availability in South Africa: a view from outside the plantation. Workshop Forests at the limit: Environmental constraints on Forest function, 11 to 17 May 1997, Skukuza, Kruger National park, South Africa. CSIR report no. ENV-S-R 9729.
- Le Maitre D.C., Scott D.F., Colvin C., 2000. Information on interactions between groundwater and vegetation relevant to South African conditions: A review. In: Sililo, O. *et al.* (Editors). Proceedings of the XXX IAH congress on Groundwater: Groundwater: Past achievements and future challenges Cape Town/South Africa, 26 November to 1 December 2000, AA Balkema, Rotterdam, pp 959-962.
- Lima W.P., 1984. The hydrology of a Eucalypt forest in Australia – a review. IPEF Piracicaba 28, 11-32.
- Lorentz S.A., 1993. The use of accurate liquid retention characteristics of porous media in hydrology. In Lorentz S *et al.* (Editors). Proceedings of the 6th South African National Hydrology Symposium. University of Natal, Pietermaritzburg. September 1993, pp 235-242.
- Lukunga G., 1998. Bowen ratio and surface temperature techniques for measuring evaporation from cabbages. Unpublished M.Sc. Agric. Thesis, University of Natal, South Africa, 166 pp.
- Malek E., 1993. Comparison of the Bowen ratio-energy balance and stability corrected aerodynamic methods for measurement of evapotranspiration. Theor. Appl. Climatol, 48, 167-178.
- Malek E., Bingham G.E., 1993. Comparison of the Bowen ratio-energy balance and the water balance methods for the measurement of evapotranspiration. J. Hydrol. 146, 209-220.
- Maree J.P., Van Tonder G.J., Millar P., 1996. Underground neutralisation of mine water with limestone. WRC Report no. 609/1/96, ISBN no. 1 86845 241 7.
- Marshall D.C., 1958. Measurement of sap flow in conifers by heat transport Plant Physiol. 33, 385-396.
- Metelerkamp B.R., 1993. The use of the Bowen ratio energy balance method for the determination of total evaporation over a grassed surface. Unpublished M.Sc. Agric. Thesis, University of Natal, South Africa, 153 pp.
- Minerals Act no. 50, 1991.
- Monteith J.L., 1963. Gas Exchange in Plant Communities Environmental Control in Plant Growth Evans L.T. (Editor.). Academic Press, New York pp 95-112.
- Monteith J.L., 1964. Evaporation and Environment. The State and Movement of Water in Living Organisms no. 19. Symp. Soc. Exp. Biol., Academic Press, New York, 205-234.

- Monteith J.L., Unsworth M.H., 1990. Principles of Environmental Physics. 2<sup>nd</sup> ed. Edward Arnold London, 291 pp.
- Munro D.S., Oke T.R., 1975. Aerodynamic boundary layer adjustment over a crop in neutral stability. *Boundary Layer Meteorol.* 9, 53-61.
- Nambiar S., 2000. Trees and water – a balanced view. In: Onwood no. 29, Winter 2000. Research updates from CSIRO Forestry and Forestry Products. <http://www.ffp.csiro.au/publicat/onwood/onwood29/story3.html> (Accessed 17/09/2002).
- National Geographic (undated)  
<http://www.nationalgeographic.com/xpeditions/atlas/index.html?Parent=africa&Rootmap=safic&Mode=d&SubMode=w> (Accessed 15/09/03).
- National Water Act no. 36, 1998.
- Nie D., Flitcroft I.D., Kanemasu E.T., 1992. Performance of Bowen ratio systems on a slope. *Agric. Forest Meteorol.* 59, 165-181.
- Ohmura A., 1982. Objective criteria for rejecting data for Bowen ratio flux calculation. *J. Appl. Meteorol.*, 21, 595-598.
- Oke T.R., 1978. *Boundary Layer Climates*. 2<sup>nd</sup> edition. London Methuen, 435 pp.
- Olbrich B.W., 1994. The application of the heat pulse velocity technique to the study of transpiration from *Eucalyptus grandis*. Unpublished Ph.D. Thesis, University of Natal, South Africa, 122 pp.
- Olbrich B.W., Poulter A.G., 1992. The establishment of a trial to determine the effect of varying espacement of water use from *Eucalyptus viminalis* at Brandspruit Colliery, Secunda. CSIR Report no. FOR-C 158.
- Olbrich B., Hudson K., Soko S., 1994. The effect of varying tree stocking densities on the water use of *Eucalyptus viminalis* trees at Brandspruit Collieries, Secunda. CSIR Report no. FOR-C 265, 20 pp.
- Ortega-Farias S.O., 1996. Daytime variation of sensible heat flux estimated by the bulk aerodynamic method over a grass canopy. *Agric. Forest Meteorol.* 81, 131-143.
- P55 series psychrometers, undated. P55 series psychrometers notes. Unpublished.
- Penman H.L., 1948. Natural evaporation from open water, bare soil and grass. *Proc. R. Soc. London Ser. A* 193, 120-145.
- Phene C.J., Hoffman G.J., Rawlins S.L., 1971. Measuring soil matric potential *in situ* by sensing heat dissipation within a porous body: I. Theory and sensor construction. *Soil Sci. Soc. Am. Proc.* 35, 27-33.

- Pieri P., Fuchs M., 1990. Comparison of Bowen ratio and aerodynamic estimates of evapotranspiration. *Agric. Forest Meteorol.* 49, 243-256.
- Rana G., Katerji N., 2000. Measurement and estimation of actual evapotranspiration in the field under Mediterranean climate: a review. *Eur. J. Agron.* 13, 125-153.
- Raper P., 2000. Water use by Trees: The Short Report no. 39. A summary of Raper P Agroforestry water use in Mediterranean regions of Australia. RIRDC Report no. 98/63 <http://www.rirdc.gov.au/pub/shortreps/sr39.htm> (Accessed 12/06/2000).
- Rawlins S.L., Dalton F.N., 1967. Psychrometric measurement of soil water potential without precise temperature control. *Soil Sci. Soc. Am. Proc.* 31, 297-301.
- Reece C.F., 1996. Evaluation of a line heat dissipation sensor for measuring soil matric potential. *Soil Sci. Soc. Am. J.* 60, 1022-1028.
- Ritchie J.T., 1972. Model for predicting evaporation from a row crop with incomplete cover. *Water Resources Res.* 8, 1204-1213.
- Rosenberg N.J., Blad B.L., Verma S.B., 1983. *Microclimate: The Biological Environment*. 2<sup>nd</sup> edition. Wiley, New York, 495 pp.
- Roux C., 1998. Ondersoek na afsterwing van bome in Secunda. Kontrak no. Oc 9820/98, 4 pp.
- Salmon D.A., 2000. Management of coal mining impacts on water resources in South Africa. In: Sililo, O. *et al.* (Editors). Proceedings of the XXX IAH congress on Groundwater: Groundwater: Past achievements and future challenges Cape Town/South Africa, 26 November to 1 December 2000, AA Balkema, Rotterdam, pp 1135-1140.
- Savage M.J., (1 July 2003). Discussion on growth parameters used in the soil water balance simulations with SWAP. Personal interview.
- Savage M.J., Cass A., De Jager J.M., 1981. Calibration of thermocouple hygrometers *Irrigation Sci.* 2, 112-125.
- Savage M.J., Wiebe H.H., Cass A., 1983. *In situ* field measurement of leaf water potential using thermocouple psychrometers. *Plant Physiol.* 73, 609-613.
- Savage M.J., Cass A., 1984. Measurement of water potential using *in situ* thermocouple hygrometers. *Adv. Agron.* 37, 73-126.
- Savage M.J., Wiebe H.H., 1987. Voltage endpoint determination for thermocouple psychrometers and the effect of cooling time. *Agric. Forest Meteorol.* 39, 309-317.
- Savage M.J., McInnes K.J., Heilman J.L., 1996. The "footprints" of eddy correlation sensible heat flux density, and other micrometeorological measurements. *S. Afr. J. Sci.* 92, 137-142.



- Savage M.J., Everson C.S., Metelerkamp B.R., 1997. Evaporation measurement above vegetated surfaces using micro-meteorological techniques. WRC Report no. 349/1/97, ISBN no. 1 86845 363 4, 227 pp.
- Scanlon B.R., Reedy R.C., Liang J., 1999. Woods A.L. (Editor). Recharge monitoring in an Interplaya setting. Amarillo National Research Centre for Plutonium. Report no. ANRCP-1999-14, 23 pp.
- Sharma M.J., 1984. Evapotranspiration from a *Eucalyptus* community. Agric. Water Manage. 8, 41-56.
- Shiva V., Bandyopadhyay J., 1983. *Eucalyptus* – a disastrous tree for India. The Ecologist 13, 184-187.
- Sikka A.K., Samra J.S., Sharda V.N., Samraj P., Lakshmanan V., 2003. Low flow and high flow responses to converting natural grassland into bluegum (*Eucalyptus globulus*) in Nilgiris watersheds of South India. J. Hydrol. 270, 12-26.
- Silberstein R., Held A., Hatton T., Viney N., Sivapalan M., 2001. Energy balance of a natural jarrah (*Eucalyptus marginata*) forest in Western Australia: measurements during the spring and summer. Agric. Forest Meteorol. 109, 79-104.
- Sinclair T.R., Allen L.H., Lemon E.R., 1975. An analysis of errors in the calculation of energy flux densities above vegetation by a Bowen ratio profile method. Boundary Layer Meteorol. 8, 129-139.
- Smith C., 14 January 2003. *E. viminalis* tree heights collected by the ICFR during species trials. Unpublished e-mail to and personal interview with Jarmain, C.
- Soares J.V., Almeida A.C., 2001. Modeling the water balance of soil water fluxes in a fast growing *Eucalyptus* plantation in Brazil. J. Hydrol. 253, 130-147.
- Soil Classification Working Group, 1991. Soil classification. A taxonomic system for South Africa. Memoirs on the Agricultural Natural Resources of South Africa no. 15. A second (revised) edition of Soil classification – A binomial system for South Africa 1977. A report on a Research Project conducted under the auspices of the Soil and Irrigation Research Institute, Department of Agricultural Development, Pretoria ISBN 0-621-10784-0, 257 pp.
- Soil Science Society of South Africa, 2001. Internet Glossary of Soil Science Terms. <http://www.soils.org/sssagloss/>. Accessed on 19/11/2003 08:46.
- South African Weather Bureau (undated)
- SOWACS, undated. <http://www.sowacs.com/sensors/psyl.html>. Last modified 8 January 1998 (Accessed on 10/10/2002 13:53).
- Spittlehouse D.L., Black T.A., 1980. Determination of forest evapotranspiration using Bowen ratio and eddy correlation measurements. J. Appl. Meteorol. 18, 647-653.

- Stannard D.I., 1997. A theoretically based determination of Bowen ratio fetch requirements *Boundary Layer Meteorol.* 83, 375-406.
- Sumner M.E., 2000 (Editor). *Handbook of Soil Science*. CRC Press, Boca Raton.
- Swanson R.H., Whitfield D.W.A., 1981. A numerical analysis of heat pulse velocity theory and practice. *J. Exp. Bot.* 32, 221-239.
- SWAP (Soil Water Atmosphere Plant model), undated. Hydrological processes at field scale. <http://www.alterra.dlo.nl/models/swap/index.htm> (Accessed 15/09/2003).
- Thom A.S., 1975. Momentum, Mass and Heat Exchange in Plant Communities. *Vegetation and the Atmosphere*. Vol. 1. Principles. Monteith J.L. (Editor). Academic Press. London, pp 57-109.
- Unland H.E., Arain A.M., Harlow C., Houser P.R., Garatuza-Payan J., Scott P., Sen O.L., Shuttleworth W.J., 1998. Evaporation from a riparian system in a semi-arid environment. *Hydrol. Processes* 12, 527-542.
- Van Dam J.C., 2000. Field-scale water flow and solute transport SWAP model concepts, parameter estimation and case studies. Ph.D. Thesis, Wageningen University, ISBN 90-5808-256-3.
- Van Dam J.C., Huygen J., Wesseling J.G., Feddes R.A., Kabat P., Van Walsum P.E.V., Groenendijk P., Van Diepen C.A., 1997. Simulation of water flow, solute transport and plant growth in the soil-water-atmosphere-plant environment. Theory of SWAP version 2.0. Report no. 71. Technical report no. 45. Department of Water Resources, Wageningen Agricultural University, Holland.
- Van der Watt H.v.H., Van Rooyen T.H., 1990. *A Glossary of Soil Science/n Verklarende Woordeboek vir Grondkunde*. Soil Science Society of South Africa, Pretoria, 356 pp.
- Van Genuchten M. Th., 1980. A closed-form equation for predicting the hydraulic conductivity of unsaturated soils. *Soil Sci. Soc. Am. J.* 44, 892-898.
- Van Genuchten, M. Th., Leij F. J., Yates S. R., 1991. *The RETC Code for Quantifying the Hydraulic Functions of Unsaturated Soils, Version 1.0*. EPA Report 600/2-91/065, U.S. Salinity Laboratory, USDA, ARS, Riverside, California, USA.  
<http://www.ussl.ars.usda.gov/models/retc.HTM>
- Versfeld D.B., Everson C.S., Poulter A.G., 1998. The use of vegetation in the amelioration of the impacts of mining on water quality – An assessment of species and water use. WRC Report no. 413/1/98, ISBN no. 1 86845 497 5, 172 pp.
- Vertessy R.A., Elsenbeer H., 1999. Distributed modelling of storm flow generation in an Amazonian rain forest catchment: Effect of model parameterization. *Water Resources Res.* 35, 2173-2187.

- Weiersbye I.M., 2002. Document for Government and the mining industry. Unpublished.
- Wescor Inc., 1998. Water potential system. Wescor Scientific products catalog. <http://www.wescor.com/environmental/index.phtml>.
- Wesseling J.G., Kroes J.G., Metselaar K., 1998. Global sensitivity analysis of the Soil-Water-Atmosphere-Plant (SWAP) model. Report no. 160, DLO-Staring Centre, Wageningen, 67 pp.
- Wever L.A., Flanagan L.B., Carlson P.J., 2002. Seasonal and interannual variation in evapotranspiration, energy balance and surface conductance in a northern temperate grassland. *Agric. Forest Meteorol.* 112, 31-49.
- White D.A., 2000. Balancing productivity and drought risk in bluegum plantations. Onwood no. 28. <http://www.ffp.csiro.au/publicat/onwood/onwood28/story5.html>. (Accessed on 17/09/2002).
- White D.A., Dunin F.X, Turner N.C., Ward B.H., Galbraith J.H., 2002. Water use by contour-planted belts of trees comprised of four *Eucalyptus* species. *Agric. Water Manage.* 53, 133-152.
- Wiebe H.H., Brown R.W., Barker J., 1977. Temperature gradient effects on *in situ* hygrometer measurements of water potential. *Agron. J.* 69, 933-939.
- Wilson K.B., Hanson P.J., Mulholland P.J., Baldocchi D.D., Wullschlegel S.D., 2001. A comparison of methods for determining forest evapotranspiration and its components: sap-flow, soil water budget, eddy covariance and catchment water balance. *Agric. Forest Meteorol.* 106, 153-168.
- Yeh G.T., Brutseart W.H., 1971. A solution for simultaneous turbulent heat and vapour transfer between a water surface and the atmosphere. *Boundary Layer Meteorol.* 2, 64-82.
- Zazueta F.S., Xin J., undated. Soil moisture sensors. <http://edis.ifas.ufl.edu/EH226> (Accessed on 10/03/2003).
- Zohar Y., Schiller G., 1998. Growth and water use by selected seed sources of *Eucalyptus* under high water table and saline conditions. *Agr. Ecosyst. Environ.* 69, 265-277.

## APPENDIX A

### SOIL DESCRIPTION FOR THE GRASSLAND AND *E. VIMINALIS* SITES

#### **A.1 Introduction**

The soil physical (particle size distribution, bulk density), chemical (electrical conductivity, soil pH, saturation extract) and water retention data for the different soil layers at the *E. viminalis* and grassland sites, and for the soil calibration samples taken at the grassland site were different. Definitions of the characteristics included in the descriptions of the soil layers, are given below.

#### **A.2 Definitions**

##### **A.2.1 Particle size distribution**

The particle size distribution defines the soil texture. It gives the percentage of each size fraction (or effective diameter) into which a dispersed soil sample has been separated (Soil Classification Working Group, 1991; Sumner, 2000).

##### **A.2.2 Bulk density**

The bulk density of a soil is defined as the mass of dry soil per unit bulk volume ( $\rho_{soil}$ ). It provides an estimate of the state of compaction and the amount of pore space in a soil (Soil Classification Working Group, 1991; Sumner, 2000).

##### **A.2.3 Van-Genuchten parameters**

The Van-Genuchten parameters are defined in Section 3.2.6.

#### **A.2.4 Porosity**

The porosity of a soil can be defined as the volume of pores in a soil sample (non-solid volume) as a fraction of the bulk volume of the sample (Soil Science Society of America, 2001).

#### **A.2.5 Electrical conductivity**

Salinity or total salt concentration can be expressed in terms of the specific electrical conductance (*EC*) (Soil Classification Working Group, 1991; Sumner, 2000).

#### **A.2.6 Soil pH**

The Soil Classification Working Group (1991) defines the soil pH as “*The degree of acidity (the negative logarithm to the base 10 of the hydrogen ion activity) of a soil at a specified soil to suspension medium (e.g. 1 to 2.5 soil:water) ratio*”. The suspension medium can be either KCl or H<sub>2</sub>O, and must be specified when reporting the pH (Soil Classification Working Group, 1991).

#### **A.2.7 Saturation extract**

Soil Classification Working Group (1991) defines the saturation extract as “*The solution which is extracted under suction from a saturated soil paste*”. These solutions can include sodium (*Na*), calcium (*Ca*), magnesium (*Mg*) and potassium (*K*).

#### **A.2.8 Sodium adsorption ratio**

The sodium adsorption ratio (SAR) provides a measure of the quality of a solution in terms of the sodium content and is approximately equal to the exchangeable sodium of the soil. The sodium adsorption ratio is given as:

$$SAR = \frac{Na}{\sqrt{\frac{Ca + Mg}{2}}} \quad A.1$$

where  $Na$ ,  $Ca$  and  $Mg$  refers to the concentration sodium, calcium and magnesium in  $\text{mmol dm}^{-3}$  (Soil Classification Working Group, 1991).

### A.2.9 Colour

Soil colour is described in terms of the Munsell notation and varies with soil water content. Soil water content status (wet or dry) therefore needs to be specified. The soil colour is described in terms of the verbal colour and a notation. The notation refers to hue, value and chroma. Hue refers to the dominant spectral colour, values to the relative lightness of colour, and chroma to the relative purity of the spectral colour and strength of the increase with decreasing greyness (Soil Classification Working Group, 1991).

### A.2.10 Structure

The structure of a soil refers to “*a natural aggregation of primary soil particles into compound units or peds which are separated from one another by planes or surfaces of weakness*”. The structure of a soil is described in terms of the type, size and distinctness of visible peds (Soil Classification Working Group, 1991).

### A.2.11 Consistence

The consistency of a soil refers to the “*degree of cohesion or adhesion within the soil mass, or its resistance to deformation or rupture*” (Soil Classification Working Group, 1991). The consistency can be described when dry or wet.

### **A.2.12 Nodules**

Nodules can be defined as bodies of a range of shapes, sizes and colour. These bodies have been hardened to a greater or lesser extent by chemical compounds. These compounds include lime, seszuioxides, animal excreta and silica. Nodules are described in terms of kind, abundance, hardness and size (Soil Classification Working Group, 1991).

### **A.3 *Properties of soil layers at field research sites, and that of calibration soil samples***

The 100-, 300-, 500-, 700- and 900-mm soil layers at the grassland and *E. viminalis* sites studied, and the soil samples used in the sensor calibration, are described in terms of their particle size distribution, bulk density, electrical conductivity, soil pH, saturation extract, Van-Genuchten parameters and porosity (Tables A.1 to A.7). The water retention characteristics (pressure head vs volumetric soil water content) of these soil layers are given in Figure A.1. The water retention characteristics up to 1 bar was determined using a controlled outflow cell technique (Lorentz, 1993) and over 1 bar using the standard pressure plate technique (Dane and Hopmans, 2002). The Van-Genuchten parameters were determined with RETC, using the data from the water retention curves (Table A.6).

The diagnostic soil horizons at the grassland and *E. viminalis* sites are described in terms of their colour, structure, consistency, and occurrence of fragments and nodules (Tables A.8 to A.10).

Table A.1 Particle size distribution, expressed as a percentage, for different soil depths at the grassland and *E. viminalis* sites studied, and for the soil samples used in the sensor calibration

Soil information		Particle size distribution			
Site	Soil form	Soil depth (mm)	Clay (%)	Silt (%)	Sand (%)
Grassland	Rensburg	100	24	24	49
		300	46	16	34
		500	56	14	30
		700	50	17	31
<i>E. viminalis</i>	Rensburg	100	36	17	43
		300	41	16	38
		500	50	13	34
		700	36	16	47
<i>E. viminalis</i>	Arcadia	100	26	20	52
		300	44	15	38
		500	48	11	39
		700	37	15	46
Calibration	Rensburg	100	21	23	56
		300	36	33	32
		500	33	27	40
		700	19	21	59

Table A.2 Bulk densities for different soil depths at the grassland and *E. viminalis* sites studied, and for the soil samples used in the sensor calibration

Soil depth (mm)	Bulk density (kg m <sup>-3</sup> )		
	Grassland	<i>E. viminalis</i>	Calibration
Soil form	Rensburg	Rensburg	Rensburg
100	1.603	1.556	1.402
300	1.526	1.383	1.401
500	1.363	1.385	1.273
700	Not available	1.360	1.519



Table A.3 Electrical conductivity for different soil depths at the grassland and *E. viminalis* sites, for the Rensburg and Arcadia soil forms

Depth (mm)	Electrical conductivity (mS m <sup>-1</sup> )		
Site	Grassland	<i>E. viminalis</i>	<i>E. viminalis</i>
Soil form	Rensburg	Rensburg	Arcadia
100	44.20	27.90	34.10
300	41.60	32.90	25.00
500	86.50	56.00	80.30
700	94.70	35.10	Not available
900	Not available	41.20	Not available

Table A.4 Soil pH (H<sub>2</sub>O) for different soil depths at the grassland and *E. viminalis* sites, for both the Rensburg and Arcadia soil forms

Depth (mm)	Soil pH		
Site	Grassland	<i>E. viminalis</i>	<i>E. viminalis</i>
Soil form	Rensburg	Rensburg	Arcadia
100	4.96	6.53	5.05
300	7.02	6.68	6.42
500	7.87	8.25	8.12
700	8.04	8.15	Not available
900	Not available	8.13	Not available

Table A.5 *Na*, *Ca*, *Mg* and *K* saturation extracts and sodium adsorption ratio (*SAR*) for different soil depths at the grassland and *E. viminalis* sites for both the Rensburg and Arcadia soil forms

Site	Soil form	Depth (mm)	Saturation extract (me L <sup>-1</sup> )				
			<i>Na</i> <sup>27</sup>	<i>Ca</i>	<i>Mg</i>	<i>K</i>	<i>SAR</i>
Grass	Rensburg	100	0.71	1.56	1.12	0.23	0.61
		300	2.18	0.93	0.88	0.02	2.29
		500	4.49	2.07	2.15	0.04	3.09
		700	5.28	2.20	2.29	0.06	3.52
<i>E. viminalis</i>	Arcadia	100	0.48	1.17	0.89	0.18	0.47
		300	0.99	0.67	0.56	0.03	1.26
		500	4.36	1.85	1.58	0.02	3.33
<i>E. viminalis</i>	Rensburg	100	1.51	0.55	0.49	0.03	2.09
		300	1.90	0.54	0.49	0.02	2.65
		500	3.35	1.15	1.13	0.03	3.14
		700	1.88	0.87	0.85	0.03	2.03
		900	2.91	0.58	0.57	0.05	3.84

<sup>27</sup> 1 cmol (+ or - charge) kg<sup>-1</sup> = 10 mmol (+ or - charge) kg<sup>-1</sup> = 1 me 100 g<sup>-1</sup> = 10 me kg<sup>-1</sup>

Table A.6 Van-Genuchten parameters estimated with RETC (Van Genuchten *et al.*, 1991) for different soil layers at the *E. viminalis* and grassland sites, and for the soil samples used in the sensor calibration

Site	Soil form	Depth (mm)	Van-Genuchten parameters				
			$\theta_S$ ( $\text{m}^3 \text{m}^{-3}$ )	$\theta_R$ ( $\text{m}^3 \text{m}^{-3}$ )	$\alpha$ ( $\text{mm}^{-1}$ )	$n$	$m$
Grassland	Rensburg	100	0.395	0	0.0088	1.0956	0.0872
		300	0.427	0	0.0132	1.0813	0.0752
		500	0.49	0	0.0086	1.114	0.1023
		700					
		Fitted	No	No	Yes		
<i>E. viminalis</i>	Rensburg	100	0.394	0	0.0276	1.0816	0.0754
		300	0.478	0	0.029	1.0834	0.0769
		500	0.482	0	0.0165	1.0346	0.0335
		700	0.495	0	0.0032	1.0547	0.0519
		Fitted	No	No	Yes		
Calibration	Rensburg	100	0.35	0	0.0008	1.2075	0.1718
		300	0.57	0	0.007	1.1028	0.0932
		500	0.52	0	0.0002	1.3267	0.2462
		700	0.44	0	0.0009	1.1632	0.1403
		Fitted	No	No	Yes		

Table A.7 Porosity for different soil depths at the grassland and *E. viminalis* sites, and for the soil samples used in the sensor calibration

Soil depth (mm)	Porosity ( $\text{m}^3 \text{m}^{-3}$ )		
	Grassland	<i>E. viminalis</i>	Calibration
Soil form	Rensburg	Rensburg	Rensburg
100	0.395	0.413	0.471
300	0.424	0.478	0.471
500	0.486	0.477	0.520
700	Not available	0.487	0.427

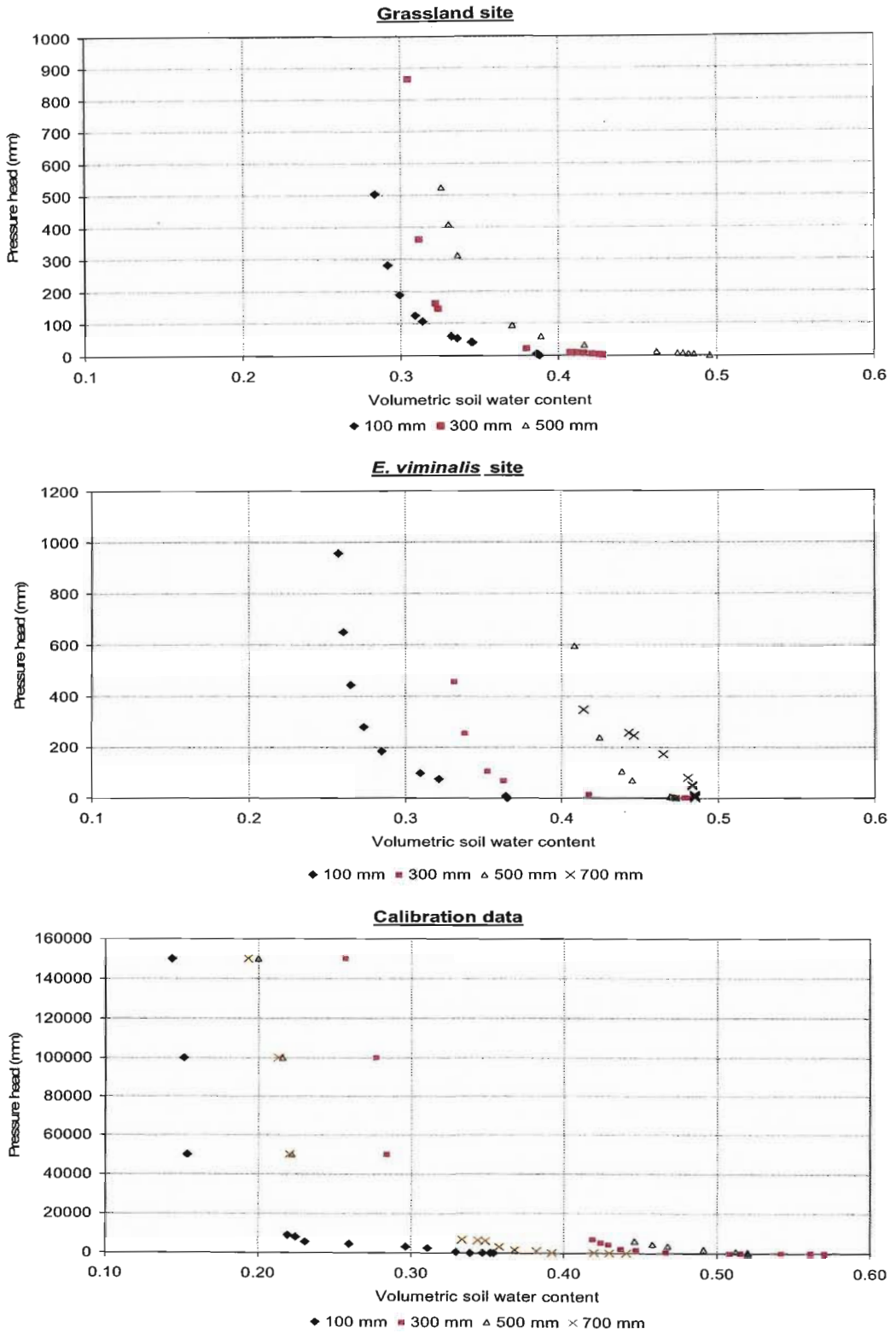


Fig. A.1 Top to bottom: Water retention functions (pressure head vs volumetric soil water content) for different soil depths at the grassland and *E. viminalis* sites, and for the soil samples used in the sensor calibration

#### **A.4 Description of soil profiles and diagnostic soil horizons at grassland and *E. viminalis* sites**

Soils at the grassland and *E. viminalis* sites were classified according to the Taxonomic Soil Classification System for South Africa (Soil Classification Working Group, 1991). Two soil forms were identified in the vicinity of the grassland and *E. viminalis* sites, namely the Rensburg and Arcadia soil forms. The Rensburg soil form was found at both the grassland and *E. viminalis* sites, whereas the Arcadia soil form was only found at the *E. viminalis* site. Du Toit (1993) noted that a broad range of soil forms (from Rensburg to Swartland) occurred within the Brandspruit Management Unit area, and included the Rensburg and Arcadia soil forms. Both the Rensburg and Arcadia soil forms consist of clays with an expansive nature. This could possibly hamper root development and would result in shallow effective soil depths. The subsoil of both the Rensburg and Arcadia soil forms are also generally prone to waterlogging during summer.

The Rensburg and Arcadia soil forms are described in terms of colour, structure and consistence (Tables A.8 to A.10) according to the Taxonomic Soil Classification System for South Africa (Soil Classification Working Group, 1991).

##### **A.4.1 Description of the Rensburg soil profile at the grassland and *E. viminalis* sites**

The Rensburg soil form consists of a Vertic A-horizon (0 to 0.50 m) overlaying a G-horizon (deeper than 0.50 m). The Vertic A-horizon has a high clay content. The smectic clay minerals possess the capacity to swell and shrink markedly in response to soil water changes. The swell-shrink potential is manifested typically by the formation of vertical cracks in the dry state and the presence, at some depth, of slicken sides (Soil Classification Working Group, 1009). The Vertic A-horizons have a characteristic appearance with a strongly developed structure, ranging from moderate blocky to strong, medium angular blocky. The Vertic A-horizon had a very dark colour, ranging from black to very dark black clay. The dark colour develops under semi-arid to sub-humid climates. The parent material is either rocks that are basic or intermediate with

regards to the base reserve, or sediments in landscape positions which receive additions of bases *via* lateral drainage of water (Soil Classification Working Group, 1990). The A-horizon has a firm consistency when moist and has a moderate to strong medium angular blocky structure. The A-horizon at the grassland site had a strong medium angular structure, with a firm consistency (Table A.8). The A-horizon of the Rensburg soil form at the *E. viminalis* site had a moderate medium angular blocky to a weak fine blocky structure when dry (Table A.9).

Table A.8 Soil profile description of the Rensburg form at the grassland site

**Form:** Rensburg

**Family:** Rietkuil

**Locality:** Secunda

**Vegetation:** Grassland

**Site:** Grassland

Soil depth (mm)	Description	Diagnostic horizons
100	<b>Colour</b> - Black (7.5YR/2.5/1) (moist) <b>Structure</b> - Moderate blocky <b>Consistence</b> - Firm	Vertic A
300	<b>Colour</b> - Very dark clay (7.5 YR/3/1) (moist) <b>Structure</b> - Strong medium angular blocky <b>Consistence</b> - Firm	
500	<b>Colour</b> - Olive grey (5y/5/2) (moist) <b>Structure</b> - Strong medium angular blocky <b>Fragments</b> - Few (20 %) angular gravel fragments (less than 10 mm) <b>Consistence</b> - firm	G
700	<b>Colour</b> - Olive grey (5 YR/5/2) (moist) <b>Fragments</b> - Common angular gravel fragments <b>Nodules</b> - Few fine soft lime and manganese nodules <b>Consistence</b> - Firm	

Table A.9 Soil profile description of the Rensburg form at the *E. viminalis* site**Form:** Rensburg**Family:** Rietkuil**Locality:** Secunda**Vegetation:** *E. viminalis***Site:** Rensburg site

Depth (mm)	Description	Diagnostic Horizons
100	<b>Colour</b> - Black clay (5 YR/2.5/1) (moist) <b>Structure</b> - Moderate medium angular blocky (dry) <b>Consistence</b> - Firm	Vertic A
300	<b>Colour</b> - Black clay (7.5YR/2.5/1) (slightly moist) <b>Structure</b> - Moderate medium angular (dry) <b>Consistence</b> - Firm	
500	<b>Colour</b> - Dark grey (10 YR/4/1) (slightly moist) <b>Structure</b> - Moderate medium angular blocky (dry) <b>Consistence</b> - Firm <b>Fragments</b> - Few fine lime	
700	<b>Colour</b> - Dark greyish brown (2.5Y/4/2) (slightly moist) <b>Fragments</b> - Few manganese and lime fragments <b>Structure</b> - Weak fine blocky (dry) <b>Consistence</b> - Slightly firm <b>Fragments</b> - Few fine manganese and lime fragments	
900	<b>Colour</b> - Dark brown (10YR/3/3) Weathering dolorite	Weathering dolorite

The G-horizon (gleyed) is generally saturated with water for long periods, unless drained. The G-horizon has an olive grey colour (grass) or a colour ranging from dark grey through to dark greyish brown. Gleying, with the reduction of ferric oxides and hydrated oxides, is the essential process to which the G-horizon is subjected. Grey, blue and green colours predominate, but stains of ferric and manganese oxides and hydrates (yellow, brown, red and black) may be present and indicate localized areas of better aeration. Grey colours are due to an absence of iron compounds, and blue and green are due to the presence of ferrous compounds.

The G-horizon at the grassland site had a slightly firm to firm consistency when wet. The structure of the G-horizon ranged from strong medium angular (500 mm) to weak fine blocky (700 mm). Angular fragments occurred, becoming common with depth. A few fine soft lime and (iron-) manganese nodules also occurred. A few fine manganese and lime fragments occurred. Lime and manganese fragments suggest higher levels of alkalinity as a result of reduced leaching in the G-horizon in this horizon compared to the Vertic A-horizon. (Usually, but not always, marked clay illuviation takes place especially in the upper part of the G-horizon) (Table A.8).

#### **A.4.2 Description of the Arcadia soil profile at the *E. viminalis* site**

The Arcadia soil form (Table A.10) consists of a Vertic A-horizon (0 to 700 mm), overlaying parent material (e.g. sandstone). The Vertic A-horizon has a black to black clay colour close to the soil surface. A very dark greyish brown layer overlies the weathering sand stone. The structure of this horizon varies between weak medium crumb (100 mm) and strong medium blocky when dry and the consistency ranged between slightly firm (300 mm) to firm when moist. Very hard, fine lime nodules occurred at depths exceeding 500 mm (Table A.10).



Table A.10 Soil profile description of the Arcadia form at the tree site

**Form:** Arcadia**Family:** Rustenburg**Locality:** Secunda**Vegetation:** *E. viminalis***Site:** Arcadia site

Soil depth (mm)	Description	Diagnostic Horizons
100	<b>Colour</b> - Black (7.5YR/2.5/1) (slightly moist) <b>Structure</b> - Weak medium crumb (dry) <b>Consistence</b> - Slightly firm (moist)	Vertic A
300	<b>Colour</b> - Black clay (7.5YR/2.5/1) (slightly moist) <b>Structure</b> - Strong medium blocky (dry) <b>Consistence</b> - Firm (moist)	
500	<b>Colour</b> - Very dark greyish brown (2.5YR/3/2) <b>Lime nodules</b> (high pH) – Very hard fine lime nodules <b>Structure</b> - Moderate fine blocky (dry) <b>Consistence</b> – Firm (moist)	
700	Sandstone	Sandstone

## APPENDIX B

### LABORATORY CALIBRATION OF SOIL SENSORS FOR SITE-SPECIFIC CONDITIONS

#### **B.1 Introduction**

As part of the field experiment, soil water content and soil water potential was estimated at different depths. These sensors were not calibrated prior to or during the field experiment. However, relationships between sensor output and soil water content and soil water potential is required to convert sensor output to soil water content (water content reflectometer) or to soil water potential (heat dissipation sensor and thermocouple psychrometer). Some sensors and their calibration relationships are sensitive to site specific conditions and application of these calibration equations to non-standard conditions could lead to inaccurate estimations of soil water content or soil water potential. For example a water content reflectometer is sensitive to the electrical conductivity, clay and organic matter content and to air temperature. Therefore, when this sensor is used under non-standard conditions (e.g. clay content greater than 30 %), the standard calibration polynomials may no longer apply (Campbell Scientific Inc., 1996). Therefore for use of the soil reflectometer sensor under non-standard conditions, individual calibration is required.

Therefore, soil water content (water content reflectometer) and soil water potential sensors (heat dissipation) used in the field experiment, were calibrated for field specific conditions. The thermocouple psychrometers were not calibrated in the laboratory since the heat dissipation calibration function was to be used to obtain a calibration function for the thermocouple psychrometer that relates sensor output to the field matric potential.

In addition to the water content reflectometers and the heat dissipation sensors, time domain reflectometers were included in the calibration. The reason for this was that these sensors are often used in research, and the question arose as to whether the equation suggested by Topp *et al.* (1980) and Ledieu *et al.* (1986) (cited by Campbell

Scientific Inc., 1992), for the calculation of the soil water content, would apply to soils with higher clay contents (greater than 30 %).

## **B.2 Materials and methods**

Block soil samples of dimensions 500 mm x 300 mm x 200 mm were removed from the grassland site at the end of the field experiment. Block samples were only taken at the grassland site, as the soil properties at the grassland and *E. viminalis* sites were similar and the clay contents within each layer were within 5 to 14 % of each other (Appendix A).

The sides of an already opened trench at the grassland site, with a depth of approximately 1 m, were shaven back. A U-shaped metal frame was subsequently carefully hammered vertically into the soil (Fig. B.1). Once the complete height (200 mm) of the frame was in the soil, the block soil sample was cut loose from the rest of the soil. A thick metal plate was hammered into the soil horizontally, below the U-shaped metal frame. Care was taken so as not to disturb the block sample and surrounding soil too much whilst removing the sample. Once the sample was cut loose from the bulk soil and removed from the trench, lids were used to cover the front, bottom and top of the soil sample. These covers kept the soil sample intact during transportation. Soil samples were taken at soil depths of 0 to 200 mm, 200 to 400 mm, 400 to 600 mm and 600 to 800 mm.

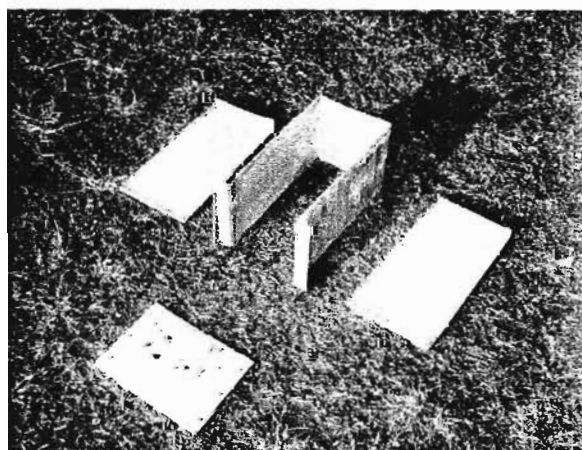


Fig. B.1 An example of one of the U-shaped metal frames used in the sampling of block soil samples at the grassland site, for the water content reflectometer calibration

The four soil samples were then transported from the research site in Secunda to a laboratory in Pietermaritzburg, approximately 500 km from the research site. In the laboratory, the front, top and bottom lids were removed, and each sample was carefully and fairly tightly wrapped first in mesh wire and then in canvas. The mesh wire and canvas kept the block soil sample intact, whilst wetting and prevented extensive swelling or expansion of the sample. The block samples were placed in a large container (about 50 l) half-filled with water, and allowed to saturate over a period of 14 days. The samples were not submerged in the water. The block samples were then removed and allowed to drain naturally.

Sets of soil sensors consisting of a water content reflectometer, heat dissipation sensor and a time domain reflectometer were then installed horizontally through the front of each block sample (Fig. B.2). A 300-mm long drill bit together with an installation guide was used to install the water content reflectometers and time domain reflectometers. A shorter drill bit was used to drill holes to install the heat dissipation sensors. Care was taken to ensure that the reflectometer rods were installed parallel to each other, and that all the sensors made good contact with the surrounding soil.

The soil sensors were subsequently connected to dataloggers. The water content reflectometers were connected to a Campbell CR23X logger, the time domain reflectometers to a CR10X datalogger, and the heat dissipation sensors to a CR7X datalogger (Fig. B.2). The water content reflectometers and heat dissipation sensors were connected to the loggers exactly as was done during the field experiment. The same datalogger programmes that were used during the field experiment were also used during the calibrations. All sensor outputs (output period, propagation velocity and temperature and change in temperature for the water content reflectometer, time domain reflectometer and heat dissipation sensors respectively) were measured every four hours.

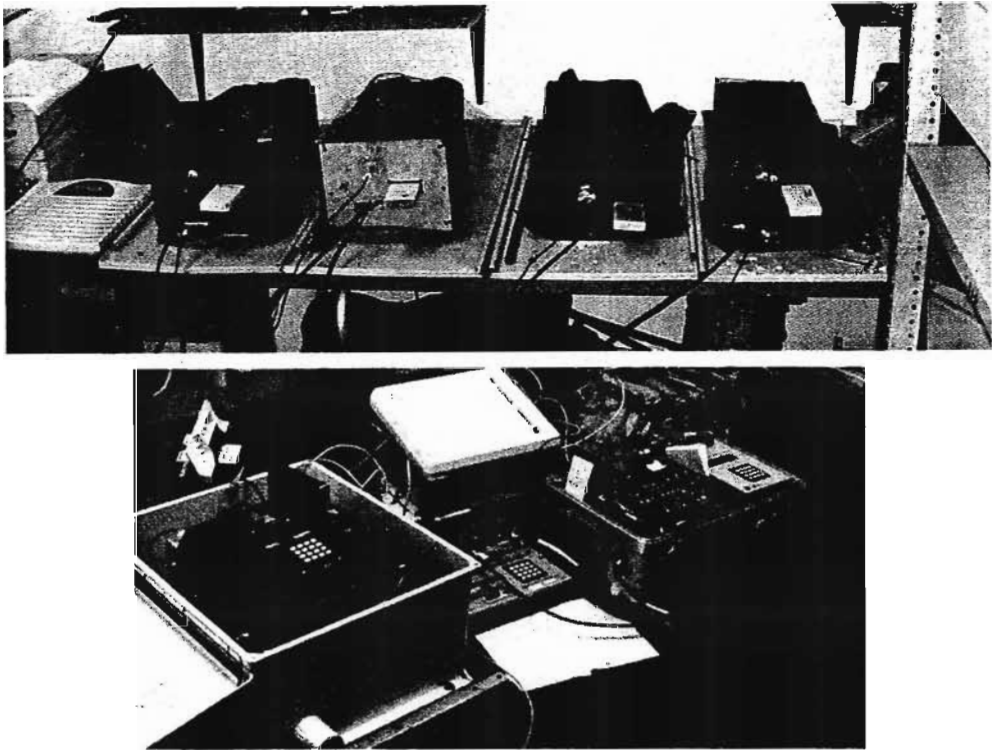


Fig. B.2 Horizontal installation of water content reflectometers, time domain reflectometers and heat dissipation sensors (top) in the block soil samples used in the sensor calibration, and the connections of the sensors to CR01X, CR23X and CR7 dataloggers (bottom)

The continuous four-hourly measurements of the sensors outputs were combined with frequent measurements of the block sample weights. The block sample weights were measured using a digital scale with a resolution of 10 g. Measurements were obtained at similar times of day, and preferably in the morning. The calibration process lasted for approximately 170 days, until signs of cracks on the outer surfaces of the block samples were visible.

At the end of this calibration period, sub-soil samples were taken from each block sample. These sub-samples were analysed in terms of the water retention characteristics and physical properties. Sub-soil samples were also used to determine the final soil water content and oven dry weight of the sub-sample. The final soil water content of each sub-sample was assumed to be the same as that of the block samples, and was used to determine the gravimetric and volumetric soil water contents of each block sample throughout the calibration process.

### **B.3 Results and discussion**

The relationship between the sensor output for each block sample and the volumetric soil water content estimated for the block sample was obtained. Second-order polynomials, as used in the factory calibrations, were fitted between the water content reflectometer period (ms) and the measured volumetric soil water content of the block sample. However, linear relationships were fitted between the inverse of the propagation velocity for the time domain reflectometer and the measured soil water content. Only the results of the water content reflectometer calibration functions will be discussed in this section. The results of the time domain reflectometer calibrations are not discussed, as it does not apply directly to the field experiment.

The actual volumetric soil water measured during the calibration process (Fig. B.3) shows the range of water contents under which the soil sensors were calibrated. The soil water content of the block samples at the beginning of the calibration period (26, 46, 52 and 39 % respectively at the 100-, 300-, 500- and 700-mm soil depths) was within 9 % of the saturated soil water contents (Table B.1) (based on the sub-soil samples). This indicates that all four block samples were close to saturation at the start of the calibration.

According to the relative saturation (Eq. 3.8), (using saturated and residual soil water contents derived for sub-soil samples) and the block sample soil water contents, the water content reflectometers were calibrated over a wide range of soil wetness (Fig. B.4). The soil wetness ranged between 14 and 73 %, 26 and 81 %, 42 and 100 % and 33 and 75 % at the 100 mm<sup>28</sup>, 300 mm, 500 mm and 700 mm soil samples respectively. The relationship between the sensor output and measured soil water content would therefore apply to both wet and dry soil conditions encountered during the field experiment.

---

<sup>28</sup>The depths 100 mm, 300 mm, 500 mm and 700 mm refer to the depth at which the block soil samples were taken, and represents the soil layers: 0 to 200 mm, 200 to 400 mm, 400 to 600 mm and 600 to 800 mm respectively.

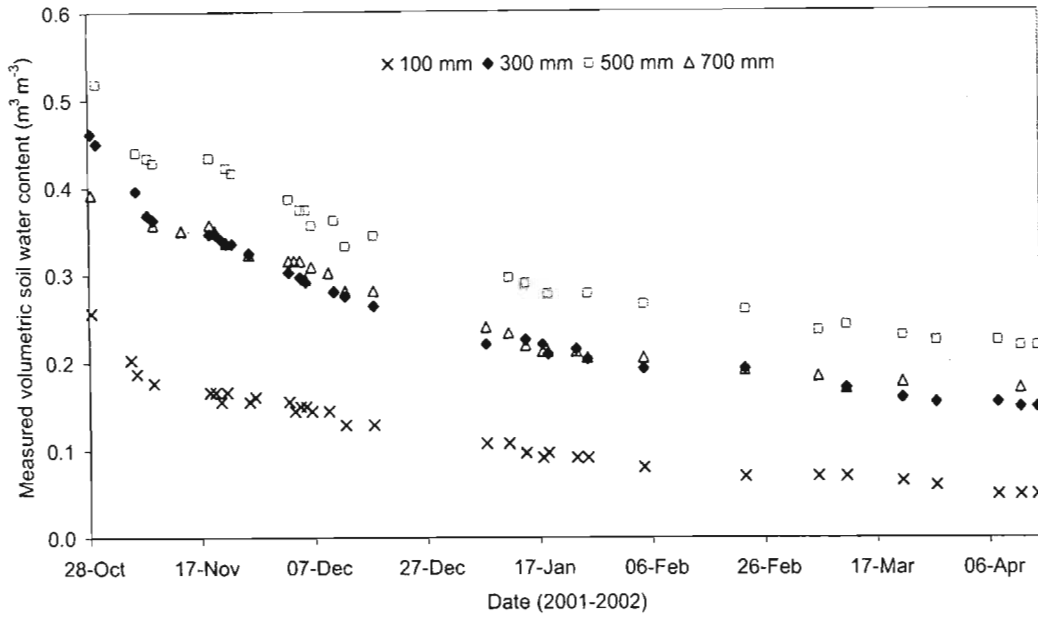


Fig. B.3 Daily measured volumetric soil water content (mass based) for four soil samples used in the sensor calibration, over a period of 170 days. 100, 300, 500 and 700 mm represent the depths at which the calibration soil samples were taken.

Table B.1 Van Genuchten water retention parameters (Eq. 3.4) for the calibration soil samples taken from different depths below the soil surface (100 to 700 mm)

Calibration data					
Van Genuchten water retention parameters estimated with RETC <sup>29</sup>					
Depth (mm)	$\theta_S$	$\theta_R$	$\alpha$	$n$	$m$
100	0.35	0	0.00076	1.20745	0.17181
300	0.57	0	0.00701	1.10275	0.09318
500	0.52	0	0.00017	1.32669	0.24624
700	0.44	0	0.00087	1.16324	0.14033

<sup>29</sup> RETC is a programme for quantifying the hydraulic functions of a unsaturated soil. RETC was developed by Van Genuchten *et al.* (1991).

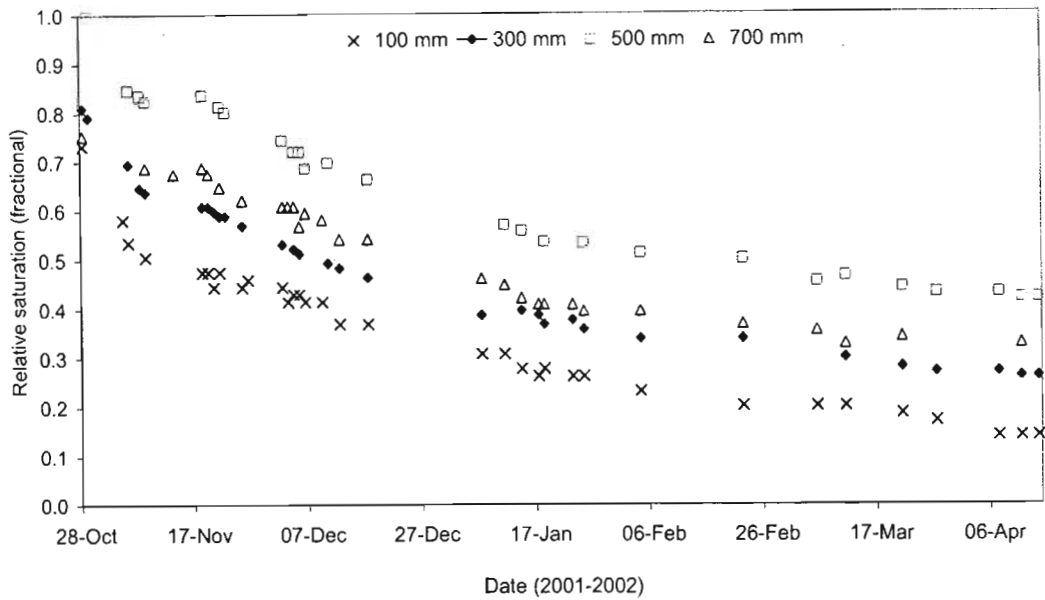


Fig. B.4 Fractional relative saturation of the four soil samples used in the sensor calibration, over a period of 170 days. 100, 300, 500 and 700 mm represent the depths at which the calibration soil samples were taken.

For the soil water content reflectometers, applying the manufacturers' calibration polynomials (Campbell Scientific Inc., 1996) to the sensor output data collected during the calibration periods, results in a consistent overestimation in the soil water contents of all four block samples (Fig. B.5<sup>30</sup>). The calculated soil water contents overestimate the soil water contents by between 2 and 71 %, irrespective of the clay content of the sample (Appendix A). The overestimation is greater at higher soil water contents (19 to 71 %) than at lower soil water contents (2 to 10 %). Site or soil specific calibration polynomials are therefore important for accurate soil water content estimations with water content reflectometers.

Statistically significant relationships ( $R^2 > 0.97$ )<sup>31</sup> were found between the water content reflectometer period outputs (ms) and the measured soil water content of all sensors and all soil block samples (Fig. B.6). The newly calculated water contents

<sup>30</sup> Statistical information on the relationship between the measured volumetric soil water content and the calculated soil water content (based on manufacturer's polynomials) for different soil depths, are given in Table B.2.

<sup>31</sup> More detailed statistical information on the relationship between the CS615 sensor output and the measured volumetric soil water content, for different soil depths, are given in Table B.3.



(using the second-order calibration polynomials), were within 3 % of the measured soil water contents ( $R^2 > 0.97$ , slope  $\approx 1$ ) (Fig. B.7)<sup>32</sup>. The second-order polynomials derived during the calibration process, therefore predict the soil water contents measured by the individual sensors accurately.

#### **B.4 Application of calibration results to field measurements**

The water content reflectometers were calibrated for four different soil layers each with a different percentage of clay ranging from 19 to 36 % (Appendix A). The clay percentage of the sub-soil samples taken from the 100- and 700-mm soil layers were less than 30 %, whereas that of the 300- and 500-mm soil layers were more than 30 %. Since the block soil samples used in the calibration were excavated in close proximity to the grassland site, the assumption was made that the calibration functions derived for each soil layer (block sample), would also apply to the corresponding soil layer at both the grassland and tree experimental sites. However, the differences in percentage clay content of the sub-soil samples of each soil layer, and that of the grassland and *E. viminalis* field sites, suggested that the calibration polynomials for each soil depth would not necessarily apply to the field experimental data.

Therefore, the question arose as to how to apply the site specific calibration functions derived for each block sample representing a different soil depth, to the field experimental data. Three different approaches were tested. Firstly, the calibration data for the soil layers with clay contents less than 30 % (100- and 700-mm) were combined, and a new calibration polynomial derived. Secondly, the same was done for soil layers with clay contents exceeding 30 % (300- and 500-mm). Lastly, all the data collected during the calibration were combined to obtain a general calibration function.

---

<sup>32</sup> More detailed statistical information on the relationship between the measured and the calculated volumetric soil water content (based on new polynomials), for different soil depths are given in Table B.4.

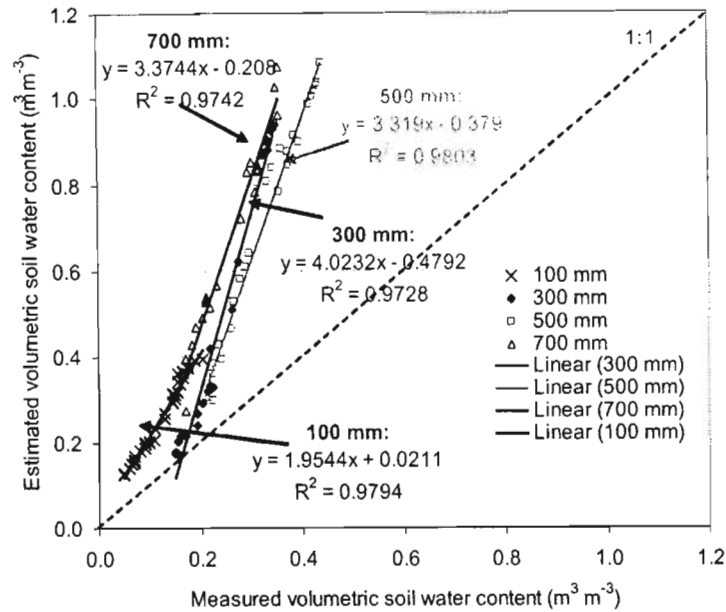


Fig. B.5 Relationship between the measured volumetric soil water content (x) and the soil water content calculated using the manufacturers' polynomials (y) for different soil samples (100, 300, 500 and 700 mm)

Table B.2 Statistical information on the relationship between the measured soil water content and the soil water contents estimated from CSI polynomials, presented in Fig. B.5

Measured soil water content vs soil water content estimated from CSI polynomials	Statistical information		Soil depth (mm)			
			100	300	500	700
	Regression Statistics	Multiple R		0.9897	0.9863	0.9901
R Square			0.9794	0.9728	0.9803	0.9742
Adjusted R Square			0.9788	0.9714	0.9795	0.9731
Standard Error			0.0129	0.0512	0.0386	0.0370
Observations			33	21	26	26
Intercept t	Coefficients		0.0211	-0.4792	-0.3790	-0.2080
	Standard Error		0.0065	0.0382	0.0323	0.0305
	P-value		0.0027	1.21208E-10	1.92939E-11	4.80141E-07
X Variable 1	Coefficients		1.9544	4.0232	3.3190	3.3744
	Standard Error		0.0509	0.1543	0.0961	0.1121
	P-value		1.01821E-27	2.44266E-16	5.61614E-22	1.41214E-20

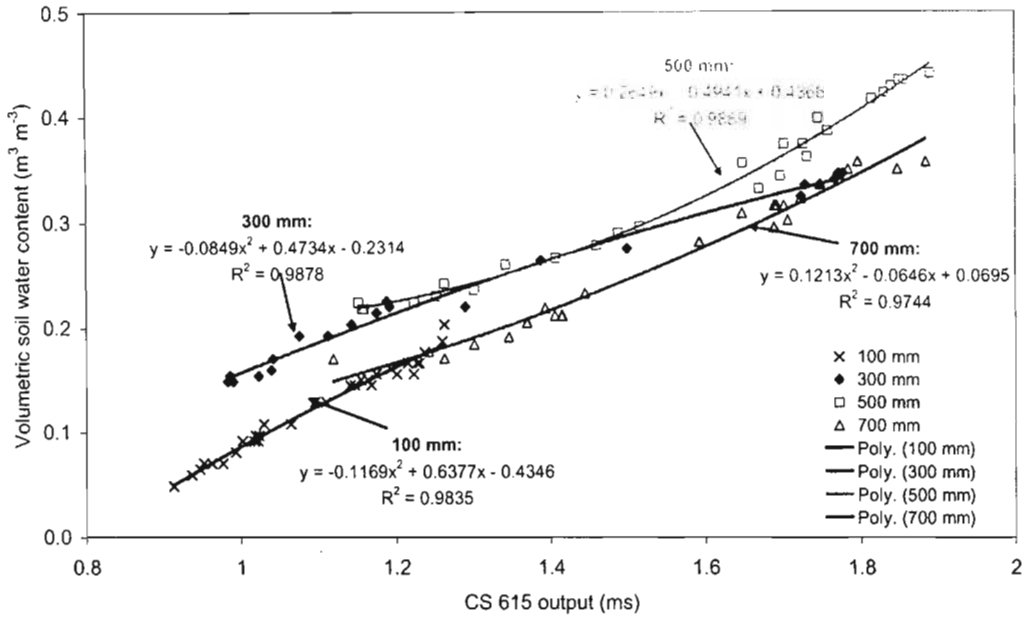


Fig. B.6 Relationship between the output of the model CS615 water content reflectometer in ms for each soil layer, and the volumetric soil water content measured

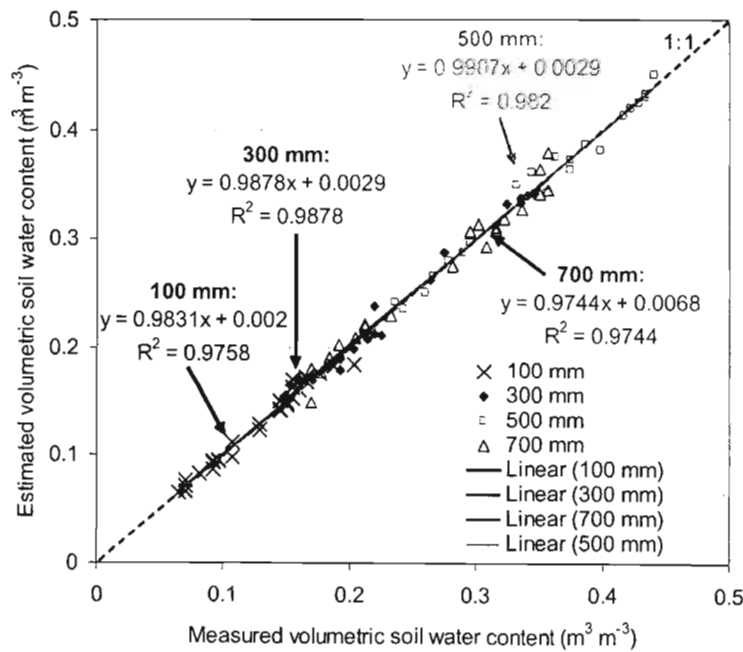


Fig. B.7 Relationship between the measured ( $x$ ) and calculated ( $y$ ) (based on new estimated polynomial functions) volumetric soil water content for each soil layer

Table B.3 Statistical information on the relationship between the CS615 output (ms) and the measured volumetric soil water content, presented in Fig. B.6

CS615 output vs measured volumetric soil water content	Statistical information		Soil depth (mm)			
			100	300	500	700
	Regression Statistics	Multiple R	0.9914	0.9919	0.9833	0.9844
R Square		0.9828	0.9839	0.9670	0.9690	
Adjusted R Square		0.9822	0.9830	0.9656	0.9677	
Standard Error		0.0060	0.0097	0.0149	0.0119	
Observations		33	21	26	26	
Intercept	Coefficients	-0.2984	-0.0747	-0.1554	-0.2077	
	Standard Error	0.0100	0.0094	0.0184	0.0174	
	P-value	1.9851E-24	1.82967E-07	1.19314E-08	1.38543E-11	
X Variable 1	Coefficients	0.3839	0.2365	0.3094	0.3056	
	Standard Error	0.0091	0.0070	0.0117	0.0112	
	P-value	6.51658E-29	1.72125E-18	2.75328E-19	1.27411E-19	

Table B.4 Statistical information on the relationship between the measured soil water content and the volumetric soil water content calculated from the new polynomials, presented in Fig. B.7

Measured soil water content vs calculated soil water content (new polynomials)	Statistical information		Soil depth (mm)			
			100	300	500	700
	Regression Statistics	Multiple R	0.9917	0.9939	0.9944	0.9871
R Square		0.9835	0.9878	0.9889	0.9744	
Adjusted R Square		0.9829	0.9871	0.9885	0.9734	
Standard Error		0.0058	0.0084	0.0086	0.0106	
Observations		33	21	26	26	
Intercept	Coefficients	0.0020	0.0029	0.0036	0.0068	
	Standard Error	0.0029	0.0062	0.0072	0.0088	
	P-value	0.5036	0.6478	0.6190	0.4483	
X Variable 1	Coefficients	0.9835	0.9878	0.9889	0.9744	
	Standard Error	0.0229	0.0252	0.0214	0.0322	
	P-value	3.50309E-29	1.2418E-19	5.51491E-25	1.27236E-20	

Good relationships ( $R^2 > 0.977$ ) were found between the sensor period outputs (ms) and the soil water contents for the new polynomials combining the 100- and the 700-mm depth data, and the 300- and the 500-mm data ( $R^2 = 0.9773$  and  $R^2 = 0.99$  for the 300- and 500-mm and 100- and 700-mm combined data sets respectively) (Table B.5). The application of new second-order polynomials showed accurate predictions the soil water content of soils with different clay contents ( $R^2 = 0.988$  and  $R^2 = 0.955$  for soil depths 100- to 700-mm, and 300- and 500-mm respectively<sup>33</sup>). These polynomials slightly underestimated (1 to 4 %) the soil water contents with these clay contents (Fig. B.8). However, applying a single polynomial, derived from all the calibration data, underestimated the soil water contents by approximately 9 % (Fig. B.8).

### **B.5 Conclusions**

Therefore, it is clear that soil samples with clay contents of more than 30 % need to be calibrated separately from the soil samples with clay contents less than 30 % as this will result in more accurate estimates of the soil water contents. Therefore, the polynomial derived from the 100-mm calibration data was used to convert the sensor outputs collected at 100-mm soil depth to soil water content at both the grassland and *E. viminalis* field experimental sites. The rest of the sensors outputs (300, 500, 700 and 900 mm) collected during the field experiment at both the grassland and *E. viminalis* sites were converted into soil water contents, using the 300- and 500-mm combination second-order polynomial.

---

<sup>33</sup> Table B.6 presents more detailed statistical information on the relationship between measured and the calculated volumetric soil water content (based on new polynomials), for different soil depths. These polynomials were derived from different combinations of measured data.

Table B.5 Information on second-order polynomials derived from different soil depths. The polynomial are based on the measured volumetric soil water content and CS615 sensor output period for different soil depths or soil depth combinations

Quadratic Fit ( $y = a + bx + cx^2$ )								
Period (ms) vs measured volumetric soil water content ( $m^3 m^{-3}$ )								
	Manufacturers ' ( $EC < 1 \text{ dS } m^{-1}$ )	Sample depth (mm)						
		100	300	500	700	100 and 700	300 and 500	100, 300, 500 and 700
<i>a</i>	-0.1870	-0.4346	-0.2314	0.4366	0.0695	-0.3267	0.0467	-0.2507
<i>b</i>	0.0370	0.6377	0.4734	-0.4941	-0.0646	0.4680	0.0313	0.3777
<i>c</i>	0.3350	-0.1169	-0.0850	0.2649	0.1213	-0.0537	0.0886	-0.0177

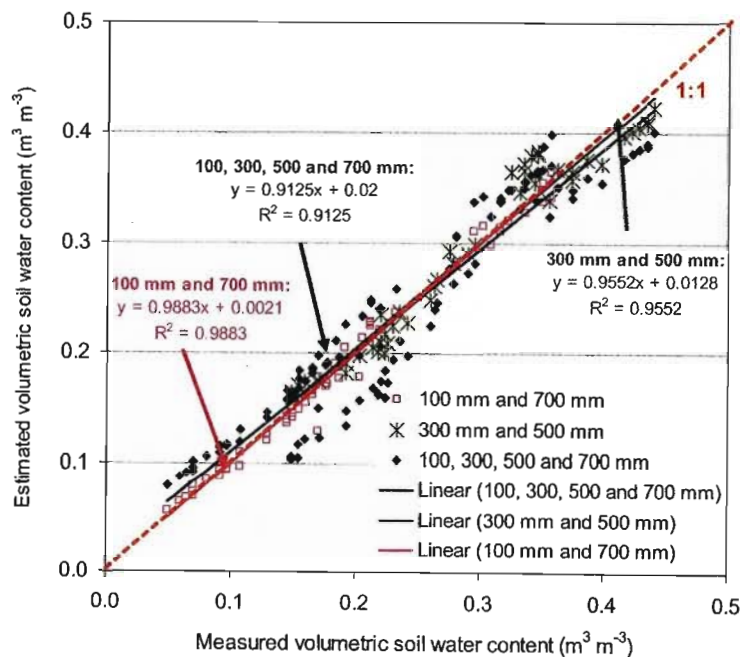


Fig. B.8 Relationship between combinations of newly calculated volumetric soil water content and measured soil water content. The newly estimated volumetric soil water content is based on polynomials derived for the data combinations collected during the calibration periods, and is indicated in the legend

Table B.6 Statistical information on the relationship between the measured soil water content and the soil water content calculated from combined polynomials, presented in Fig. B.8

Measured soil water content vs calculated soil water content (combined polynomials)	Statistical information		Soil depth (mm)			
			100 and 700	300 and 500	100, 300, 500 and 700	
Regression Statistics	Multiple R		0.9941	0.9773	0.9552	
	R Square		0.9883	0.9552	0.9125	
	Adjusted R Square		0.9881	0.9542	0.9117	
	Standard Error		0.0099	0.0186	0.0294	
	Observations		59	47	106	
Intercept	Coefficients		0.0021	0.0128	0.0200	
	Standard Error		0.0029	0.0092	0.0070	
	P-value		0.4645	0.1718	0.0048	
X Variable 1	Coefficients		0.9883	0.9552	0.9125	
	Standard Error		0.0142	0.0308	0.0277	
	P-value		9.137E-57	5.45637E-32	7.90339E-57	

## APPENDIX C

### RELATIONSHIP BETWEEN THE SOIL WATER CONTENT AND THE SOIL WATER POTENTIAL

#### **C.1 Introduction**

To illustrate the effect of different vegetation types on the profile soil water contents and the water movement within the soil profiles, three different types of soil sensors were used. Water content reflectometers, heat dissipation sensors and soil psychrometers were used to cover the possible range of soil water contents and soil water potentials within the soils, ranging from periodically saturated to very dry soils.

In order to compare soil water content estimated using water content reflectometers with soil water potential estimated using heat dissipation sensors and soil psychrometers, soil water content was converted to soil water potential using the Van Genuchten (1980) relationship (Eq. 3.4). As the soil depths of the grassland site were near saturation for extended periods during the field experiment (Fig. 6.1), the soil water potentials calculated at the *E. viminalis* site were compared. The response of different soil sensors, at the *E. viminalis* site to wetting and drying periods following rainfall periods, will be compared.

#### **C.2 Comparison of the soil water potentials estimated with water content reflectometers, heat dissipation sensors and thermocouple psychrometers**

Water content reflectometers, heat dissipation sensors and thermocouple psychrometers all responded to changes in soil water potential due to rainfall and soil water movement. The sensors responded differently at different soil depths. Differences in soil water potential estimated using the different sensors were clear when comparing the:

- responses of the sensors to changes in soil water potential using the surface and sub-surface soil depths,



- soil water potential during a wetting period,
- soil water potential following a rainfall event, and
- soil water potential during a drying period.

As differences in the soil water potential estimated using different sensors existed, trends are discussed rather than quantitative values.

When comparing the soil water potential estimated with the different sensors, it is clear that more negative (lower) soil water potentials were in general estimated at the soil depth closest to the surface, than at greater depths (Fig. C.1). Although the full scale of measurements are not shown in Fig. C.1, it is clear that the soil water potentials estimated with the water content reflectometer close to the surface (100 mm) were less than -500 MPa, whilst that estimated with the heat dissipation sensors were an order of magnitude greater, and that estimated with the thermocouple psychrometers, much larger (about  $10^3$  times) and of the order of -1200 kPa under fairly wet conditions.

The very low soil water potentials estimated with the water content reflectometers and heat dissipation sensors at this soil depth (100 mm) compared to that estimated with the thermocouple psychrometer, illustrates the sensitivity of these sensors and techniques to surface contact between soil and sensor. At depths close to the surface, where the climatic conditions play an important role in drying the soil, the soil water potentials change quickly following rainfall events. Therefore, as soon as small cracks are formed around the sensors or the soil moves away from the sensor during a shrinking action of the soil, the sensor loses contact with the soil and low soil water potentials are estimated. The very low soil water potentials estimated at greater soil depths (300 mm, 500 mm, 700 mm and 900 mm) with especially the heat dissipation sensors, are probably also the result of loss of surface contact between sensor and soil (Fig. C.1).

The soil sensors at the soil depths close to the surface also responded to less significant rainfall events than the sensors installed at greater depths. The changes in soil water potential for the shallower depths (100 mm) were also more rapid prior to and following the rainfall event compared to that at greater depths. For example, only the soil water potential sensors at 100-mm depth responded to rainfall events (2 to 56 mm d<sup>-1</sup>) from 1 January to 19 February 1999.

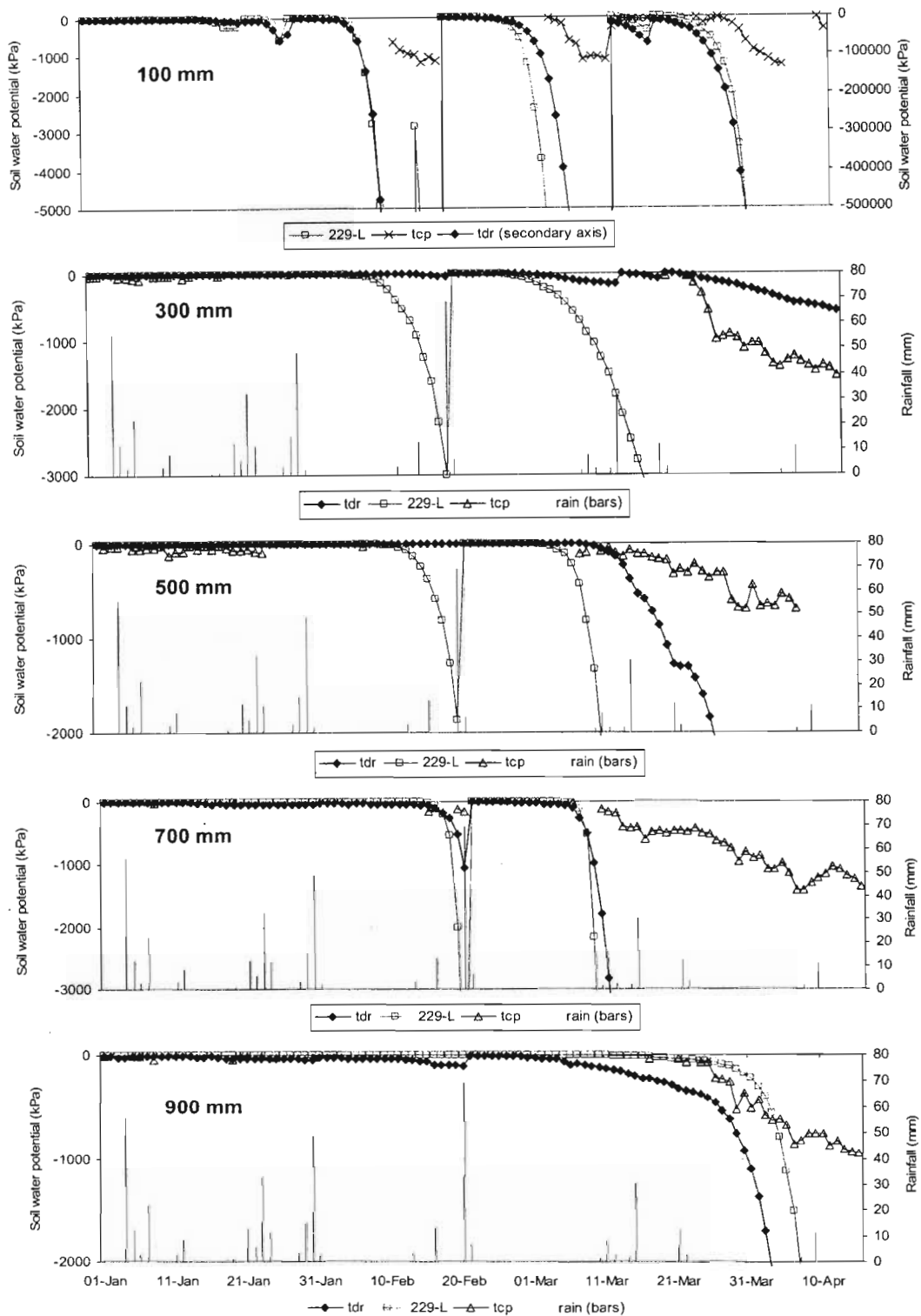


Fig. C.1 Daily soil water potentials for the 100-mm, 300-mm, 500-mm, 700-mm and 900-mm soil depths (top to bottom) at the *E. viminalis* site. Soil water potentials estimated with water content reflectometers measurements (tdr), heat dissipation sensors (229-L) and thermocouple psychrometers (tcp). Bars represent the daily rainfall

On 29 January 1999, with a rainfall event of 49 mm, the soil water potential at this depth estimated with a water content reflectometer and a heat dissipation sensor respectively, increased from -60680 kPa and -530 kPa respectively to close to 0 kPa. The soil water potentials at all of the other depths were close to 0 kPa, following 831 mm accumulated rainfall from the start of the season.

However, following a rainfall event of 69 mm towards the end of summer (21 February 1999), the soil water potential at the 100-mm soil depth, estimated with water content reflectometers and heat dissipation sensors, increased close to 0 kPa (Fig. C.1). Within the layers of greater depth, the soil water potentials also increased close to 0 kPa. This increase in the soil water potentials was especially noticeable for the heat dissipation sensor data. The water content reflectometer soil water potentials, did not show a significant change. Prior to this increase and rainfall event (approximately 20 days) the soil water potentials, estimated using water content reflectometers and heat dissipation sensors, decreased continually.

From the end of February 1999 until mid-April, the soil water potential at all soil depths and as estimated with different sensors, decreased from 0 kPa (Fig. C.1). Higher soil water potentials were maintained for longer with the water content reflectometers and heat dissipation sensors at 300-mm and 900-mm soil depths. However, from the end of March until mid-April, during the soil drying period, the soil water potential estimated using thermocouple psychrometers exceeded that estimated using water content reflectometers and heat dissipation sensors. The exceptions were the soil water potential estimated at the 300-mm soil depth and periodically at the 900-mm soil depth. The higher soil water potentials estimated with the thermocouple psychrometers suggest a slower response by these sensors to changes in soil water potential, as a result of saturation of the soil. Alternatively, the lower soil water potentials estimated with the heat dissipation sensors and thermocouple psychrometers mean that these sensors lost contact with the soil.

### ***C.3 Possible reasons for discrepancies between soil water potentials estimated with different soil water sensors***

Although similar trends in the soil water potentials estimated with different sensors were found, the actual soil water potentials were different. The relationships between the soil water potentials estimated with the different techniques at each soil depth were also different. There may be many reasons for the discrepancies between the soil water potentials estimated within a specific soil layer.

#### **C.3.1 Conversion of soil water content into soil water potential**

The water content reflectometers provide an estimate of soil water content, whereas the heat dissipation sensors and the thermocouple psychrometers estimate soil water potential. The soil water content estimated with water content reflectometers was converted into soil water potential using water retention relationships. The accuracy of the conversion of soil water content into soil water potential will therefore be dependent on the accuracy of the parameters of this retentivity relationship. The accuracy of these parameters will in turn depend on whether they were determined from representative sub-soil samples, taken from the particular soil depth in question.

#### **C.3.2 Conversion equations (sensor output vs soil water potential)**

The outputs of the heat dissipation sensors (temperature differences) as well as the thermocouple psychrometers (voltage differences) were converted into soil water potentials using generalised equations as suggested by Jovanovic and Annandale (1997) and Brown (1970) respectively and not using site or sensor specific equations. Site or sensor specific calibration equations might have yielded more accurate estimates of soil water potential and better relationships between the soil water potentials estimated for the different types of sensors.

The soil water content estimated from the water content reflectometer period output was calculated using second-order polynomial functions determined in the laboratory. However, as the clay contents of the calibration samples (taken at the grassland site) and the field samples (taken at the grassland and *E. viminalis* sites) were different, the calibration results were extrapolated. Generalized calibration equations were derived for clay contents exceeding 30 % and for clay contents less than 30 %, combining the calibration results. Individual field calibrations of the water content reflectometers installed at the different soil depths at each site may have yielded more accurate soil water content and soil water potential estimates. This may have resulted in an improved comparison between soil water potentials estimated using the different sensors.

Therefore, in order to compare results from different sensors, field or laboratory calibrations are imperative. More accurate calibrations however would not have solved the problem of the soil occasionally losing contact with the sensor through soil shrinking under drying conditions, irrespective of the type of sensor.

### **C.3.3 Soil water potential vs soil matric potential**

Differences between soil water potential estimated using different sensors could also be attributed to the fact that the heat dissipation and water content reflectometer conversions provide estimates of matric potential whereas the thermocouple psychrometer provided estimates of the total soil water potential<sup>34</sup>. If for example osmotic potential, a component of total soil water potential, played an important role at the research sites, the exclusion of this term in the comparison would have caused differences between the results of the water content reflectometer and heat dissipation sensor, and the soil psychrometer. However, as the electrical conductivity for the different soil depths at the grassland and *E. viminalis* sites only ranged between 0.025 and 0.095 S m<sup>-1</sup>, this was not expected.

---

<sup>34</sup> Total soil water potential includes matric potential, osmotic potential and gravitational potential.

### **C.3.4 Disadvantages and limitations of, and damage to soil sensors**

Insufficient surface contact between a water content reflectometer or a heat dissipation sensor and the soil, may cause different soil water potential estimates, especially during dry periods. This is especially the case with the water content reflectometers, where surface contact should be maintained over the whole length (300 mm) of each of the two rods.

Intensive drying periods during winter at both the grassland and *E. viminalis* sites have resulted in cracking of the ceramic of all the heat dissipation sensors installed at both sites. The soil water potential estimates using these sensors, following the formation of the cracks, were therefore variable and the data discarded.

## **C.4 Summary**

This section compared the soil water potentials estimated with different sensors: water content reflectometers, heat dissipation sensors and soil psychrometers. The results suggest that when applying these sensors to non-standard conditions, site-specific calibrations are required. More accurate calibrations however would not have solved the problem of the soil occasionally losing contact with the sensor through soil shrinking under drying conditions, irrespective of the type of sensor. This section also provided possible reasons for discrepancies between the soil water potentials estimated with the different techniques. The psychrometer should, in theory, be less sensitive to non-contact problems since the technique involves water vapour pressure equilibration between the pore space of the soil and the cavity of the psychrometer. All of the other techniques are critically dependent on good contact between soil and sensor.

## APPENDIX D

### SEASONAL CHANGES IN THE TOTAL EVAPORATION OF GRASSLAND AND TRANSPIRATION OF *E. VIMINALIS* TREES

#### **D.1 Introduction**

The hypothesis of this study is that a change in vegetation, from grassland to *E. viminalis* trees, will reduce the drainage of water beyond the root-zone and into the underground mine workings. The potential reduction in drainage following afforestation with *E. viminalis* trees is the result of the modification of the other soil water balance components and their relationships (increased total evaporation and decreased soil water storage), over the short- and long-term.

The seasonal changes in the total evaporation component of a grassland and *E. viminalis* trees observed during the field experiment, and the climatic conditions experienced during the field experiment, are presented below. These seasonal changes in the total evaporation and transpiration are related to changes in climatic conditions (and atmospheric demand), plant growth (leaf area index, root density distribution) and soil water availability experienced during the field experiment. From these it is possible to deduce the possible effect of a change in vegetation, from grassland to *E. viminalis* trees, on the total evaporation.

#### **D.2 Total evaporation for the grassland site**

##### **D.2.1 Introduction**

The total evaporation of a grassland estimated with the Bowen ratio energy balance technique, includes (a) evaporation from the soil surface, (b) transpiration by the grass and (c) evaporation of water intercepted by the grass canopy. The Bowen ratio energy balance technique requires measurement of net irradiance and soil heat flux densities, and the estimation of the sensible and latent heat flux densities (Eq. 2.1). The latent heat flux density is subsequently converted into total evaporation (Eq. 2.8). Seasonal changes in the total evaporation of a grassland is therefore directly related to the seasonal changes in the energy balance components. These seasonal changes in the

grassland energy balance are discussed in Appendix E. The focus here is on the latent heat component (evaporation) of the energy balance.

### D.2.2 Seasonal variation in total evaporation of a grassland

Due to an incomplete total evaporation data set<sup>35</sup>, seasonal trends rather than quantitative values are explored in this section.

After the onset of rainfall (9 September 1998), the Bowen ratio energy balance total evaporation increased from 1.5 mm d<sup>-1</sup> during early spring (3 October 1998) to 7.9 mm d<sup>-1</sup> towards the end of spring (14 November 1998) (Fig. D.1). The increase in the total evaporation over this period was the result of the increased soil water availability following 217.7 mm of rainfall, an increase in air temperature and solar radiant density of 6.3 °C and 6.1 MJ m<sup>-2</sup> respectively (Fig. D.2), and increased growth through an increased leaf area index of up to 6 (Fig. D.3). During this period in spring, the total evaporation (Fig. D.4) varied and responded to daily changes in the climatic conditions. For example, the total evaporation decreased from 5.6 to 3.7 mm d<sup>-1</sup> (19 to 20 October 1998 respectively), following the decrease in the radiant density (27 to 26 MJ m<sup>-2</sup>) (Fig. D.4).

Maximum daily total evaporation of 6 to 8 mm d<sup>-1</sup> (Fig. D.1) was reached at the end of spring (November 1998) and during summer (December 1998, January 1999) and coincided with maximum average daily air temperatures (19.7 °C), solar radiant density (31.1 MJ m<sup>-2</sup>) (Fig. D.2), and maximum leaf area index of 6 (Fig. D.3).

The maximum total evaporation estimated in this study was higher than that recorded for other grassland sites. Versfeld *et al.* (1998) measured total evaporation for grassland in the Secunda area over a short period in summer of 1 and 3 mm d<sup>-1</sup>. Wever *et al.* (2002) found the total evaporation of a northern temperate grassland to reach a maximum of 4.5 mm d<sup>-1</sup>, whereas Everson *et al.* (1998) found total evaporation for moist upland grassland during summer to be between 3 and 7 mm d<sup>-1</sup>.

---

<sup>35</sup> Due to rejected data, broken sensors for example damaged fine wire thermocouples and unfavourable weather conditions, the Bowen ratio energy balance evaporation data were incomplete.



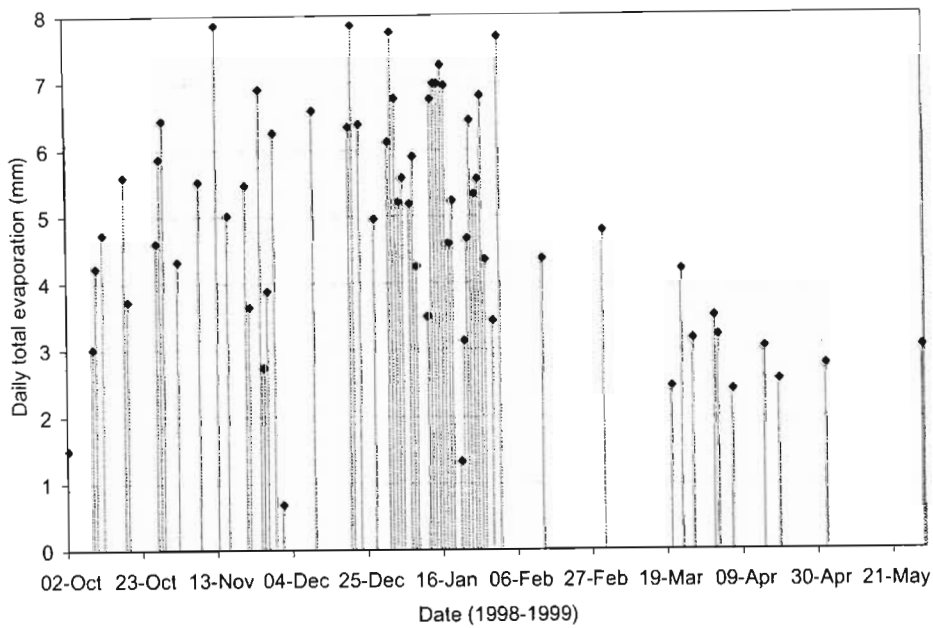


Fig. D.1 Daily total evaporation of grassland estimated with the Bowen ratio energy balance technique for the period 3 October 1998 to 30 May 1999

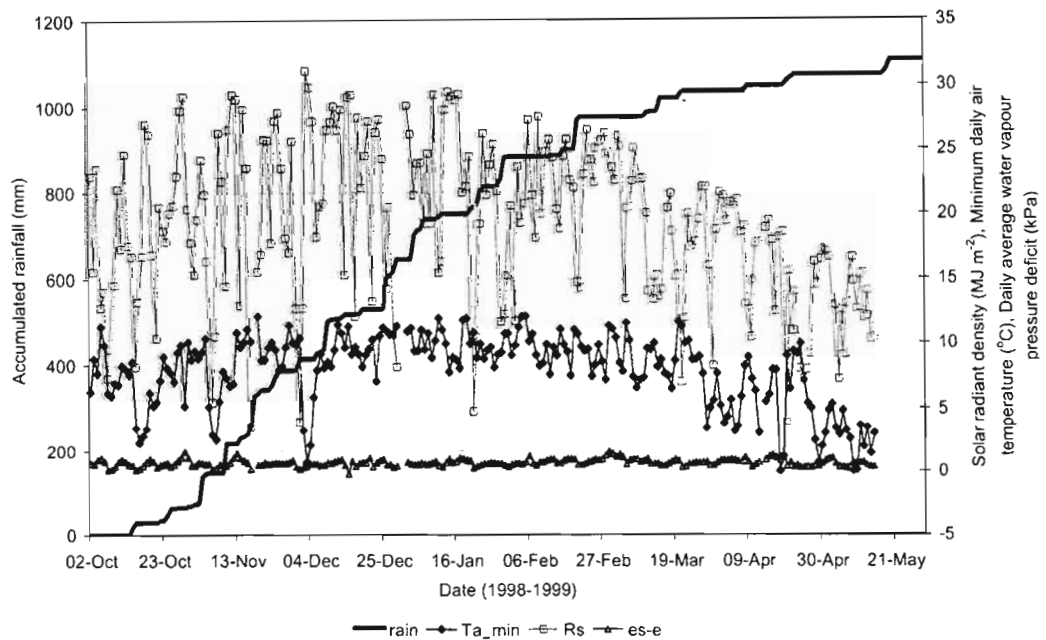


Fig. D.2 Climatic conditions for the period 3 October 1998 to 30 May 1999:

Accumulated rainfall (rain), daily minimum air temperature ( $T_{a\_min}$ ), daily solar radiant density ( $R_s$ ) and daily average water vapour pressure deficit ( $es-e$ )

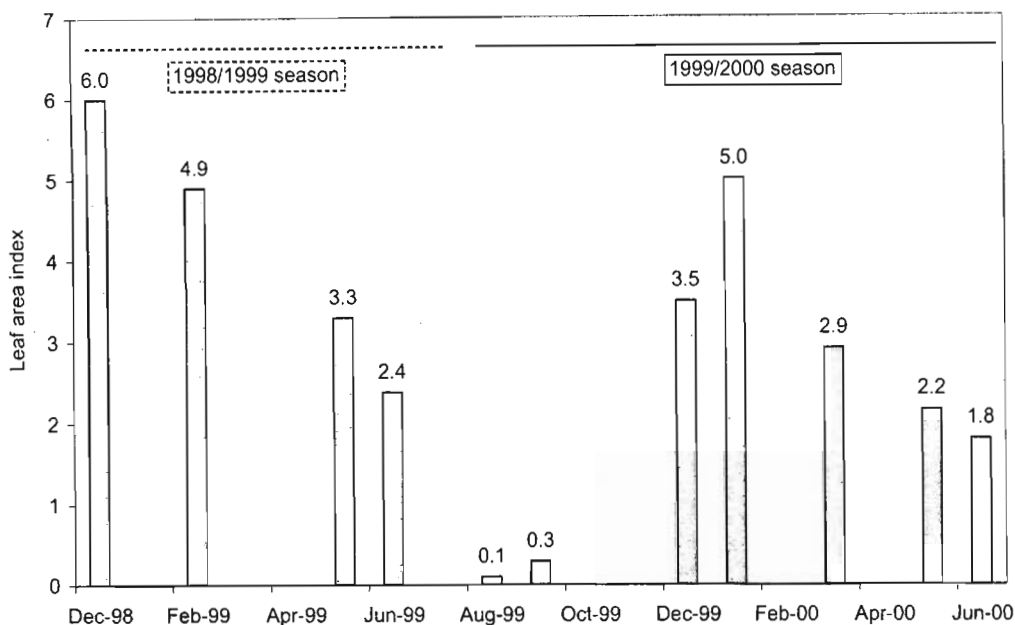


Fig. D.3 Leaf area index variations at the grassland site for the period December 1998 to June 2000

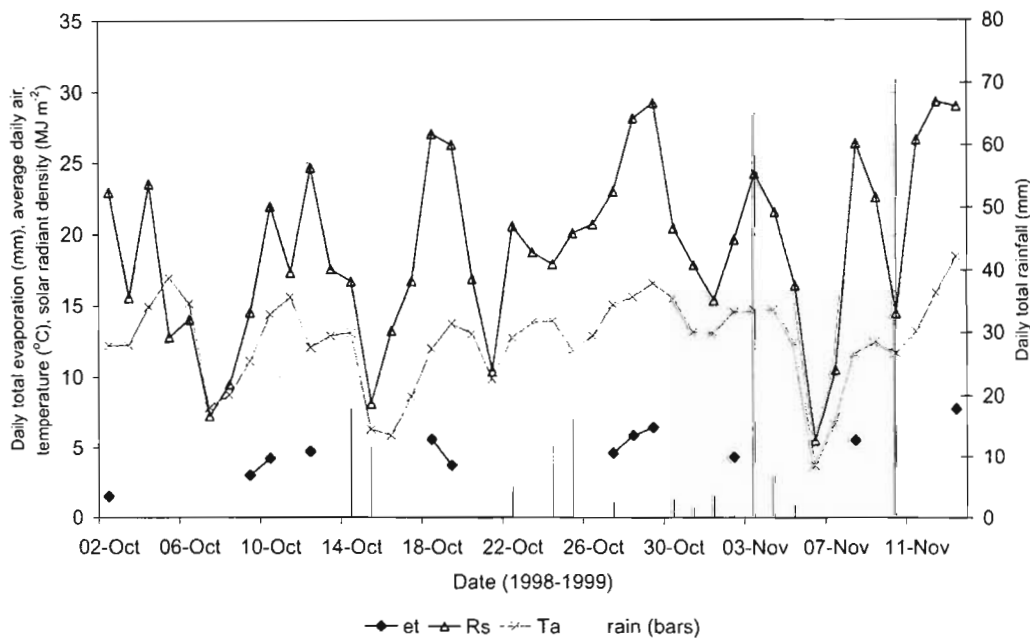


Fig. D.4 Daily total evaporation of grassland as estimated with the Bowen ratio energy balance technique (et), solar radiant density (Rs), average daily air temperature (Ta) and daily total rainfall (rain) for the period 3 October 1998 to 14 November 1999

The high total grassland evaporation estimated in this study can be attributed to the high leaf area index (up to 6) (Fig. D.3) and the consistently high soil profile saturation during summer (also discussed in *Chapter 6*).

The maximum total evaporation during summer was followed by a decrease in total evaporation from about 7.8 to 3.0 mm d<sup>-1</sup> (January 1999 to May 1999). The decrease in the total evaporation (Fig. D.1) over this period was the result of decreases in: air temperature (16.7 to 7.2 °C), solar radiant density (27.2 to 10.4 MJ m<sup>-2</sup>), rainfall (142 to 21.4 mm month<sup>-1</sup>) (Fig. D.2) and leaf area index (6 to 2.4) (Fig. D.3).

The air temperature, solar radiant density, rainfall and leaf area indices decreased further to reach seasonal minimum values during June 1999 (Fig. D.2). No evaporation data is available for this winter period, but total evaporation is expected to decrease below the 3 mm d<sup>-1</sup> estimated during autumn, to less than 1 mm d<sup>-1</sup> during winter (June 1999), following the onset of frost on 10 May 1999 and the subsequent senescence of the grass. Examples of minimum total evaporation of grassland include that by Wever *et al.* (2002) (less than 0.5 mm d<sup>-1</sup>), Versfeld *et al.* (1998) (0.5 mm d<sup>-1</sup>) and Everson *et al.* (1998) (less than 1 mm d<sup>-1</sup>).

### **D.3 Transpiration by *E. viminalis* trees**

#### **D.3.1 Introduction**

The transpiration rates of six *E. viminalis* trees were monitored during 1998/1999 and 1999/2000 using the heat pulse velocity technique. The discussion on the seasonal changes in transpiration and variation in transpiration between individual trees and is limited to three of the six trees studied. The data for the other trees are not as complete. The trees are referred to as Tree1, Tree2 and Tree3 in the discussion below. At the end of the study the tree diameters (at breast height) and heights were 115 mm, 145 mm and 107 mm respectively and 11.3 m, 11.1 m and 11.4 m respectively.

### D.3.2 Seasonal variation in the transpiration of three *E. viminalis* trees

The transpiration during autumn (for example autumn 1999) decreased from between 2.5 and 4 mm d<sup>-1</sup>, to less than 1 mm d<sup>-1</sup> during winter (Fig. D.5). This decreasing trend in transpiration corresponded to decreases in: air temperature (8.8 to 6.2 °C), solar radiant density (15.5 to 11.5 MJ m<sup>-2</sup>), rainfall (35.8 to 0 mm month<sup>-1</sup>) (Figs 5.3 and D.5) and leaf area index (2.6 to 0.9) (Fig. D.6). Minimum transpiration rates (0.4 to 0.6 mm d<sup>-1</sup>) were only reached at the end of winter (August 1999) and the beginning of spring (September 1999), just before the onset of the new rainy season.

Minimum transpiration rates of less than 1 mm d<sup>-1</sup> for all three trees were reached just before the onset of rainfall in spring. The transpiration by Tree1 was the lowest at 0.4 mm d<sup>-1</sup>, followed by 0.5 mm d<sup>-1</sup> by Tree2 and 0.6 mm d<sup>-1</sup> by Tree3 (Fig. D.7). Therefore, the minimum transpiration rates were very similar, within 0.13 mm d<sup>-1</sup> of each other, but Tree3, the tree with the smallest diameter had the highest minimum transpiration rate during winter. Therefore, all three trees were probably experiencing similar amounts of water stress at that time which resulted in winter transpiration rates of less than 1 mm d<sup>-1</sup>.

Lima (1984) found the minimum transpiration of *Eucalyptus* spp. to be 1.5 mm d<sup>-1</sup>, slightly higher than that estimated here, whereas Olbrich *et al.* (1994) and Versfeld *et al.* (1998) found transpiration of *E. viminalis* trees within the same range of that estimated in this experiment: 0.42 mm d<sup>-1</sup> and 0.5 mm d<sup>-1</sup> respectively.

After the first rains of 1999/2000 (mid September 1999), the transpiration of Tree2 and Tree3 increased by about 1 mm d<sup>-1</sup> and that of Tree1 by about 0.3 mm d<sup>-1</sup> (Fig. D.5). The transpiration of all three trees decreased again to about 1 mm d<sup>-1</sup> due to the lack of rainfall until mid October 1999. Following a number of rainfall events exceeding 20 mm d<sup>-1</sup> each from October to December 1999, the transpiration rates of all three trees continued to increase and reached maximum rates of up to 9 mm d<sup>-1</sup> (Tree3) during January 2000 (Fig. D.5). The transpiration of Tree2 increased to a maximum of 3.66 mm d<sup>-1</sup>. By comparison, the transpiration of Tree1 increased from 2.52 mm d<sup>-1</sup> at the start of December 1999 to similar transpiration of Tree3 (about 9 mm d<sup>-1</sup>) towards the end of December 1999 and January 2000 (Fig. D.7).

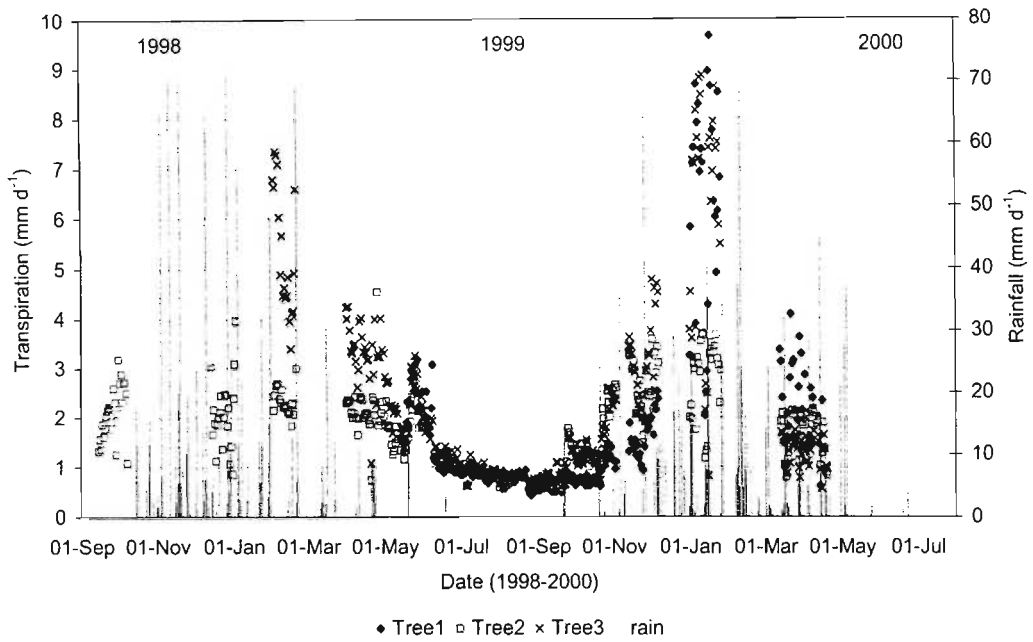


Fig. D.5 Daily transpiration of three *E. viminalis* trees (Tree1, Tree2 and Tree3) representing different diameter classes for the period 1 September 1998 to 30 July 1999

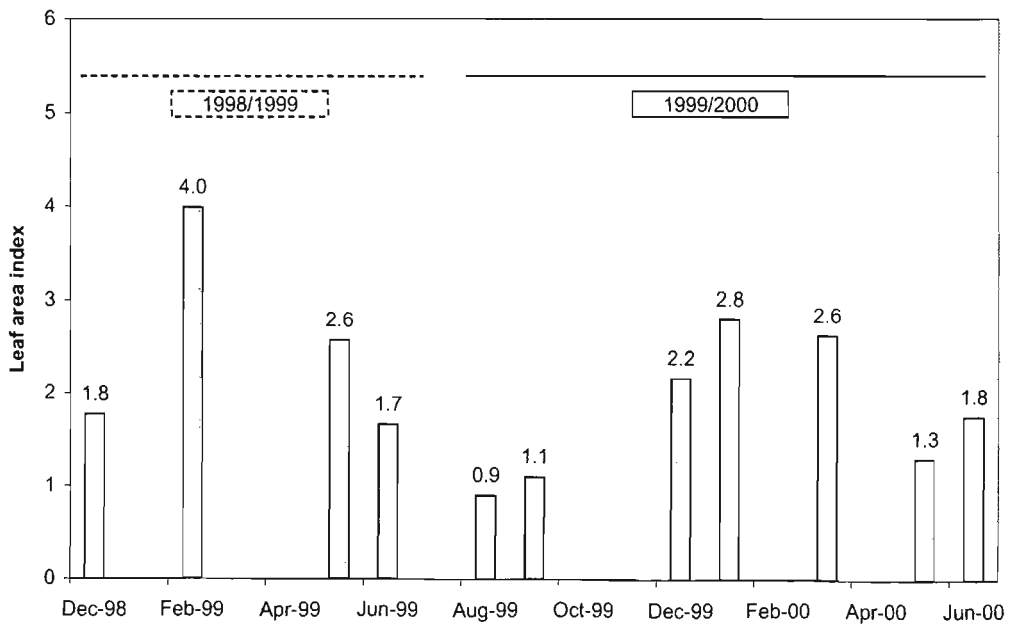


Fig. D.6 Leaf area index variation at the *E. viminalis* site for the period 1998 to 2000

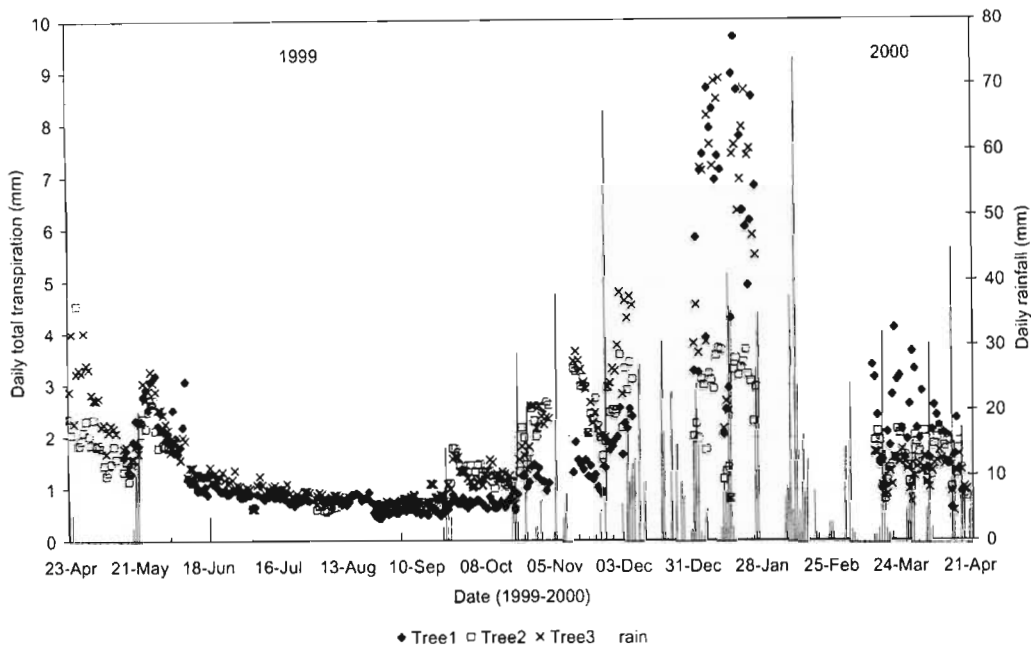


Fig. D.7 Daily total transpiration of Tree1, Tree2 and Tree3, and daily rainfall (rain) represented by the bars, for the period April 1999 to April 2000

The increasing trend in the transpiration was the result of increases in air temperature, solar radiant density, leaf area index and rainfall. The maximum transpiration rates coincided with the maximum solar radiant density, rainfall and growth ( $20.99 \text{ MJ m}^{-2}$ ,  $124.8 \text{ mm month}^{-1}$  and LAI of 2.8 respectively) (Figs 5.3 and D.6) reached during January 2000. The increases in transpiration throughout this period seem very sensitive to rainfall. The transpiration rates during this period often increased by about  $2 \text{ mm d}^{-1}$  following a rainfall event, but decreased when rainfall stopped (for example November 1999) (Fig. D.5). Olbrich *et al.* (1994) also found that the transpiration rates of *E. viminalis* trees were sensitive to soil water deficits.

These maximum transpiration rates of up to  $9 \text{ mm d}^{-1}$  estimated for *E. viminalis* trees were in accordance with transpiration of *E. viminalis* and other *Eucalyptus* tree species within the study area and other areas. Olbrich *et al.* (1994) found maximum summer transpiration *E. viminalis* trees in the Secunda area of  $6 \text{ mm d}^{-1}$ . Versfeld *et al.* (1998) reported maximum transpiration rates by *Eucalyptus* species in the Secunda area to be as high as  $12 \text{ mm d}^{-1}$ . Other examples of high maximum total evaporation and transpiration rates by *Eucalyptus* species are given by Lima (1984) ( $6 \text{ mm d}^{-1}$ ),

Honeysett *et al.* (1992) ( $5$  to  $6$   $\text{mm d}^{-1}$ ) (cited by Hunt and Beadle, 1998) and Zohar and Schiller (1998) ( $5.1$   $\text{mm d}^{-1}$ ) and Jarmain and Everson (2002) ( $9$   $\text{mm d}^{-1}$ ).

Following the maximum transpiration rates reached in summer, the transpiration decreased again, responding to decreases in air temperature ( $3.2$   $^{\circ}\text{C}$ ), solar radiant density ( $8.84$   $\text{MJ m}^{-2}$ ), rainfall ( $55.4$   $\text{mm month}^{-1}$ ) (Figs 5.2 and 5.3) and leaf area index ( $1.5$ ) (Fig. D.6), to reach transpiration rates of  $2$  to  $4$   $\text{mm d}^{-1}$  during autumn. The autumn transpiration was  $2$  to  $5$   $\text{mm d}^{-1}$  less than that estimated during summer. During April 2000, the transpiration of Tree1 during April 2000 was about  $1$   $\text{mm d}^{-1}$  higher than that of Tree2 and Tree3, which had similar transpiration rates (Fig. D.7). The high transpiration of Tree1 during autumn 2000, suggested that although this tree possibly experienced water stress during winter 1999, and was in a poor condition at the start of 1999/2000, it recovered well following the rainfall of 1999/2000. Tree1 was able to maintain high transpiration rates of  $2$  to  $4$   $\text{mm d}^{-1}$  during autumn, which was higher than that of Tree2 and Tree3 during 1999/2000 ( $1$  to  $2$   $\text{mm d}^{-1}$ ), however similar to that during autumn 1998/1999.

#### **D.4 Summary**

This section showed how the total evaporation of grassland and transpiration of three *E. viminalis* trees change over the season in response to changes in rainfall, air temperature, solar radiant density and leaf area index. It showed the sensitivity of total evaporation and transpiration of grassland and different *E. viminalis* trees respectively to rainfall and minimum air temperature, especially during the drier months (autumn, winter and spring).

**APPENDIX E**

**SEASONAL CHANGES IN THE ENERGY BALANCE COMPONENTS**

**OF A GRASSLAND**

**E.1 Introduction**

An analysis of the Bowen ratio energy balance data, consisting of net irradiance flux densities ( $R_n$ ), soil heat flux densities ( $G$ ) and sensible ( $H$ ) and latent heat flux densities ( $\lambda E$ ), highlighted important seasonal differences and helped to explain the effect of climatic and soil conditions on the total evaporation. The energy balance components are related through Eq. 2.1.

**E.2 Estimation of the net irradiance as a function of solar irradiance**

**E.2.1 Introduction**

The net irradiance ( $R_n$ ) is required in the estimation of the latent heat flux density (and subsequently total evaporation) with the Bowen ratio energy balance technique through Eq. 2.7 and 2.8. However, hourly midday net irradiance was not measured during the period 25 August 1998 to 16 April 1999. Solar irradiance available from a nearby automatic weather station was used to estimate the net irradiance for the missing periods using Eq. 2.25, and as a linear function of the solar irradiance. The relationship between the hourly measured and estimated (simulated) net irradiance revealed the accuracy of the estimation, and where Eq. 2.25 was used, the most suitable reflection coefficient to be used.

**E.2.2 Estimation of net irradiance using Eq. 2.25**

Statistically significant relationships were found between net irradiance measured and that estimated as a function of the solar irradiance (Eq. 2.25) (Table E.1, Fig. E.1).



Table E.1 Statistical information on the relationship between the measured ( $x$ ) and the estimated ( $y$ ) net irradiance for a grassland, using different reflection coefficients, where  $y = mx + c$  where  $m$  is the slope of the relationship and  $c$  is the offset

Month	Measured vs estimated net irradiance			
	1998 and 1999			
	Surface reflection coefficient (unitless)	slope $m$	offset $c$	$R^2$
Aug	0.01	0.9969	20.89	0.9721
Sep	0.05	0.9946	27.25	0.9655
Oct	0.01	0.9622	14.48	0.9700
Nov	0.01	0.9647	6.203	0.9506
Dec	0.01	0.9758	16.29	0.9557
Jan	0.11	0.9953	14.42	0.9197
Feb	0.01	0.9213	10.11	0.9743
Mar	0.01	0.9165	11.25	0.9733
Apr	0.01	0.9218	8.706	0.9859

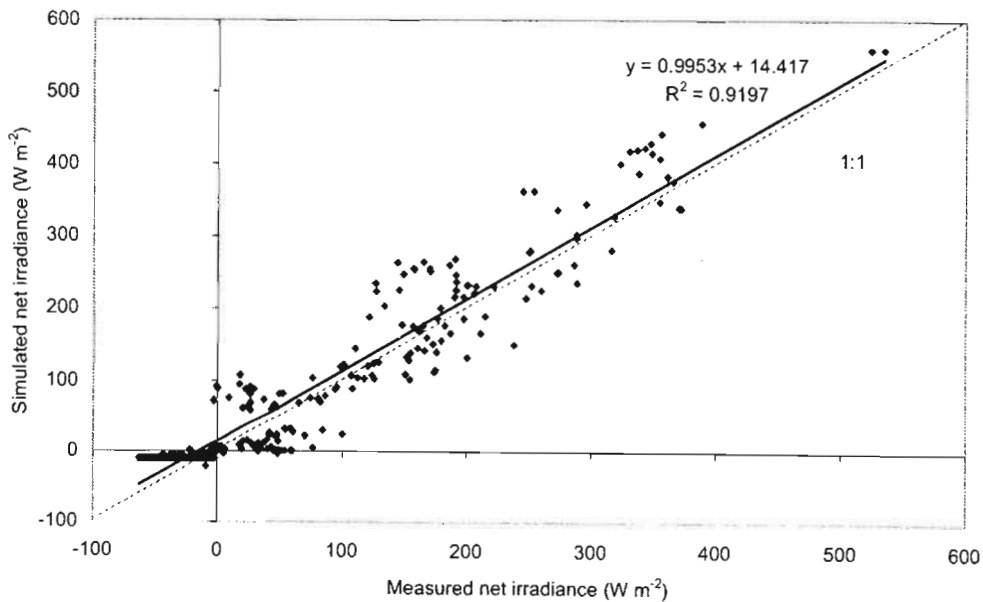


Fig. E.1 Hourly measured ( $x$ ) vs estimated ( $y$ , simulated) net irradiance for grassland during January 1999. Note: The dotted line indicates the 1:1 relationship between the measured and estimated net irradiance, and the solid line the linear relationship between  $x$  and  $y$ . Each data point represents a 20-minute average

The slopes ( $m$ ) of these relationships were close to 1 and the coefficients of determination ( $R^2$ ) exceeded 0.9 (Table E.1). These relationships indicated that the net irradiance can be estimated accurately using the measured solar irradiance and a seasonal, canopy specific reflection coefficient using Eq. 2.25.

### **E.2.3 Estimation of net irradiance as a site-specific linear function of *only* solar irradiance**

Although statistically significant relationships were found between the measured and estimated net irradiance in Section E.2.2, the surface reflection coefficients (albedo's) used in the estimation of the net irradiance (Table E.1) was much lower than values quoted in the literature (Table E.2). The relationship between the measured net irradiance and solar irradiance were therefore studied (Table E.3). This was done to determine whether the linear relationship between the hourly values of net irradiance and solar irradiance could be used to estimate missing net irradiance values, with accuracies close to that obtained with Eq. 2.25 (Table E.1).

Statistically significant relationships ( $R^2 > 0.9$ ) were found between the measured solar irradiance ( $x$ ) and measured net irradiance ( $y$ ) (Table E.3). These linear relationships were subsequently used to calculate the net irradiance. The calculated net irradiance was compared to the measured net irradiance (Table E.3). Statistically significant relationships were found between the measured net irradiance and the net irradiance calculated as a linear function of the solar irradiance, ( $m > 0.93$ ,  $R^2 > 0.95$ ). For August 1998 to December 1998 the net irradiance estimated from the solar irradiance (linear function) underestimated the net irradiance by between 3 % (August 1998) and 7 % (December 1998). The linear relationships between the net irradiance and solar irradiance can therefore be used to calculate the net irradiance to within 7 % accuracy (Table E.3).

Table E.2 Published surface reflection (unitless) coefficients for grassland

<i>Surface</i>	<i>Surface reflection coefficient</i>	<i>Source</i>
<i>Mixed grass</i>	0.22	<i>Kalma and Badham (1972)</i>
<i>Moist upland grassland</i>	0.14 (following burning), 0.42 (summer)	<i>Everson et al. (1998)</i>
<i>Grass</i>	0.24	<i>Jones (1992) (cited by Sumner, 2002)</i>
<i>Green grass</i>	0.16 and 0.27	<i>Van Wijk and Scholte Ubing (1963) (cited by Sumner, 2002)</i>
<i>Dried grass</i>	0.16 to 0.19	<i>Van Wijk and Scholte Ubing (1963) (cited by Sumner, 2002)</i>
<i>Short grass (0.02 m)</i>	0.26	<i>Oke (1978) (cited by Sumner, 2002)</i>
<i>Long grass (1 m)</i>	0.16	<i>Oke (1978) (cited by Sumner, 2002)</i>

Table E.3 Statistical information on the relationship between solar irradiance ( $x$ ) and the net irradiance ( $y$ ) where  $y = mx + c$ ,  $m$  is the slope of the relationship,  $c$  is the offset of the relationship and  $R^2$  is the coefficient of determination, and the relationship between the measured net irradiance ( $x$ ) and the net irradiance calculated as a function of the solar irradiance ( $y$ )

<i>Month (1998)</i>	<i>Statistical information on the relationship between the Solar and net irradiance</i>			<i>Statistical information on the relationship between the measured net irradiance and net irradiance calculated as a linear function of the solar irradiance</i>		
	<i>m</i>	<i>c</i>	<i>R<sup>2</sup></i>	<i>m</i>	<i>c</i>	<i>R<sup>2</sup></i>
<i>August</i>	0.8210	0.9714	0.9714	0.9714	-39.642	0.9713
<i>September</i>	0.7999	0.9664	0.9664	0.9664	-42.080	0.9664
<i>October</i>	0.8515	0.9408	0.9408	0.9408	-27.285	0.9723
<i>November</i>	0.8546	0.9688	0.9688	0.9688	-18.190	0.9615
<i>December</i>	0.8100	0.9345	0.9345	0.9345	-21.764	0.9147

#### **E.2.4 Use of the estimated net irradiance**

The net irradiance estimated using Eq. 2.25 and as a linear function of the solar irradiance, yielded statistically significant relationships when compared to the measured net irradiance (Tables E.1 and E.3). The linear relationship underestimated the net irradiance more than Eq. 2.25 (3 to 7 % vs 1 to 4 % respectively) during the period August to December 1998. Therefore, the measured net irradiance was subsequently combined with the net irradiance estimated with Eq. 2.25, and used in the calculation of the Bowen ratio energy balance total evaporation (Eq. 2.8). However, it is suggested that the surface reflection coefficients used in these estimations of net irradiance in Eq. 2.25 (Table E.1) are not used for the estimation of net irradiance above other grassland surfaces.

#### **E.3 Changes in the partitioning of the available energy ( $R_n-G$ ) into sensible and latent heat flux density at a grassland site**

During spring and early summer (Fig. E.2 top), the net irradiance ( $R_n$ ) reached maximum values of about  $780 \text{ W m}^{-2}$ . The net irradiance increased a further 13 % to reach midday maximums of about  $900 \text{ W m}^{-2}$  (Fig. E.2 middle) during mid-summer. These net irradiance values corresponded with midday maximum solar irradiances of  $1000 \text{ W m}^{-2}$ . These maximum irradiance values (net and solar) decreased steadily towards winter (Figs E.2 and 5.3). During autumn, maximum net and solar irradiance values of  $650 \text{ W m}^{-2}$  and  $700 \text{ W m}^{-2}$  respectively, were reached during the day (Fig. E.2 bottom).

For the period 1998 to 2000, the soil heat flux densities ( $G$ ) (Table E.4) were only a small fraction of the net irradiance:  $G:R_n < 14 \%$  (Fig. E.2). Most modelling studies apply a  $G:R_n$  of 10 % during the day, and  $G:R_n$  of 50 % during the night (Campbell, 1992). Approximately 11 % of the net irradiance was partitioned into the soil heat flux density during winter and only 3 % during summer (Table E.4) for the grassland site. The small  $G:R_n$  ratios during summer coincided with the maximum seasonal leaf area indices ( $LAI$ ) of up to 6 measured at the grassland site during summer (Fig. E.3).

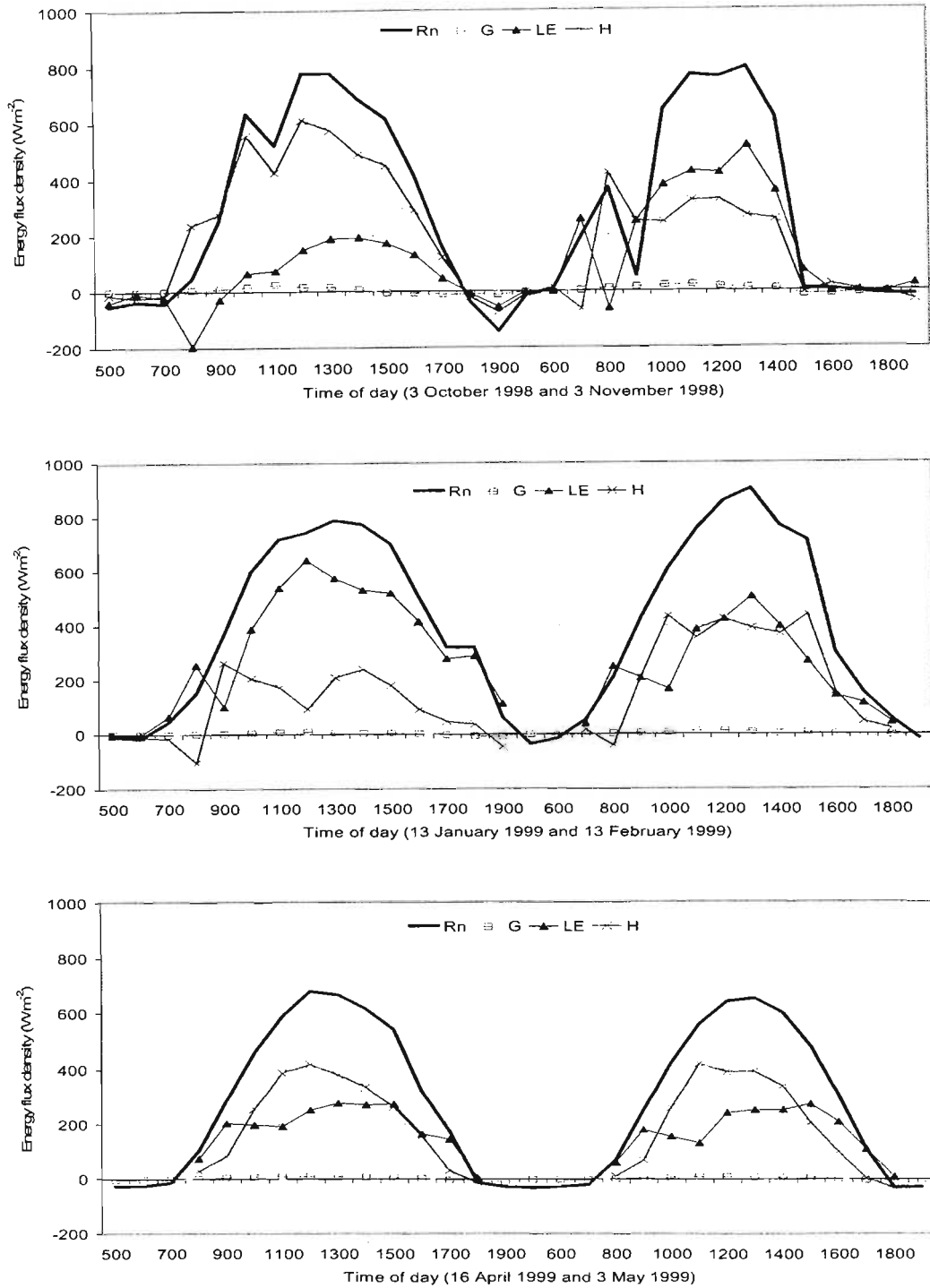


Fig. E.2 Energy flux densities (Rn, G, LE and H) for a grassland site during different times of the year (1998 to 1999). Rn represents net irradiance flux density, G soil heat flux density, LE latent heat flux density and H sensible heat flux density. From top to bottom: 3 October and 3 November 1998 (top); 13 January and 13 February 1999 (middle); 16 April and 3 May 1999 (bottom).

Table E.4 Relationship between the soil heat flux density and the net irradiance ( $G:R_n$ ) measured at the grassland site, where the soil heat flux density is a percentage of the net irradiance for each month of measurement from July 1998 to June 2000

Month	Jul	Aug	Sep	Oct	Nov	Dec	Jan	Feb	Mar	Apr	May	Jun
1998/ 1999	n/a	11	11	4	3	3	3	4	4	5	7	10
1999/ 2000	10	11	11	13	12	13	8	5	3	7	10	10

The high leaf area indices (LAI = 6 during December 98) during summer, decreased to 3.30 during autumn (May 1999) and to 0.10 during winter following mowing and a veld fire. The decrease in the leaf area from 6 to 0.10, corresponded to the increase in the  $G:R_n$  fractions from 3 to 13 % (Table E.4).

Applying the simplified energy balance (Eq. 2.1), the difference between the net irradiance and soil heat flux density ( $R_n - G$ ), provides an estimate of the energy flux density partitioned between the sensible and latent heat flux densities. The available energy flux densities ( $R_n - G$ ) were partitioned into different ratios of sensible ( $H$ ) to latent heat flux densities ( $\lambda E$ ) during 1998/1999 and 1999/2000 (Fig. E.2).

During spring (Fig. E.2 top), most of the available energy flux density (85.5 % or 14 MJ m<sup>-2</sup>) was partitioned into the sensible heat flux density. The remaining energy flux density (2.36 MJ m<sup>-2</sup>) was partitioned into the latent heat flux density. The differences in the sensible and latent heat flux densities were the result of the large profile air temperature differences (-0.3 to 3.5 °C) and small water vapour pressure (-0.03 to 0.09 kPa) differences, that existed during spring (Fig. E.4). This shows that before the onset of rainfall and the start of the grass growing season, most of the available energy was used to heat up the air, and very little (14.5 %) used to drive evaporation.

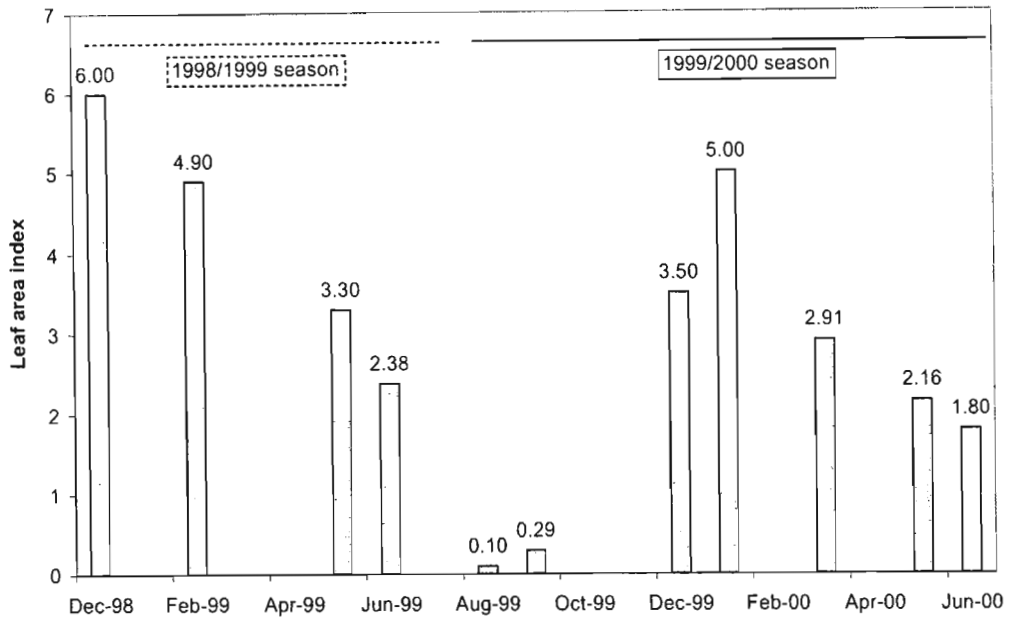


Fig. E.3 Leaf area index at the grassland site for the period December 1998 to June 2000

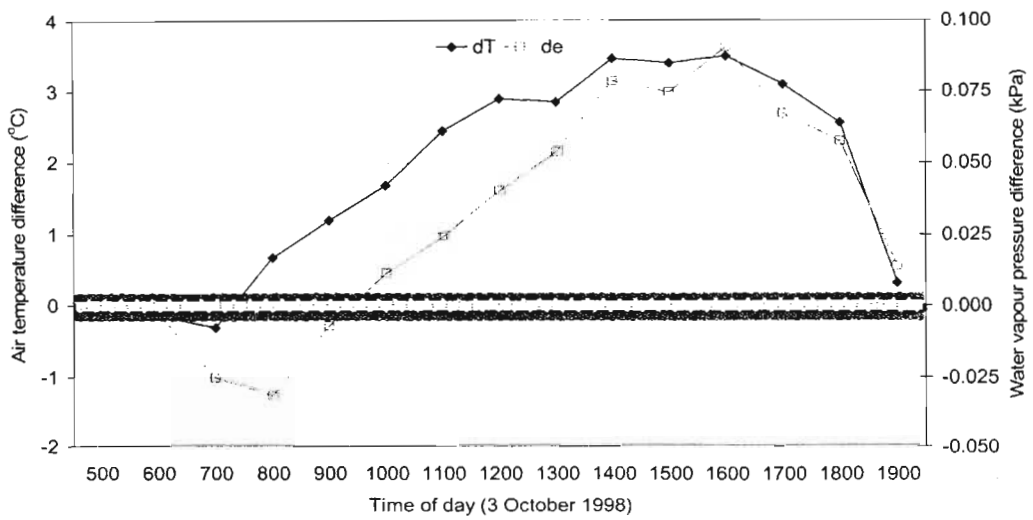


Fig. E.4 Air temperature ( $dT$ ) and water vapour pressure profile differences ( $de$ ) measured at the grassland site during spring (3 October 1998). Profile differences are measured between two sampling arms of the Bowen ratio energy balance system installed at different heights above the grassland. Note: The dotted lines indicate the air temperature and water vapour pressure rejection ranges

However, during summer (Fig. E.2 middle), 42.5 to 61.5 % more available energy flux density was partitioned into latent heat flux density (57 % and 76 % or  $9.5 \text{ MJ m}^{-2} \text{ d}^{-1}$  and  $16.5 \text{ MJ m}^{-2}$  respectively) when compared to spring (Fig. E.2 top). During summer only 43 to 24 % ( $7.2$  to  $5.4 \text{ MJ m}^{-2}$ ) of the available energy flux density was partitioned into sensible heat flux density. This was the result of proportionally lower air temperature differences ( $-0.16$  to  $-0.59 \text{ }^\circ\text{C}$ ) and proportionally higher water vapour pressure differences during summer (Fig. E.5) compared to spring (Fig. E.4). Therefore, during summer with higher available soil water (rainfall) (Fig. 5.3), high atmospheric demands ( $ET_o$ ) (Fig. 5.3), and high  $LAI$ 's through an actively growing crop, up to three quarters of the available energy flux density is used to drive evaporation.

Towards the end of summer and the end of the growing season the available energy flux density (Fig. E.2 middle) was partitioned into almost equal amounts of latent to sensible heat flux densities (51 and 49 % respectively). Thereafter, during autumn, the daily latent and sensible heat flux densities remained similar (45 to 54 % for the latent and the sensible heat flux densities respectively) (Fig. E.2 bottom). These similar flux densities show that evaporation is still taking place, but is not sustained throughout the day. From the diurnal changes in the sensible and latent heat flux densities, it is clear that more available energy flux density is partitioned into the latent heat flux density during early morning and late afternoon, whereas more available energy flux density is partitioned into sensible heat flux density during midday (Fig. E.2 bottom). The higher latent heat flux densities during the morning suggests low canopy resistances, which increases during the afternoon as water becomes less available and this results in a decrease in the latent heat flux densities.

#### **E.4 Summary**

The components of the shortened energy balance of a grassland changed over the season. The changes in the energy balance components are related to the climatic conditions and the grassland plant characteristics. Changes in the energy partitioning affect the latent heat flux density and subsequently the total evaporation.



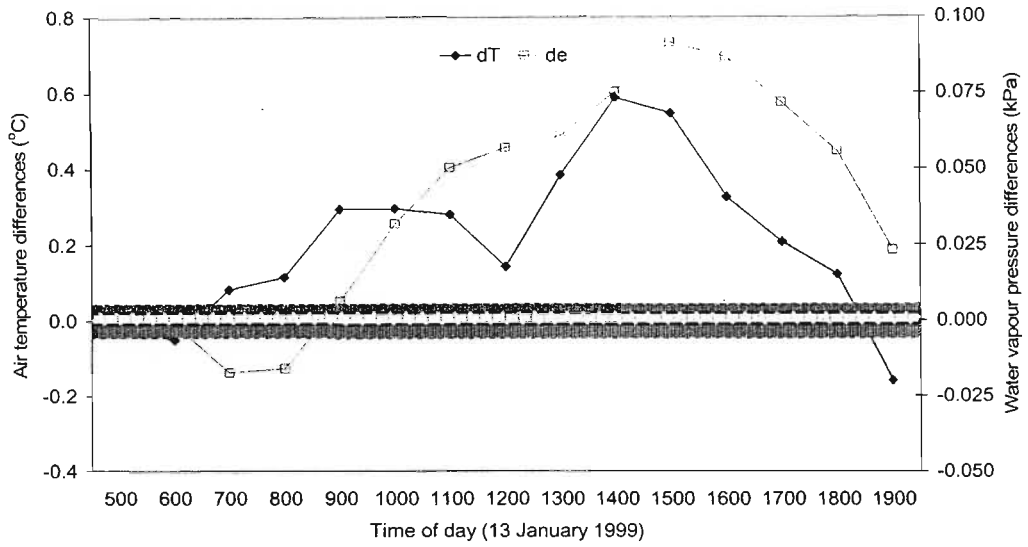


Fig. E.5 Air temperature ( $dT$ ) and water vapour pressure profile differences ( $de$ ) measured at the grassland site during spring (13 January 1999). Profile differences are measured between two sampling arms of the Bowen ratio energy balance system installed at different heights above the grassland. Note: The dotted lines indicate the air temperature and water vapour pressure rejection ranges

## APPENDIX F

### SWAP MODEL INPUT PARAMETERS FOR THE

#### *E. VIMINALIS* AND GRASSLAND SITES

##### **F.1 Introduction**

SWAP has a number of inputs and outputs (Tables F.1 and F.2). The inputs of the model are utilized to calculate the components of the soil water balance at a daily time step. Model inputs for this study include data from the field experiment, data from experiments conducted under similar circumstances, data generated, and data obtained from the literature and through personal communication (Tables F.3 to F.9). The model inputs can be divided in general inputs, and inputs concerning the atmosphere, plants, soil and water.

##### **F.2 General data inputs**

General information required by SWAP for the *E. viminalis* and grassland sites are given in Table F.3.

---

Table F.1 A summary of the SWAP model inputs

---

<b>Component</b>	<b>Examples of model inputs</b>
Atmosphere	General meteorological data
Plant	Growth period, leaf area index, soil cover fraction, canopy height, root density and distribution over time
Soil	Ponding depth, water retention characteristics, hydraulic function, physical properties
Water	Water management, irrigation, drainage

Table F.2 A summary of the SWAP model outputs<sup>36</sup> in  $\text{cm a}^{-1}$ 

Initial soil water content	
Final soil water content	
Change in the soil water content	
<b>Into the profile</b>	<b>Out of the profile</b>
Rainfall	Runoff
Irrigation	Interception
Deep percolation (Bottom flux)	Soil evaporation
	Transpiration
	Drainage
	Crack flux

Table F.3 General information relating to the simulations for both the grassland and *E. viminalis* sites

<i>Parameter</i>	
<i>Start of simulation run</i>	<i>01/07/1964</i>
<i>End of simulation run</i>	<i>30/06/1994</i>
<i>First month of agricultural year</i>	<i>7</i>
<i>Latitude</i>	<i>26.0° South</i>
<i>Altitude (m)</i>	<i>1600</i>
<i>Use ETRef<sup>37</sup> from meteorological files</i>	<i>Yes</i>
<i>Simulation of drainage</i>	<i>No</i>

<sup>36</sup> The components of the soil water balance simulated with SWAP are output in cm

<sup>37</sup> ETRef refers to the reference total evaporation estimated from the automatic weather station data.

### **F.3 Atmospheric data inputs**

Meteorological data for the period 1964 to 1994 were used in the long-term simulations. Long-term daily rainfall and minimum and maximum air temperature data for the region were used in a climatic generator programme (CLIMGEN, undated), to generate the required climatic inputs over this 30 year period. These climatic inputs included: daily total solar radiant density ( $\text{kJ m}^{-2}$ ), minimum and maximum air temperature ( $^{\circ}\text{C}$ ), average relative humidity (kPa), windspeed ( $\text{m s}^{-1}$ ), rainfall ( $\text{mm d}^{-1}$ ) and reference evapotranspiration ( $\text{mm d}^{-1}$ ). The reference evapotranspiration was calculated using the Penman-Monteith equation.

### **F.4 Plant data inputs**

The *E. viminalis* site consists of *E. viminalis* trees with an understorey of *Cymbopogon* grass and other weeds, whereas the grassland site consists of *Cymbopogon* grass and cosmos and other weeds. Both sites have more than one species, and the *E. viminalis* site requires understorey growth modelling whereas the grassland site requires a model that allows for more than one overlapping growing season. However, SWAP does not allow the simulation of growth of an understorey canopy separate from the main canopy, and it also does not make provision for overlap between more than one growing season. Therefore, in the modelling exercises, the inputs for the *E. viminalis* simulations combine the *E. viminalis* tree and grassland information to represent a complete canopy. The inputs for the grassland simulations, combines the *Cymbopogon* and the cosmos and other weed information. The *E. viminalis* and grassland root information was according to Knight (1999), and Versfeld (1998) respectively. The *E. viminalis* height information was supplied by ICFR and was obtained over a trial rotation, where as the *E. viminalis* LAI for a closed canopy was supplied by Dye (2003). The rest of the parameters were obtained from the field experiment data, literature, or through personal communication.

#### F.4.1 Growth calendar

General information on the growth simulations are given in Table F.4.

---

Table F.4 Information regarding the growth simulations used for both sites

---

<i>Parameter</i>	
<i>Number of crops per season</i>	<i>1</i>
<i>Type of crop model</i>	<i>Simple</i>
<i>Emergence of crop</i>	<i>01/07</i>
<i>Forced end of crop growth</i>	<i>30/06</i>

#### F.4.2 Simple growth model data inputs

SWAP has three crop growth model options with varying degrees of complexity and detail required. Due to data limitations at both research sites, the simple crop growth model was selected for simulations at both sites. Key parameters are given in Tables F.5 to F.7.

Table F.5 Growth information<sup>38</sup> required in the simple model parameterisation

<i>Parameter</i>	<i>E. viminalis</i>	<i>Grassland</i>
<i>Length of crop cycle (d)</i>	<i>365 or 366</i>	<i>365 or 366</i>
<i>Extinction coefficient:</i>		
<i>Diffuse visible radiation</i>	<i>0.5</i>	<i>0.4</i>
<i>Direct visible radiation</i>	<i>0.5</i>	<i>0.4</i>
<i>Yield response as a function of development stage</i>	<i>1.0</i>	<i>1.0</i>
<i>Water and salt stress functions:</i>		
<i>No water extraction at higher pressure heads (cm)</i>	<i>-10</i>	<i>-10</i>
<i>H<sup>39</sup> below which water extraction starts for top layer (cm)</i>	<i>-25</i>	<i>-25</i>
<i>H below which water extraction starts for sub layers (cm)</i>	<i>-25</i>	<i>-25</i>
<i>H at which water uptake reduction starts at high Tpot (cm)</i>	<i>-500</i>	<i>-300</i>
<i>H at which water uptake reduction starts at low Tpot (cm)</i>	<i>-1500</i>	<i>-1000</i>
<i>No water extraction at lower pressure heads cm</i>	<i>-15000</i>	<i>-15000</i>
<i>Level of high atmospheric demand (cm d<sup>-1</sup>)</i>	<i>1.1</i>	<i>1.1</i>
<i>Level of high atmospheric demand (cm d<sup>-1</sup>)</i>	<i>0.1</i>	<i>0.1</i>
<i>Minimum canopy resistance (s m<sup>-1</sup>)</i>	<i>70</i>	<i>70</i>
<i>ECsat<sup>40</sup> at which salt stress starts (dS m<sup>-1</sup>)</i>	<i>0.6</i>	<i>2.0</i>
<i>Decline of rootwater uptake above % (dS m<sup>-1</sup>)</i>	<i>0.1</i>	<i>0.1</i>
<i>Interception coefficient Von Hoyningen-Hune and Braden (cm)</i>	<i>0.35</i>	<i>0.25</i>
<i>Relative root depth vs density</i>	<b><u>Depth</u></b>	<b><u>Depth</u></b>
	<b><u>Density</u></b>	<b><u>Density</u></b>
	<i>0.08 0.54</i>	<i>0.38 0.80</i>
	<i>0.17 0.19</i>	<i>0.75 0.15</i>
	<i>0.25 0.06</i>	<i>1.00 0.05</i>
	<i>0.33 0.03</i>	
	<i>0.42 0.02</i>	
	<i>0.50 0.01</i>	
	<i>0.58 0.01</i>	
	<i>0.67 0.01</i>	
	<i>0.83 0.01</i>	
	<i>0.92 0.005</i>	
<i>1.00 0.005</i>		

Table F.6 Growth information required in the simple model parameterisation at the grassland site as a function of development stage

<sup>38</sup> These parameters were chosen in discussions with Savage (2003).

<sup>39</sup> H refers to the pressure head of a soil layer and this value is negative.

<sup>40</sup> ECsat refers to the electrical conductivity level of salt stress.



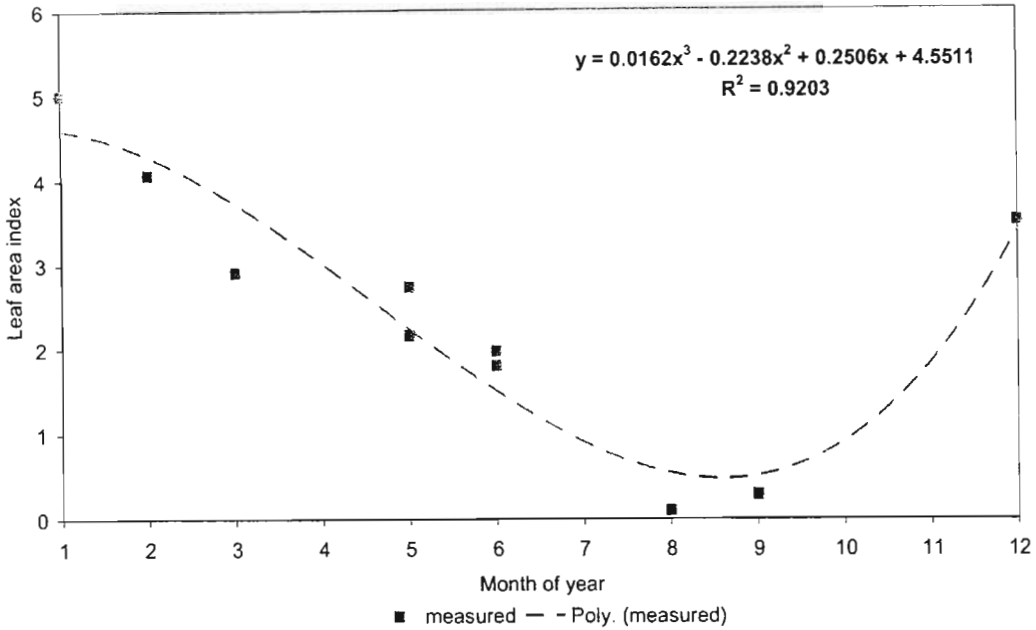


Fig. F.1 Average leaf area index ( $y$ ) as a function of the month of the year ( $x$ ) measured for grassland during the field experiment. Dotted line represents the third order polynomial fitted to the data.

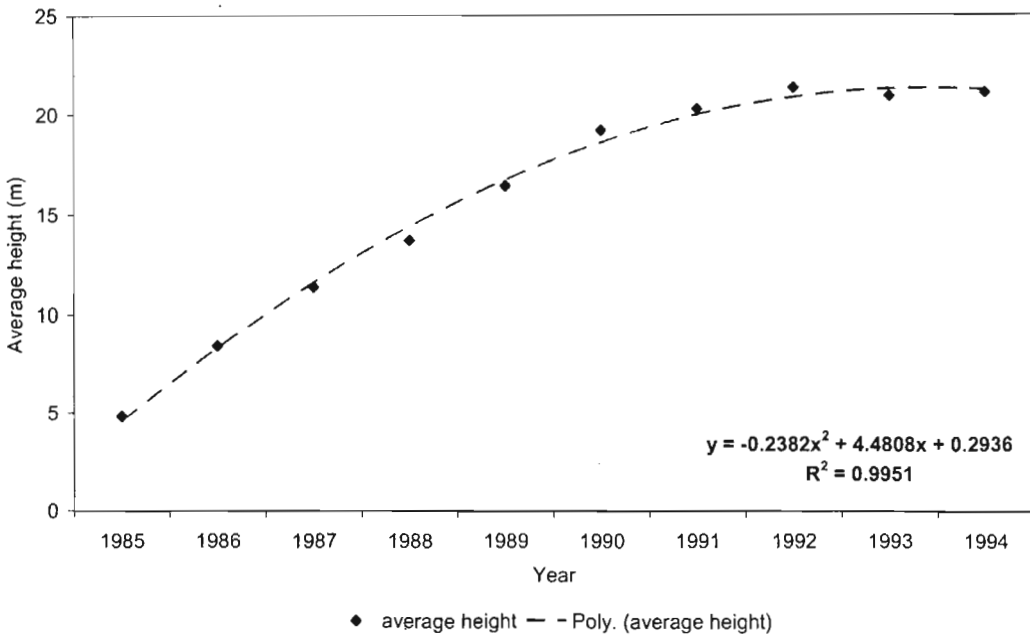


Fig. F.2 Average canopy height ( $y$ ) over time ( $x$ ) measured for *E. viminalis* during field trials by the ICFR. Dotted line represents the second order polynomial fitted to the height data, as a function of time



### F.5 Soil data inputs

The SWAP model was parameterised for both the grassland and *E. viminalis* sites using the Rensburg soil information/parameters collected at the *E. viminalis* site (Tables F.8 and F.9). This ensures that any difference in the soil water balance components – *E. viminalis* vs grassland site – is the result of differences in the canopy/plant types and not in the soils.

#### F.5.1 Profile description

Table F.8 Profile description used for both the *E. viminalis* and grassland sites

<b><i>Parameter</i></b>	
<i>Ponding thickness (cm)</i>	5
<i>Reduction in soil evaporation to:</i>	<i>Maximum Darcy flux</i>
<u><i>Richards equation time discretization:</i></u>	
<i>Minimum time step (d)</i>	1.00E-05
<i>Maximum time step (d)</i>	0.16
<i>Type of scheme</i>	<i>Richards equation solved until convergence</i>
<i>Number of soil layers</i>	5
<i>Number of soil compartments</i>	40
<i>Hysteresis</i>	No
<i>Similar media scaling</i>	No
<u><i>Preferential flow simulation:</i></u>	
<i>Due to immobile water</i>	No
<i>Due to soil cracks</i>	No
<i>Vertical distribution of drainage</i>	No
<i>Initial moisture conditions: pressure head at each compartment (cm)</i>	-8000
<i>Maximum rooting depth (cm)</i>	120

### F.5.2 Layer property inputs

Table F.9 Soil layer properties at the *E. viminalis* and grassland sites

<i>Parameter</i>	<i>Soil layer depth below soil surface (mm)<sup>41</sup></i>				
	<i>100</i>	<i>300</i>	<i>500</i>	<i>700</i>	<i>900</i>
<i>Sand</i>	0.43	0.38	0.34	0.47	0.46
<i>Silt</i>	0.17	0.16	0.13	0.16	0.15
<i>Clay</i>	0.36	0.41	0.5	0.36	0.37
<i>Organic matter</i>	0.04	0.04	0.03	0.02	0.02
<i>Residual soil water content (m<sup>3</sup> m<sup>-3</sup>)</i>	0.0000	0.0000	0.0000	0.0000	0.0000
<i>Saturated soil water content (m<sup>3</sup> m<sup>-3</sup>)</i>	0.3940	0.4780	0.4820	0.4950	0.4950
<i>Saturated hydraulic conductivity (cm d<sup>-1</sup>)</i>	7.255	0.06	0.06	1.51089	1.51089
<i>Alpha main drying curve (cm<sup>-1</sup>)</i>	0.2763	0.2897	0.1653	0.0323	0.0323
<i>Exponent in hydraulic conductivity function</i>	0.7540	0.0770	0.0335	0.0519	0.0519
<i>Parameter n</i>	1.0816	1.0834	1.0346	1.0547	1.0547
<i>Alpha main wetting curve (cm<sup>-1</sup>)</i>	0.2763	0.2897	0.1653	0.0323	0.0323

### F.6 Water data inputs

The bottom boundary conditions at both the *E. viminalis* and grassland sites were set to simulate free drainage of the bottom of the soil profile.

<sup>41</sup> The parameters were used within different depths. The parameters specified for the 100-, 300-, 500-, 700- and 900-mm soil depth were applied to the 0 to 299 mm, 300 to 499 mm, 500 to 699 mm, 700 to 1200 mm soil layers.